Prediction of Continental Shelf Sediment Transport

Using a Theoretical Model of the Wave-Current Boundary Layer

by

Margaret Redding Goud

B.S. Stanford University, Stanford, California

(1978)

SUBMITTED IN PARTIAL FULFILLMENT OF THE

REQUIREMENTS FOR THE DEGREE OF

DOCTOR OF PHILOSOPHY

at the

MASSACHUSETTS INSTITUTE OF TECHNOLOGY

and the

WOODS HOLE OCEANOGRAPHIC INSTITUTION

September, 1987

Signature of Author_____.

Joint Program in Oceanography,
Massachusetts Institute of Technology and
Woods Hole Oceanographic Institution
August 31, 1987

Certified by_____.

Ole Secher Madsen
Thesis Supervisor

Accepted by_____.

Marcia K. McNutt
Chairman, Joint Committee for Marine Geology and Geophysics
Massachusetts Institute of Technology/Woods Hole Oceanographic Institution

PREDICTION OF CONTINENTAL SHELF SEDIMENT TRANSPORT USING

A

THEORETICAL MODEL OF THE WAVE-CURRENT BOUNDARY LAYER

by

MARGARET REDDING GOUD

Submitted to the Massachusetts Institute of Technology-

Woods Hole Oceanographic Institution

Joint Program in Oceanography

on August 31, 1987 in partial fulfillment of the

requirements for the Degree of Doctor of Philisophy

This thesis presents an application of the Grant-Madsen-Glenn bottom boundary layer model (Grant and Madsen, 1979; Glenn and Grant, 1987) to predictions of sediment transport on the continental shelf. The analysis is a two-stage process. Via numerical experiment, we explore the sensitivity of sediment transport to variations in model parameters and assumptions. A notable result is the enhancement of suspended sediment stratification due to wave boundary layer effects. When sediment stratification is neglected under conditions of large wave bottom velocities (i.e. $u_b \geq 40\frac{cm}{sec}$), concentration predictions can be more than an order of magnitude higher than any observed during storm conditions on the continental shelf.

A number of limitations to application emerged from the analysis. Solutions to the stratified model are not uniquely determined under a number of cases of interest, potentially leading to gross inaccuracies in the prediction of sediment load and transport. Load and sediment transport in the outer Ekman Layer, beyond the region of emphasis for the model, can be as large or larger than the near-bottom estimates in some cases; such results suggest directions for improvements in the

theoretical model.

In the second step of the analysis, we test the ability of the model to make predictions of net sediment transport that are consistent with observed sediment depositional patterns. Data from the Mid-Atlantic Bight and the Northern California coast are used to define reasonable model input to represent conditions on two different types of shelves. In these examples, the results show how the intensification of wave bottom velocities with decreasing depth can introduce net transport over a region. The patterns of erosion/deposition are shown to be strongly influenced by sediment stratification and moveable bed roughness. Also predicted by the applications is a rapid winnowing out of fine grain size components when there is even a small variation of bed grain size texture in the along-flow direction.

Thesis supervisor: Ole Secher Madsen
Title: Professor of Civil Engineering

ACKNOWLEDGEMENTS

I owe debts of gratitude to too many people to name here, who have lent their kindness and support to me over the course of my graduate career. I can only begin to express my appreciation.

Two men made this work possible. Bill Grant offered me the opportunity to do this project and contributed insight, enthusiasm, and confidence whenever I needed them. He demonstrated how one should take joy in both work and life. There is a hole in the world without him.

Ole Madsen stepped in as my thesis advisor when Bill was unable to continue to work. Through his skill as an educator, curiosity as a scientist and kindness as a friend, he has taught me, more than anyone else, how to be a researcher.

I would like to thank my thesis committee, David Aubrey, Elazar Uchupi, and Charlie Hollister, for their help throughout the formulation and completion of the research. Sandy Williams served as chairman for my defense, for which I am very grateful. In addition, Nick McCave, Hans Graber, and Dave Cacchione read the thesis and provided helpful suggestions.

I have profited from discussions with any number of the staff and students at WHOI. Scott Glenn not only provided the theoretical and computational foundations for this work, but also answered questions on anything from basic fluid dynamics to details of the boundary layer model. I especially appreciate the talks with Harry Jenter as we were both figuring out the model. I learned a lot about how to approach science in talks with John Wilkin, Tom Gross and Rocky Geyer. Paul Dragos was a very patient tutor on the computer. Vincent Lyne had good insight into the model when I was first learning how it works. Brad Butman was very generous with information and ideas whenever I asked him for help.

The WHOI Education Office provided financial and moral support: many

thanks to Jake Peirson, Abbie Jackson, and Mary Athanis. I also want to thank the Ocean Engineering Department for adopting me, and Gretchen McManamin for always knowing the answer to whatever questions I asked her. Betsey Hirschell skillfully drafted a number of figures on very short notice.

I am indebted to the WHOI security guards, who were always ready with a kind word, a friendly smile, a cup of coffee and the occasional late night lift. Being a night owl would be no good without them.

I couldn't have made it without the help of my friends, who reminded me that there was more to life than work. Thanks to Stephanie Pfirman for sharing so much of Woods Hole with me; to Gabe Benoit for the Copley, the Red Sox, Bickford Pond and Dave McKenna; to Donna Blackman for taking care of me at crucial junctures; to Julie Jones for being mostly sane; to Bill Schwab for being mostly not sane; to David Rudd for the cartoons; to Paul Thogersen for the key to his house in Boston, no advance notice needed; to Sarah Griscom for moving out here to live with me; to Su Green for telling me to move back to San Francisco; to Merryl Alber for sharing enthusiasm; to Ron Smith for not giving up on me; to Doug Toomey for lots of music; to Betsy Welsh for always questioning the assumptions; to Dave Musgrave for lightness, usually; to Nancy Murphy for perspective; to Mary Athanis for clothing me; to Ray Howard for anarchy in snow.

John Collins did everything he could for me, including a lot of the worrying.

Finally, I thank my family for their support and confidence over the years. My mother Ruth, my father Allan, my brothers Allan and Richard, my sister Libba: they raised me to be unafraid to try anything, and stood behind me regardless of what it was I tried. This thesis is dedicated to them.

FINANCIAL SUPPORT

I received support during the course of this work from the WHOI Education Office, from the National Science Foundation (grant no. OCE-84-03249) and from the Office of Naval Research (contract no. N00014-86-K-0061).

Contents

List of Figures

List of Tables

Table of Symbols

A_b wave excursion amplitude at ocean bottom, from linear wave theory

C_{bed} concentration of a given grain size on the surface of the seafloor $(\frac{cm^3}{cm^3})$

C_D drag coefficient, relating boundary shear stress to flow velocity

C_m coefficient of added mass = 0.5

$C(z)$ volumetric sediment concentration at height z above the bottom $(\frac{cm^3}{cm^3})$

$C(z_0)$ sediment reference concentration at height z_0 above the bottom

d grain diameter (cm)

f Coriolis parameter $= O(\frac{10^{-4}}{sec})$ at temperate latitudes

f_{cw} combined wave-current friction factor, used to relate shear stress to fluid velocity at bottom

f'_{cw} skin friction component of total wave-current friction factor

g gravitational acceleration $= 980\frac{cm}{sec^2}$

h water depth (m)

H trough-to-crest surface wave height (m)

i $\sqrt{-1}$

k wavenumber for surface gravity waves $= \frac{2\pi}{\Lambda}$ (m^{-1})

k_b physical bottom roughness length (cm)

L Monin-Obukov length $= \frac{|u_*^3|\bar{\rho}}{\kappa g \overline{\rho' w'}}$ (cm)

Load total volume of sediment suspended in water column over a given area $= \int C(z)dz$ $(\frac{cm^3}{cm^2})$

p pressure $(\frac{gm}{cm^3})$

$\vec{q}_s$ rate of sediment transport $= \int C(z)\vec{u}(z)dz$ $(cm^3/cm/sec)$

$q_{s,x}, q_{s,y}$ components of sediment transport at a single point in the x- and y-directions, respectively

q_{bed} bedload sediment transport rate

R_* boundary Reynolds number $= \frac{u_* d}{\nu}$

S normalized excess shear stress $= \frac{\tau_0 - \tau_c}{\tau_c} = \frac{\psi}{\psi_c}$

S_* non-dimensional grain size $= \frac{d}{4\nu}\sqrt{(s-1)gd}$

s relative density of sediment in water $= \frac{\rho_{sed}}{\rho}$

T wave period (sec)

t time (sec)

u x-component of velocity, defined in the numerical model as the cross-shelf direction and in theory explanation as the wave direction $(\frac{cm}{sec})$

u_{ref} current velocity at some specified reference height within the current boundary layer

U current velocity above current boundary layer

$u(z)$ current velocity at a height z above the bottom

$\langle u'w' \rangle, \langle v'w' \rangle$ Reynolds average of vertical turbulent fluctuations, representing turbulent shear stress

u_a reference current velocity at some undefined height within the wave boundary layer, used to define boundary shear stress

u_b maximum wave horizontal velocity at the bottom, from linear wave theory

u_{cw} combined wave and current velocity

u_w instantaneous wave velocity

u_* shear velocity $= \sqrt{\frac{\tau_0}{\rho}}$ $(\frac{cm}{sec})$

u_{*c} current shear velocity, representing the boundary shear stress on the (quasi-) steady flow

u_{*cw} wave-current shear velocity, representing the maximum shear stress exerted on the bottom by the combined wave and current flow

u_{*w} wave shear velocity, representing maximum boundary shear stress for pure wave motion

u', v', w' turbulent velocity fluctuations in the x, y, z directions

V_2 a function of the the time-averaged near-bottom velocities used to calculate the current shear velocity

v y-component of velocity, defined as along-shelf $(\frac{cm}{sec})$

w z-component of velocity, defined as the vertical $(\frac{cm}{sec})$

w_f sediment fall velocity $(\frac{cm}{sec})$

x, y horizontal distances

$\Delta x, \Delta y$ horizontal grid spacings in numerical model of continental shelf

z vertical distance from bottom (cm)

$\frac{z}{L}$ stability parameter for a stratified flow

z_0 physical bottom roughness felt by flow within the wave boundary layer, $= z_{0,B} + z_{0,T} + z_{0,n}$

$z_{0,B}$ bottom roughness due to flow over bedforms $= \eta\frac{\eta}{\lambda}$

$z_{0,T}$ bottom roughness due to sediment transport $= 5.3(s + C_m)d\psi_c[(\frac{\psi_m}{\psi_c})^{.5} - 0.7]^2$

$z_{0,n}$ bottom roughness due to grain roughness $= \frac{d}{30}$

z_{0c} wave-enhanced bottom roughness, as felt by (quasi-) steady flow above the wave boundary layer

α a function of the maximum near-bottom wave-current velocity, used to calculate the wave-current shear velocity

β empirical constant derived from atmospheric studies of stratified flows =4.7

γ empirical constant derived from atmospheric studies of stratified flows =0.74

γ_0 empirical reference concentration parameter; in this thesis $.0005 \leq \gamma_0 \leq .005$

δ boundary layer thickness $= O(\frac{\kappa u_*}{\sigma})$ (cm)

δ_c thickness of current boundary layer

δ_w thickness of wave boundary layer $= O(\frac{\kappa u_{*cw}}{\omega})$

ς net erosion or deposition of sediment over a period of time (cm)

ζ_s stability parameter measuring effects of sediment stratification on boundary layer flow

η_p sediment porosity = 0.6

η sediment ripple height on seafloor (cm)

θ_{bed} direction of bedload transport with respect to wave direction

θ_{cur} angle of mean current with respect to the alongshelf direction

θ_w angle of wave direction with respect to the alongshelf direction

κ von Karman's constant = 0.4

Λ wavelength of surface waves (m)

λ sediment ripple wavelength on seafloor (cm)

ν fluid kinematic viscosity = 0.013 for seawater $(\frac{cm^2}{sec})$

$\nu_{t,cw}$ enhanced turbulent eddy viscosity in the wave boundary layer due to waves and current $(\frac{cm^2}{sec})$

ν_t turbulent eddy viscosity in unstratified flow

ν_{tm} turbulent eddy viscosity of momentum in a stratified flow $= \frac{\nu_t}{1+\beta\frac{z}{L}}$

ν_{ts} turbulent diffusivity of sediment mass

ρ fluid density $\approx 1.0\frac{gm}{cm^3}$

ρ_{sed} sediment grain density

σ radian frequency of fluid motion $= 2\pi/T$; (sec^{-1})

τ turbulent shear stress in vertical direction $= \rho\langle u'w'\rangle = \nu_t \frac{\partial u}{\partial z}$ $(\frac{gm}{cm-sec^2})$

τ_0 boundary shear stress

τ_{0c} enhanced time-averaged boundary shear stress

τ_{0cw} maximum instantaneous wave-current boundary shear stress

τ_0' skin friction component of bottom shear stress, in this case the maximum instantaneous wave-current boundary shear stress

ϕ_c angle between direction of reference current and direction of wave, $0° \leq \phi_c \leq 90°$

ψ Shields parameter for initiation of sediment motion $= \frac{\tau_0}{(s-1)\rho g d}$

ψ' Shields parameter based on skin friction boundary shear stress

ψ_β breakoff Shields parameter, designating shear stress at which ripples begin to be washed out $= 1.8 S_*^{0.6}$

ψ_c critical Shields parameter for initiation of motion of a given grain size

ψ_m maximum Shields parameter generated by a given flow

ω frequency of surface wave motion $= \frac{2\pi}{T}$ $O(10^0 - 10^{-1} sec^{-1})$

Chapter 1

INTRODUCTION

The transport of sediment is affected strongly by the presence of surface waves, particularly by the large waves associated with storms on the continental shelf. This intuitively obvious statement introduces a significant complication into the field of continental shelf sedimentology. Observations of flow and suspended sediment during storms are difficult to make; the response of sediments to waves is difficult to quantify; models, once made, are hard to verify. Marine sedimentology has therefore been limited, usually, to conceptual and generally qualitative models of sediment transport and sedimentation. These models are based largely on extrapolation from local studies, limited in temporal and spatial extent, sometimes augmented by laboratory studies. Such models are of limited use outside their immediate study area, and there has been a recognized need for a predictive model of erosion, deposition, and depth of reworking which could be applied in a wide variety of continental shelf environments.

Interest in sediment transport is not limited solely to sedimentologists and stratigraphers. Shelf physical oceanographers are concerned with the effect of suspended sediment on the drag generated by the seafloor. Coastal engineers must consider sediment transport in any continental shelf construction or pipeline project. Contaminants often attach themselves to sediment grains, so the range and rate of sediment transport is of concern for pollution control. The methods developed for

these other areas of study can be applied to aspects of the geological question, and the results may prove useful for all.

This dissertation presents an application of recently-developed boundary layer theory toward the goal of a predictive, general sediment transport model for the continental shelf. The aim here is to demonstrate how the physical elements controlling transport are represented in the theoretical model, then test the model to see which factors are most important in calculating sediment transport and load.

The model used here has grown out of the theory to predict boundary shear stress due to the nonlinear interaction of waves and currents developed by Grant and Madsen (1979). That model was combined with a moveable bed roughness model (Grant and Madsen, 1982) by Scott Glenn (1983; Grant and Glenn, 1983), who also added stratification by suspended sediments to the formulation. With minor modifications, the theory and computer programs generated by Glenn were used in this work.

The explanation and application of the model proceeds as follows. The remainder of the Introduction is devoted to an overview of continental shelf physical systems and the role of sediments in them, and a brief history of the development of geological models of shelf sediment transport. In Chapter 2, a physical description of the elements of the boundary layer model is presented. Then, in Chapter 3, the theory is developed quantitatively; that is, the relationships of the parameters are demonstrated using the equations of the theoretical model rather than descriptions of the physical relationships. The calculation scheme used by the model is demonstrated in Chapter 4.

Presentation of results begins in Chapter 5 with a sensitivity analysis which demonstrates the response of sediment load and transport predictions to variation in input parameters. In Chapter 6, the boundary layer model is used to calculate net erosion or deposition and reworking depth under wave and current conditions

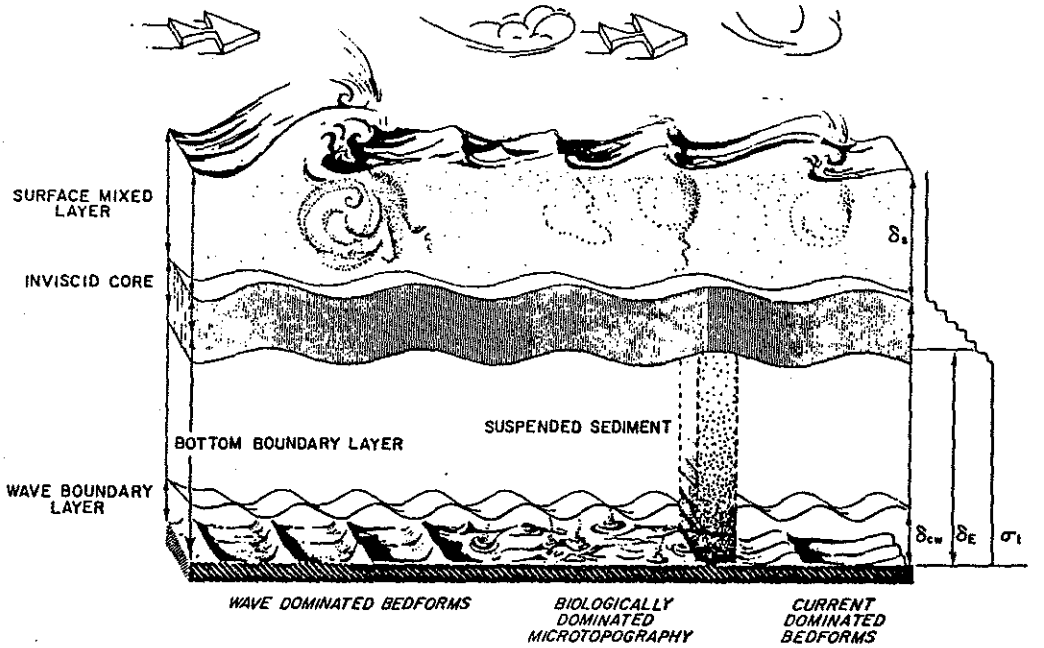

Figure 1.1: Schematic diagram of the major elements of the continental shelf physical system, emphasizing the boundary layers ($\delta_w, \delta_E, \delta_s$). Note the vertical extent (not necessarily to scale) of the surface and bottom boundary layers. Temperature (σ_t) is usually used in physical oceanographic studies to define the limits of the surface and bottom mixed layers. (from Grant and Madsen, 1986).

representative of storms on continental shelves of the Mid-Atlantic Bight and the Northern California coast. Chapter 7 states the conclusions of the study and suggests plans for improving and applying the model.

1.1 Sediments Within Shelf Physical Systems

Modelling sediment transport on the continental shelf is closely bound to physical oceanographic modelling of surface waves and currents on the continental shelf (Figure 1.1). The forcing mechanisms that control processes in the bottom boundary layer where sediment resuspension and transport take place represent entire fields of study in and of themselves. Shelf physical oceanographers devote careers to modelling, theoretically and numerically, the response of the surface and core flows to winds, pressure gradients, and topography. The development and disper-

sion of wind waves are the subject of numerous theories. Transport of sediment by these forces is influenced by processes representing still more independent disciplines: The generation of bedforms by steady or oscillatory flows is an empirical field, with predictive models based on laboratory flume studies; benthic biological studies define the effects of biota in binding together and reworking the surface sediments, and in generating roughness elements through their own mass or the sediment mounds they build. Advances in each of these fields are necessary to a complete shelf sediment transport model.

The connections between the processes represented by these fields of study are complex, involving feedback between the forcing and response elements of the system (Figure 1.2). The bottom boundary layer, for example, exists in response to wave and current flows generated by winds and pressure gradients. The interaction of the bottom boundary layer flow with the bottom, however, can generate roughness elements which feed back to influence the bottom boundary layer flow. Appendix A contains a more detailed diagram of the specific elements of a complete continental shelf physical model and a point-by-point description of the elements and their interactions.

Each element can be studied, modelled, and tested separately. As each becomes better understood on its own, the influence of other factors can be added. This generates the need for reliable models of what would have been called 'extraneous effects' in the initial stages of study. In this way, physical oceanographers have become more interested in the effects of waves and, to a more limited degree, sediments on the frictional drag on currents. In this dissertation, available models of boundary shear stress, sediment entrainment, bedform development, suspended load reference concentration, vertical diffusion of mass and momentum, sediment concentration and velocity profiles, and stratification by suspended sediments have been combined into a predictive sediment model, forming a framework into which

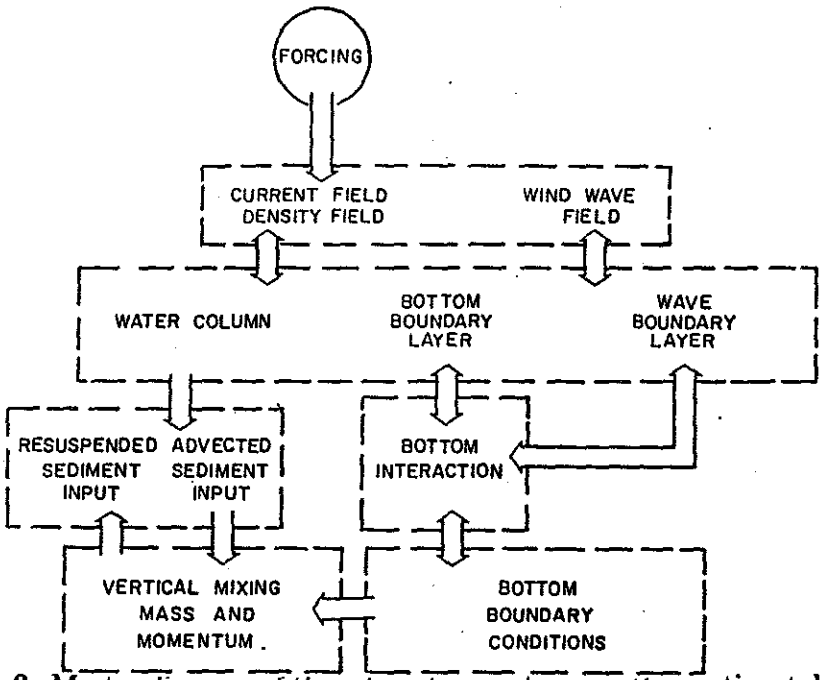

Figure 1.2: Master diagram of the interacting systems on the continental shelf, extending from the atmosphere to below the water-sediment interface. Arrows indicate forcing and feedback between systems. (Grant and Graber, unpublished)

future modelling developments can be placed.

1.2 Development of Geological Models of Shelf Sediment Transport

The geological utility of quantitative predictions of sediment transport is threefold. First, qualitative models that have been formulated from observations of input and depositional patterns can be tested. Second, the rates and episodicity of transport can be modelled accurately. Finally, models that have been formulated to explain stratigraphic components of the geological record for which there are no contemporary counterparts also can be tested.

Early geologic models presented the shelf, qualitatively, as a profile of equilibrium between sea level, sediment input and the action of waves and currents. Dietz (1963, 1964) and Moore and Curray (1964) traced the development of the

concepts of 'wave base', 'wave cut terraces' and 'profile of equilibrium'. 'Wave base' had been the most basic classification for marine sedimentology, and some workers even suggested the depth of the shelf edge was determined by wave base (Figure 1.3). Dietz and Moore and Curray, using the increasing data base of seismic profiles and samples of the continental shelf, as well as fundamental concepts of wave theory and initiation of sediment motion, emphasized that the morphological generation of the shape of the continental shelf was controlled primarily by tectonics and sea level variation. Waves are important for their capacity to erode bedrock in the surf zone, they contended, but in water deeper than a few meters, the term 'wave base', used geologically, can refer only to the wave's capacity to move unconsolidated sediment. No absolute depth could be set for such a definition, since it would depend on the wave height and period and the grain size and areal distribution.

The complexity of continental shelf processes has generated a number of complementary approaches. By the 1970s, geologists such as Swift (1974) were characterizing continental shelves based on the wave and current climate (i.e. storm- or tide-dominated) and the origin and distribution pattern of the sediments (i.e. palimpsest, autochthonous). Patterns and rates of sediment transport were being related to observed environmental conditions, and specific causes of transport were being isolated in detailed laboratory and field studies (see, e.g., papers in Swift, Duane, and Pilkey, 1972).

In general, regional geological studies combine a variety of observations in a particular locale in attempting to determine the modern and recent processes shaping the distribution. For example, Kulm et al.(1975) used sediment cores, bottom photos, current measurements, transmissometer profiles, and CTD (conductivity, temperature and depth) profiles to construct the model of sedimentation illustrated in Figures 1.4 and 1.5. The model indicates that sedimentation is sensitive to a

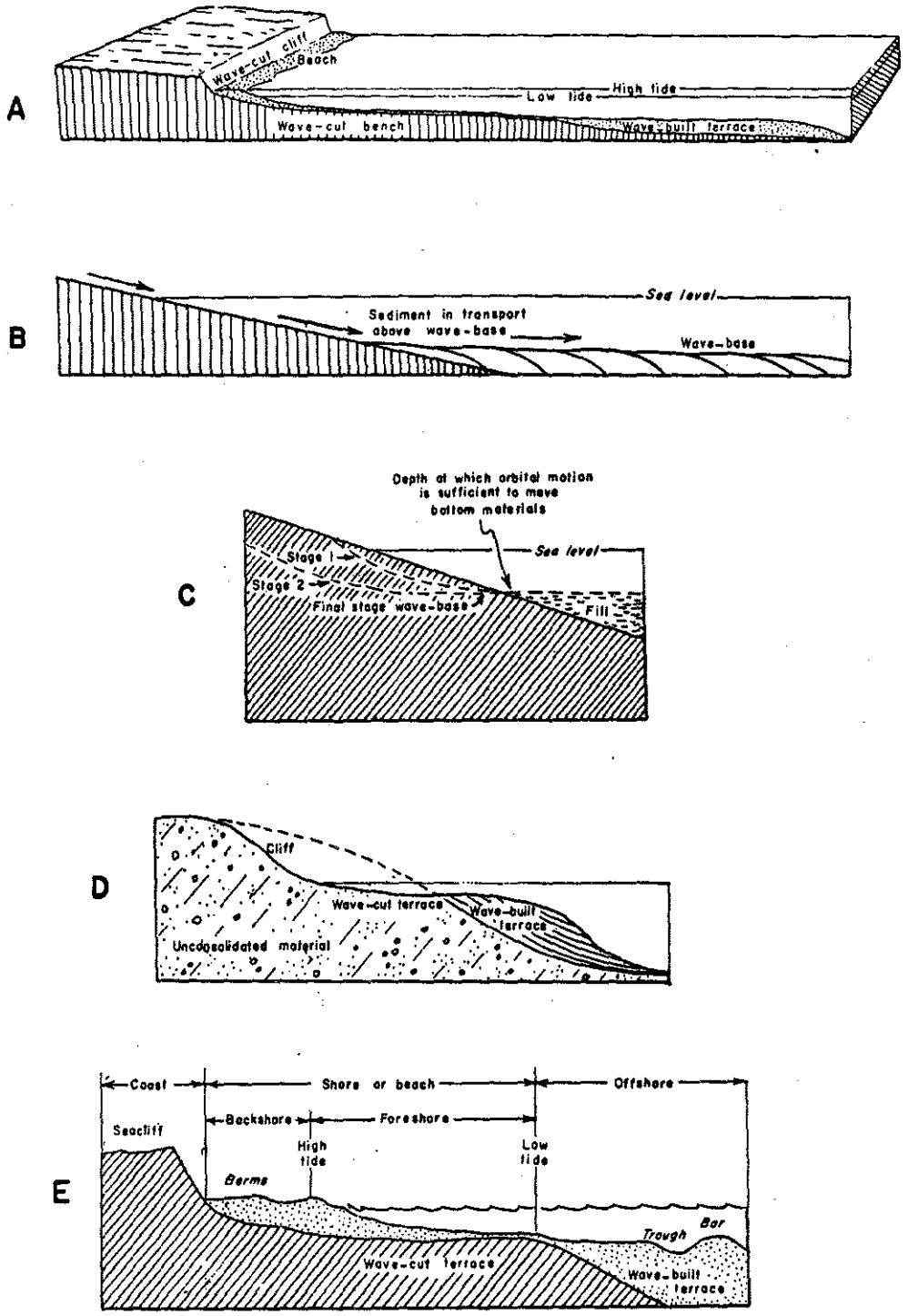

Figure 1.3: Views of the origin of the continental shelf, each implying a controlling effect of wave base. After: A) Longwell et al. (1948), B) Clark and Stern (1960), C) Garrels (1951), D) Von Engeln(1942) and E) Leet and Judson (1958) (illustration from Dietz, 1963).

wide variety of variables in this location: seasonal waves and currents, sediment input, stratification in the water column, biological activity, topographic variation and irregularities, bedforms and grain size. However, the relative importance of each variable can only be estimated using, generally, physical intuition. Controlled field experiments to examine the effect of variation of each variable on a regional scale are prohibitively expensive or impossible.

Since the 70s, advances have been made in combining field, laboratory, and theoretical work from disparate fields such as boundary layer dynamics, physical oceanography, geology, and biology. Progress on a number of these fronts is reviewed in Nowell (1983). Interdisciplinary field work such as the experiments of Cacchione and Drake (1982) and Butman (1987a and 1987b) attempt to explain local transport depositional patterns by combining physical oceanographic observations with theoretical predictions.

Some of the theoretical tools for constructing a numerical sediment transport model have been devised. The elements and their state of development at that time were described by Smith (1977). Kachel (1980, Kachel and Smith, 1986) applied Smith's theoretical concepts in a model to explain patterns of deposition on the Washington continental shelf.

The remainder of this dissertation describes the approach taken and the results gained in applying the boundary layer model of Grant, Madsen, and Glenn to the sediment transport problem. This theoretical model has been described in the literature in a series of papers and reports (Grant and Madsen, 1979; Grant and Madsen, 1982; Grant and Glenn, 1983; Glenn, 1983; Glenn and Grant, 1987). These will be referred to collectively hereafter as GMG.

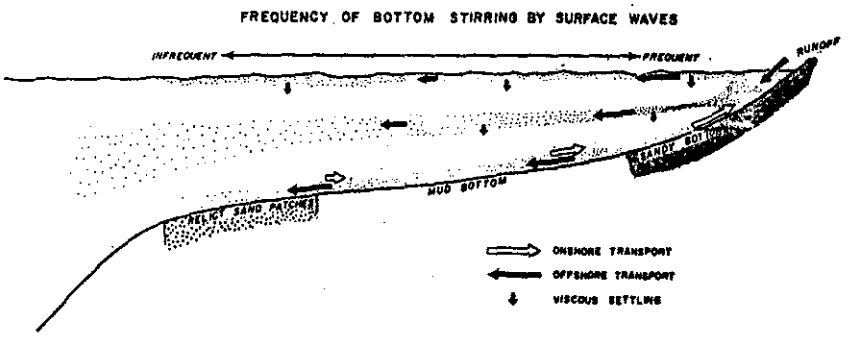

Figure 1.4: Model of suspended sediment transport across the northern Oregon shelf (from Kulm et al. 1975), indicating influences of various processes on sediment movement.

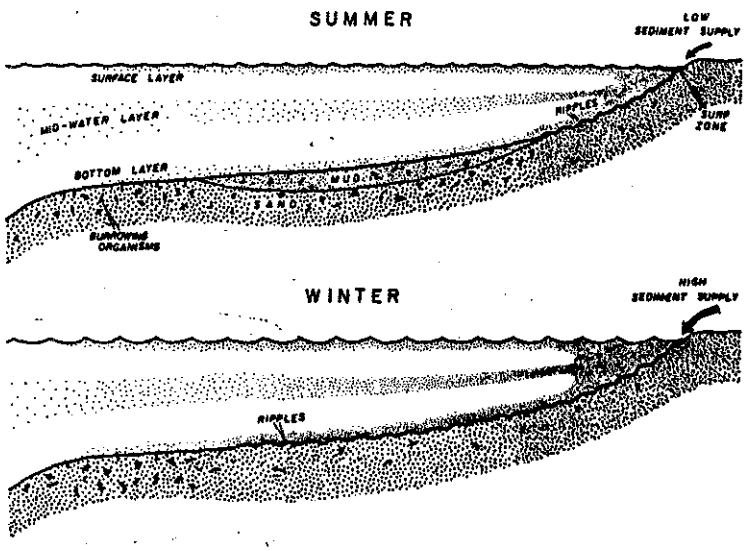

Figure 1.5: Seasonal variation in sedimentation for northern Oregon shelf (from Kulm et al., 1975), showing the influence of increased river runoff and larger swell and storm waves in winter.

Chapter 2

Model Background: Concepts

In this section, the key elements of continental shelf sediment transport are discussed in terms of fluid dynamics, but to the extent possible without resorting to equations. The presentation follows the formulation developed in GMG. A theoretical section follows (Chapter 3), elaborating and expanding on the concepts introduced here. All of the elements of the theoretical treatment are introduced in the present section, however, so that the reader who wants to avoid wading through the mathematical treatment can skip from the end of the present section to the Sensitivity and Application sections (Chapters 5 and 6) and understand the physical significance of the results presented therein. Many of the symbols used in the theoretical sections are introduced here, and they provide the continuity between the physical descriptions of this discussion and the precise mathematical definitions of the theoretical section.

2.1 The Continental Shelf Boundary Layer

This discussion of sediment transport by waves and currents begins with an examination of the bottom boundary layer. The boundary layer is the region of vertical velocity shear at a boundary. The *turbulent bottom boundary layer* refers to the region above the bottom where the flow is turbulent because of flow interaction with

the ocean floor. (The laminar boundary layer is not of concern here) Turbulent eddies are the mechanism by which the flow sets sediment in motion and keeps it suspended, so the boundary layer is the focus for study of resuspension and subsequent transport of sediment. There is no mechanism for sediment resuspended from the bottom to go higher than the boundary layer since the core flow (between the surface mixed layer and the bottom boundary layer) is defined as inviscid and therefore free of turbulent shear stress (Figure 1.1).

The existence of a boundary layer hinges upon the presence of a flow in the core layer driven by some outside force such as tides, winds, waves, or a large scale pressure gradient (this is often called the outer layer forcing). In shallow water and/or under strong wind forcing, the surface and bottom boundary layers can meet, so that the bottom boundary layer is driven more directly by surface forcing. This complication is not treated in this model, however.

The velocity of the fluid in contact with the bottom is by definition zero; this follows from the conclusion of fluid dynamicists, based on numerous experiments with liquids and gases, that the micro-layer of fluid in direct contact with a solid surface adheres to that surface. This boundary condition is known as the *no-slip condition* (see e.g. Schlichting, 1968), and sets up the boundary layer region of vertical velocity shear between the bottom and the core. Bottom roughness triggers the formation of turbulent eddies, which transport low-momentum fluid upward and higher-momentum fluid downward (Figure 2.1). The drag exerted on the flow due to these turbulent eddies is known as *Reynolds stress* or *turbulent shear stress.*

2.1.1 Boundary shear stress

The shear stress exerted on the flow immediately above the seafloor is known as the *boundary shear stress*, τ_0. The magnitude of the boundary shear stress sets

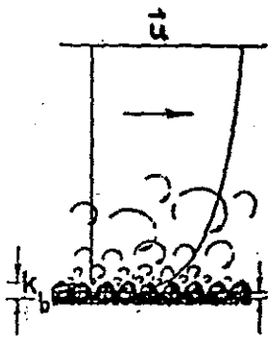

Figure 2.1: Schematic representation of turbulent eddies in the bottom boundary layer (after Yalin and Karahan,1979)

the level of turbulent energy for the boundary layer. Initiation of sediment motion and resuspension in the bottom few centimeters of the flow depend directly on the boundary shear stress.

In the study of sediment transport, the drag exerted on the seafloor by a steady flow of fluid (or, conversely, in physical oceanography the resistance imposed by the seafloor on a steady flow) is often represented using a *drag coefficient*, C_D. The drag coefficient can be used in a quadratic drag law to relate the boundary shear stress to a measured current velocity (u_{ref}) at some height above the bottom (see, e.g., Monin and Yaglom, 1965):

$$\tau_0 = \rho C_D u_{ref}^2 \tag{2.1}$$

where ρ is fluid density and C_D is $O(10^{-3})$; its exact value is a function of boundary roughness and height of the reference velocity above the seafloor.

In an analogous fashion, Grant and Madsen (1979) use a wave-current friction factor (f_{cw}) to relate the instantaneous boundary shear stress to the combined wave and current velocity close to the bottom, both of which vary with the phase of the wave. To determine the drag on the steady flow, the instantaneous shear stress values are time-averaged over the period of the wave to yield the enhanced current boundary shear stress, τ_{0c}. In the few centimeters closest to the bottom, the turbulent intensity is assumed to be governed by the maximum instantaneous

boundary shear stress, τ_{0cw}, based on the assumption that the time scale for decay of momentum-carrying eddies is long compared with the wave period (Grant and Madsen, 1979; Smith, 1977). These assumptions about the mean and maximum boundary shear stresses are fundamental to this work; their ramifications are presented below. For now it is simply noted that different shear stresses control turbulence at different heights above the bottom.

It is useful to represent the bottom shear stress in terms of a velocity scale; this is accomplished by defining a shear velocity u_*:

$$u_* = \sqrt{\frac{\tau_0}{\rho}} \tag{2.2}$$

2.1.2 Boundary layer height

The thickness of the continental shelf boundary layer (δ) is dependent on two factors: 1) the time available for the transport of turbulent energy away from the bottom, represented by the inverse of the temporal frequency (σ, signifying the radian frequency) of the flow, and 2) the velocity scale of the turbulent eddies, represented by the shear velocity u_*. The height of the boundary layer is calculated (Grant and Madsen, 1979):

$$\delta = O(\frac{\kappa u_*}{\sigma}) \tag{2.3}$$

where $\kappa = 0.4$ is von Karman's constant (Clauser, 1956).

To demonstrate how flow frequency limits boundary layer height, oscillatory flow will be used as an example. The sense of vorticity of turbulent eddies depends on flow direction. Changes in direction of the flow, therefore, change the sense of vorticity of the eddies being generated. When flow direction changes in oscillatory flow, newly-created eddies begin to cancel those with opposite vorticity, inhibiting their spread upward. For example, the tidal current boundary layer has a thickness on the order of $\delta_c = O(\frac{\kappa u_{*c}}{\sigma}) \approx \frac{(0.4)O(\frac{1cm}{sec})}{O(\frac{10^{-4}}{sec})} \approx O(10m)$ (σ here is the tidal frequency).

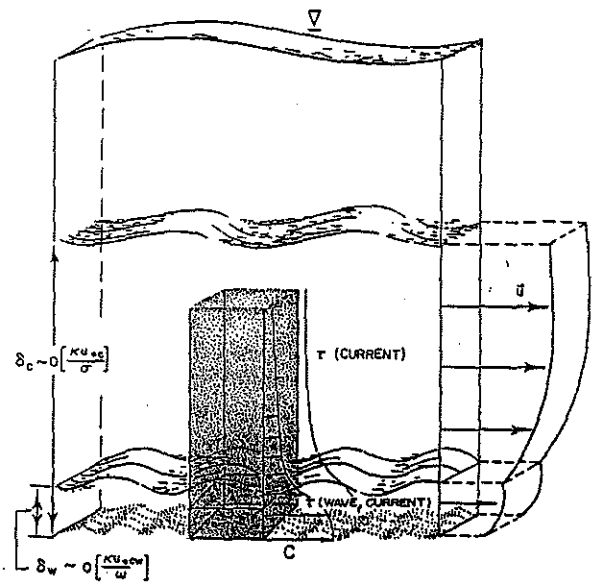

Figure 2.2: Schematic diagram of the continental shelf boundary layer illustrating the nested wave and current boundary layers (after Glenn, 1983).

The boundary layer due to waves is much thinner. The maximum bottom shear stress associated with waves, τ_{cw}, is often up to an order of magnitude larger than the mean boundary shear stress τ_c. However, the wave frequency, ω, is much higher than that of the mean flow. The wave boundary, therefore, has a thickness $\delta_w = O(\frac{\kappa u_{*w}}{\omega}) \approx \frac{(0.4)O(\frac{10cm}{sec})}{O(\frac{10^0-10^{-1}}{sec})} \approx O(10cm)$. The height of the boundary layer, therefore, is governed by the distance vorticity is transported away from the boundary in the time limits imposed by the flow.

On the continental shelf, both surface gravity waves and quasi-steady flow due to wind-driven, density-driven, or tidal currents are usually present. As the calculations in the last paragraph suggest, the boundary layers associated with the two processes are orders of magnitude different in scale, with the wave boundary layer nested inside the current boundary layer (Figure 2.2). For sediment transport prediction, the wave boundary layer is a critical element in the model, since it provides the boundary conditions for both velocity and concentration profiles.

Wave boundary layers

Maximum near-bottom velocities on the mid-to-outer shelf are often similar for waves and currents, although during storms wave velocities can be much higher. Even when the velocities are similar, the smaller length scale associated with the wave (δ_w) creates a maximum velocity shear much greater than the current shear, generating a much stronger instantaneous shear stress in the wave boundary layer than above it. The bottom shear stress in the wave boundary layer is a nonlinear function of the instantaneous wave plus current velocity, which varies over the period of the wave (Smith, 1977; Grant and Madsen, 1979). As noted in Section 2.1.1, the intensity of turbulence in the wave boundary layer is assumed to be controlled by the maximum wave-current shear stress. Therefore, the maximum boundary shear stress, $\tau_{0,max} = \tau_{0cw}$ is used to define the properties of the wave boundary layer, including the shear velocity u_{*cw} and the wave boundary layer height:

$$\delta_w = N\frac{\kappa u_{*cw}}{\omega} \tag{2.4}$$

Based on the approach of the predicted wave velocity to the free-stream velocity, Grant and Madsen (1979) suggested a value for the scaling constant of N=2; Trowbridge and Madsen (1984) suggest N=1 based on agreement with higher-order models. Variation of this parameter is of little importance for load and transport calculations because sediment is well-mixed in the wave boundary layer, so concentration at δ_w is not strongly dependent on N. Unless otherwise noted, the value $N = 2$ is used in this thesis.

Current boundary layers

Above the wave boundary layer, all turbulent transport is assumed to be associated with the current. The shear velocity u_{*c} represents, in this case, the boundary shear stress (τ_{0c}) felt by the current. In the no-wave case, the drag felt by a given steady

current is governed by the bottom roughness: more energetic eddies are produced and more low-momentum fluid is transported upward if the bottom is rougher. The effect of the wave is also to increase turbulent energy in the region very close to the bottom. The wave-generated turbulence therefore can be treated as a roughness element acting on the flow above the wave boundary layer; u_{*c} is greater because the current "feels" a rougher boundary.

The frequency governing the boundary layer height associated with the mean current on the shelf is the Coriolis parameter f (Grant and Madsen, 1986), defined as

$$f = 2(\frac{1}{24hours}) \sin \phi \tag{2.5}$$

where ϕ is the latitude. For mid-latitudes $f = \frac{O(10^{-4})}{sec}$. The scale height of the current boundary layer is therefore defined, using the wave-enhanced current shear velocity, as

$$\delta_c = \frac{\kappa u_{*c}}{f} \tag{2.6}$$

Like the tidal current boundary layer, the characteristic scale of the mean flow is $O(10m)$, with 40-60m not uncommon during storms.

2.2 Initiation of Sediment Motion

Sediment motion is initiated when the shear stress felt by the seafloor is greater than the critical shear stress for moving sediment. The boundary shear stress τ_0 defines the effects of turbulence on the flow in the boundary layer. This stress can be viewed as resulting from two separate components: 1) the interaction of the fluid with the solid boundary and 2) the turbulence generated due to pressure gradients introduced by roughness elements on the bottom. These two components of the boundary shear stress are referred to as *skin friction* and *form drag.* The medium sand and smaller grains ofprimary interest for suspended sediment transport are

not set in motion by the pressure gradients that make up the form drag component. For the purposes of this model, initial sediment motion is considered to result from the skin friction component, denoted by the symbol τ_0'. Turbulent transport of mass and momentum in the boundary layer is governed by the total boundary shear stress.

A sediment grain responds nearly instantaneously to turbulent fluctuations. Therefore, critical shear stress for initiation of motion might be expected to be related to the skin friction component of the maximum boundary shear stress, τ_{0cw}, (Section 2.1.1). In controlled laboratory settings, initiation of motion and bedload transport in oscillatory flow were found to be predicted quite successfully using the maximum shear stress (Madsen and Grant, 1976). In those laboratory tests, the bed was flat, so the maximum shear stress was equal to the skin friction shear stress. In the calculations of this study, the skin friction component of the maximum combined boundary shear stress is used for all initiation of motion and bedload transport predictions.

A commonly used empirical criterion for determining the critical shear stress for initiation of motion of non-cohesive sediments is the Shields parameter, which is defined:

$$\psi = \frac{\tau_0}{(s-1)\rho g d} \tag{2.7}$$

The numerator represents the force trying to move the particle and the denominator represents the gravitational force (per unit area) on the particle, which resists motion ($s = \frac{\rho_{sed}}{\rho}$, ρ_{sed} = grain density, g = gravity, and d = grain diameter). When the critical value of Shield's parameter for the non-cohesive grains in the bed is exceeded by the flow, sediment is moved. The critical value is designated ψ_c.

Critical values for the Shields parameter have been determined empirically in a series of laboratory experiments, beginning with those used to generate the original Shields Diagram (Shields, 1936). That original diagram plotted ψ_c versus the

boundary Reynolds number $R_* = \frac{u_* d}{\nu}$. This can be reformulated to make the independent variable a function of sediment and fluid properties only (e.g. Yalin, 1972; Madsen and Grant, 1976). The modified Shields Diagram plots ψ versus S_*, where

$$S_* = \frac{d}{4\nu}\sqrt{(s-1)gd} \tag{2.8}$$

The original flume experiments on which the diagram was based were performed using only large grain size material, corresponding to grain diameters of medium sand or larger (R_* and $S_* > 1$). Later investigators did experiments with grains as small as $d = .0016$ cm (medium silt) and used machine oil to increase viscosity, thereby extending the Shields Diagram from $R_* = 1.0$ to $R_* = 0.05$ (White, 1970; Mantz, 1977; Yalin and Karahan, 1979). For this study, this extended Shields Diagram has been adapted to the S_* formulation(Figure 2.3). The initiation of motion criterion can be increased by biological adhesion of sediment grains (Nowell, Jumars, and Eckman, 1981; Grant, Boyer and Sanford, 1982) or electrochemical cohesion, due to the presence of clays in even small quantities. This is especially true for silt-sized grains; interpretations of sediment load and transport results must be made with this uncertainty in mind.

2.3 Sediment Suspension

Once sediments are dislodged from the seabed, they are available for transport upward by turbulent eddies. The strength of these eddies governs the mixing of mass and momentum in the boundary layer and is determined by the boundary shear stress, τ_0. Mixing occurs because vertical eddies are transporting high-concentration fluid up and low-concentration fluid down, so there is a net upward flux of sediment. This flux is balanced by the tendency of the sediment to fall out of suspension due to gravity.

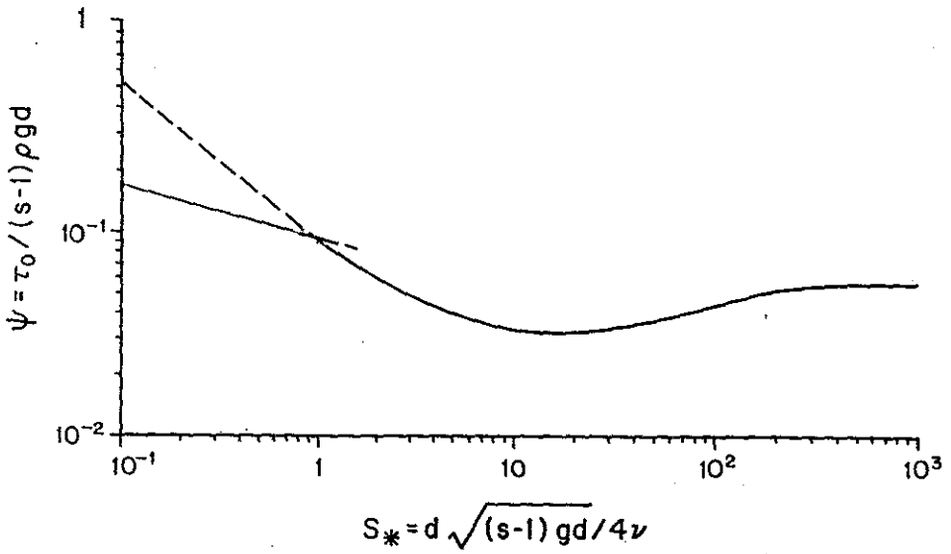

Figure 2.3: Modified Shields diagram. The extension of the initiation of motion criteria to include recent laboratory results for fine grain is shown by the solid line to the left of the break in slope at $S_* = 1$. The dashed line shows the criterion generated by linearly extending the trend established by Shields' coarse grain data (modified from Madsen and Grant, 1976).

The tendency of sediment to fall is measured by the particle fall velocity w_f and is determined to first order by balancing the submerged particle weight with the fluid drag on the particle, the weight being determined by particle size and density (Figure 2.4). Stokes drag law holds for grains for which the nondimensional sediment parameter S_* is less than one (representing, for quartz grains, a diameter of 0.012 cm, or fine sand size), and the fall velocity is calculated (Madsen and Grant, 1976):

$$\frac{w_f}{[(s-1)gd]^{\frac{1}{2}}} = \frac{2}{9}S_* \tag{2.9}$$

In nature, the fall velocity of a particle can be affected by flocculation or biological aggregation, so that *in situ* measurements of the fall velocity are desirable. However, the medium silt to medium sand grain sizes considered in this work are not usually subject to aggregation. The high wave boundary layer shear stresses discussed here would, at any rate, likely disaggregate many aggregates (McCave, 1984). The calculated fall velocity is, therefore, probably reasonable, but may be

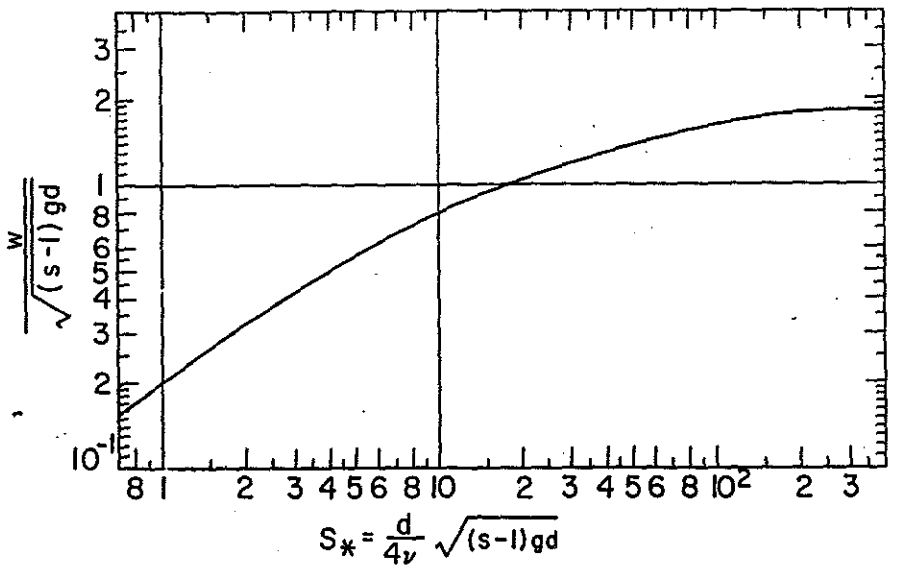

Figure 2.4: Nondimensionalized particle fall velocity as a function of S_* (nondimensionalized grain diameter; after Madsen and Grant, 1976).

a little low at the lower end of the grain size spectrum.

By using shear velocity u_* to characterize the energy of turbulent eddies, the concentration profile near the seafloor can be characterized by the ratio $\frac{u_*}{w_f}$. The more energetic the turbulence, the greater the flux upward; the larger the particle, the greater the flux down.

Stratification by suspended sediments

The introduction of sediment into the flow from the bottom causes a vertical density gradient, with the highest density at the bottom. This configuration is known as stable stratification and tends to damp turbulence. The mechanism by which stratification damps turbulence can be understood in terms of energy conservation. Turbulent kinetic energy in a boundary layer is generated by the interaction of mean velocity shear with the Reynolds stress, as the interaction of the flow with the seafloor transforms the kinetic energy of the outer layer forcing into turbulent energy. If the fluid is stably stratified, then some of the kinetic energy is expended in displacing the denser fluid upward, rather than in the maintenance of turbulence.

The effect of stratification on the turbulent energy depends on the density gradient and the turbulent energy of the flow. In the extreme case where the density gradient is small and the energy is large, then the stratification has little effect on the turbulence, and turbulent mixing may destroy the stratification. This is exemplified in the surface- and bottom- "mixed layers" on the continental shelf, where temperature and salinity stratification have been destroyed by boundary layer turbulence. At the opposite extreme, where the density gradient is large and turbulent energy is small, the turbulence may not be sufficiently energetic to displace the higher density fluid upward, and all turbulent mixing between the layers may be stifled. This situation is not unusual in estuaries where a turbulent fresh water layer may flow over a turbulent saline layer without substantial mixing. In intermediate cases, stratification lessens, but does not entirely wipe out, turbulent mixing.

The degree of stratification is generally denoted using a Richardson Number, which is derived from the turbulent kinetic energy equation. It is the ratio of the production of turbulent kinetic energy due to interaction of the mean shear with Reynolds stress to the production (or absorption) of turbulent kinetic energy due to buoyancy.

Stable stratification of the flow by sediments can affect both the velocity and concentration profiles. To explain the effects, the case of a steady flow without waves will be examined first. Consider a flow in the inviscid core of velocity U, over a rippled seafloor (Figure 2.5a). The ripples interact with the flow to generate turbulent eddies, which advect low velocity fluid up into the water column. At some height z_1 above the bottom, the flow has been retarded to a velocity $U - u_1$. If sediments stratify the flow, less turbulent energy is available to mix low-momentum fluid up from the bottom. This leads to a larger vertical velocity shear, so the velocity at z_1 is higher $(U - u_2$, where $u_1 > u2)$ and the drag due to the boundary

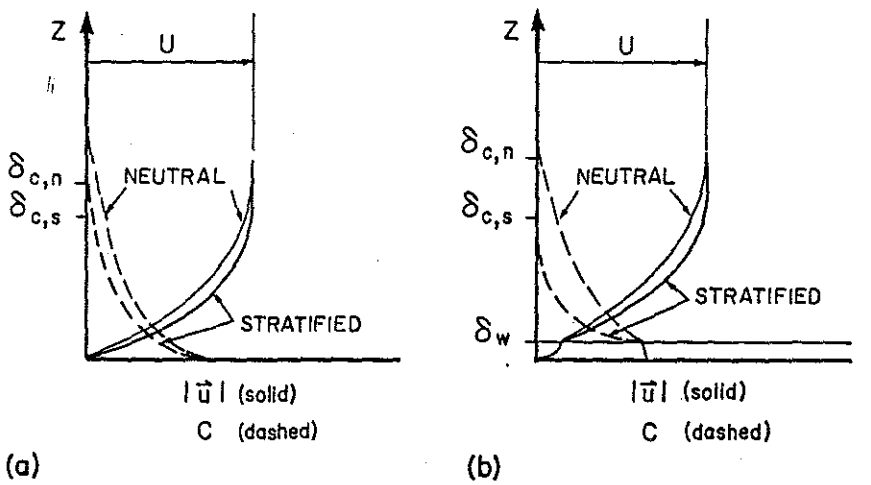

Figure 2.5: Schematic diagram showing the predicted effects of sediment stratification on velocity and concentration profiles in the bottom boundary layer. Velocity profiles are solid lines; concentration profiles are dashed. (a) Current profiles with no wave motion. (b) Wave and current profiles.

dies out closer to the bottom ($\delta_{c,s}$ versus $\delta_{c,n}$). The latter effect means that the height of the current boundary layer δ_c is smaller when there is stratification due to suspended sediments in the water column.

The effect on concentration profiles is analogous to that on the velocity. If concentration profiles are calculated without taking stratification into account, the concentration at z_1 reflects the balance between the upward flux of sediment due to turbulence and the downward flux due to gravity. Since stratification decreases the boundary layer turbulent energy, a larger concentration gradient is necessary to maintain the balance of upward and downward fluxes, and the concentration at z_1 is therefore lower when stratification is taken into account.

The presence of a wave boundary layer can amplify the effect of stratification. The high energy associated with the wave-generated eddies cause the wave boundary layer to be well-mixed. That is, the sediment concentration in the wave boundary layer is high throughout. If wave bottom velocities are large relative to the near-bottom current velocities, the turbulent energy will drop quickly over a

short distance as the effects of the waves die out.

The rapid decrease in turbulent intensity translates to a rapid decrease in sediment concentration, and therefore an increase in stratification effects. As formulated in GMG and used here, with a discontinuity in eddy viscosity at the top of the wave boundary layer, the flow immediately above the wave boundary layer is suddenly able to hold substantially less sediment in suspension, causing strong stratification and drastically reducing the transfer of mass and momentum above the wave boundary layer. Under strong waves, this wave-enhanced stratification causes dramatic increases in the vertical gradients of sediment concentration and velocity above the wave boundary layer (Figure 2.5b), and dramatic decreases in predicted load and transport. The decreases due to stratification are discussed in detail in the sensitivity analysis (Chapter 5). The stratification effect due to waves is artifically enhanced by telescoping the distance over which wave effects die out down to a point at δ_w. The stratification effects discussed here are, therefore, end member cases for the wave, current and sediment conditions presented.

Determination of the effect on the flow of stable stratification by sediments is complicated by the fact that the sediment concentration profile is itself a function of the turbulent energy of the flow. The feedback between the concentration profile $(C(z))$ and the turbulent energy (u_*) means that the calculation process must be iterative; the method used is described in Chapter 4.

2.4 Sediment Transport

The discussion so far has been concerned with velocity and sediment concentration profiles in the boundary layer at a point for a single set of conditions. These quantities, by themselves, can be used to calculate the depth of reworking and the net flux past the point over a given period of time. To predict the net sediment

transport, that is, erosion or deposition, for a finite region on the continental shelf over a finite time, a model must account for spatial variation of one or more environmental parameters. The parameter variation could take a number of forms, such as a variation in wave height due to water depth change; a variation in bottom roughness due to biological activity; a variation in grain size; or a variation in current speed or direction. In cases where there is no horizontal change, the input of sediment to an area would equal the output from it, and there would be neither net erosion nor deposition.

For purposes of this exercise we let a region of any continental shelf be represented by a square (Figure 2.6), defined by four points at its corners, over which sediment, wave, and/or current parameters are allowed to vary. The box defined by the grid square and the boundary layer directly above it comprises the field of interest. The horizontal extent chosen for a grid square is dependent on the spatial homogeneity of conditions in the region of interest and the sensitivity of the predictions to changes in the parameters. For example, changes in water depth change the wave parameters at the bottom so that a length scale might be determined by the bottom slope.

The Grant, Madsen, and Glenn model is a steady state model, reflecting the assumption that flow and sediment profiles adjust to changes in forcing (waves and currents) quickly relative to the duration of the flow conditions. This assumption is reasonable for the near-bottom layer under all circumstances, as the eddy diffusivity associated with the current will mix mass and momentum to a height of about 10 meters in a matter of minutes. Storm conditions typically last for one to three days, and stationarity in storm conditions can be assumed for a matter of hours. The question of time variance is left to future models.

At the corners of the box, the sediment load and sediment flux must be calculated. To do so requires the calculation of the velocity profile and the sediment

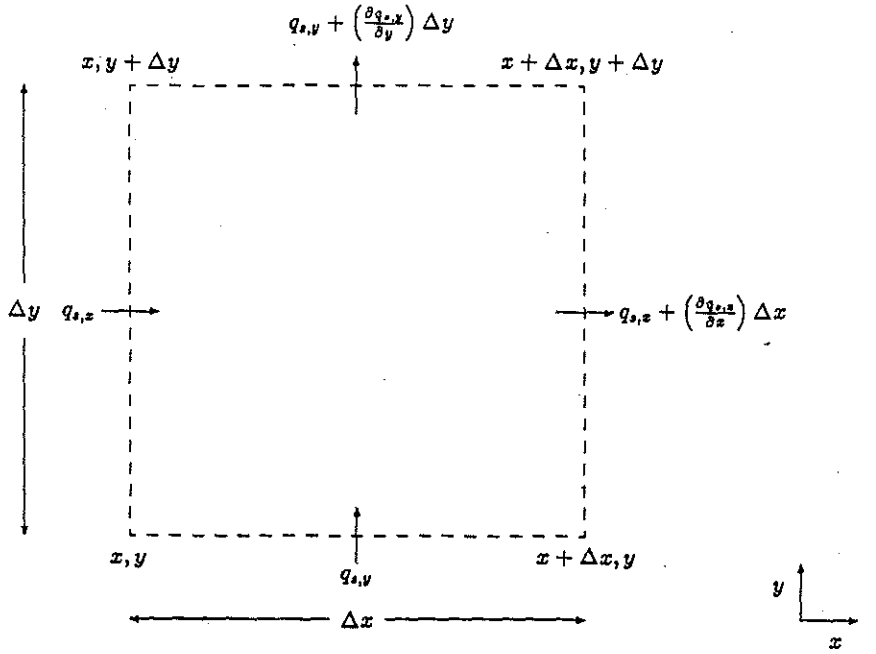

Figure 2.6: Sample horizontal grid square for calculating net transport on an area of the continental shelf

concentration profile in the bottom boundary layer. This can be accomplished using GMG; the method of calculation is described in the next two sections. The average erosion or deposition for the grid square is determined by vector averaging the transport predictions at each corner and dividing the net transport by the area of the square. The average depth of reworking is calculated by averaging the sediment load predictions at the four corners and dividing by the bed grain concentration, here taken to be 0.6 (Yalin, 1972).

Chapter 3

Model background: Theory

There are three quantities of interest in this study of sediment transport: 1) the net erosion or deposition of sediment over a period of time; 2) the sediment load, or total volume of sediment stored in the water column, from which the reworking depth can be calculated; and 3)sediment transport, or rate at which the sediment moves across the seafloor. These three quantities are related through the equation of conservation of sediment mass:

$$(1-\eta_p)\frac{\partial \varsigma}{\partial t} = -\frac{\partial}{\partial t}\int C dz - \nabla_H \cdot \vec{q_s} \tag{3.1}$$

The net erosion or deposition is represented in the left-hand side of this equation, where $\frac{\partial \varsigma}{\partial t}$ is the change in level of the seafloor (ς) over time (t), and η_p = sediment porosity. The two terms on the right-hand side represent 1) changes in the load with time and 2) the horizontal transport divergence, where:

$$Load(\frac{cm^3}{cm^2}) = \int C(z)dz \tag{3.2}$$

$$\vec{q_s} = Transport(cm^3/cm/sec) = \int C(z)\vec{u}(z)dz \tag{3.3}$$

The symbol ∇_H is the mathematical vector operator "del", applied in the horizontal plane, defined by $\nabla_H = \mathbf{i}\frac{\partial}{\partial x} + \mathbf{j}\frac{\partial}{\partial y}$. The dot product of ∇_H and the transport vector is designated the 'horizontal divergence' and represents spatial change in transport

volume. It is defined:

$$\nabla_H \cdot \vec{q_s} = \frac{\partial}{\partial x} q_{s,x} + \frac{\partial}{\partial y} q_{s,y} \tag{3.4}$$

where $q_{s,x}$ and $q_{s,y}$ are the x and y components of the transport vector and represent the net rate of sediment flux into a control square of unit size. The quantities that must be calculated are the velocity and sediment concentration profiles. In this study, these are generated using GMG. The theoretical foundations for these calculations are discussed briefly here; they can be studied in more detail in GMG.

3.1 Near-bottom Boundary Layer: No Suspended Sediments

3.1.1 Governing Equations

The horizontal flow in the boundary layer is governed by the Reynolds averaged equations of momentum:

$$\frac{\partial u}{\partial t} - fv = -\frac{1}{\rho}\frac{\partial p}{\partial x} - \frac{\partial}{\partial z}\langle u'w' \rangle \tag{3.5}$$

$$\frac{\partial v}{\partial t} + fu = -\frac{1}{\rho}\frac{\partial p}{\partial y} - \frac{\partial}{\partial z}\langle v'w' \rangle \tag{3.6}$$

where (x, y) and (u, v) are horizontal directions and velocities, respectively; and w is the vertical velocity, positive upward. Primed variables represent turbulent velocity components; p is pressure. The terms $\langle u'w' \rangle = \frac{\tau_x}{\rho}$ and $\langle v'w' \rangle = \frac{\tau_y}{\rho}$ represent the Reynolds stresses defined in Section 2.1; they result from Reynolds averaging the turbulent velocity components over a time that is long compared to the time scale of the turbulence. The terms in these equations show that the velocity profile is determined by the Coriolis force, horizontal pressure gradients, and Reynolds stresses. The assumptions underlying this form of the equations are that the flow, the boundary, and the roughness elements are all horizontally homogeneous, so that variations in x and y directions can be neglected.

The velocity and pressure terms can be divided into wave and current contributions, assuming wave motion is in the positive x direction:

$$u = u_c + u_w \tag{3.7}$$

$$p = p_c + p_w \tag{3.8}$$

Wave Governing Equation

After substituting these into the momentum equation (Equation 3.5), the terms governing the mean current motion can be separated from those governing the wave motion. The equation governing the wave motion becomes:

$$\frac{\partial u_w}{\partial t} = -\frac{1}{\rho}\frac{\partial p_w}{\partial x} - \frac{\partial}{\partial z}\langle u'w' \rangle \tag{3.9}$$

Current Governing Equations

The current is assumed to be steady over the time scales of interest, so that variations in time are neglected. Assuming also that the flow is driven by Coriolis forcing in the inviscid core, the pressure terms can be replaced using the geostrophic equations:

$$-fv_\infty = -\frac{1}{\rho}\frac{\partial p_c}{\partial x} \tag{3.10}$$

$$fu_\infty = -\frac{1}{\rho}\frac{\partial p_c}{\partial y} \tag{3.11}$$

The equations governing the mean flow become:

$$-f(v - v_\infty) = -\frac{\partial}{\partial z}\langle u'w' \rangle \tag{3.12}$$

$$f(u_c - u_\infty) = -\frac{\partial}{\partial z}\langle v'w' \rangle \tag{3.13}$$

Coriolis effects can be neglected close to the bottom where the assumption of a constant stress layer is made; for simplicity in the discussion, waves and currents

are assumed to be collinear. The momentum equations governing the mean flow in the near-bottom layer (Equations 3.12 and 3.13) then simplify to a single equation:

$$\frac{\partial}{\partial z}\langle u'w'\rangle = 0 \tag{3.14}$$

The assumption of wave-current collinearity is not necessary for the calculation, and the model is equipped to handle differences in wave and current direction.

The constant stress region is referred to throughout this work as the near-bottom region, distinguishing it from what is referred to as the outer Ekman region, where shear stress drops and the current direction veers due to Coriolis accelerations. The largest volume of shelf sediment transport is concentrated in the bottom few meters of the water column under most circumstances. The near-bottom region is the focus of the GMG model, and the determination of its vertical limits are based on the current shear stress as discussed in Section 3.2.4.

In the outer Ekman layer, the effects of changes in direction must be taken into account, and the full Ekman layer equations (Equations 3.12 and 3.13) must be solved using a numerical solution. This is not done in the present model; instead, the model calculates a rough estimate of the total load and transport in the outer Ekman layer based on the values of sediment concentration and eddy viscosity at the outer edge of the constant stress layer. The method used to make the estimates is described in Section 3.2.4. In cases where the load and transport in the outer Ekman layer are the same as or greater than the near-bottom transport, the volume and direction of predictions of total transport must be treated with caution.

3.1.2 Turbulent Closure

To solve the simplified wave and current momentum equations (Equations 3.9 and 3.14) for the near-bottom velocity profiles, the Reynolds stresses must be made tractable. By analogy with molecular frictional shear stress, the Reynolds

stress can be modelled using an eddy viscosity, ν_t:

$$-\langle u'w' \rangle = \frac{\tau_x}{\rho} = \nu_t \frac{\partial u}{\partial z} \tag{3.15}$$

where eddy viscosity is a parameterization of the intensity of the turbulence based on the flow velocity and the length scale of the eddies (cf. the fluid viscosity ν which is a property of the fluid). The turbulent eddy viscosity model for the near-bottom layer chosen by GMG and used in this work is time invariant and linear with distance from the bottom:

$$\nu_t = \kappa u_* z \tag{3.16}$$

Distance from the bottom, z, is included because, close to the bottom, the vertical length scale of the turbulent fluctuations can be no larger than the distance from the bottom. The shear velocity, u_*, is a measure of the shear stress on the bottom, as defined in Equation 2.2. Close to the boundary, the turbulent shear stress has been observed to be approximately constant and equal to the boundary shear stress, τ_0. The region where this approximation holds is referred to as the *constant stress region.* Substituting the eddy viscosity representation of the Reynolds stress into the near-bottom momentum equation governing the mean flow (Equation 3.14) and solving it with the boundary condition that the bottom shear stress is equal to τ_0 leads to the constant stress layer definition:

$$\nu_t \frac{\partial u}{\partial z} = \frac{\tau_0}{\rho} = u_*^2 \tag{3.17}$$

Recall from the discussion of boundary layers (Section 2.1.1) that the characteristic shear velocity is different for the wave boundary layer and the current boundary layer. In the wave boundary layer, turbulent energy is assumed to reflect the maximum combined wave and current boundary shear stress:

$$\tau_{0cw} = \tau_{0c} + \tau_{0w,max} = \mathcal{F}(u_c + u_{w,max}) \tag{3.18}$$

where $\mathcal{F}$ represents a functional relationship. Above the wave boundary layer, turbulent eddies are associated with the time-averaged current shear stress τ_{0c} alone. This means that eddy viscosity is defined differently inside the wave boundary layer and above it:

$$\nu_{t,cw} = \kappa u_{*cw} z \qquad z \leq \delta_w \tag{3.19}$$

$$\nu_t = \kappa u_{*c} z \qquad z > \delta_w \tag{3.20}$$

The limits of the constant stress layer and the eddy viscosity model for the outer region of the current boundary layer are discussed in more detail in Section 3.2.4.

3.1.3 Boundary Shear Stress Calculation

The characteristic boundary shear stresses and shear velocities are calculated from the instantaneous boundary shear stress. The instantaneous boundary shear stress is defined in GMG using a quadratic drag law:

$$\vec{\tau}_0 = \frac{1}{2}\rho f_{cw}(u^2+v^2)[\frac{u}{(u^2+v^2)^{\frac{1}{2}}}, \frac{v}{(u^2+v^2)^{\frac{1}{2}}}] \tag{3.21}$$

where u, v are the x, y components of a combined wave and current reference velocity vector close to the bottom. In this discussion, however, the wave and current are assumed to be collinear in the x-direction. f_{cw} is the combined wave and current friction factor, analogous to Jonsson's (1966) wave friction factor for pure oscillatory motion. The characteristic shear stress in the wave boundary layer ($\tau_{0cw} = \rho\ u_{*cw}^2$), as discussed in Section 2.1, is defined as the maximum value of Equation 3.21. For the current boundary layer, τ_{0c} ($= \rho u_{*c}^2$) is calculated by time averaging Equaion 3.21. The solutions for the shear velocities are:

$$u_{*cw} = [\frac{1}{2} f_{cw} \alpha(\frac{u_a}{u_b})]^{\frac{1}{2}} u_b \tag{3.22}$$

$$u_{*c} = [\frac{1}{2} f_{cw} V_2(\frac{u_a}{u_b})]^{\frac{1}{2}} u_b \tag{3.23}$$

where α and V_2 are functions of the maximum and time-averaged velocities, respectively, in the wave boundary layer. u_b is the maximum wave bottom velocity, calculated using linear wave theory:

$$u_b = \frac{H}{2}\frac{\omega}{\sinh kh} \tag{3.24}$$

where H = trough-to-crest wave height, $k = \frac{2\pi}{\Lambda}$ is wave number, and Λ is wavelength.

u_a is a representation of the velocity of the mean flow in the wave boundary layer, so $\frac{u_a}{u_b}$ is a representation of the relative strength of the mean versus the maximum oscillatory flow in the wave boundary layer. The value of f_{cw} is calculated using these definitions and the wave velocity profile. The solutions for the friction factor and the wave velocity profile are found in Appendix B. The functional depencence of f_{cw} is:

$$f_{cw} = \mathcal{F}(u_b, u_{ref}, \phi_c, k_b, A_b) \tag{3.25}$$

where u_b is the maximum wave bottom velocity, ϕ_c is the angle between wave and current directions, k_b is the bottom roughness, and A_b is the bottom excursion amplitude for the wave, defined:

$$A_b = \frac{u_b}{\omega} \tag{3.26}$$

3.1.4 Velocity Profile Solutions

With the definitions of shear velocity and eddy viscosity given in Sections 3.1.2 and 3.1.3 and the bottom roughness discussed in Section 3.3, solutions for the steady and oscillatory velocity profiles can be determined from Equations 3.14 and 3.9.

As discussed in Section 2.1.2, the effects of the boundary on wave motion are limited to a thin layer close to the bottom, the wave boundary layer. The shear velocity in that region is a function of the combined wave-current velocity near the bottom. Above the wave boundary layer, the turbulent momentum flux associated

with the wave is small. The solution for fluid motion due to the wave is simply the linear wave solution for inviscid flow, predicting sinusoidal motion decreasing in amplitude with depth (e.g., LeBlond and Mysak, 1978, sec. 11). For waves that generate significant velocities at the seafloor, (see Section 5.1), the wave motion at the top of the wave boundary layer is:

$$u_w = u_b \sin \omega t \tag{3.27}$$

The solution for the momentum equation for the waves inside the wave boundary layer (Equation 3.9) is not explicitly of interest for the present problem, though it is necessary for the calculation of the boundary shear stress. The solution is given in Appendix B.

Because of the difference in turbulent mixing in the wave boundary layer and the area above it, the solution for the mean (current) velocity is different inside and above the wave boundary layer. The profiles are calculated from Equation 3.17, using the different values of eddy viscosity inside and outside the wave boundary layer as defined in Equations 3.19 and 3.20:

$$u(z) = \frac{1}{\kappa} u_{*c} \frac{u_{*c}}{u_{*cw}} \ln \frac{z}{z_0} \qquad z \leq \delta_w \tag{3.28}$$

$$u(z) = \frac{1}{\kappa} u_{*c} \ln \frac{z}{z_{0c}} \qquad z > \delta_w \tag{3.29}$$

The influence of the enhanced boundary shear stress on the mean flow inside the wave boundary layer is demonstrated by the $\frac{u_{*c}}{u_{*cw}}$ term in Equation 3.28. Since the combined wave-current shear velocity u_{*cw} is by definition larger than u_{*c}, the mean flow is reduced in the wave boundary layer relative to what it would be if turbulent intensity were governed entirely by the mean shear stress. The lower velocities reflect the increased drag on the flow caused by wave-generated turbulence.

The value of z_0, where the calculated flow velocity goes to zero, is based on the bottom roughness. The method used to calculate it is discussed in Section 3.3. The

enhanced bottom roughness, z_{0c}, represents the total roughness felt by the mean flow, including the effects of the increased eddy viscosity due to the presence of the wave. The value of z_{0c} is determined by matching the calculated velocities for each region (Equations 3.28 and 3.29) at the top of the wave boundary layer, δ_w:

$$z_{0c} = z_0 \left(\frac{\delta_w}{z_0}\right)^{1-\frac{u_{*c}}{u_{*cw}}} \tag{3.30}$$

Since $\delta_w > z_0$ by definition, z_{0c} is likewise greater than z_0. This reflects the increased transport by wave-generated turbulence of low-momentum fluid up from the seafloor to the top of the wave boundary layer.

3.2 Near-Bottom Boundary Layer: With Suspended Sediments

The last section introduced the concepts underlying the study of combined wave boundary layers. The neutral velocity profile solutions (Equations 3.28 and 3.29) are sufficient for the study of flow in the boundary layer when the bottom is bedrock or sediment grains so large that they will not go into suspension. The focus of this study, however, is the effect of waves on sediment transport, rather than the effect of waves on the drag encountered by the current. Although the sediment concentration profile is a function of the turbulent mixing capacity of the flow, as represented by u_*, the results from the neutral boundary layer model cannot simply be applied to the calculation of a concentration profile. This is because stratification by sediments, as discussed in Section 3.2, can damp the turbulent transfer of mass and momentum up from the seafloor, affecting the values of u_{*c}. To calculate a velocity profile that takes stratification into account, the sediment concentration profile also must be determined. Since the concentration profile is itself dependent on the stratification correction, the procedure has to be iterative.

Governing Equations

The simplified, Reynolds-averaged conservation of momentum equations for waves and currents (Equations 3.9 and 3.14) still govern the flow. Again, for ease of discussion, co-directional waves and currents in the x-direction in the near-bottom layer are assumed. The mean distribution of sediment in the water column is governed by the conservation of mass equation for sediment (also known as the sediment continuity equation):

$$w_f \frac{\partial}{\partial z} C + \frac{\partial}{\partial z} \langle C'w' \rangle = 0 \tag{3.31}$$

where C is the time-averaged volumetric sediment concentration and $\langle C'w' \rangle$ represents the Reynolds averaged turbulent fluctuation of sediment flux. Inside the wave boundary layer, there is a fluctuating instantaneous concentration associated with the oscillatory wave velocity, which is taken into account in calculating the reference concentration.

Analogous to the eddy viscosity representation for turbulent stress, turbulent mixing of sediment likewise can be modelled using an eddy diffusivity, so that

$$\langle C'w' \rangle = -\nu_{ts} \frac{\partial C}{\partial z} \tag{3.32}$$

It is most often assumed that the eddy diffusivity and eddy viscosity can be represented in boundary layer flows using similar forms, and ν_{ts} can be written as

$$\nu_{ts} = \frac{\nu_t}{\gamma} = \frac{\kappa}{\gamma} u_* z \tag{3.33}$$

where γ is an empirical parameter, assumed to be 0.74, based on Businger and Arya (1974). The GMG model assumes steady state conditions, with a balance between upward turbulent transport and gravitational transport down. Thus Equation 3.31 can be written

$$w_f C + \nu_{ts} \frac{\partial C}{\partial z} = 0 \tag{3.34}$$

This is satisfied by

$$C(z) = C(z_0)(\frac{z}{z_0})^{-\frac{\tau_{wf}}{\kappa u_{*cw}}} \qquad z_0 < z < \delta_w \tag{3.35}$$

$$C(z) = C(\delta_w)(\frac{z}{\delta_w})^{-\frac{\tau_{wf}}{\kappa u_{*c}}} \qquad z > \delta_w \tag{3.36}$$

where $C(z_0)$ is a reference sediment concentration, discussed in Section 3.2.3, and $C(\delta_w)$ is the concentration at the top of the wave boundary layer, determined from Equation 3.35.

3.2.1 Stratification Effects

The effect of stratification on velocity and concentration profiles is treated using the eddy viscosity models. By analogy with atmospheric models, the eddy viscosity for momentum in the presence of stratification is defined:

$$\nu_{tm} = \frac{\nu_t}{\phi_m} \tag{3.37}$$

and the eddy diffusivity for mass is defined:

$$\nu_{ts} = \frac{\nu_t}{\phi_s} \tag{3.38}$$

where ν_t is the neutral eddy viscosity, and ϕ_m and ϕ_s are the nondimensional velocity and concentration gradients, respectively, defined:

$$\phi_m = 1 + \beta\zeta_s \tag{3.39}$$

$$\phi_s = \gamma + \beta\zeta_s \tag{3.40}$$

where β is another empirical parameter, with value 4.7 (Businger and Arya, 1974). ζ_s is a stability parameter, derived from the Richardson number, which measures the effect of stratification on the flow. The stability parameter in the near-bottom flow (where the constant stress assumption holds) is defined:

$$\zeta_s = \frac{z}{L} \tag{3.41}$$

where L is the Monin-Obukov Length, a parameterization of the ratio of the production of turbulent kinetic energy by mean shear to its dissipation by stratification (or production by buoyancy; Long, 1981):

$$L = \frac{|u_*|^3}{\kappa \frac{g}{\rho} \langle \rho' w' \rangle} \tag{3.42}$$

Near the bed, all density fluctuations are assumed to be caused by the vertical sediment concentration gradient, and so the turbulent fluctuation of mass is modelled using an eddy diffusivity and the sediment concentration profile (Long,1981):

$$\langle \rho' w' \rangle = \rho(s-1)\langle C' w' \rangle = -\rho(s-1)\nu_{ts}\frac{\partial C}{\partial z}$$

Before installing this expression into the stability parameter, the differential is disposed of by substituting in from the steady-state equation of conservation of mass (Equation 3.34), so that

$$\frac{z}{L} = \frac{\nu_t g(s-1) w_f C(z)}{u_*^4} \tag{3.43}$$

The value of the stability parameter varies from near zero, when stratification effects are very small, and is of order one when stratification effects are large.

3.2.2 Velocity and Concentration Profile Solutions

Using the definitions of eddy viscosity altered by stratification effects (Equations 3.37 and 3.38), the solutions for the steady current can be determined. The solution for the current above the wave boundary layer becomes:

$$u(z) = \frac{1}{\kappa} u_{*c} [\ln \frac{z}{z_{0c}} + \beta \int_{\delta_w}^{z} \frac{1}{L} dz] \quad z > \delta_w \tag{3.44}$$

The effects of stratification are shown in the second term on the right hand side of Equation 3.44. The equation demonstrates the effect mentioned in Section 2.3 that, for a given boundary shear stress u_*, a higher velocity is measured at a height

z if there is stratification by sediments. Conversely, for a measured velocity in the field at a height z above the bottom, less shear stress is felt on the bottom if there is sediment stratification.

Because the high energy of the eddies in the wave boundary layer is expected to keep that region well mixed, the stratification correction is not included in the calculation of the velocity below δ_w and the solution for the current profile is unchanged from Equation 3.19. The validity of this assumption for the GMG model is demonstrated in an analysis by Glenn (1983), where the maximum expected correction to velocity due to stratification in this model is shown to be an order of magnitude too small to affect turbulent fluxes.

The concentration profile inside the wave boundary layer is likewise unchanged from the neutral case (Equation 3.35). The solution for the concentration profile above the wave boundary layer is:

$$C(z) = C(\delta_w)(\frac{z}{\delta_w})^{-\frac{\gamma w_f}{\kappa u_{*c}}} \exp\{-\frac{\beta w_f}{\kappa u_{*c}} \int_{\delta_w}^{z} \frac{1}{L} dz\} \quad z > \delta_w \tag{3.45}$$

Note that the exponential decay of the concentration increases with an increase in the stability parameter. The integral in the exponential term must be solved numerically.

The calculation of the concentration above the wave boundary layer (Equation 3.45) depends directly on the calculation of the concentration at the top of the boundary layer, $C(\delta_w)$, as calculated using Equation 3.35. In addition to the decay in concentration due to the balance of the fall velocity with the turbulent mixing as in the wave boundary layer, the exponential decay term reflects the reduction in turbulence due to stratification. If the fall velocity is small relative to the shear velocity ($w_f << u_*$), the concentration decays relatively slowly and stratification has little effect on the concentration and velocity profiles. For relatively large fall velocities ($w_f \geq u_*$), the concentration decays rapidly regardless of

stratification, so stratification again has relatively little effect. The exception to this rule occurs when there is a strong wave and relatively weak current so that $u_{*cw} >> u_{*c}$. In this case, the concentration will drop off rapidly above the wave boundary layer regardless of grain size, creating a strong stratification effect. This tendency is investigated in the Sensitivity section.

The discussion has addressed only the case of a single grain size in the seabed. This is for ease of presentation; the GMG model can accomodate up to ten grain size classes. The procedure is the same, with grain diameter and bed concentration being specified for each class. The stratification correction is calculated using the sum of the concentrations for all categories.

3.2.3 Reference Sediment Concentration

The solution for the sediment concentration profile requires that a reference concentration be specified ($C(z_0)$ in Equation 3.35). The reference concentration is calculated in the model using the form suggested by Smith and McLean(1977):

$$C(z_0) = C_{bed}(\frac{\gamma_0 S}{1 + \gamma_0 S}) \tag{3.46}$$

where C_{bed} is the bed concentration of the grain. γ_0 is an empirical reference concentration parameter, and estimates of its value range from 0.0001 to 0.005 (Glenn, 1983; Wiberg and Smith, 1983). S is the normalized excess skin friction

$$S = \frac{\tau_0' - \tau_c}{\tau_c} = \frac{\psi'}{\psi_c - 1}$$

The primes refer to the skin friction component of the total boundary shear stress. The skin friction component is determined by calculating the combined wave-current friction factor f_{cw} using the dominant grain size as the bottom roughness scale rather than the physical boundary roughness (Equation B.1). To accomodate the presence of waves in this model, the instantaneous normalized excess shear

stress is used to calculate instantaneous reference concentrations which then are averaged over a wave period to find the mean reference concentration.

The reference concentration is directly dependent on the critical shear stress, as determined by the Shields parameter. However, the critical Shields parameter is an empirical value based on laboratory flume experiments on single grain-size sands. Mixed grain sizes and biological binding or mixing, as found in field situations, may affect the critical shear stress. The effects of these uncertainties in transport and load predictions are addressed in the Sensitivity section.

3.2.4 Sediment in Outer Ekman Layer

The Grant-Madsen-Glenn near-bottom model calculates velocity and concentration profiles only for the constant stress region of the boundary layer flow. For estimates of sediment load and transport, it is necessary to specify a height limit over which the concentration profile is to be integrated, so a vertical limit to the constant stress layer must be specified. Turbulent mixing extends beyond the constant stress region, however, so it is possible that significant proportions of the total sediment load are located above the constant stress region, in what will be referred to as the outer Ekman layer. To estimate the magnitude and relative importance of the outer Ekman layer transport, the GMG model was altered as discussed below. In the near-bottom layer, eddy size scales with distance from the bottom, so z is an appropriate length scale for the eddy viscosity. This region can be modelled as a constant stress layer with a linearly increasing eddy viscosity; numerous experiments have found that this approximation provides good agreement with observed velocity profiles. Above the constant-stress region, the velocity profile is relatively slowly-varying and the magnitude is insensitive to the form of the eddy viscosity. Ellison (1956) and Businger and Arya (1974) suggest a form for the eddy viscosity which is linear close to the bottom, but which is modulated by an exponential

decay:

$$\nu_t = \kappa u_* z e^{-\frac{z}{h}} \tag{3.47}$$

The eddy viscosity, then, reaches a maximum at $z = h$, and decays as $z \rightarrow \infty$; that is, approaching the top of the boundary layer. Long (1981) solved the neutral momentum equations (Equations 3.12 and 3.13) using the exponential form for the eddy viscosity and found

$$h = \frac{1}{6}\frac{u_*}{f}$$

where $\frac{u_*}{f}$ represents his boundary layer scale height. Above the constant-stress layer, Ekman turning becomes significant, so that the direction of flow is not the same as the direction of the bottom stress.

Numerical solutions for the velocity and concentration profiles in the outer boundary layer have been approached by Long (1981) and Glenn (1983). In the present work, an estimate of outer Ekman layer load and transport which can be solved analytically is used instead. Following Smith and Long (1976), the assumption is made that the eddy viscosity above the constant stress layer can be set to a constant value. This leaves open the choice of what height to choose as the beginning of the outer Ekman layer and what eddy viscosity to apply there.

Under the assumption that transport of sediment is controlled by the most energetic eddies, a logical choice for the outer Ekman layer eddy viscosity is the maximum value determined using the exponential form (Figure 3.1). This value occurs at

$$z = h = \frac{1}{6}\frac{1}{\kappa}\frac{\kappa u_*}{f} = \frac{\delta_c}{2.4}$$

At this height, the value of the eddy viscosity, as defined by the exponential model, is:

$$\nu_{t,max} = \kappa u_{*c}\frac{\delta_c}{2.4}\frac{1}{e}$$

The height where the linear model produces this same value will be defined as the top of the near-bottom region. Using the linear eddy viscosity model, this value of the eddy viscosity is reached at a height

$$z = \frac{\delta_c}{2.4e} \approx \frac{\delta_c}{6}$$

Figure 3.1 shows the linear (Equation 3.16), the modulated (3.47), and the combined eddy viscosity profiles. Using the combined (linear near-bottom and constant outer Ekman layer) eddy viscosity model, the eddy viscosities in the outer Ekman layer are defined. For the neutral case

$$\nu_{t,Ek} = \kappa u_* \frac{\delta_c}{6} = \frac{(\kappa u_*)^2}{6f} \tag{3.48}$$

and for the stratified case

$$\nu_{tm,Ek} = \frac{\nu_{t,Ek}}{1 + \beta \frac{\frac{\delta_c}{6}}{L_{\frac{\delta_c}{6}}}} \tag{3.49}$$

$$\nu_{ts,Ek} = \frac{\nu_{t,Ek}}{\gamma + \beta \frac{\frac{\delta_c}{6}}{L_{\frac{\delta_c}{6}}}}. \tag{3.50}$$

where the Ek subscript refers to the constant value used in the outer Ekman layer and $L_{\frac{\delta_c}{6}}$ refers to the value of the Monin-Obukov length at the top of the constant stress layer.

Use of the constant eddy viscosity in the outer Ekman layer means that for the outer boundary layer, the sediment continuity equation (Equation 3.31) takes the form

$$\nu_{ts,Ek} \frac{\partial C}{\partial z} + w_f C = 0 \tag{3.51}$$

This equation, solved with a boundary concentration given at $z = \frac{\delta_c}{6}$ has the solution:

$$C(z) = C(\frac{\delta_c}{6}) \exp[-\frac{w_f}{\nu_{ts,Ek}} z'] \tag{3.52}$$

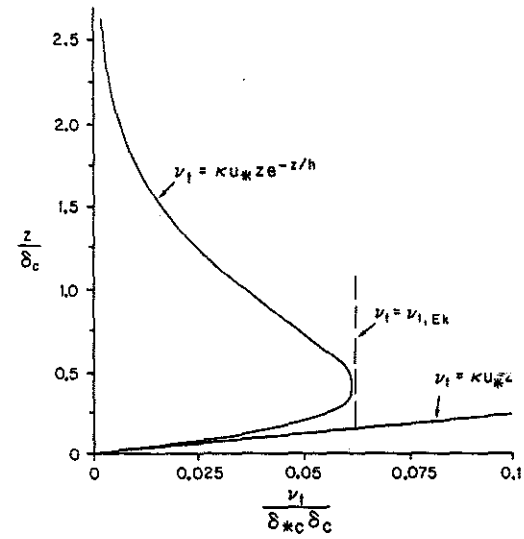

Figure 3.1: Dimensionless eddy viscosity as a function of nondimensional distance from the bottom. Solid curved line is exponentially decaying model; dashed line shows constant outer layer value; straight, solid line is linear model (after Glenn,1983)

where $z' = z - \frac{\delta_c}{6}$. Rather than calculate the concentration profile, the fact that the formula has an exact solution when integrated from zero to infinity is used to estimate the entire load in the outer boundary layer:

$$\int_0^\infty C(\frac{\delta_c}{6}) \exp[-\frac{w_f}{\nu_{ts,Ek}} z'] dz' = C(\frac{\delta_c}{6}) \frac{\nu_{ts,Ek}}{w_f}$$

To estimate the volume of transport in the outer layer, we multiply the total load by the velocity calculated at $z = \frac{\delta_c}{6}$, since this height represents the limit of the constant stress layer where velocity varies rapidly. The velocity profile is approaching the geostrophic value at this point and velocity growth is slow, so that matching estimated values for the logarithmic profile and the velocity deficit profile calculated from the geostrophic boundary layer equations gives an estimate of error of no more than 25% and a 20-degree maximum turning angle, which is acceptable given the fact that, under most circumstances, transport is expected to be concentrated in the near bottom layer.

This estimate has two significant applications. First, the relative significance of the sediment load and transport in the outer Ekman layer can be assessed. While in most cases sediment is expected to remain concentrated in the lower part of the

boundary layer, fine sediment in a strong current could diffuse upward in significant concentrations much higher in the boundary layer. In these cases, it is necessary to include Ekman turning to represent accurately the direction of transport, and results of the model should be interpreted cautiously. This estimate shows when Ekman turning can be neglected for calculation of transport; that is, when the constant stress layer model described and used in this thesis is sufficient.

On the other hand, the load and transport estimates are accurate enough for estimating net transport as the model is used here. The depth of reworking predicted under given wave-current conditions may be increased by the outer Ekman layer load: this technique provides an estimate of that depth. When calculating net transport (erosion or deposition) for an area, the conditions will be slowly-varying enough from one grid point to the next that the outer Ekman layer transport directions and volumes should be similar. Most of the error in direction and volume introduced by assuming that transport is in the direction of and controlled by the near-bottom steady current is therefore cancelled in calculating the net transport for a grid square.

3.3 Bottom Roughness

The calculation of the velocity profile inside the wave boundary layer (Equation 3.28) depends explicitly on the physical bottom roughness length z_0. This length is also necessary for the calculation of the friction factor, f_{cw}, on which the calculation of the shear velocities depends. The roughness changes in response to the flow, due to bedform development and the formation of a layer of sediment in motion.

The model used in this work for movable bed roughness under a combined wave and current flow was developed by Grant and Madsen (1982); that work will be

described briefly here.

The physical roughness felt by the near-bottom flow is the sum of three components: 1) the roughness due to the individual grain diameters in the bed (skin friction); 2) the roughness due to ripples and mounds on the seafloor (form drag); and 3) a roughness associated with dissipation due to moving sediment in the near-bed layer. The effect of these elements will be parameterized in terms of a Nikuradse equivalent sand grain roughness, k_b. As used here, the roughness height is expressed as:

$$k_b = k_{b,n} + k_{b,B} + k_{b,T} \tag{3.53}$$

where the three terms on the right hand side represent the roughness due to grains, ripples, and sediment transport, respectively.

The grain roughness, $k_{b,n}$, is represented by the grain diameter d. For a flat bed, the grain roughness is the only roughness element, and the skin friction is the total roughness. In most continental shelf situations, however, there are either hydrodynamically or biologically generated roughness elements at least an order of magnitude greater than the grain size, so that grain roughness can be neglected. It should be noted, however, that the sand grain size is the appropriate roughness length for the skin friction component of the total boundary shear stress, on which initiation of motion and bedload calculations depend.

The form drag component of shear stress is generated by the formation of eddies in the wake of the roughness element and the reattachment of the flow between elements. The roughness is dependent on the shape and distribution of the elements. Using the analysis of roughness elements of Wooding et al. (1973), Grant and Madsen (1982) derive an expression for roughness associated with a two-dimensional wave-generated ripple:

$$k_{b,B} = 27.7\eta(\frac{\eta}{\lambda}) \tag{3.54}$$

where η and λ are ripple height and length. Grant and Glenn (1983) include an expression for a generalized roughness where the height, shape and concentration of the elements are known. It is not used in the model since that information is not generally available; as information about the seafloor becomes more detailed, that element of the model can be determined more precisely.

The dimensions of the ripple are determined best from direct observation of the seafloor. When this is impossible, or when the roughness is in transition, empirical bedform formulas can be used. The model used in this work, since the cases of interest are wave-dominated, is a model of wave-generated ripples discussed in Grant and Madsen (1982). For boundary shear stress only slightly greater than that needed to initiate motion, Grant and Madsen found that ripples change slowly in what they refer to as 'equilibrium range'. At some higher shear stress, ripples height decreases rapidly as they are washed out. The shear stress at which the washing out process begins is designated by a breakoff Shields parameter:

$$\psi_B = 1.8 S_*^{0.6} \psi_c \tag{3.55}$$

where S_* is a non-dimensionalized measure of grain diameter (Equation 2.8) and ψ_c is the critical Shields parameter for initiation of motion. The empirical relationships for ripple geometry under waves given by Grant and Madsen are:

$$\frac{\eta}{A_b} = 0.22\left(\frac{\psi'}{\psi_c}\right)^{-0.16}$$

$$\psi_c < \psi' < \psi_B$$

$$\frac{\eta}{\lambda} = 0.16\left(\frac{\psi'}{\psi_c}\right)^{-0.04}$$

and

$$\frac{\eta}{A_b} = 0.48 S_*^{0.8}\left(\frac{\psi'}{\psi_c}\right)^{-1.5}$$

$$\psi' > \psi_B$$

$$\frac{\eta}{\lambda} = 0.28 S_*^{0.6}\left(\frac{\psi'}{\psi_c}\right)^{-1}$$

These values are used in Equation 3.54 to calculate ripple roughness in the model. Larger scale bed roughness which would not be perceived by the wave, but which would affect the mean flow, is not treated here, as it would be more appropriate to a general circulation model.

The roughness associated with sediment transport is based on arguments advanced by Owen (1964) that the wake structure around sediment grains in the near-bed transport layer cause the flow to feel a roughness proportional to the thickness of the layer. This concept was applied by Smith and McLean (1977) to

steady flow in the Columbia River, and by Grant and Madsen (1982) to oscillatory flow.

Grant and Madsen derive an expression for the layer thickness by balancing the initial kinetic energy of a particle put into motion with the potential energy at its highest elevation. The roughness length they derive using data from Carstens et al. (1969) is expressed:

$$k_{b,T} = 160(s + C_m)d\psi_c[(\frac{\psi'}{\psi_c})^{\frac{1}{2}} - 0.7]^2 \tag{3.56}$$

where $C_m = 0.5$ is the coefficient of added mass of a sphere.

The roughness length z_0 in fully turbulent flows as considered in the boundary layer model is equal to $\frac{k_b}{30}$, or approximately

$$z_0 = (\eta\frac{\eta}{\lambda}) + 5.3(s + C_m)d\psi_c[(\frac{\psi'}{\psi_c})^{.5} - 0.7]^2 + \frac{d}{30} \tag{3.57}$$

The three terms on the right hand side represent, respectively, ripple roughness ($z_{0,rip}$), sediment transport roughness ($z_{0,s.t.}$), and grain size roughness.

3.4 Sediment Transport

The Grant-Madsen-Glenn model is concerned primarily with prediction of velocity and concentration profiles. The method used to apply these to the predictions of suspended sediment transport and a method for estimating bedload transport are described here; these applications are not explicitly covered in GMG.

Three quantities derived from the boundary layer predictions are examined in the sensitivity analysis and applications: 1) the net transport for a given location, which can be used to determine whether a given area is undergoing erosion or deposition; 2) the total transport over time, which can be used to estimate the residence time of sediment on the shelf; and 3) the reworking depth, which demonstrates the degree to which sediment is mobilized during a transport event, and which may prove useful in interpretation of the conditions necessary to generate observed geological strata. The first can be calculated by integrating the transport calculations over time:

$$q_{s,tot} = \int [(\int_{z_0}^{\infty} Cudz) + \vec{q}_{bed}]dt \tag{3.58}$$

where the first term on the right hand side is suspended transport, calculated us-

ing velocity and concentration profiles as discussed above, and the second term is bedload transport. Because this quantity is integrated over time, any errors in the transport calculations are multiplied as the time interval is increased. Integration over time also introduces an assumption of spatial homogeneity in sediment concentration profiles over the area from which sediment is being advected into the region being modelled. For these reasons, estimates of total transport are generated here only for fairly short time periods, such as the duration of a single storm.

The net transport is the divergence of the transport vector, defined in Equation 3.4, which is calculated numerically for a point inside the grid square illustrated in Figure 2.6, using transport values calculated at the corners:

$$\begin{aligned}\nabla_H \cdot \vec{q}_s &= \frac{\partial}{\partial x} q_{s,x} + \frac{\partial}{\partial y} q_{s,y} \\ &= \frac{1}{2}\Big(\frac{q_{s,x}(x+\Delta x, y) + q_{s,x}(x+\Delta x, y+\Delta y) - q_{s,x}(x,y) - q_{s,x}(x,y+\Delta y)}{\Delta x} + \\ &\qquad \frac{q_{s,y}(x,y) + q_{s,y}(x+\Delta x, y) - q_{s,y}(x,y+\Delta y) - q_{s,y}(x+\Delta x, y+\Delta y)}{\Delta y}\Big)\end{aligned}$$

where the subscripts denote the direction of transport, the values in parentheses designate the grid point, and Δx and Δy represent the grid spacing between points in the $x-$ and $y-$ directions, respectively (Figure 2.6). The resultant transport rate is a small value reflecting the small difference between relatively large numbers. Considering the uncertainties in the component models and data inputs, the error would have to be expected to be large. The flux should be integrated over only relatively small time periods–a shelf storm, for example– and the prediction should be interpreted as classifying the region as erosive, depositional or steady-state and suggesting order of magnitude of transport rate. A more precise interpretation of the net transport predictions would be spurious.

3.4.1 Bedload Calculation

Bedload is not expected to be a significant portion of the total load in the wave-dominated shelf conditions on which this study focuses except in cases where transport is relatively small, and GMG does not consider this transport element. Since many of the world's continental shelves are sand-covered, however (Emery, 1968), there is a significant number of shelves where bedload makes up a large percentage of the transport under most conditions.

For this reason, a method of estimating the relative importance of bedload to the quantity and direction of transport is developed here, using a semi-empirical bedload formula. While the order of magnitude and direction of transport calculated using this method are reasonable, they should be considered only rough estimates for purposes of characterization of transport regimes. The focus of this study is near-bottom suspended transport.

Empirical bedload formulations often base their predictions on estimates of the skin friction component of boundary shear stress, raised to some power. The Meyer-Peter and Müller (1948) formulation, an empirical formula based on an extensive set of laboratory experiments in steady flow, raises the excess shear stress to the $\frac{3}{2}$ power:

$$\frac{q_{s,bed}}{d\sqrt{(s-1)gd}} = 8(\psi' - \psi_c)^{\frac{3}{2}} \tag{3.59}$$

where $q_{s,bed}$ is bedload transport in $cm^3/cm/sec$ and the prime indicates that the Shields parameter is calculated using the skin friction component of the boundary shear stress. To apply this or any other bedload formula, which is formulated for steady, unidirectional flow, to the combined wave-current flow, we assume that the response time for the sediment is small relative to the unsteady time scale (as demonstrated in Madsen and Grant, 1976) .

For this study, a modified version of the Meyer-Peter and Müller bedload for-

mula (Equation 3.59) is used. For ease in calculation, it is assumed that if the maximum skin friction-based Shields Parameter (ψ'_m) is less than the critical value for initiation of motion, then there is no bedload transport. However, if the maximum is greater than the critical we make the conservative assumption that transport occurs throughout the wave cycle, in proportion to the instantaneous bottom boundary shear stress. This method is conservative in that it will tend to overpredict the bedload transport.

The instantaneous bedload transport is thus calculated from :

$$\frac{q_{s,bed}}{d\sqrt{(s-1)gd}} = 8\psi'^{\frac{3}{2}} \tag{3.60}$$

where ψ' (Equation 2.7)is proportional to the skin friction component of the instantaneous shear stress τ'_0, which is calculated as in Equation 3.15:

$$\vec{\tau'_0} = \frac{1}{2}\rho f'_{cw}|\vec{u}|\vec{u}$$

where f'_{cw} is the skin friction component of the wave-current friction factor and $\vec{u}$ is the instantaneous wave plus current velocity in the wave boundary layer, which varies over the wave period. To estimate the time-averaged bedload transport, the velocity terms are raised to the $\frac{3}{2}$ power and time-averaged over a wave period. The x- and y-components of the instantaneous velocity are defined:

$$\begin{aligned} u &= u_b \cos\omega t + u_a \cos\phi_c \\ v &= u_a \sin\phi_c \end{aligned}$$

where ϕ_c is the angle between the wave (which is defined as the x-direction) and the current, and $\cos\omega t$ defines the phase of the wave.

Inserting these definitions into the shear stress equation raised to the $\frac{3}{2}$ power gives:

$$
\begin{aligned}
(\tau'_{0,x})^{\frac{3}{2}} &= (\frac{1}{2}\rho f_{cw,sf})^{\frac{3}{2}} u_b^3 \times \\
&\quad [\cos^3 \omega t + 3\frac{u_a}{u_b}\cos^2 \omega t \cos\phi_c + (\frac{u_a}{u_b})^2 \cos\omega t + 2(\frac{u_a}{u_b})^2 \cos\omega t \cos^2\phi_c + (\frac{u_a}{u_b})^3 \cos\phi_c] \\
(\tau'_{0,y})^{\frac{3}{2}} &= (\frac{1}{2}\rho f_{cw,sf})^{\frac{3}{2}} u_b^3 [\frac{u_a}{u_b}\cos^2 \omega t \sin\phi_c + 2(\frac{u_a}{u_b})^2 \cos\omega t \cos\phi_c \sin\phi_c + (\frac{u_a}{u_b})^3 \sin\phi_c]
\end{aligned}
$$

where $\tau'_{0,x}$ and $\tau'_{0,y}$ are the x- and y-components respectively of boundary shear stress.

Time-averaging these values over the wave period gives values of:

$$
\begin{aligned}
\langle \tau'^{\frac{3}{2}}_{0,x} \rangle &= (\frac{1}{2}\rho f'_{cw})^{\frac{3}{2}} u_b^3 (\frac{3}{2}\frac{u_a}{u_b} + (\frac{u_a}{u_b})^3) \cos\phi_c \\
\langle \tau'^{\frac{3}{2}}_{0,y} \rangle &= (\frac{1}{2}\rho f'_{cw})^{\frac{3}{2}} u_b^3 (\frac{1}{2}\frac{u_a}{u_b} + (\frac{u_a}{u_b})^3) \sin\phi_c
\end{aligned}
$$

where the brackets indicate time-averaged quantities. From these expressions the magnitude of the bedload transport can be calculated using Equation 3.60 and the direction can be determined:

$$\theta_{bed} = \arctan \frac{\langle \tau'^{\frac{3}{2}}_{0,y} \rangle}{\langle \tau'^{\frac{3}{2}}_{0,x} \rangle} \tag{3.61}$$

where θ_{bed} is the angle between the direction of the mean bedload transport and the wave direction.

Chapter 4

Model Background: Calculation Method

The interconnections of these disparate elements, and the generation of the results, can be illustrated best by using a step-by-step examination of how the boundary layer model works. The programs used in the application of the model were developed by Scott Glenn (1983), and modified slightly for the present work. The near-bottom model Fortran code can be found in Grant and Glenn (1983c). The computational procedure, as discussed in the preceding sections and applied here, is traced in Figure 4.1. Each line in the flow chart is labelled, and those labels are referred to in this discussion.

There are three inputs (Line 1) to the model at each point: (1) current velocity (u_r) at some height within the current boundary layer and above the wave boundary layer, (2) wave conditions, consisting of maximum wave bottom velocity (u_b) and wave excursion amplitude (A_b) (or, equivalently, wave height (H) and period (T) and water depth (h)), and (3) sediment size (d), density (ρ_s) and texture. For simplicity, co-directional wave and current and a single grain size bed are assumed in this discussion. The example presented is a moderate storm wave, with a 26 cm/sec current measured one meter above a bottom composed of coarse silt (Table 4.1).

The first step in the model is to estimate the contribution of the current to boundary shear stress on the bottom (Line 2a). This is represented as $\frac{u_a}{u_b}$, where

Input parameters for sample model run			
u_b	40 $\frac{cm}{sec}$	A_b	96 cm.
H	2.6 meter	T	15 seconds
h	50 meters	γ_0	0.002
u_r	26 $\frac{cm}{sec}$	z_r	1.0 meter
d	0.006 cm.	ρ_s	2.65 $\frac{gm}{cm^3}$

Table 4.1: Input parameters for sample model run discussed in text

u_a represents the mean velocity at some unspecified height within the wave boundary layer. The parameters α and V_2, used to calculate the shear velocities in Equations 3.22 and 3.23, are direct functions of $\frac{u_a}{u_b}$. The model's initial estimate is $\frac{u_a}{u_b} = \frac{u_r}{u_b}$.

This shear stress estimate is used with the grain roughness (d) to calculate the skin friction component of the friction factor (f'_{cw}; Line 2b; Equation B.1). This friction factor is necessary to test for initiation of sediment motion. It is used with Equation 3.22 to calculate the skin friction component of the maximum bottom shear stress $\tau'_{0,cw}$ and, from that, the maximum Shields parameter for the flow (Equation 2.7). If the Shields parameter is less than the critical value for the sediment on the seafloor, no sediment moves (Lines 2c- 2e). In that case, the skin friction shear stress is the same as the total shear stress, unless some roughness element representing pre-existing bedforms has been included as input. For now, we use only the movable bed roughness estimates.

If sediment is moving, then, the boundary roughness due to ripples and sediment transport is calculated according to Equation 3.57, and that roughness is used in Equation B.1 to calculate the total friction factor f_{cw} (Line 2f). The total f_{cw} is used to calculate the mean and maximum shear velocities (Equations 3.22 and 3.23; Line 2g). From these, the first estimate of the predicted reference velocity

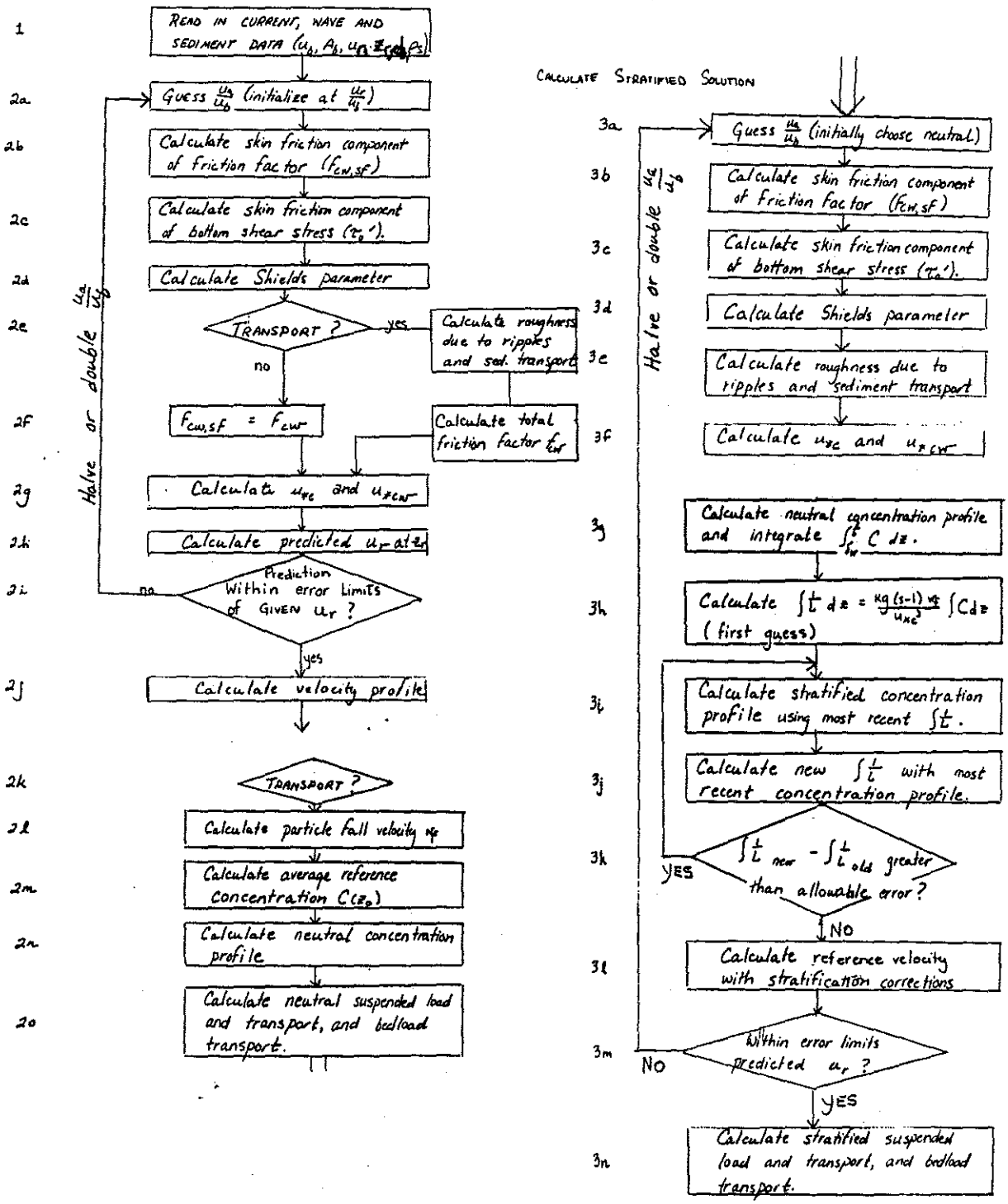

Figure 4.1: Flow chart tracing computational procedure for boundary layer model. Labels are referred to in text

is calculated using Equation 3.29 (Line 2h). If the predicted velocity is not within one per cent of the given reference velocity (as it certainly will not be on the initial try), the model chooses another value of $\frac{u_a}{u_b}$, and proceeds again through the steps just described.

If the predicted value was too high, the value of $\frac{u_a}{u_b}$ is halved; if too low, the parameter is multiplied by a factor of 2.05 (this factor is chosen rather than 2.0 to avoid a halving-doubling flip-flop in iterations). Iterations continue until the predicted and given currents match within one per cent. At that point,the neutral velocity profile is calculated using Equation 3.29 (Line 2j).

If sediment was put in motion, the sediment concentration profile is calculated, first without including stratification corrections to either velocity or concentration profiles. The particle fall velocity is determined from Equation 2.9 and the sediment reference concentration is determined from Equation 3.46. These are used in Equations 3.35 and 3.36 to calculate the sediment concentration profile (Line 2n).

Finally, the velocity and concentration profiles are integrated to determine the neutral load and transport predictions (Equations 3.2 and 3.3). The estimated bedload is calculated using Equation 3.60. The estimated outer Ekman layer load and transport are calculated from Equation 3.51.

The neutral results for the wave case described above are shown in Table 4.2. Note that the value of u_a drops by a factor of three from the first estimate. Most of the roughness is generated by ripples (compare $z_{0,rip}$ vs. $z_{0,s.t.}$), and the additional roughness beyond the grain diameter increases the friction factor significantly (compare f'_{cw} vs. f_{cw}). The wave-current shear velocity is more than twice the current shear velocity. The predicted bedload transport is insignificant compared with the suspended transport. The outer Ekman layer load and transport, however, are estimated at more than three and a half times the near-bottom load and transport for this coarse silt, suggesting that in some cases, at least, more attention must be

Neutral results for sample model run			
$\frac{u_a}{u_b}$	.203	f'_{cw}	4.745×10^{-3}
ψ'_m	0.5657	f_{cw}	2.907×10^{-2}
z_0	8.837×10^{-2}cm	ψ_c	0.1226
$z_{0,c}$	1.432 cm	$z_{0,s.t.}$	2.591×10^{-2}cm
u_{*cw}	5.802 cm/sec	$z_{0,rip}$	6.226×10^{-2} cm
u_{*c}	2.46 cm/sec	δ_w	11.13 cm
N.B. susp. load	$0.6294 \frac{cm^3}{cm^2}$	$\frac{\delta_a}{6}$	16.41 m
O.E. susp. load	$2.027 \frac{cm^3}{cm^2}$	bedl. trans.	$.0114 \frac{cm^3}{cm}/sec$
N.B. susp. trans.	$22.65 \frac{cm^3}{cm}/sec$	O.E. susp. trans.	$87.82 \frac{cm^3}{cm}/sec$

Table 4.2: Some results for neutral, near-bottom model run for a moderate storm wave on the continental shelf, as described in text. N.B. refers to near-bottom load and transport ($z < \frac{\delta_a}{6}$). O.E. refers to the outer Ekman layer load and transport ($z > \frac{\delta_a}{6}$). Input parameters are shown in Table 4.1.

paid to the outer Ekman layer transport. More attention is devoted to this question in the sensitivity analysis. The predicted neutral velocity and concentration profiles are shown in Figure 4.2 (a) and (b).

The stratified calculation begins, as does the neutral one, with an estimate of $\frac{u_a}{u_b}$. Initially, the value that produced the neutral case solution is used. This results in a prediction of reference velocity which is too high, since stratification increases velocities above the wave boundary layer. The same steps as for the neutral case are followed through calculation of the shear velocities at Line 3f in the flow diagram (Figure 4.1). At this stage, the calculation of the stratification-corrected concentration profile begins.

First, the concentration profile without the stratification correction is calculated, as for the neutral case. That profile is integrated and used in Equation 3.39 to procure an initial estimate for the integrated Monin-Obukov Length ($\int \frac{1}{L} dz$; Lines 3g and 3h). This value is used to calculate a stratification-corrected concentration profile (Equation 3.45), which is then integrated to generate a revised

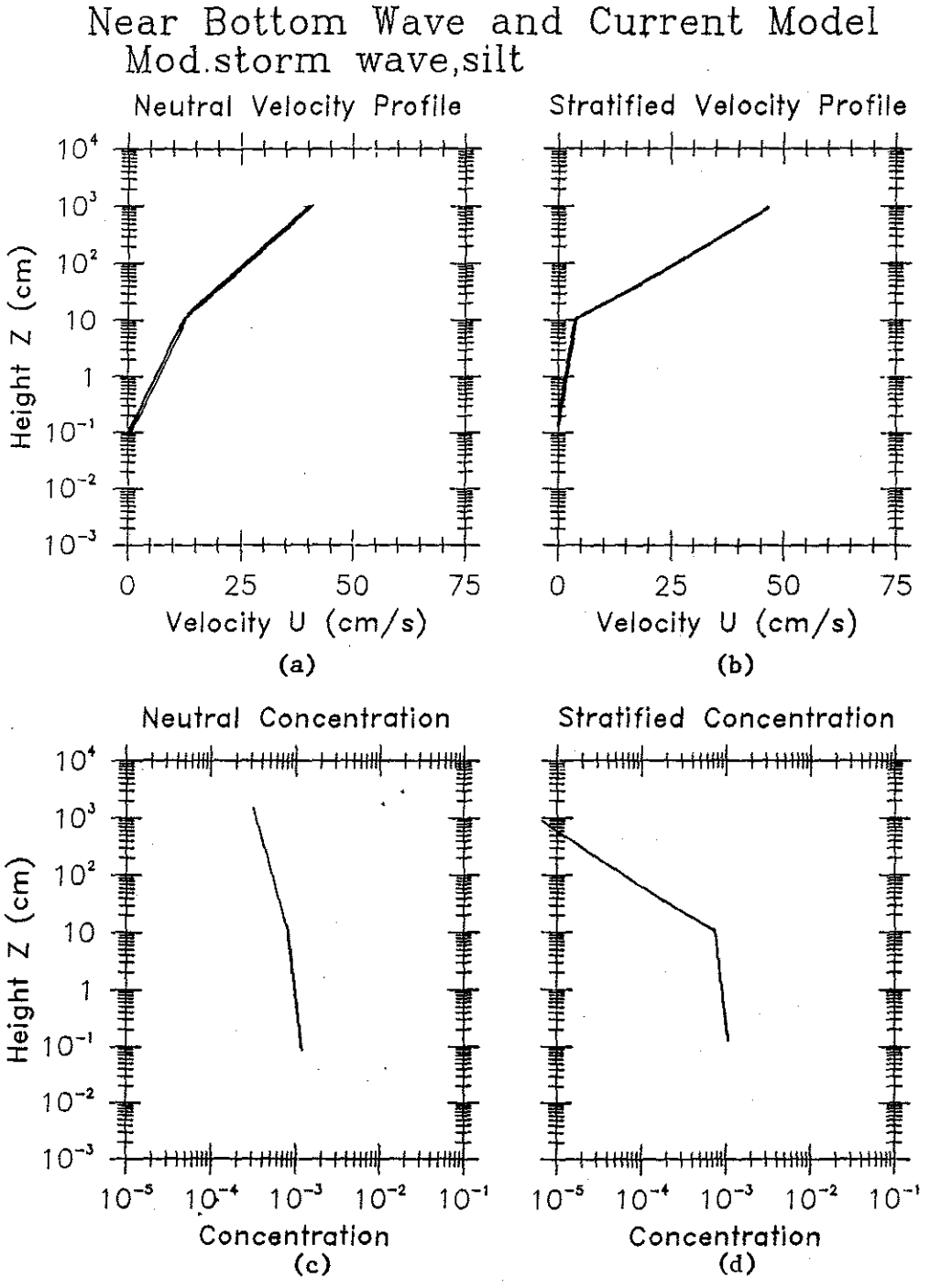

Figure 4.2: Predicted neutral and stratified velocity and concentration profiles for a moderate storm wave with a reference current at one meter above the bottom of 26 cm/sec. The velocity and concentration profiles extend only to the top of the near-bottom layer, $\frac{\delta_a}{6}$

estimate of the integrated Monin-Obukov Length (Lines 3i-3j). If the difference between the old and new integrated values of L is greater than the allowable error, the new value is used to calculate another revised concentration profile. These iterations (Lines 3i-3k) continue until the integrated Monin-Obukov Length values converge.

Once the concentration profile is determined for this $\frac{u_a}{u_b}$ value, the new reference velocity prediction including stratification effects can be calculated using Equation 3.44. As in the neutral case, if the predicted and given values are outside acceptable error limits (which we take to be one per cent since the mean current is not measurable more precisely than this), iterations begin again with a new $\frac{u_a}{u_b}$ value, revised in the same manner described above for the neutral case (Figure 4.1, Lines 3a-3m). Once the velocity values converge, the final stratified velocity and concentration profiles and the transport and load predictions are calculated.

The stratified results for the wave case described above are shown in Table 4.3 and Figure 4.2 (c) and (d). The results differ markedly from the neutral case results shown in Table 4.2 and Figure 4.2 (a) and (b). The bottom line of Table 4.3 notes that the neutral case $\frac{u_a}{u_b}$ value gave a reference velocity prediction of 39 cm/sec. That is, stratification led to an increase in predicted velocity at one meter above the seafloor of about 50 %. The sharp drop in concentration and increase in velocity above the wave boundary layer can be seen by comparing the neutral and stratified profiles in Figure 4.2.

The largest changes from the neutral case result from the reduced current shear velocity: u_{*c} is approximately one-half the neutral value. For this reason, $\frac{\delta_e}{6}$ drops to 9.4 m in the stratified case from 16.4 m, and the near-bottom suspended load and transport estimates drop by an order of magnitude or more. Even more notable, the estimates of outer Ekman layer load and transport drop by two or more orders of magnitude, so that the near-bottom load and transport volumes are about three

Stratified results for sample model run			
$\frac{u_a}{u_b}$	0.054	f'_{cw}	4.86×10^{-3}
ψ'_m	0.445	f_{cw}	3.66×10^{-2}
z_0	0.132 cm	ψ_c	0.1226
$z_{0,c}$	3.646 cm	$z_{0,s.t.}$	1.794×10^{-2}cm
u_{*cw}	5.702 cm/sec	$z_{0,rip}$	1.135×10^{-1} cm
u_{*c}	1.418 cm/sec	δ_w	10.95 cm
N.B. susp. load	$3.73 \times 10^{-2} \frac{cm^3}{cm^2}$	$\frac{\delta_a}{6}$	9.45 m
O.E. susp. load	$5.8 \times 10^{-3} \frac{cm^3}{cm^2}$	bedl. trans.	$3.07 \times 10^{-3} \frac{cm^3}{cm}/sec$
N.B. susp. trans.	$0.746 \frac{cm^3}{cm}/sec$	O.E. susp. trans.	$0.2714 \frac{cm^3}{cm}/sec$
Predicted u_r, with $\frac{u_a}{u_b} = 0.203$:			39.0 cm/sec

Table 4.3: Some results for stratified near-bottom model run for a moderate storm wave, strong current, and a silt bed on the continental shelf. Predicted velocity on bottom line is the result for the neutral current shear stress. N.B. refers to near-bottom load and transport ($z < \frac{\delta_a}{6}$). O.E. refers to the outer Ekman layer load and transport ($z > \frac{\delta_a}{6}$). Input parameters are shown in Table 4.1.

to six times larger than those in the outer Ekman layer.

Parameters which reflect only wave boundary layer conditions change much less. The wave-current shear velocity u_{*cw} and wave boundary layer height δ_w are essentially the same. The roughness prediction rises by 67 % in the suspended stratified case because the ripples are left intact by the smaller shear stress, even though the sediment transport roughness ($k_{b,T}$) drops by 30 %. Bedload transport drops by only 25 %, but is still insignificant compared with suspended transport.

Chapter 5

Sensitivity Analysis

The sediment transport and load predictions made by the boundary layer model depend on a broad array of parameters and assumptions (Table 5.1). As described in the Introduction and Background Sections, the influence of each parameter on sediment transport is related in a complex way to the others, so that the effects of changing a parameter are not readily predictable. For example, a decrease in grain size under constant wave and current conditions might suggest that the volume of sediment load would go up. However, the grain size is strongly related to the stratification correction and to roughness (z_0), not so much because the grain roughness $k_{b,n}$ is important, but because grain size governs ripple dimensions and sediment transport layer roughness ($k_{b,B}$ and $k_{b,T}$). If conditions are such that roughness decreases and stratification increases, the effect of decreasing grain size could be only a very small increase, or even a decrease, in total load and transport.

The purpose of this chapter is to establish the relative significance of the various parameters in the model's predictions of load and transport. This serves three useful purposes. First, the examples provide physical intuition on the roles of parameters and their interactions. Second, this analysis demonstrates strengths and weaknesses of the theoretical model: it identifies circumstances where the model's results are physically reasonable, but also defines conditions where field and lab-

Model parameters describing physical environment

H	wave height
T	wave period
h	water depth
u_r	reference current velocity at 100 cm off bottom
d_n	grain size(s)
k_b	physical boundary roughness $= z_0 \times 30$
$k_{b,B}$	part of boundary roughness due to ripples
η, λ	ripple height and wavelength
δ_w	wave boundary layer thickness
ϕ_c	angle between waves and current

Empirical parameters

γ_0	sediment reference concentration parameter
β, γ	stratification parameters

Implicit assumptions in theory and/or model formulation

Effects of stratification on velocity and concentration profiles can be modeled by revising the eddy viscosity to $\frac{\nu_t}{\gamma+\beta\frac{z}{L}}$.

The wave spectrum can be represented by a single wave height and frequency, such as the frequency of the spectral peak.

Grain distribution can be represented by 1 or 2 modal grain sizes.

Effects of armoring can be modeled so that there is equilibrium between calculated load and bottom concentrations.

Parameters vary slowly enough in time and space so that there is steady state in the vertical concentration and velocity profiles.

Table 5.1: Parameters and assumptions in the boundary layer model

oratory experiments are needed to constrain the model's predictions. Third, it provides initial estimates of the relative volumes of sediment transport in different circumstances, thus discriminating between the importance of storms versus everyday regional currents in transporting sediments.

The organization of this section reflects the focus of this study on the influence of waves on sediment dynamics. As far as sediment response is concerned, the general climate is set by the waves, and so the sediment transport results are presented by wave condition. The variation of transport and load due to other factors is discussed within the context of a particular set of wave parameters.

In the first subsection the depth limit of wave influence, as imposed by wave period, is discussed. Each of three subsequent subsections treats a single wave condition (represented by bottom velocity u_b and excursion amplitude A_b) representative of a general physical climate. The first of these examines the effect of moderate storm waves on transport. It is used as a case study of the effects of stratification on load and transport, and contains detailed explanations for the observed changes due to stratification. Results for the other five wave conditions are discussed in the final section, primarily in contrast with the three that are examined in detail. Within each subsection, the effects of variation of several of the environmental parameters listed in Table 5.1 are described.

5.1 Maximum Depth of Wave Influence

"Wave base", or the maximum depth at which waves affect the bottom, is often described as one-half the deepwater wavelength (Λ). This depth is derived from the dispersion relationship of linear wave theory, which relates wave period (T), water depth (h), and wavelength (see, e.g., LeBlond and Mysak, 1978):

$$\omega^2 = gk \tanh kh \tag{5.1}$$

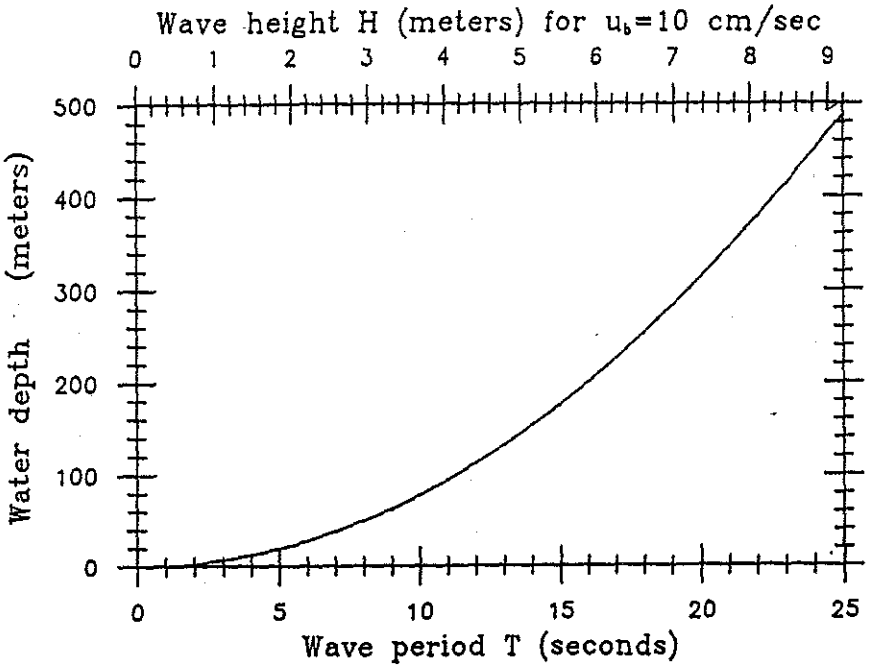

Figure 5.1: The approximate maximum depth of influence of waves, calculated as one-half Λ. Top axis shows wave height required to generate a 10 cm/sec maximum wave velocity at that depth

In this equation, $\omega = \frac{2\pi}{T}$ is wave frequency, g is gravity, and $k = \frac{2\pi}{\Lambda}$ is the wavenumber. For short waves or deep water ($kh \gg 1$), the hyperbolic tangent approaches unity. The wavelength in deep water can, therefore, be calculated directly from the wave period, as the dispersion relationship reduces to:

$$\Lambda = \frac{g}{2\pi} T^2 \tag{5.2}$$

This formula is accurate within one per cent for $h/L > \frac{1}{2}$; shallower than this, water depth becomes significant in calculating Λ. This 'wave base' (Figure 5.1) can be used in conjunction with the formula for calculating wave bottom velocities (Equation 3.24) to establish a rough criterion for maximum depth of influence for waves.

The significance of the wave for sediment transport is dependent on the maximum wave bottom velocity, u_b. The maximum wave bottom velocity at the depth

$h = \frac{\Lambda}{2}$ (Figure 5.1) is calculated, using Equation 3.24,

$$u_b = \frac{H}{T} \frac{\pi}{\sinh \frac{2\pi}{\Lambda} \frac{\Lambda}{2}} = .27 \frac{H}{T}$$

To sustain a particular bottom velocity at a depth of $\frac{1}{2}\Lambda$, therefore, wave height must increase linearly with period. The wave height necessary to generate a velocity of 10 cm/sec is plotted on the top axis of Figure 5.1. (A 5 cm/sec velocity would require waves one-half as high; 20 cm/sec would require waves twice as high, etc.) Using this graph, one can quickly determine whether a particular wave would significantly affect the seafloor at a particular depth. For example, for a wave to generate a bottom velocity of 10 cm/sec at a depth of one hundred meters, it must be at least 4.2 meters high and have a period of eleven and one half seconds. Deeper water would require higher and longer waves. This constraint is of particular importance on the central and outer continental shelf, where only swell and very large storm waves would affect the bottom.

5.2 Sensitivity Test Conditions

Wave conditions

The boundary layer model was run for 8 different wave conditions (Table 5.2) to represent a broad range of wave conditions that might affect sediment transport on the continental shelf. The primary consideration was to test a range of wave bottom velocities. The lowest velocity chosen was $20\frac{cm}{sec}$, because lower velocities set little or no sediment in motion. Wave bottom velocities were increased by $20\frac{cm}{sec}$ steps, and at least two wave periods were used for each bottom velocity in order to demonstrate the effect of period on sediment transport predictions. One case is presented for $u_b = 100\frac{cm}{sec}$, to demonstrate the results under extreme wave conditions. Wave periods from 10 to 20 seconds were used in order to encompass

Wave Climates Tested				
Waves	$u_b \frac{cm}{sec}$	$A_b(cm)$	$T(sec)$	H(in m,if $h = 50m$)
Moderate windsea	20	32	10	2.5
Low swell	20	64	20	1.1
Large storm, early	40	64	10	5.0
Moderate storm, late	40	96	15	2.6
Moderate swell	40	128	20	2.2
Large storm, late	60	144	15	3.9
Large swell	60	191	20	3.3
Extreme swell	100	319	20	5.4

Grain sizes tested		
	$d(cm)$	$w_f(\frac{cm}{sec})$
Fine sand	.0200	1.965
Very fine sand	.0100	0.950
Coarse silt	.0060	0.250
Medium silt	.0025	0.043

γ_0 *values tested*					
0.0005	0.001	0.002	0.003	0.004	0.005

Table 5.2: Variation of parameters in sensitivity analysis

the range of waves affecting most shelf depths.

Each wave bottom velocity and period condition is given a qualitative label, to reflect an example of the surface wave conditions which could impose the bottom parameters (Table 5.2). These labels, from moderate windsea and low swell to extreme swell conditions, do not signify the only surface conditions applicable to the bottom wave conditions they describe. Both stratified and neutral predictions are made for every input condition.

Sediment grain sizes

For each wave condition, the model was run using 4 sediment grain size classes ranging from fine sand to medium silt (Table 5.2). These represent grain sizes typically found on continental shelves. They also cover a size range that is susceptible to suspended transport, but not subject to cohesive forces, where cohesion is defined as the electrochemical binding forces by grains less than 10^{-3}cm (McCave, 1984) which can bind sediments into a plastic mass. However, biologically-produced mucous can cause sediments to stick together, increasing the initiation of motion criterion and fall velocity. Both biological and electrochemical adhesion become increasingly effective and increasingly common as the mean grain size of the seabed decreases. For these reasons, no sediments smaller than medium silt ($d = 2.5 \times 10^{-3} cm$) are included in the sensitivity analysis, since factors not considered in this model are so important in determining such fundamental properties as fall velocity and initiation of motion for smaller grains (McCave, 1984).

Although sands and medium silts, especially the latter, are not completely immune to adhesive forces, it is assumed in this study that binding effects are limited to an increase in the critical Shields parameter for the initiation of motion, which directly affects only the sediment reference concentration (Equation 3.46). The same effect on load and transport predictions is thus achieved by varying the sediment reference concentration parameter γ_0.

Reference concentration parameter

Sediment load and transport depend not only on grain size but also on how much sediment is mobilized by the bottom shear stress, expressed in this work as a reference concentration, $C(z_0)$ (Equation 3.35). The reference concentration is directly dependent on the empirical parameter γ_0(Equation 3.46). Estimated values

for γ_0 range from $5 \times 10^{-4}$to 4×10^{-3} (Glenn, 1983; Wiberg and Smith, 1983). To gauge the effect of varying the reference concentration boundary condition, the model was run using six values of γ_0, representing an order of magnitude variation for each grain size (Table 5.2). This variation in γ_0 also reflects the uncertainty in all parameters involved in calculating the concentration at the top of the wave boundary layer, including initiation of motion criteria (ψ_c), exact values of the skin friction component of boundary shear stress (τ_0' and, therefore, ψ'), and the height of the wave boundary layer.

Current velocities

Finally, for each wave condition, for each grain size, and for each reference concentration, sediment transport and load were calculated for a range of current shear stress values. This variation is expressed as a reference velocity calculated at one meter above the seafloor, and ranges from a few centimeters per second to 30-100 cm/sec for each grain size and wave condition. The reason for the variation in reference velocity range from case to case is that the velocity is an intermediate result of the model; the results reflect variation in bottom shear stress, which is translated into a velocity prediction, as discussed below.

Presentation of results: format

In the interest of brevity, full discussions of the results are presented for only three of the wave conditions investigated; the other cases are discussed more generally in relation to those three. The three wave conditions detailed are listed in Table 5.2 as low swell, moderate storm, and large swell. For each of those three cases, a set of 16 plots is presented that demonstrates the effects of stratification on predicted load and transport, and of the variation of grain sizes, reference concentration, and current velocity on both neutral and stratified load and transport .

The contour plots that serve as the fundamental illustrations for these sections embrace a great deal of information; unfortunately, they are not readily interpreted. A detailed explanation of the format is presented here, referring to Figures 5.2-5.5 as examples. Each figure shows results of model runs for moderate storm wave conditions ($u_b = 40\frac{cm}{sec}, A_b = 96\ cm$), where the seabed is covered with sediment of a single grain size. Each figure consists of four contour plots showing variation in predicted near-bottom load or transport for that grain size by that wave, including or neglecting the effects of sediment stratification as labeled. The load and transport volumes are calculated by integrating the predicted concentration and velocity profiles (Equations 3.2 and 3.3) to a height $\delta_c/6$ equal to one-sixth the Ekman depth (Section 3.2.4). Bedload transport and outer Ekman layer load and transport are not included in these graphs. Note that the use of 'near-bottom' here conforms with its use in GMG as the lowest few meters of the water column.

Each 'x' represents a load or transport value calculated by the model. These are the data points on which the contours are based. The locations of the points with respect to the x-axis show the value of the concentration at the top of the wave boundary layer ($C(\delta_w)$) for the given set of wave, current, and sediment conditions.

The variation in load and transport predictions within each plot results from changing two of the model's parameters: the sediment concentration parameter (γ_0) and the current contribution to the boundary shear stress within the wave boundary layer (u_a). Rather than use these parameters as the axes of the plots, however, I have chosen to use physically significant intermediate results of the model's calculations that, under most circumstances, are uniquely determined by the parameters being varied (that is, γ_0 and u_a). The x-axis ($C(\delta_w)$) represents a potentially measurable quantity. The y-axis is the current velocity at one meter above the bottom, u_r, non-dimensionalized by the maximum wave bottom velocity u_b. The reference current is a physical parameter used to specify the problem, and

is used as the matching condition for the model iterations. That is, the velocity calculated by the model, based on its guess of the bottom shear stress and stratification effects, is matched against the specified velocity to determine the end of calculations (see Chapter 7). Its variation with respect to input parameters is therefore important, and circumstances where it is not uniquely determined by the model require an additional boundary condition, as discussed below.

$C(\delta_w)$ represents the sediment available at the top of the wave boundary layer for transport by the current (Equation 3.35). It is chosen rather than γ_0 as the x-variable for a number of reasons. First, it is linearly related to γ_0, so that the order-of magnitude change in γ_0 results in a similar variation in $C(\delta_w)$. Unlike γ_0, however, $C(\delta_w)$ is a measurable physical quantity, so that it provides insight into the predicted conditions near the boundary, and can be judged as realistic or unrealistic on physical grounds. Second, $C(\delta_w)$ is also related directly to the seabed concentration of the sediment, C_{bed}, and the excess bottom shear stress S (Equations 3.35 and 3.46). Although the figures in this section were produced by varying γ_0, they could just as well result from varying the critical boundary shear stress, the skin friction component of shear stress, or the bed concentration. Using $C(\delta_w)$ as the x-axis variable, therefore, shows the sensitivity of load and transport predictions to four variables that are subject to uncertainty, rather than one. Third, the magnitude of $C(\delta_w)$ indicates the degree of sediment response to shear stress in the wave boundary layer. Compare the ranges of the x-axes in Figures 5.2 and 5.4, for example. For the same wave and current conditions, the concentration of the finer sediment (Figure 5.4) at the top of the wave boundary layer is as much as twice that of the coarser sediment (Figure 5.2).

Because the velocities represented by the y-axis are calculated by the model (Equation 3.29 or 3.44), vertical range of the data points varies within a wave condition between neutral to stratified cases and between grain sizes. To make

comparison easier, the y-axis maximum is the same for all plots for a single wave condition, although the contours only extend as far as the limits of the 'data'. This is the reason for the frequent blank spots in the figures.

The predicted load values are easily translated to estimates of erosion depth, or reworking depth once the sediment settles back down after the transporting event, by dividing by the bed concentration (0.6 in this work). In Figure 5.2, for example, the load of 0.16 $\frac{cm^3}{cm^2}$ at the location circled on the plot would signify a reworking depth of 0.27 cm.

5.3 Results: Moderate Storm Waves

On some continental shelves, moderately large storms generate waves up to several meters in height, with periods of 15 seconds or more. The wave discussed in this section, with a maximum bottom velocity of 40 cm/sec and an excursion amplitude of 96 cm (denoting a 15 second period), would could occur in such a storm. In 50 meters water depth, a 2.6 meter wave height would be required to generate that velocity.

The four figures accompanying this section (Figures 5.2-5.5) are contour plots of sediment load and transport, with and without the effects of stratification by sediments in suspension. The neutral plots are primarily for reference: although one might be interested in velocity profiles for the neutral case, ignoring stratification by sediments is inconsistent in the calculation of a sediment profile. In some cases, however, sediment stratification effects are small, and the iteration needed to solve for the stratification effects produce immeasurably small changes in the concentration profile. In those cases the concentration profile above the wave boundary layer can be predicted without the stratification correction (Equation 3.36). The contrasts between the stratified and unstratified load and transport predictions

suggest the amount of error introduced by using the simpler procedure and can provide guidelines for conditions under which the neutral model is sufficient.

5.3.1 Neutral results

The results for the unstratified cases (Figures 5.2-5.5) are easily predictable from the neutral equations for the velocity profiles (Equations 3.28 and 3.29) and concentration profiles (Equations 3.35 and 3.36). These equations and the two for calculating load and transport (Equations 3.2 and 3.3) should be referred to in the discussion that follows.

In parts (a) and (c) of each figure, both the neutral sediment load and the neutral transport are seen to depend directly on the sediment reference concentration (the x-axis): doubling $C(\delta_w)$ leads to doubling of the load or transport for any velocity. This follows from the proportionality of the concentration profile to the concentration at the top of the wave boundary layer.

In the neutral case, a higher reference velocity always implies a higher current shear velocity u_{*c}. The shear velocity affects the sediment concentration profile in two ways: First, the concentration decays exponentially with $-\frac{w_f}{u_{*c}}$. Higher u_{*c} values generate smaller concentration gradients. Second, higher u_{*c} increases the height of the current boundary layer (δ_c; Equation 2.6). This increases the vertical distance over which load and transport are integrated ($\delta_c/6$). The slower decay of concentration with height and longer integration distance combine to increase the predicted values of load and transport. Transport predictions depend directly on the velocity profile also (Equation 3.3), so transport values rise more rapidly with increasing current velocity than load values do.

The similar concave curves of all of the neutral plots (Figures 5.2-5.5 (a) and (c)) illustrate the predictability of the response of neutral predictions to variations in current and reference concentration. In fact, the neutral load and transport plots

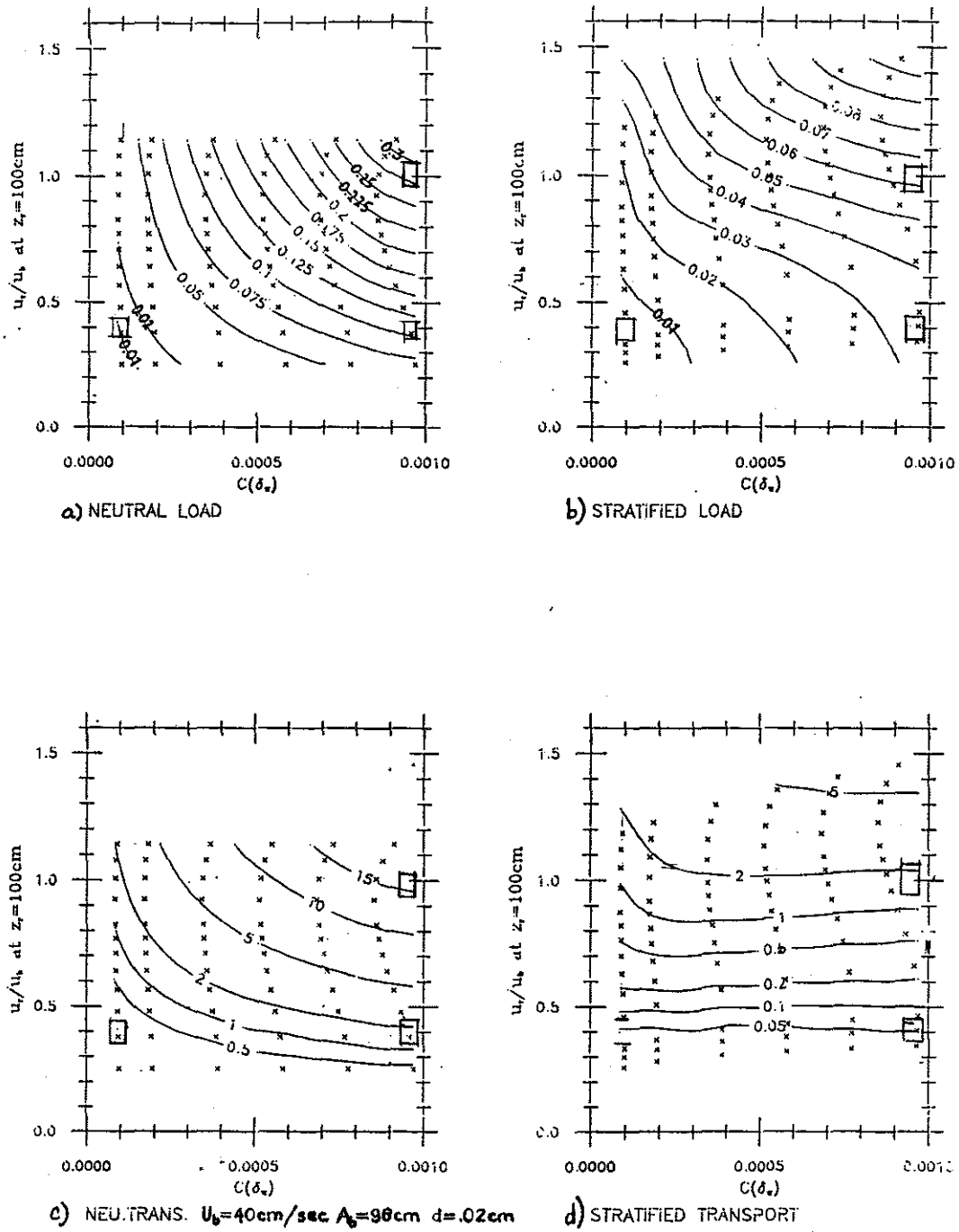

Figure 5.2: Predicted near-bottom load ($\frac{cm^3}{cm^2}$) and transport ($cm^3/cm/sec$) values for fine sand in moderate storm waves. T=15 sec, and the wave height in 50 m of water would be 2.6m. u_r is reference current velocity. δ_w ranges from 21-25 cm; $\frac{\delta_c}{\delta}$ ranges from 12 to 38 m.

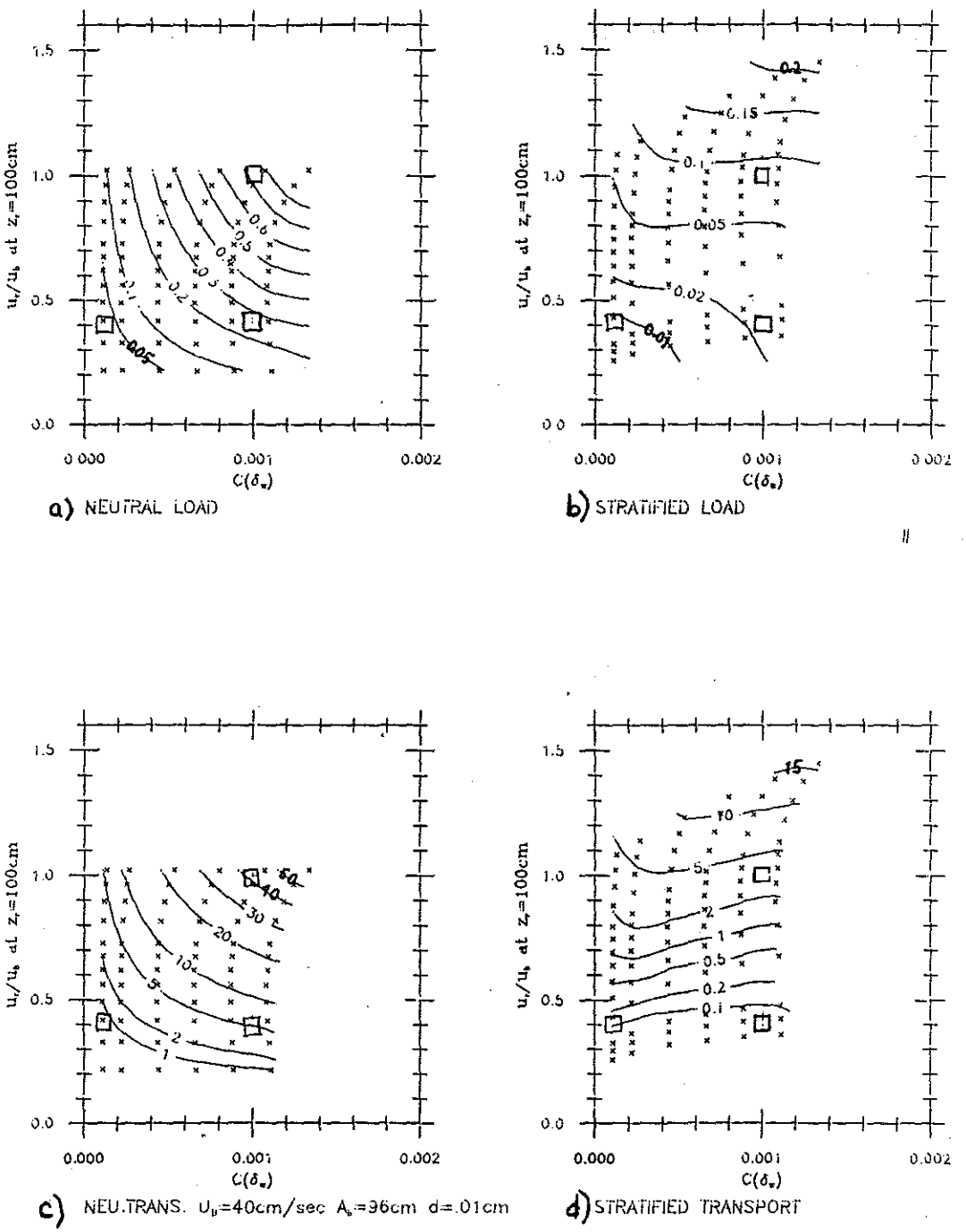

Figure 5.3: Predicted near-bottom load ($\frac{cm^3}{cm^2}$) and transport ($cm^3/cm/sec$) values for very fine sand in moderate storm waves. δ_w ranges from 15-16 cm; $\frac{\delta_c}{6}$ ranges from 8 to 27 m.

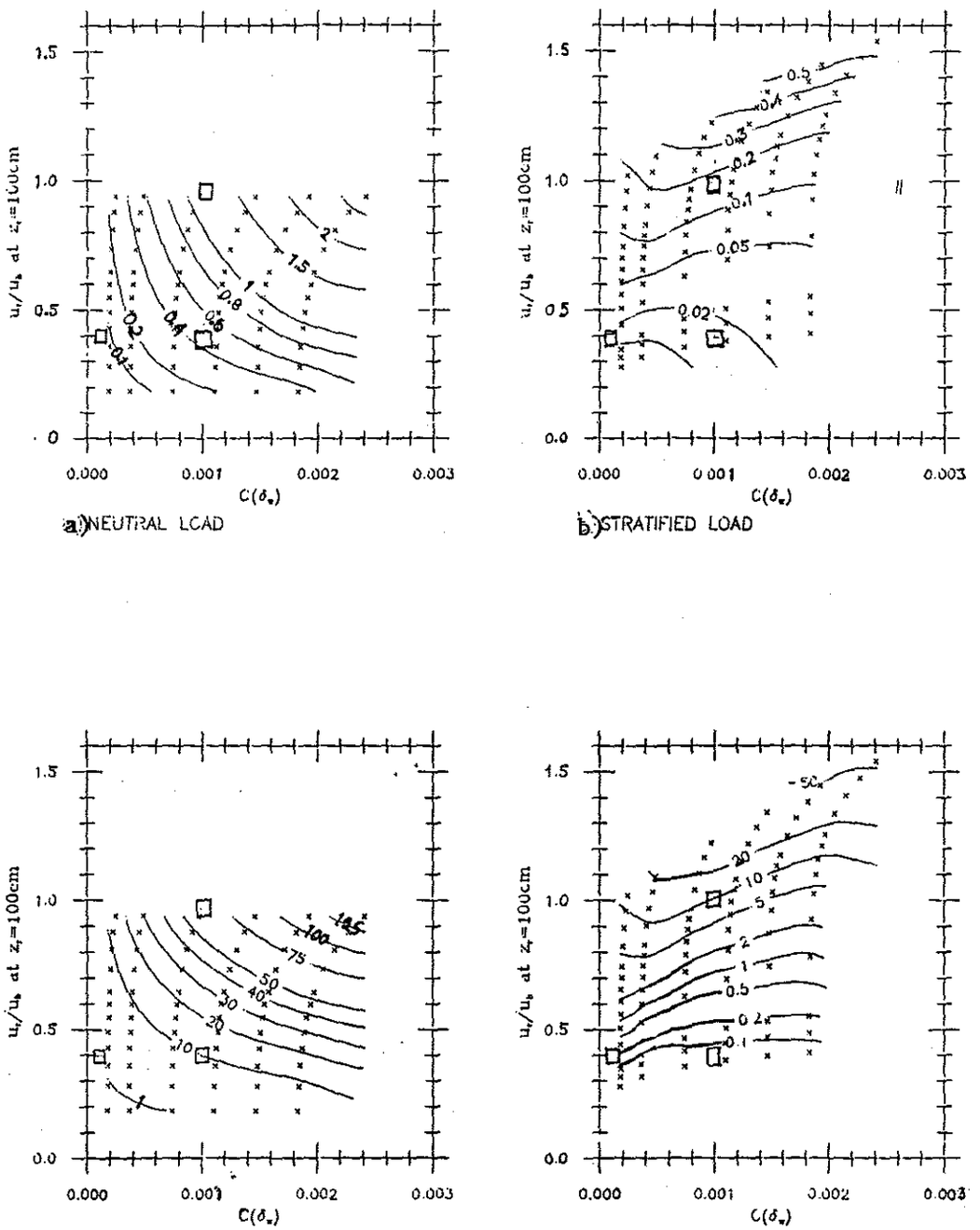

Figure 5.4: Predicted near-bottom load ($\frac{cm^3}{cm^2}$) and transport ($cm^3/cm/sec$) values for coarse silt in moderate storm waves. δ_w ranges from 11-12 cm; $\frac{\delta_a}{6}$ ranges from 5 to 21 m.

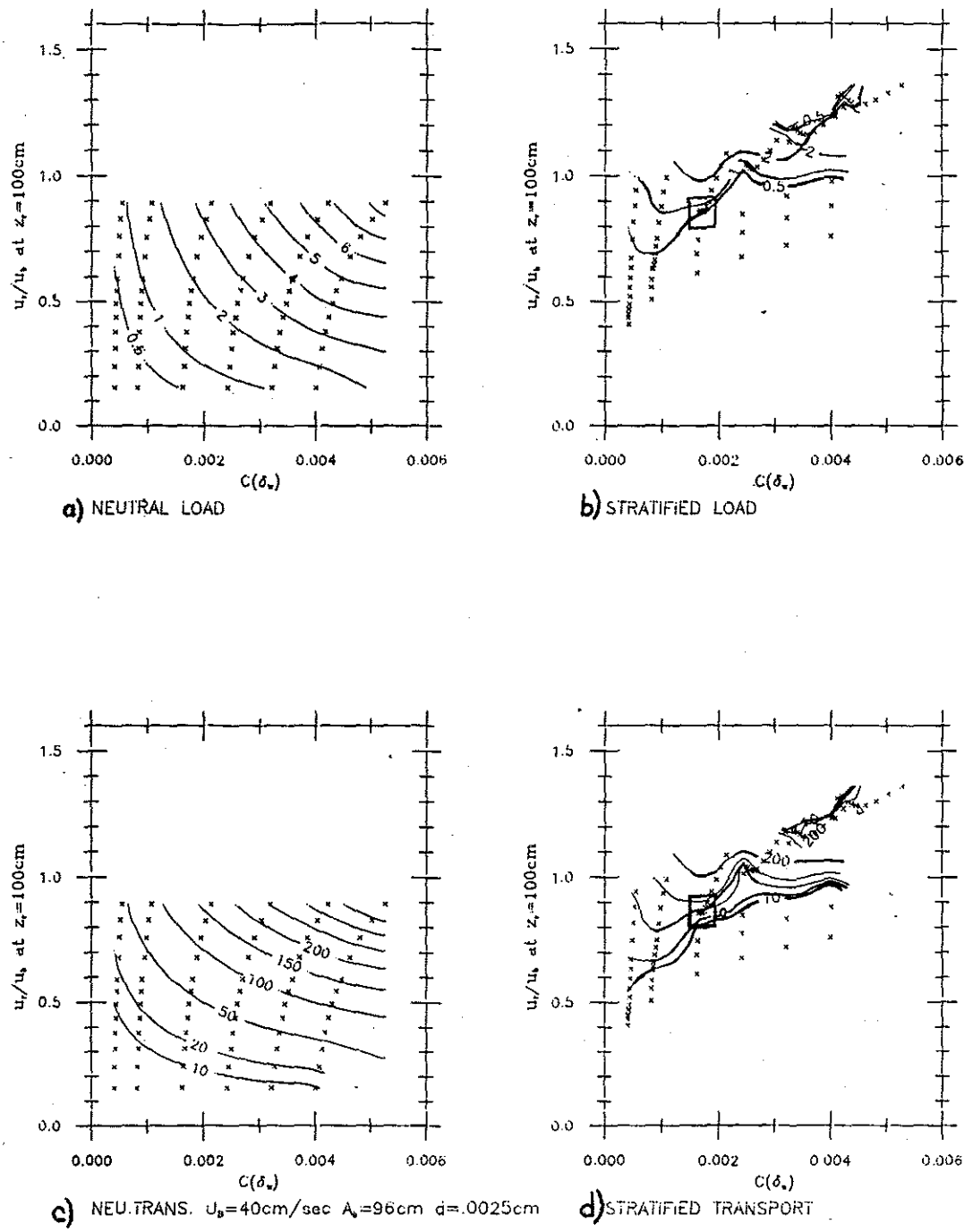

Figure 5.5: Predicted near-bottom load ($\frac{cm^3}{cm^2}$) and transport ($cm^3/cm/sec$) values for medium silt in moderate storm waves. The irregular contour patterns for the stratified plots occur in regions where the model gives non-unique solutions, as discussed in text. δ_w ranges from 8-10 cm; $\frac{\delta_a}{6}$ ranges from 4 to 18 m.

for all eight wave conditions tested share this pattern of response to increasing velocity and $C(\delta_w)$. The scale of the response (i.e. the values of the contours) is set by wave conditions and grain size. Because of this predictability, the neutral results are not examined in detail in the other discussions of results.

Bedload and outer Ekman Layer transport

In the neutral case for the moderate storm wave, bedload is generally insignificant, but transport in the outer Ekman layer is often very important. The contours in the plots of Figures 5.6-5.9 show the relative magnitudes of the bedload transport and outer Ekman layer transport, compared with the near-bottom transport. The format is the same as that of the load and transport contour plots, except that the velocities on the y-axes are dimensional. These plots are included only for the moderate storm wave case, in order to demonstrate typical patterns of variation. For other wave conditions, the results are discussed in the text, but plots are not included.

In the neutral case, bedload under this strong wave is uniformly insignificant compared with the near-bottom transport (plot (a) in Figures 5.6-5.9). The largest bedload contribution is one per cent of the near-bottom transport; this occurs only for the coarsest grain size at the lowest current velocity and reference concentration (Figure 5.6(a), lower left-hand corner). The relative value of bedload decreases with decreasing grain size and with increasing current because, although the predicted bedload volume rises with each of those variations, the suspended transport rises much faster. The ratio of bedload transport to near-bottom transport in the neutral case also decreases with increasing reference concentration since near-bottom transport rises with $C(\delta_w)$, as discussed above. Bedload is uninfluenced by that parameter in this formulation because it reflects an increase in γ_0, of which bedload is independent.

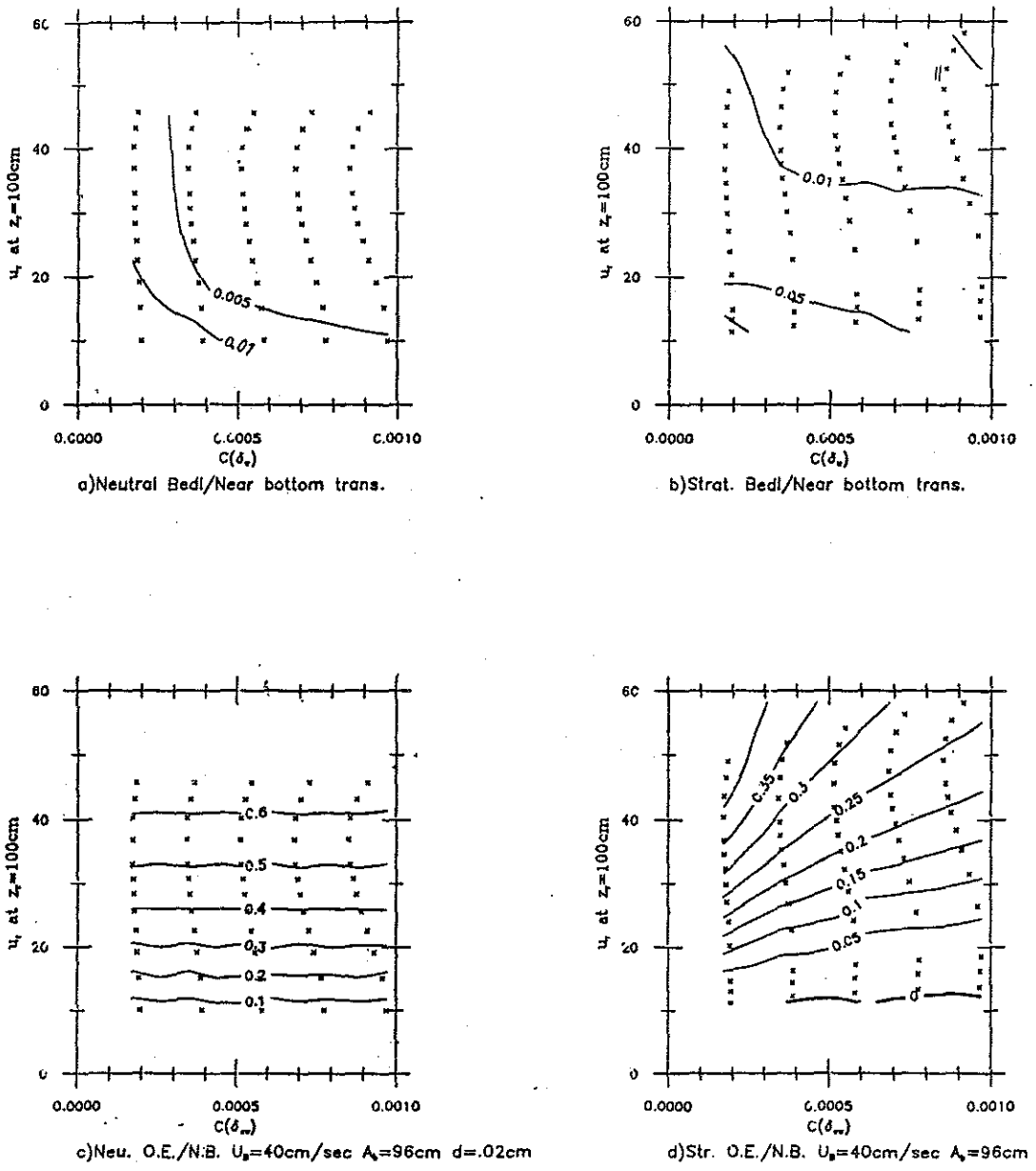

Figure 5.6: Relative values of bedload and outer Ekman layer transport, compared with near bottom transport, for fine sand in moderate storm waves.

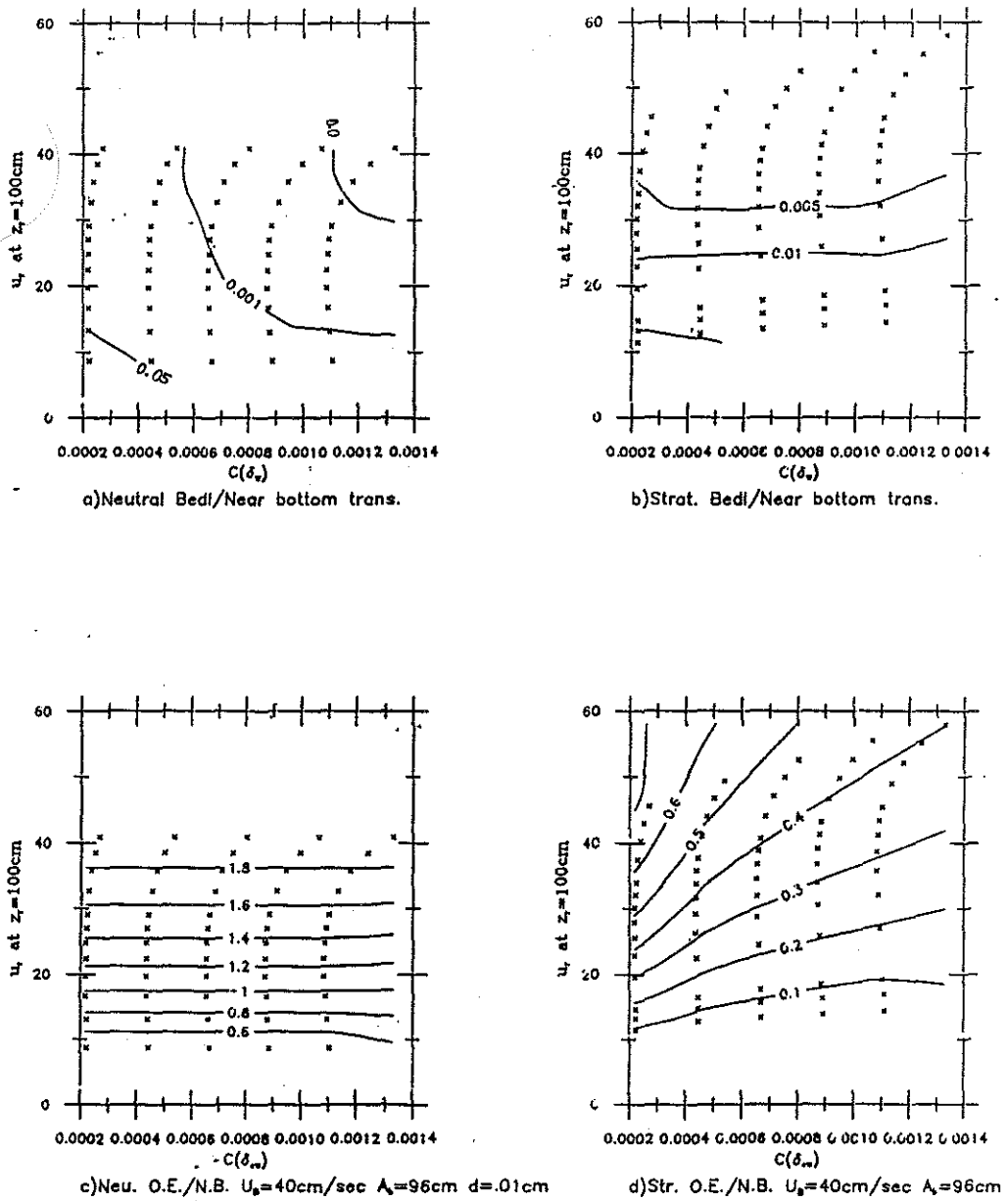

Figure 5.7: Relative values of bedload and outer Ekman layer transport, compared with near bottom transport, for very fine sand in moderate storm waves.

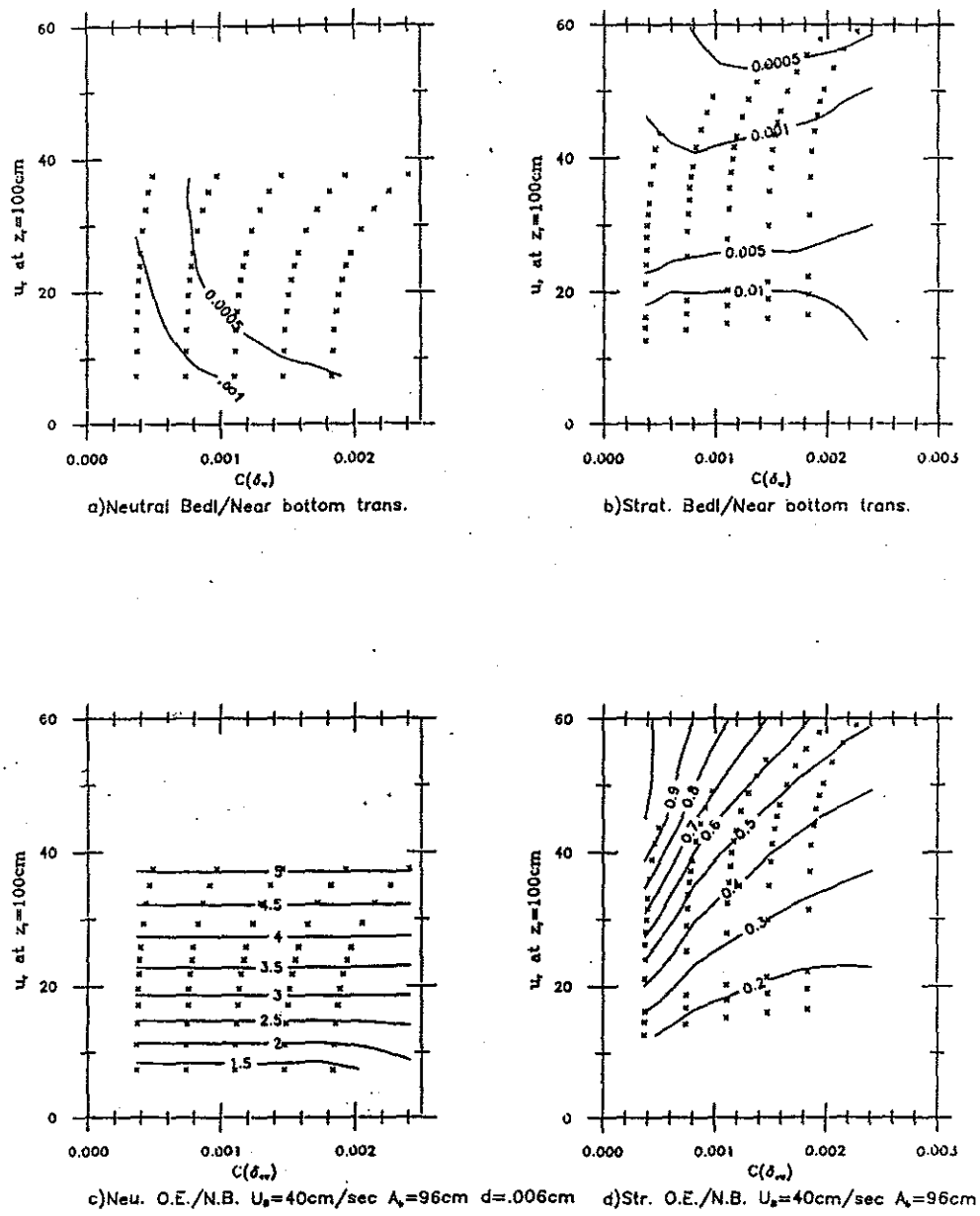

Figure 5.8: Relative values of bedload and outer Ekman layer transport, compared with near bottom transport, for coarse silt in moderate storm waves.

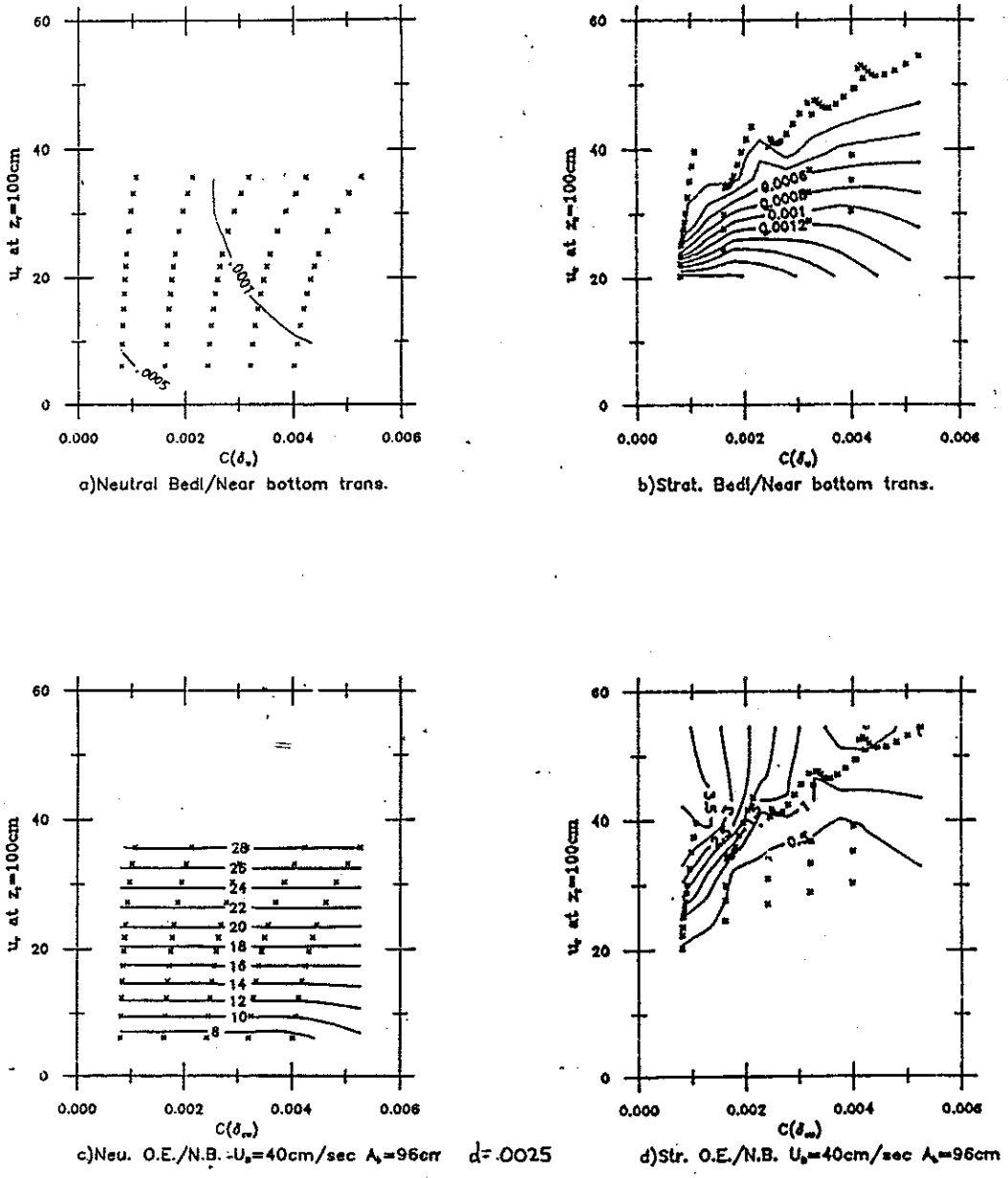

Figure 5.9: Relative values of bedload and outer Ekman layer transport, compared with near bottom transport, for medium silt in moderate storm waves. The contours for the stratified results demonstrate the effects of the nonunique solutions to the model, and are discussed in detail in the text.

Outer Ekman layer transport (Section 3.2.4) is much more likely than bedload to be a significant factor in predicting neutral transport volume (plot (c) in Figures 5.6-5.9). Since both neutral near-bottom and outer-Ekman layer transports are proportional to the reference concentration, there is no variation with $C(\delta_w)$ (the x-axis) in their relative values. This accounts for the uniformly flat contours. Since the concentration profile decays exponentially with $-\frac{w_f}{u_{*c}}$ (Equation 3.36), however, the relative value of outer Ekman layer transport rises with increasing current and with decreasing grain size. An increase in current from 10 to 40 $\frac{cm}{sec}$ causes a three- to six-fold increase in the proportion of the transport that occurs in the outer Ekman layer.

The relative rate of outer Ekman layer transport is strongly dependent on grain size, but in a sense opposite to the relative bedload transport rate. The outer Ekman layer transport is ten to sixty per cent of the near-bottom transport for fine sand (Figure 5.6(c)), but is eight to twenty-eight times greater than the near-bottom transport for medium silt (Figure 5.9(c)). Estimates of relative load for the outer Ekman layer are slightly lower than the relative transport rates, ranging from 0.013 to 0.44 for fine sand, 0.21 to 1.6 for very fine sand, 0.9 to 4.3 for coarse silt and 5.6 to 24.6 for medium silt.

These large proportions of transport in the outer Ekman layer might be cause for some concern, since the present work concentrates on calculating the near-bottom sediment profile. The large proportions are tempered by four factors, however: 1) stratification, as discussed in Section 5.3.2; 2) sediment availability, since these predictions assume an infinite mixing depth; 3) temporal and vertical spatial limitations, since the water depth may be less than the predicted Ekman layer thickness or there might not be adequate time to establish equilibrium sediment concentration conditions for the full water column (as opposed to the near-bottom layer) before environmental conditions change; and 4) predicted suspended sedi-

ment concentration values, some of which are up to an order of magnitude or more greater than any ever observed in continental shelf environments.

The third factor implies that the large outer Ekman layer load and transport reflect a problem in the method used to calculate them. This is true under some circumstances: the heights of the 'near-bottom' layer ($\frac{\delta_e}{6}$) for these cases are as large as 38 meters in the stronger currents (Figures 5.2-5.5). Obviously, integrating sediment concentration over a water column six times that depth violates the depth constraints imposed by the continental shelf. This problem can be addressed simply by limiting integration to the water depth; however, that introduces the complication of merging of the surface and bottom boundary layers and the need to model a fully mixed shelf. That problem will therefore be deferred, particularly in light of the other considerations.

The other three reservations with respect to the neutral model results reflect near-bottom processes. Silt concentrations of $O(10^{-3})$ are predicted in some cases at heights up to 20 m or more above the seafloor; these are one to two orders of magnitude greater than concentrations observed during continental shelf storms, even much closer to the bottom (e.g. Butman, 1987a). These large overpredictions cannot be corrected simply by adjusting the reference concentration parameter or initiation of motion criteria. At least under the conditions of this model run, the neutral model does not give physically reasonable results.

Stratification offers one remedy for the excessive concentrations, to wit, that the sediment is responding to a different turbulent structure than the one the neutral model produces. Specifically, the stratified model works on the assumption that the sediment itself modifies the turbulent structure and decreases the concentration.

Bed armoring of a seafloor with mixed grain sizes provides another possible solution. If the bottom shear stresses and sediment responses occur as modelled in the neutral case, then the flow would suspend the supply of fine sediments in

the surface layer, leaving a layer of coarser grains to armor the surface. The large differential in predicted reworking depths ($\frac{Load}{0.6}$) for different grain sizes under the same wave-current conditions suggests that this could be at least partly responsible for the overprediction of sediment concentrations in the neutral case.

5.3.2 Stratification effects

In the neutral case, the concentration gradient decays with the ratio of the fall velocity to the shear velocity. When stratification is included, the concentration gradient is influenced not only by $-\frac{w_f}{u_{*c}}$, but also by the gradient itself. In a stratified flow with only one length scale (a current boundary layer without waves, for example), stratification is significant only when the fall velocity is large enough so that the sediment is not mixed homogeneously through the entire constant stress layer, but is not so large that all the sediment falls out very close to the bottom (Glenn, 1983). In a stratified flow with two length scales such as those considered here, the gradient in turbulent intensity between the wave boundary layer and the current boundary layer introduces more stratification. The wave shear stress mobilizes sediment from the seafloor and transports it up into the water column. Over a short distance, however, the wave-generated shear stress dies out and only the current-generated turbulence is available to transport sediment higher. The a sediment concentration gradient depends on the ratio of u_{*cw} to u_{*c}, and reflected in the change in eddy viscosity over that short distance. The effect of stratification on the sediment load and transport predictions in this case hinges on three factors: reference concentration $C(z_0)$, the ratio of the sediment fall velocity to the shear velocity ($\frac{w_f}{u_{*c}}$), and the value of the stability parameter ($\frac{z}{L}$) immediately above the wave boundary layer.

The effects of sediment stratification on sediment load and transport predictions are shown in Figures 5.2-5.5(compare (a) and (c) with (b) and (d)). These effects

are less easily predictable from inspection of the governing equations than are variations in the neutral cases. Initial inspection shows three primary changes: 1) changes in contour shape, 2) decrease in maximum transport and load values, and 3) smaller blank areas at the top of the plots. These will be explained in reverse order.

The smaller blank areas result from the effect of stratification on the velocity profile (Section 2.3). The neutral and stratified cases in each figure represent the same range of bottom shear stress. Because the stratification dampens the transfer of low-momentum fluid up from the bottom, however, the predicted velocities at one meter above the bottom are higher in the stratified case than in the neutral case. This effect is demonstrated in the distribution of the 'data' points (xs) in the plots. The magnitude of the effect of stratification on the velocity can be gauged by comparing the location of the corresponding neutral and stratified data points. Each of the circled points in Figure 5.2, plots (a) and (b) represents the same u_{*c} and u_{*cw} values for this wave and reference concentration ($C(\delta_w) \sim 5 \times 10^{-4}$) for fine sand. The predicted neutral current velocity, however, is $\sim 40 \frac{cm}{sec}$ ($\frac{u_r}{u_b} \sim 1.0$), and the predicted stratified current velocity is $\sim 50 \frac{cm}{sec}$ ($\frac{u_r}{u_b} \sim 1.25$). The difference of 10 cm/sec represents the value of the stratification term in the velocity profile calculation (Equation 3.44).

A decrease in predicted sediment load and transport is expected, since the upward transfer of mass, like the upward transfer of momentum, is damped by stratification. The magnitude of the response to stratification is strongly dependent on the relative wave-current and current shear stresses. The response of the sediment load and transport predictions to stratification will be discussed in three categories: 1) small concentrations at the top of the wave boundary layer; 2) low current velocity; and 3) high reference concentrations with large currents. Within these categories, the sediment response hinges on the balance of terms in the sim-

plified sediment continuity equation (Equation 3.34). For the sake of reference in the discussion, the equation is repeated here:

$$w_f C + \nu_{ts} \frac{\partial C}{\partial z} = 0$$

Note that the product of the stratification-corrected eddy viscosity (ν_{ts}) and the concentration gradient is balanced by the product of the fall velocity and the concentration.

Small $C(\delta_w)$, Large current velocity

Under this relatively strong wave forcing, when the sediment concentration at the top of the wave boundary layer is small ($O(10^{-4})$) and there is a strong current, the response to stratification is minor. These conditions are demonstrated in Figures 5.2-5.5 by the range of contours near the left hand margin of each plot. The highest values vary only slightly between the stratified and neutral cases. For example, the upper left hand data points in Figure 5.2(a) and (c) are located at the vertical coordinate 1.15 and have load and transport values of 0.04 cm^3/cm^2 and 2.0 $cm^3/cm/sec$ respectively; the corresponding point for plots (b) and (d) are at the vertical coordinate 1.2 and have values of about 0.028 and 1.7. Stratification does not substantially alter the load, transport, or velocity value for this fine sand case, and the same is true for the other three grain sizes. In terms of the sediment continuity equation, the small concentration and relatively large eddy viscosity (since u_{*c} is relatively large) mean that the concentration gradient is relatively small, regardless of the fall velocity. The stability parameter, which lowers the value of the eddy viscosity, and is a function of the concentration gradient, stays fairly small.

Physically, this corresponds to a situation where the currents are strong enough to suspend enough of the small boundary concentration to preclude a strong con-

centration gradient. In the calculation procedure, the dependence on $C(\delta_w)$ can be seen in the stratification terms of the solutions for the velocity and concentration profiles (Equations 3.44 and 3.45). Both depend on the integral of the concentration. A small boundary concentration therefore leads to small stratification effects.

Low current velocity

A small current relative to the wave results in strong stratification effects at the top of the wave boundary layer. Load and transport may drop by an order of magnitude or more. The effect is intensified with increasing $C(\delta_w)$ and with decreasing grain size. In Figure 5.2(a) and (b), for $\frac{u_r}{u_b} = 0.4$ ($u_r = 16\frac{cm}{sec}$), stratification leads to a decrease in load of approximately 50% when $C(\delta_w) = 10^{-4}$. The values on which these comparisons are based are marked by boxes on the plots and enumerated in Table 5.3(a) and (b). Moving to the right across the plots to the points marked at $C(\delta_w) = 10^{-3}$, the decrease in load due to stratification is about 70%. At the same current level ($\frac{u_r}{u_b} = 0.4$), the decrease in load for very fine sand ranges from 67% to 90% for $C(\delta_w) = 10^{-4} - 10^{-3}$ (marked on Figure 5.3(a) and (b)). For coarse silt, the same range of concentrations at the same velocity level yields decreases in load of 83-96% (marked on Figure 5.4).

The effect on transport calculations is even more pronounced since, in stratified flow, the sediment that makes up the load is concentrated near the bottom where velocities are lowest. In the same four figures (marked on Figures 5.2-5.5, plots (c) and (d)) at the same current level ($\frac{u_r}{u_b} = 0.4$) for the same range of $C(\delta_w)$ ($10^{-3} - 10^{-4}$), the transport of fine sand drops by 83-97% due to stratification; transport of very fine sand drops by 89-98%; and transport of silt drops by 90-99% (again, compare top two sections of Table 5.3).

The first order effect of stratification in this large wave environment where

$\frac{u_r}{u_b}$	$C(\delta_w)$	$d(cm)$	load(neu)	load(strat)	trans(neu)	trans(strt)
a) *Low current, low* $C(\delta_w)$						
0.4	10^{-4}	0.02	0.01	0.005	0.3	0.05
percentage change			-50%		-83%	
0.4	10^{-4}	0.01	0.03	0.009	0.9	0.1
percentage change			-67%		-89%	
0.4	10^{-4}	0.006	0.09	0.015	2.0	0.2
percentage change			-83%		-90%	
0.4	10^{-4}	0.0025	0.27	0.026	5.5	0.37
percentage change			-90%		-93%	
b) *Low current, high* $C(\delta_w)$						
0.4	10^{-3}	0.02	0.11	0.034	1.8	0.05
percentage change			-70%		-97%	
0.4	10^{-3}	0.01	0.25	0.025	5.0	0.08
percentage change			-90%		-98%	
0.4	10^{-3}	0.006	0.45	0.018	10.0	0.08
percentage change			-96%		-99%	
0.4	10^{-3}	0.0025	1.33	0.018	27.4	0.06
percentage change			-99%		-99%	
c) *High current, high* $C(\delta_w)$						
1.0	10^{-3}	0.02	0.28	0.065	16	1.8
percentage change			-77%		-89%	
1.0	10^{-3}	0.01	0.70	0.08	41	3.5
percentage change			-88%		-92%	
1.0	10^{-3}	0.006	1.2	0.18	60	10
percentage change			85%		-83%	
1.0	10^{-3}	0.0025	5.04	2.4	300.0	241
percentage change			-52%		-20%	

Table 5.3: Values of load and transport in a moderate storm, picked from Figures 5.2-5.5 for ranges of conditions as discussed in text. For each current category, results are shown for (top-to-bottom) fine sand, very fine sand, and coarse silt. Magnitudes of decreases due to stratification are shown. Load units are $\frac{cm^3}{cm^2}$; transport units are $cm^3/cm/sec$.

the current is small is such a drastic decrease in predicted load and transport that the second-order effects of grain size and reference concentration might seem gratuitous. For example, there appears to be little difference between 97%, 98%, and 99% decreases in transport for fine sand, very fine sand, and silt in low current, high $C(\delta_w)$ conditions (Table 5.3(b)). The difference is made obvious, however, by observing that instead of an order of magnitude increase in transport from fine sand to silt, transport predictions for all three grain sizes in a $16\frac{cm}{sec}$ current with relatively high reference concentration are nearly the same. For the same wave, current and reference concentration conditons, the predicted load for silts is a factor of two smaller than the predicted load for fine sand. Thus stratification may nullify or reverse the expected result that, for a given wave and current condition, finer sediment leads to greater suspended load and transport.

This counter-intuitive result is caused by the feedback between stratification and shear velocity. If the holding capacity for suspended sediment of the current-generated turbulence is much less than that due to the wave-current enhanced shear stress in the wave boundary layer, then the stratification due to the suspended sediment concentration gradient at the top of the wave boundary layer acts to damp the mean shear stress (but not the maximum shear stress, because it is dependent primarily on the wave), thereby enhancing the stratification. The effect increases with smaller grains (for the same wave and current conditions) and with increased reference concentration (for the same grain size) for the same reason: the stratification terms depend on the integral of the concentration, and a large boundary concentration introduces the possibility of a large concentration gradient.

In terms of the sediment continuity equation, this translates to a relatively small eddy viscosity (since u_{*c} is small) requiring a relatively large concentration gradient to balance the product of fall velocity with concentration. The larger gradient generates a larger stability parameter, which leads to a smaller eddy viscosity, and

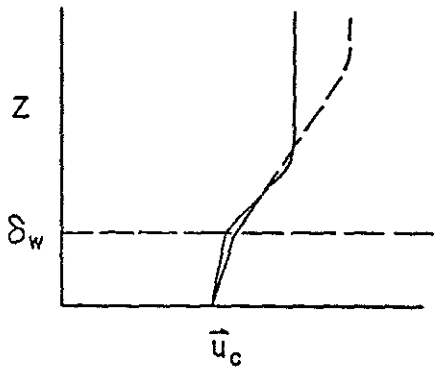

Figure 5.10: Schematic diagram of alternative solutions to stratified velocity profile for near-bottom wave and current boundary layer flow. Solid line is low current shear stress case with strong stratification; dashed line is high current shear stress case.

therefore the gradient must be still larger. This is the reason for the drastic drop in expected load and transport when the current is small.

The medium silt results present a special case for the stratified results, as a look at the contours for the stratified case suggests (Figure 5.5 (b) and (d)). The small fall velocity and large concentration require a large sediment gradient when the current eddy viscosity is small, in order to balance terms in the sediment continuity equation. The current eddy viscosity decreases with an increased concentration gradient, leading to a stronger gradient to balance the sediment continuity equation, and so on until convergence.

The velocity profile is likewise affected by the enhanced stratification. The velocity profile is the sum of a stratification term and a logarithmic term (Equation 3.44). If the stratification term increases more rapidly in the strongly stratified case than the logarithmic term does in the less-strongly stratified case, then the velocity profiles can overlap at some heights above the bottom (Figure 5.10). If the reference velocity is specified in the vicinity of these heights, then there is more than one solution, and predictions of load and transport for the solutions can vary a lot.

While the results for relatively low reference concentrations are similar to those for larger grain sizes, stratification effects are increased when grains are small, the

	(1)	(2)	(3)	(4)	(5)	(6)
$\frac{u_a}{u_b}$	0.175	0.15	0.125	0.10	0.075	0.05
u_{*cw}	4.57	4.47	4.37	4.27	4.17	4.06
u_{*c}	1.84	1.70	1.55	1.39	1.20	0.97
u_r	35.2	34.7	34.4	34.3	34.5	34.2
u_r, neu. contrib.	22.1	20.1	17.9	15.5	12.8	10.0
u_r, str. contrib.	13.1	14.6	16.5	18.8	21.6	24.2
N.B. Load	0.97	0.79	0.63	0.47	0.32	0.18
N.B. Trans.	70.7	54.5	39.5	26.2	15.0	6.5

Table 5.4: Six sets of model parameters representing the six load and transport predictions in the boxed region of Figure 5.5(b) and (d). The matching parameter for model convergence, u_r, is effectively the same for all six cases, but the near-bottom (N.B.) load and transport vary by factors of 5 and 10, respectively. The model solution is not uniquely determined in this case.

concentration at the top of the wave boundary layer is greater than 10^{-3} and the mean shear stress is low. To illustrate this point a detailed examination of the conditions defining the boxed region in Figure 5.5(b) will be undertaken. The six points in the box represent parameter ranges as listed in Table 5.4.

The values listed in Table 5.4 for the reference velocity u_r calculated by the model are nearly identical: they vary by less than the resolution of field measurements, certainly, and are within the one per cent convergence criterion for the model. The load and transport predictions, however, vary by factors of five to eleven over this essentially identically-specified range of solutions. The difference in u_{*cw} values is very small, but u_{*c} values double over the range. The reason for this ambiguity is found in lines 5 and 6 of Table 5.4. Note that the stratification contribution to the reference velocity increases at the same rate that the logarithmic contribution decreases as u_{*c} goes down. The stability parameter at z_r combines with the variation in u_{*c} to give this ambiguous result.

The similarity in predicted velocities leads to the difficulty in applying the

model because convergence is set on u_r. As Table 5.4 demonstrates, the same u_r can be obtained from very different mean shear stress values. The predicted velocity profiles for points (3) and (5) of Table 5.4 are shown in Figure 5.11, plotted linearly to show detail. Obviously, the model could converge on either of these solutions if z_r were specified between about 0.2 and 1.4 meters, and the difference in predicted load and transport is a factor of two. Similar plots could be shown for the other four points, so that the possible range in predicted load is a factor of five, and in transport a factor of eleven. To choose between these options, a velocity or concentration measurement somewhere higher in the water column would have to be specified. More fundamentally, this result calls into question the representation of stratification using a stability parameter to modify the eddy viscosity, in some circumstances. It is not clear that the stability parameter should be allowed to grow so large, or that it is an accurate representation of the physical world when it does. This set of wave-current-sediment predictions needs to be tested in controlled field or laboratory conditions.

Large $C(\delta_w)$, large current

In contrast to the high reference concentration and low current scenario just discussed, a higher current restores the expected pattern of increased load and transport with decreasing grain size when observed wave and current conditons are the same. The predictions used to demonstrate this point are those for a current of $40\frac{cm}{sec}$ ($\frac{u_r}{u_b} \sim 1$), marked by boxes on Figures 5.2-5.5 and listed in Table 5.3(c).

Again, the first order effect on load and transport values is stratification: the stratified load predictions are fifty-two to eighty-eight per cent lower than the neutral ones. In looking at the percentage decreases, however, note that the largest change in the stratification effect, with respect to the low current case, occurs in the fine grain size cases. For medium silt, instead of a ninety-six to ninety-nine per

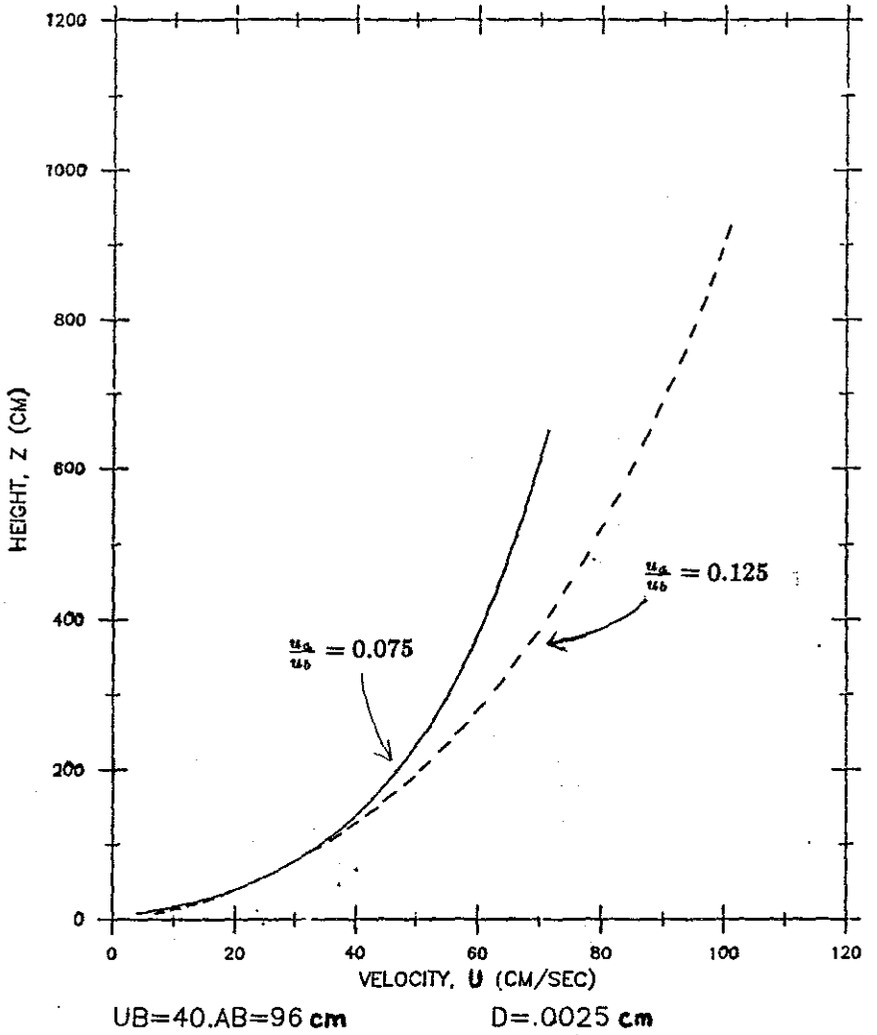

Figure 5.11: Velocity profiles, plotted linearly to show detail, illustrating how stratification effects can lead to non-unique model solutions. Specification of the reference velocity between 0.2 and 1.4 m could yield either of these velocity profile solutions. These profiles represent velocity profile predictions (3) and (5) for the wave-current-velocity results shown in Table 5.4.

cent decrease in load and transport due to stratification, there is an eighty-three to eighty-five per cent decrease, a change of eleven to sixteen per cent. The increase in load and transport relative to the neutral case for medium silt is even greater.

What these changes mean is that the load increases with decreasing grain size, as expected. Even more pronounced is the change in transport patterns. Rather than being practically the same, transport of coarse silt is an order of magnitude greater than transport of fine sand (1.8 vs. 10 $cm^3/cm/sec$) and transport of medium silt is an order of magnitude higher still (241 $cm^3/cm/sec$).

The shapes of the contours in the plots of stratified predictions result from the reconciliation of the tendency of the stratification effects to grow with increasing $C(\delta_w)$ and to shrink with increasing current. The regular, hyperbolic shapes of the neutral contours are suggested in the small-concentration regions at the left-hand edge of some of the plots. The curves begin to flatten in all cases, since stratification makes the flow less competent to hold sediment. In some cases the curves remain flat, indicating that the effects of increasing reference concentration and increasing velocity balance. For smaller grain sizes, the curves rise to the right, suggesting that an *increase* in available sediment leads to a *decrease* in total load or transport. As discussed earlier, this results from the larger concentration gradient at the top of the wave boundary layer.

Grain size effects

The influence of grain size on stratification effects was discussed above. As a general rule, smaller grain sizes enhance the effect of stratification due to the gradient in eddy viscosity at δ_w when the wave is large and the current small. Grain size also influences the value of $C(\delta_w)$ in three ways: 1) the $\frac{w_f}{u_{*c}}$ ratio determines the concentration gradient (Equation 3.35); 2) the critical Shields parameter for initiation of motion is a factor in the reference concentration; and 3) the bottom rough-

ness is determined by the grain size, whether through the size of ripples, sediment transport layer or grain roughness itself (Section 3.3). This is very important in the calculation of boundary shear stress. Ultimately, grain size is the determining factor in the quantity of sediment that can be carried by a flow.

The variation of the concentration at the top of the wave boundary layer with grain size is most easily seen in the x-axes of Figures 5.2-5.5. The x-axes' maxima, in decreasing order of grain size, are: 10^{-3}, 1.5×10^{-3}, 3×10^{-3} and 6×10^{-3}. Since all of these plots represent approximately the same ranges of wave and current velocities, the variation in $C(\delta_w)$ results entirely from initiation of motion criteria, movable bed roughness, and vertical decay inside the wave boundary layer. In these cases, where wave shear stress is very large, the differences are due primarily to initiation of motion criteria and roughness.

The effect of roughness on $C(\delta_w)$ for a single grain size is demonstrated in the plots. If one ignores the contours, the data points (xs) represent an x-y plot of the variation of $C(\delta_w)$ with reference velocity. If roughness had no effect on u_{*cw}, and therefore on $C(\delta_w)$, the data points in each plot would be a set of six near-vertical lines, curving slightly to the right in response to the slight increase in boundary shear stress ($\tau_{0,cw}$) due to incremental increases in current contribution. However, with increases in current and shear stress, the bottom roughness either increases because bedforms and sediment transport layers grow, or decreases because ripples are washed out. If the roughness increases, then the shear stress in the wave boundary layer increases and the concentration at the top of the wave boundary layer increases. The data points in Figures 5.3-5.5 show increases in $C(\delta_w)$ with increases in current (i.e. they curve to the right). This reflects the bedform roughness element ($k_{b,B}$) due to the building of ripples in the sand case, and the sediment transport roughness ($k_{b,T}$) due to formation of a transport layer in the silts. The decrease in $C(\delta_w)$ with increasing current in the fine sand case, demonstrated in

the data points' curve to the left in Figure 5.2, indicates that ripples are being washed away because of the increasing bottom shear stress.

These effects demonstrate the interconnections between waves, currents, grain diameter, bottom roughness, and concentration. Since the predictions of stratified load and transport for a given grain size depend only weakly on changes in $C(\delta_w)$, its variation is more significant between grain sizes than within one grain size when the wave is large.

Bedload and Outer Ekman Layer Load and Transport

In a storm wave environment the effects of stratification on the values of the outer Ekman layer load and transport are more pronounced than the stratification effects on bedload transport in a storm wave environment. The proportion of bedload transport compared with near-bottom transport in the stratified storm wave case is similar to that in the neutral case (Figures 5.6(b)-5.9(b)). The smaller total transport values make the bedload proportion slightly higher, but the maximum is still only ten per cent of the near-bottom transport (Figure 5.6(b)). In general, bedload transport is less than five per cent of the stratified near-bottom suspended transport.

Stratification makes a big difference in the predicted outer Ekman layer load and transport. Most important for the application of this model, the predicted transports are, in general, less than or equal to the near-bottom transports even for the finer-grained sediments (Figures 5.6(d)-5.9(d)). Since the focus of this work is the near-bottom transport, and the predictions for the region farther from the bottom are more poorly constrained (Section 3.2.4), this pattern is reassuring with respect to the usefulness of the present results.

In addition to the changes in the magnitudes of the contours, the patterns of the contours are different for the stratified vs. neutral outer Ekman to near bottom

transport. The ratio increases with increasing current in the stratified case as it does in the neutral case. However, since the stratified concentration profile is a nonlinear function of the concentration at the top of the wave boundary layer, with effects of stratification increasing as $C(\delta_w)$ increases, the proportion of sediment transport in the outer Ekman layer decreases with increasing $C(\delta_w)$.

What this means is that for large waves, the transport in the outer Ekman layer is relatively unimportant except when both large currents and small grains are present. These cases must be approached with caution for a number of other reasons, as discussed in relation to the neutral case: time-dependence of the model, merging of the surface and bottom Ekman layers, armoring of mixed grain sizes, and variations of fall velocity and critical Shields parameter due to adhesion and cohesion. However, the unrealistically high sediment concentrations above the wave boundary layer characteristic of the neutral case are not found in the stratified results. The inclusion of stratification thus provides one physically reasonable approach to eliminating unsatisfactory results from the neutral model. For most cases, the proportion of the total load in the outer Ekman layer is small enough that error in the method used to calculate the estimate of its volume is acceptably low.

Total load and transport

The discussion of both neutral and stratified results so far has focused on the relative importance of various parameters and conditions to the calculation of sediment transport values. The amount of sediment involved is most easily grasped by converting the volumetric load values into estimates of the reworking depth, by dividing the load by the bed concentration, here taken to be 0.6.

The reworking depth is very grain-size dependent. For the neutral, near-bottom load, each step up in grain size corresponds to a decrease in load and transport

Ranges of reworking depths, Moderate Storm Near-bottom load only		
$d(cm)$	neutral (cm)	stratified (cm)
0.02	0.01 - 0.53	0.007 - 0.175
0.01	0.02 - 1.6	0.005 - 0.35
0.006	0.055 - 4.6	0.008 - 0.97
0.0025	0.22 - 14.2	0.03 - 7.6

Table 5.5: Reworking depth ranges for the moderate storm wave showing how stratification effects are amplified with decreasing grain size. Note that the neutral and stratified predictions for the same grain sizes represent the same range of wave-current shear stress values, but not the same range of reference current values.

by a factor of $\sim 2-3$. Eight to 10 times as much coarse silt as fine sand would, therefore, be lifted from the seafloor and transported under these neutral wave and current conditions (Table 5.5).

In the stratified cases, the erosion and transport values are lower, but the pattern of increase, at least for the high velocity and high $C(\delta_w)$ cases, is similar to the neutral. For each increase in grain size, the values of load and transport predictions drop by a factor of $\sim 1.5-2$ (Figures 5.2-5.5). For the low velocity cases, however, the stratification effects are stronger for smaller grain sizes, so there may be little or no change in predicted load due to grain size. The ranges in predicted reworking depths are approximately halved relative to the neutral case (Table 5.5), but higher reference current velocities are needed to generate the smaller loads.

5.3.3 Summary

While a wave with a bottom velocity of 40 cm/sec can put much more sediment in motion than could a current alone, the stratification generated by the gradient in turbulent energy beyond the wave boundary layer tempers drastically the erosive potential of the combined wave-current force. The load and transport are depen-

dent on grain size, current velocity and reference concentration, but the maximum expected erosion due to a moderate storm appears to be on the order of 1-5 cm, even in very strong currents. Neutral predictions for load and transport under large waves and currents appear to overpredict concentrations by at least an order of magnitude. This effect is countered by stratification, which may be an important factor in limiting transport.

5.4 Results: Low Swell

On some continental shelves, low, long period swell waves occur as forerunners of an approaching storm or as remnants of a distant storm. Swell is characterized by its long period, monochromatic character. Periods can be up to 25 or 30 seconds. This set of model runs treats a 20 second wave generating bottom velocities of 20 cm/sec. Such a wave would have a height of 1.1 m in 50 m water depth. Figures 5.12-5.15 show the variation in load and transport predictions with $C(\delta_w)$ and $\frac{u_r}{u_b}$, in the same format as discussed in detail at the end of Section 5.2.

These contours are much simpler than those for the cases with larger wave bottom velocities. The most striking feature of these plots, though, is the blank space in the lower half of each plot. Before examining the load and transport results, this phenomenon will be explained.

Unlike the last wave case, the small wave considered here does not generate sufficient boundary shear stress to put sediment into motion except in the finest sediment class considered (medium silt). In the fine sand case, for example (Figure 5.12), only when $\frac{u_r}{u_b}$ is approximately equal to one does sediment begin to move. At lower velocities, the data points plot onto the y-axis to signify a reference concentration of zero. The blank areas on the plots, then, signal conditions under which no motion is predicted: for example, on a seabed of very fine sand in low

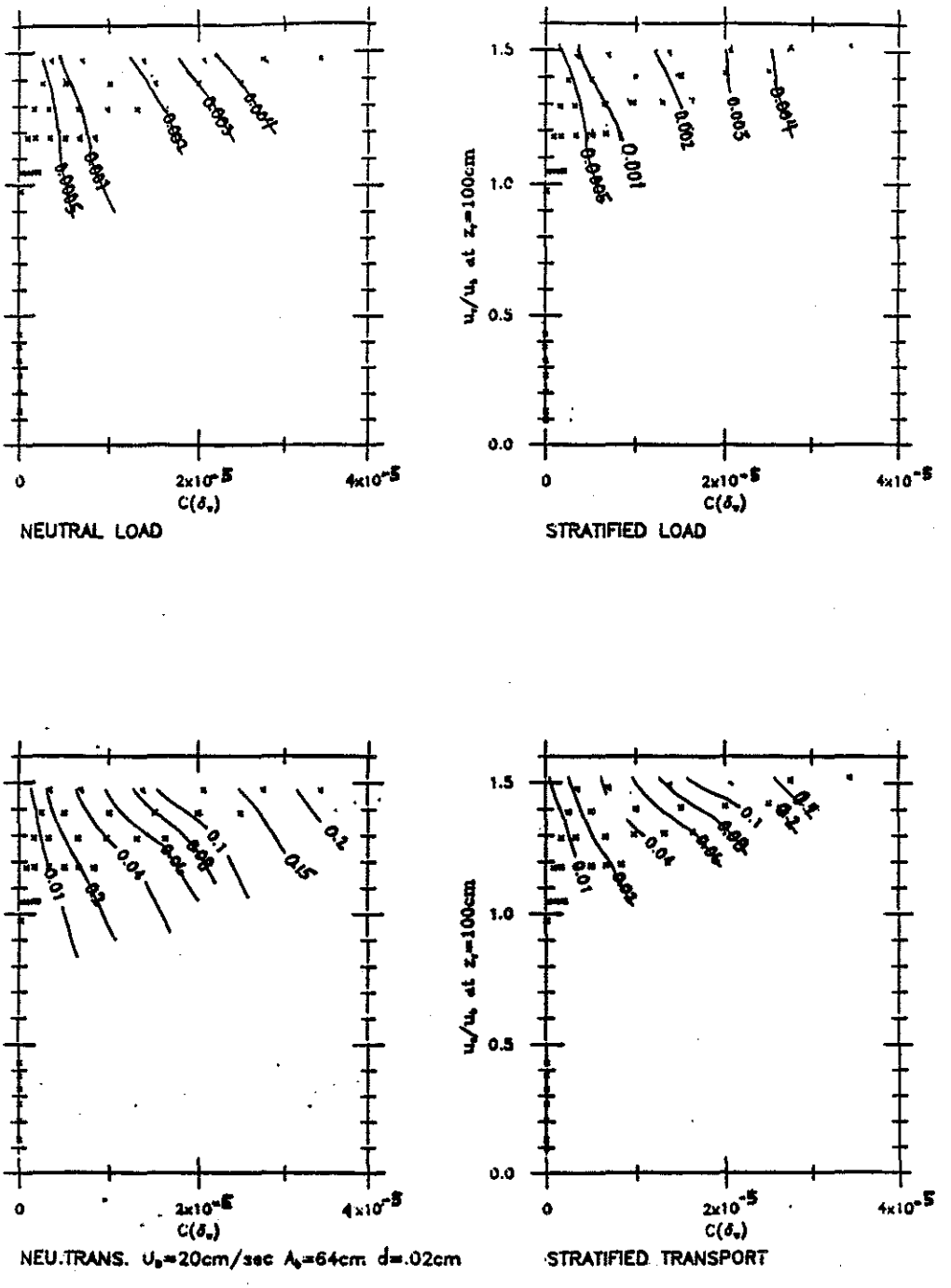

Figure 5.12: Predicted near-bottom load ($\frac{cm^3}{cm^2}$) and transport ($cm^3/cm/sec$) values for fine sand in low swell waves. T=20 sec, and the wave height in 50 m of water would be 1.1m. u_r is reference current velocity. δ_w ranges from 3-21 cm; $\frac{\delta_a}{6}$ ranges from 1 to 28 m.

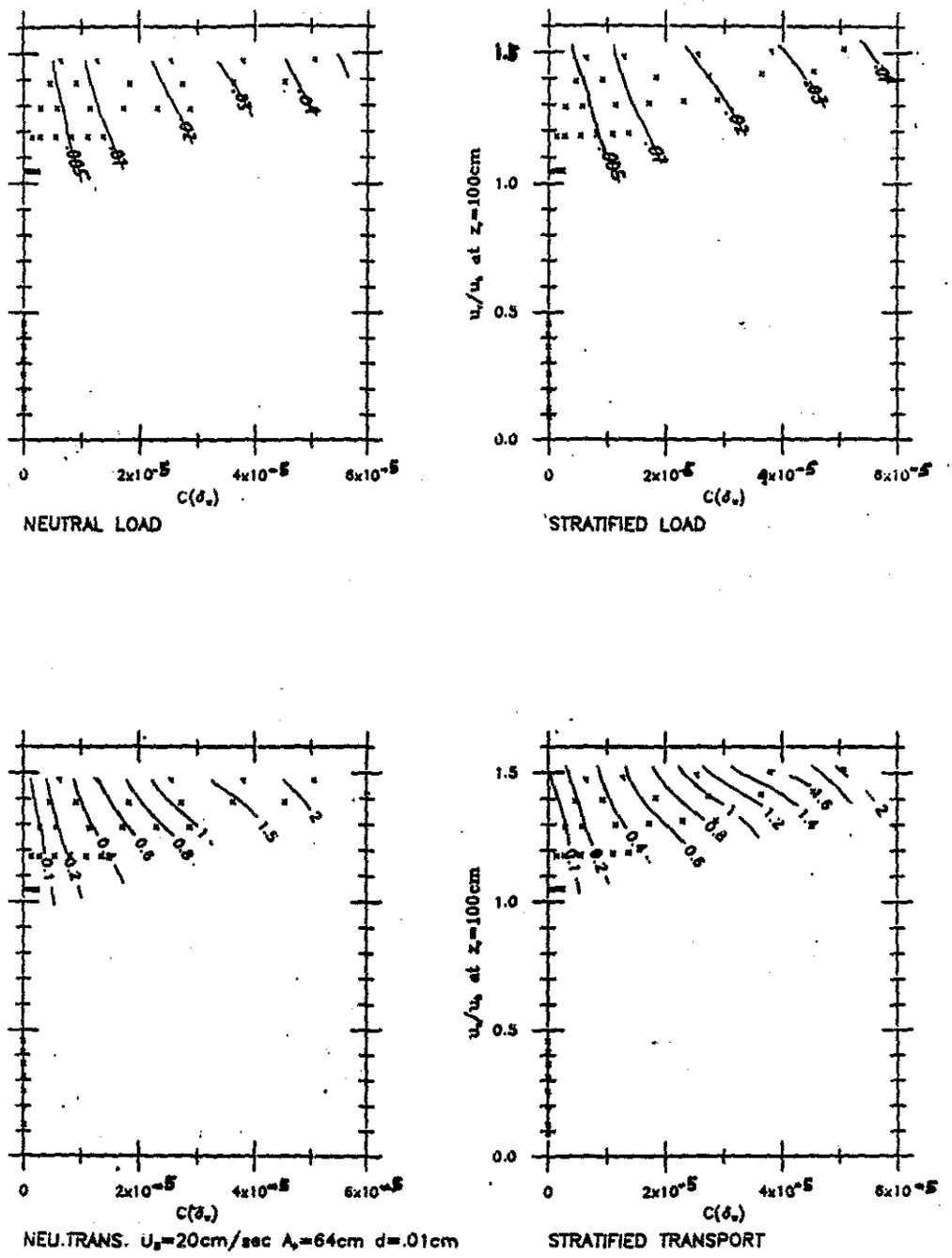

Figure 5.13: Predicted near-bottom load $(\frac{cm^3}{cm^2})$ and transport $(cm^3/cm/sec)$ values for very fine sand in low swell waves. δ_w ranges from 3-21 cm; $\frac{\delta_s}{\delta}$ ranges from 1 to 28 m.

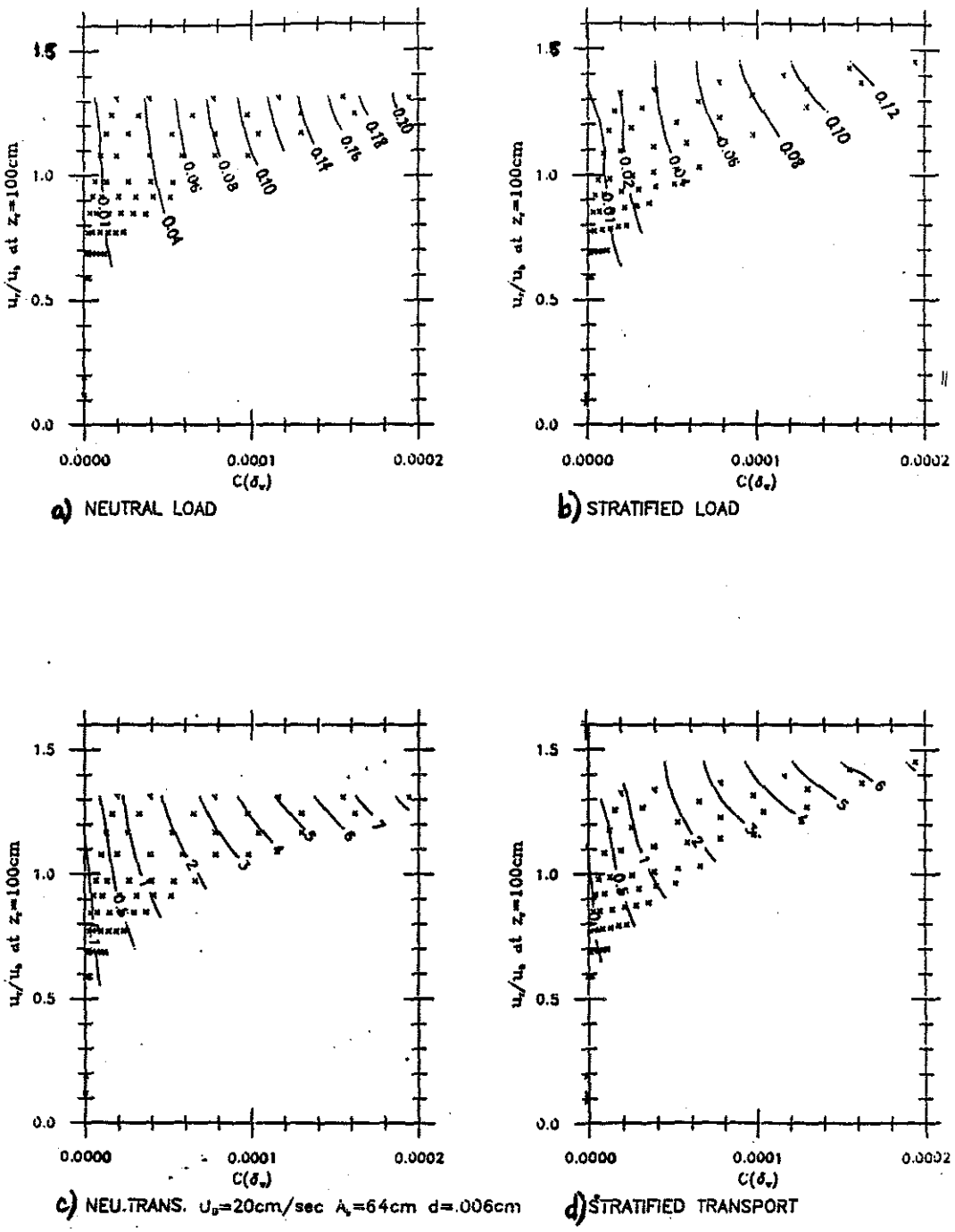

Figure 5.14: Predicted near-bottom load ($\frac{cm^3}{cm^2}$) and transport ($cm^3/cm/sec$) values for coarse silt in low swell waves. δ_w ranges from 3-17 cm; $\frac{\delta_a}{6}$ ranges from 1 to 20 m.

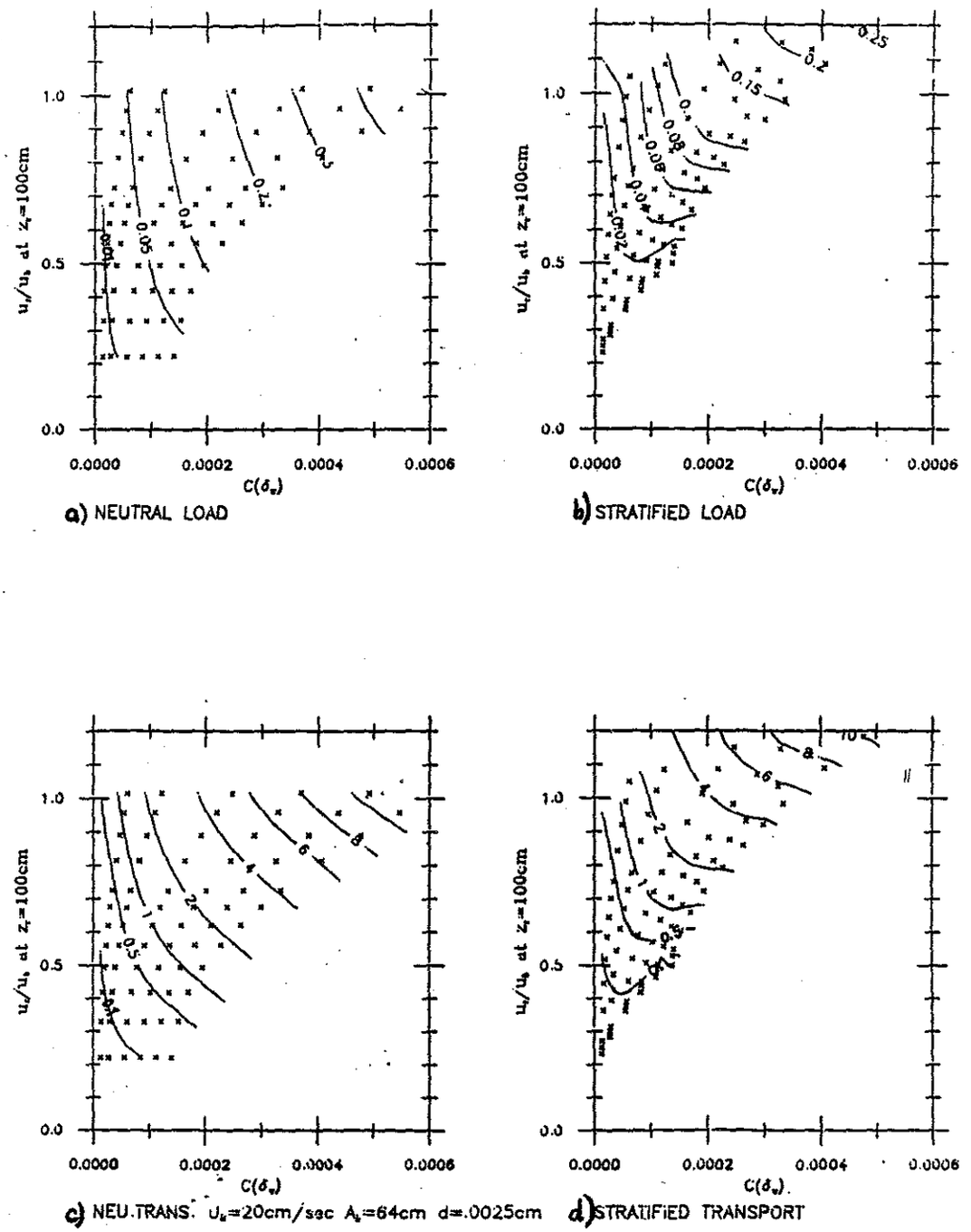

Figure 5.15: Predicted near-bottom load ($\frac{cm^3}{cm^2}$) and transport ($cm^3/cm/sec$) values for medium silt in low swell waves. δ_w ranges from 7.7-8.1 cm; $\frac{\delta_a}{\delta}$ ranges from 3 to 10 m.

swell of this sort, with a current of 10 cm/sec ($\frac{u_r}{u_b} = 0.5$), one would not expect to find $C(\delta_w) = 10^{-3}$ (Figure 5.13).

When the moveable bed roughness model is used, the only roughness element under conditions of no motion is the grain size roughness $k_{b,n}$. Such small roughnesses generate very little turbulence, so the model predicts small u_{*cw} and u_{*c} values and, therefore, very low current values. Once the skin friction shear stress exceeds the critical value, however, the movable bed roughness model generates roughness estimates based on equilibrium bedform and sediment transport models, causing a discontinuity between the grain roughness when there is no sediment motion and the bedform roughness which is as much ;as an order of magnitude or more greater.

The roughness discontinuity leads to a discontinuity in predicted reference velocity: the increased roughness leads to increased turbulence and a jump in the predicted velocity. Note, for example, that $\frac{u_r}{u_b} = 0.45$ in Figure 5.12a is the largest velocity at which there is no sediment motion (data point plots on the y-axis). The non-dimensionalized reference velocity jumps to $\frac{u_r}{u_b} = 0.98$ (the next highest data point) with the next incremental increase in $\frac{u_a}{u_b}$ because sediment motion has begun and the moveable bed roughness model is predicting ripple formation. This large change in predicted reference velocity, however, represents only an incremental change in the skin friction component of bottom shear stress. The ripples increase the turbulent intensity, so that the current feels more drag (u_{*c} is greater), and the transport capacity jumps dramatically.

This signals a logistical problem for the model: what if the input condition it is trying to match is a reference velocity of $15\frac{cm}{sec}$ ($\frac{u_r}{u_b} = 0.75$) when waves and currents are as shown in Figure 5.12. The model's iterations would skip back and forth between a no-motion case (which would give a velocity too low) and a rippled bed case, which gives a velocity that is too high. There is no value of $\frac{u_a}{u_b}$ that would

give the specified reference velocity.

There is a simple solution: include a bed roughness as input, based on observed or expected animal mounds and ripples, rather than using the moveable bed roughness model. This is a realistic solution, since the ocean floor would not be expected to be flat, and the small wave-current velocities under which this problem occurs would not likely be the factors controlling bed roughness.

Like the storm wave cases, the effects of stratification grow pronounced with decrease in grain size and with increase in concentration. Because the model predicts no motion at small current velocities for all but the medium silt, it is the only case to display the effects of the gradient in turbulent energy at the top of the wave boundary layer. Note the lowest contours flattening toward horizontal (Figure 5.15); the effect of stratification on load and transport of medium silt is a decrease of as much as 80%. Since the total transport is so small, however, that translates to a maximum difference in reworking depth of only 2 mm even for silt.

In general, the concentrations at the top of the wave boundary layer are very small compared with those generated by the large wave examined above. These low concentration and the low wave-current shear stresses lead to small differences between neutral and stratified predictions, generally 30% or less. In all cases, the difference is beyond the resolution of field measurements.

The outer Ekman layer transport is negligible in fine sand applications, reflecting the reduced mobility of the sediment under the small wave. Silt and very fine sand have outer Ekman layer transport approximately equal to the near-bottom values for all currents greater than 20 cm/sec. Bedload transport remains less than 10% of near-bottom transport in all silt cases, but forms most of the (very small) sand transport in currents smaller than about 20 cm/sec.

The ranges of reworking depths resulting from the near-bottom load for this wave are, not surprisingly, much smaller than for the larger wave (Table 5.6. In-

Ranges of reworking depths, Low swell Near-bottom load only		
$d(cm)$	neutral (cm)	stratified (cm)
0.02	0.0 - 0.01	0.0 - 0.008
0.01	0.0 - 0.10	0.0 - 0.075
0.006	0.0 - 0.35	0.0 - 0.23
0.0025	0.005 - 0.87	0.003 - 0.57

Table 5.6: Reworking depths for low swell, showing that stratification reduces the near-bottom load by less than a factor of two in all cases.

cluding the outer Ekman layer load increases the maximum reworking depth to 0.01 cm for fine sand, to 0.1 cm for very fine sand, to 0.6 cm for coarse silt, and to 1.1 cm for medium silt. Maximum reference currents are about 30 cm/sec; higher currents would of course result in higher loads.

In summary, low swell in the presence of only small currents is relatively ineffective as a means of sediment transport. If only medium and coarser sand-sized grains are present, transport is likely to be limited to bedload. Silt-sized grains may be transported in moderately large quantities if currents are strong.

5.5 Results: Large swell

Occasionally on the continental shelf, the remnants of a large, distant storm will bring high, long period waves that generate substantial bottom velocities at all shelf depths. The case examined here is a 20 second wave generating bottom velocities of 60 cm/sec; such a wave would be 3.3 m high at 50 m water depth (Figures 5.16-5.19).

The most notable thing about these plots is their striking similarity to the corresponding plots for the moderate storm wave case (Figures 5.2-5.5). Since all stratification and grain size effects appear similar between the two, I comment

only on the relative magnitudes of the sediment concentrations, load, and transport values.

The $C(\delta_w)$ values are in general twice as high as those for the smaller wave, reflecting the increased turbulent energy in the wave boundary layer. As in the storm wave case, the effects of stratification dampen or wipe out most of the variation in load and transport predictions due to changes in $C(\delta_w)$.

In all cases, the higher wave bottom velocity generates larger load and transport predictions for the neutral case than for the moderate storm wave with a similar current velocity. This follows from the increased shear stress associated with the wave. In the stratified case, however, the increase in wave bottom velocity and excursion amplitude does not necessarily correspond to an increase in total load when the reference velocity is the same. (In comparing the plots, keep in mind that the velocity scales are not the same. In Figures 5.2-5.5, the top of the scale represents $u_r = 64\ cm/sec$. In Figures 5.16-5.19, the top of the scale represents $u_r = 72\ cm/sec$.) The change in load from the moderate storm case to the large swell case varies with grain size, and is strongly influenced by the stratification effect at the top of the wave boundary layer. For fine sand (Figure 5.16 and Figure 5.2), the larger wave causes an increase in load of about 50% when currents are strong. This is about the same increase seen for very fine sand (Figure 5.17 and Figure 5.3). The increase in load for coarse silt at high current velocities is about a factor of 2 (Figure 5.18 and Figure 5.4). The medium silt shows an increase of about a factor of about 4 (Figure 5.19 and Figure 5.5).

The magnitude of the increases gradually declines with lower current velocities in all cases. In the three coarsest sediments, the difference becomes very small at low velocities; in some cases the predicted load and transport are the same. The differences in predictions between grain sizes is also very small or nonexistent: the problem has again become dominated by stratification effects.

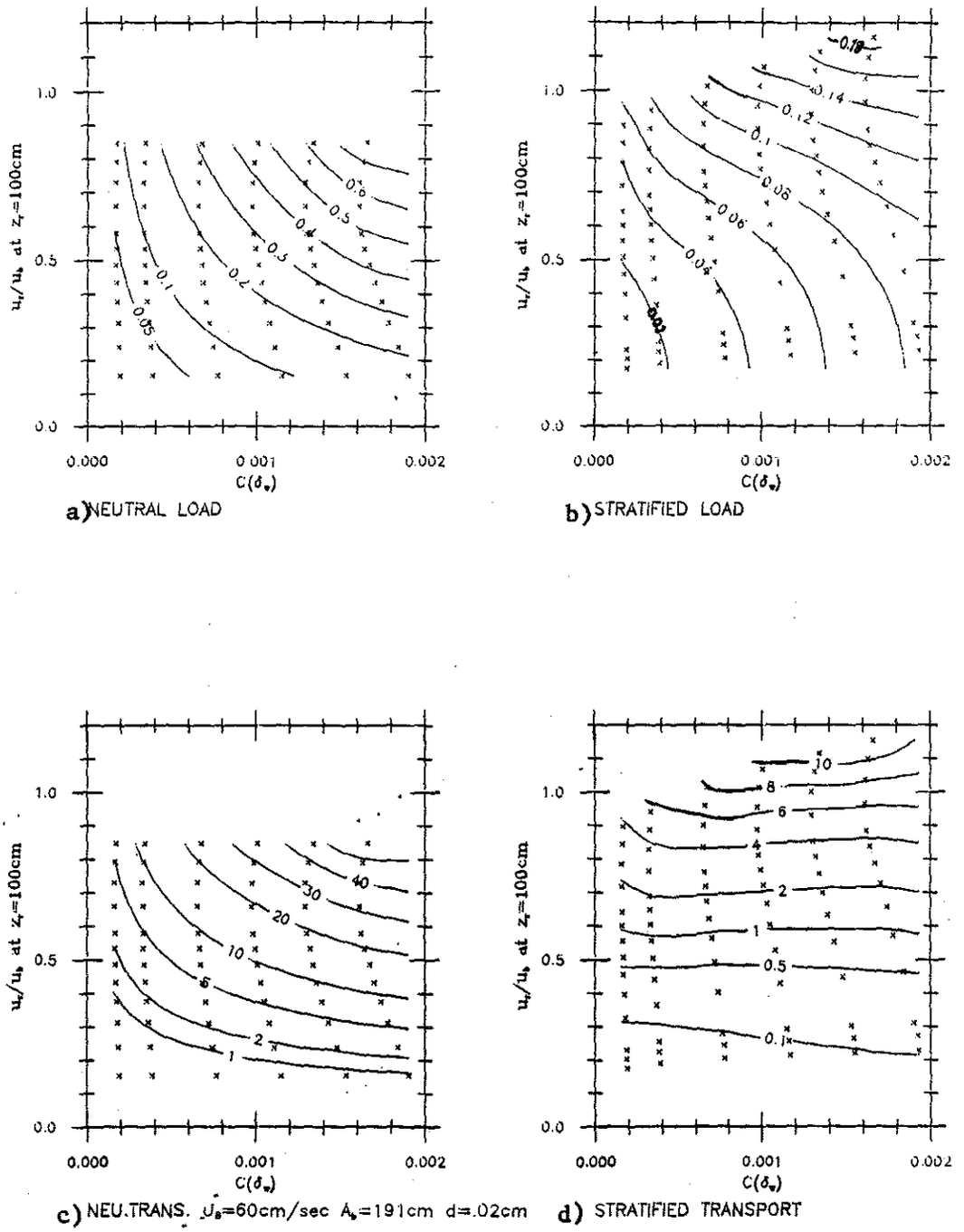

Figure 5.16: Predicted near-bottom load ($\frac{cm^3}{cm^2}$) and transport ($cm^3/cm/sec$) values for fine sand in large swell waves. T=20 sec, and the wave height in 50 m of water would be 3.3m. u_r is reference current velocity. δ_w ranges from 29-31 cm; $\frac{\delta_s}{d}$ ranges from 11 to 39 m.

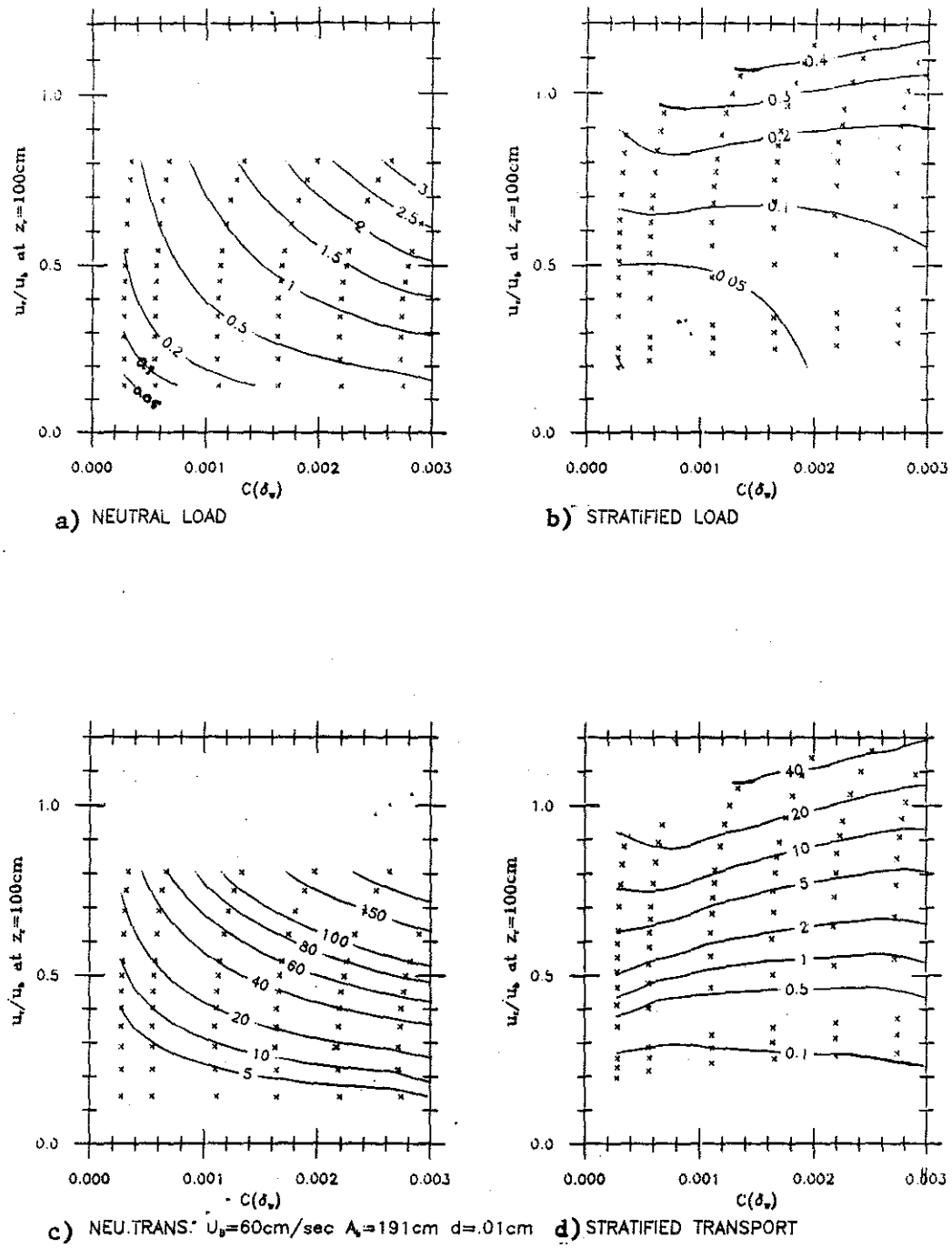

Figure 5.17: Predicted near-bottom load ($\frac{cm^3}{cm^2}$) and transport ($cm^3/cm/sec$) values for very fine sand in large swell waves. δ_w ranges from 22-24 cm; $\frac{\delta_a}{\delta}$ ranges from 7 to 32 m.

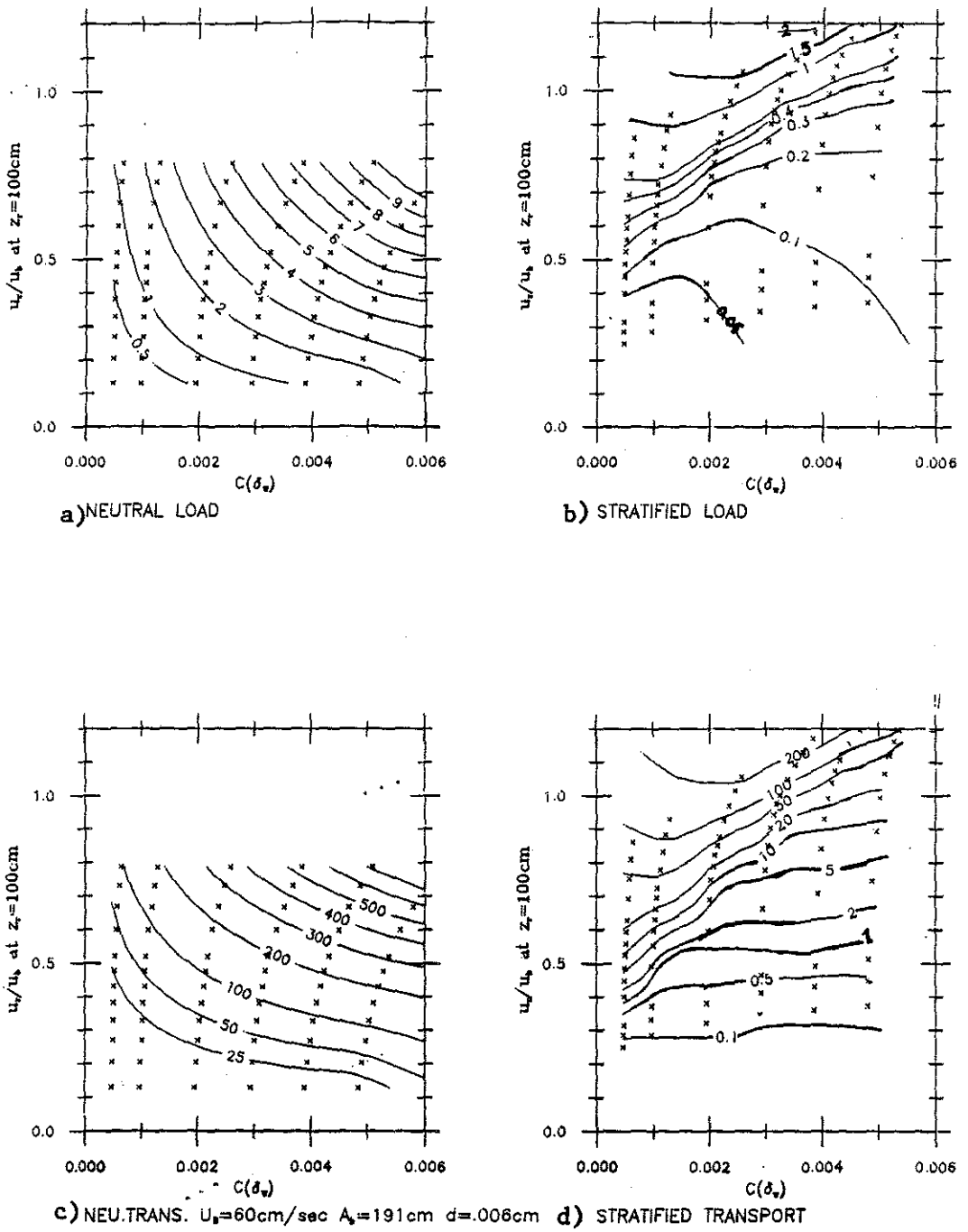

Figure 5.18: Predicted near-bottom load ($\frac{gm^3}{cm^2}$) and transport ($cm^3/cm/sec$) values for coarse silt in large swell waves. δ_w ranges from 17-21 cm; $\frac{\delta_a}{6}$ ranges from 6 to 29 m.

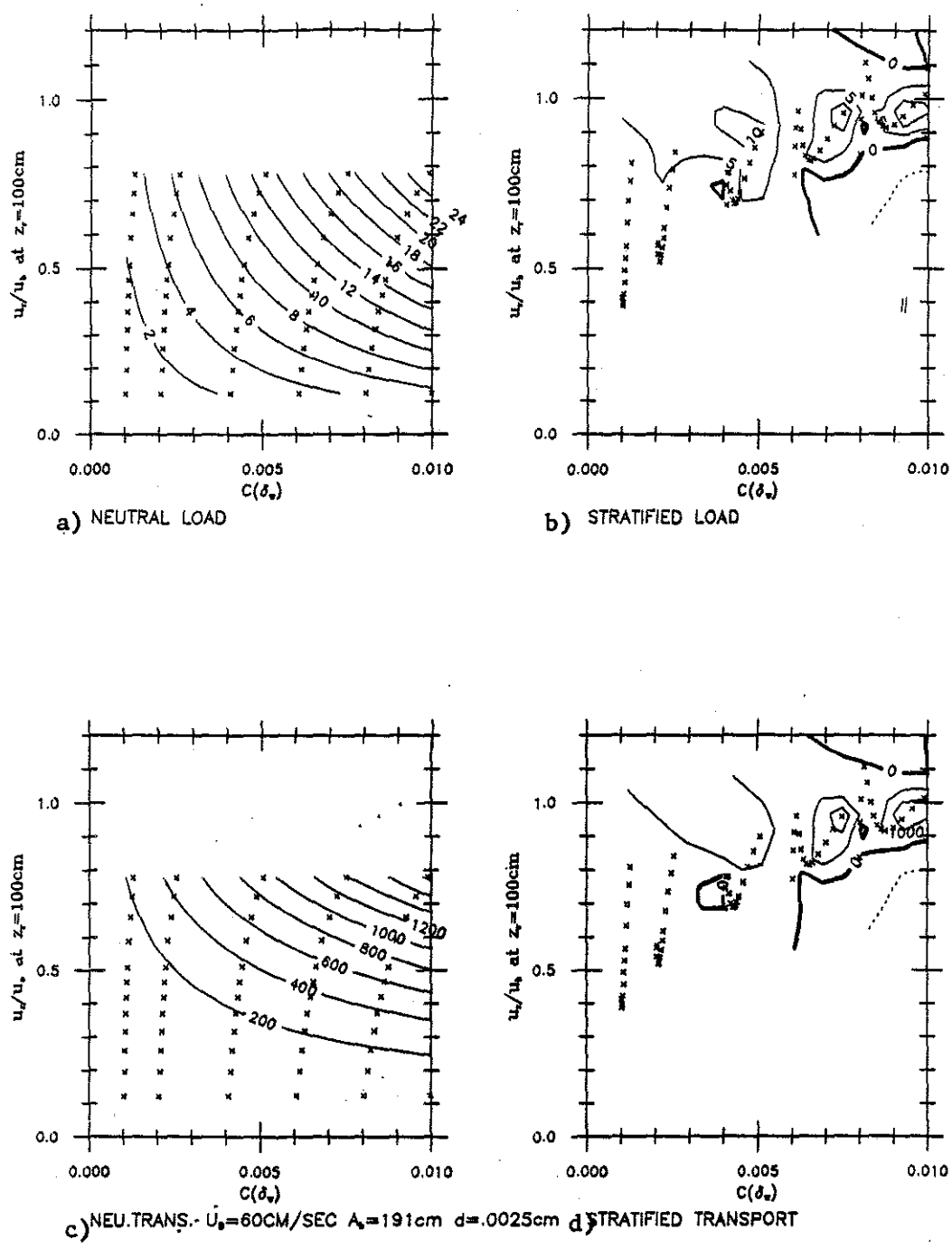

Figure 5.19: Predicted near-bottom load ($\frac{cm^3}{cm^2}$) and transport ($cm^3/cm/sec$) values for medium silt in large swell waves. The irregular contour patterns for the stratified plots occur in regions where the model gives non-unique solutions, as discussed in text. δ_w ranges from 14-21 cm; $\frac{\delta_a}{\delta}$ ranges from 5 to 28 m.

Ranges of reworking depths, Large swell Near-bottom load only		
$d(cm)$	neutral (cm)	stratified (cm)
0.02	0.027 - 1.29	0.015 - 0.32
0.01	0.062 - 6.44	0.015 - 0.95
0.006	0.22 - 20.45	0.025 - 3.89
0.0025	0.92 - 53.0	0.014 - 33.0

Table 5.7: Reworking depths for large swell, showing large decrease in ranges due to stratification effects. The maximum reworking depths for the neutral silt cases reflect the unrealistically high predicted concentrations discussed in the text.

Like the storm wave case, bedload transport is insignificant in this wave environment, approaching ten percent of the suspended transport volume only for the coarsest grains and the smallest currents. The larger reference concentrations yield even larger stratification effects on the outer Ekman layer load and transport estimates, so that for all but the smallest grain size, outer Ekman layer transport is less than 0.8 times the near-bottom transport, and outer Ekman layer load is less than 0.4 times the near-bottom load. The predicted outer Ekman layer load and transport values for medium silt are a factor of two to three greater than the near bottom values, however. The large values may be limited by factors such as water depth and bed armoring, so the model's results must be interpreted in light of local conditions especially in applications involving fine sediments in large storms.

The reworking depths due to near-bottom suspended load, including the effects of stratification, for the four grain sizes in this wave environment are very small for sands, always less than one centimeter (Table 5.7). In both the silt cases, the predicted concentrations are within expected limits in all but the strongest current velocities, which overcome much of the effect of stratification.

5.6 Results: General Wave Effects

The results discussed so far cover most of the patterns observed in the model runs for all eight wave cases. Plots of the other load and transport predictions are included in Appendix C. The present discussion summarizes those results.

The effects of waves on sediment transport can be most generally classified by bottom wave velocity, u_b. The ranges of predicted loads and transports (Tables 5.8-5.11) show that, for each 20 cm/sec increase in u_b, the maximum and minimum ranges for load and transport predictions increase by an order of magnitude when grain size is constant. The exceptions to this pattern of increase are due to strong stratification effects, also controlled by the wve bottom velocities. For example, a current of 30 cm/sec in wave conditions with a 10 second wave period and 20 cm/sec wave bottom velocities can suspend 0.02-0.1 cm^3/cm^2 from a silt bottom, depending on reference concentration (Figure C.3b); if the wave bottom velocity is 40 cm/sec, the load is 0.04-0.06 cm^3/cm^2 (Figure flgste3b). The approximate equality of the ranges is due to stratification effects: the ranges predicted by the neutral model are 0.02-0.2 cm^3/cm^2 for the smaller bottom wave velocity and 0.2-2.0 cm^3/cm^2 for the larger one.

The effect of period on sediment transport is smaller and less direct. The wave bottom velocity has direct control over shear velocity u_{*cw}, which controls the sediment motion directly (Equation 3.22). The wave period effect comes through the relation of the wave period to the height of the wave boundary layer (δ_w; Equation 2.4), and the relation of δ_w to the roughness length for the mean flow (z_{0c}; Equation 3.30). A shorter wave period generates a thinner wave boundary layer, which means less roughness is felt by the flow and the sediment load is expected to be slightly smaller. The response to change in period is barely visible in predicted load for silts for the neutral case (Figure C.7a versus Figure C.11a, as

Ub	Ab	T(sec)	d(cm)	load		transport	
				(max)	(min)	(max)	(min)
20.00	32.00	10.053	0.020	.7000E-02	.0000E+00	.2550E+00	.0000E+00
20.00	64.00	20.106	0.020	.5000E-02	.0000E+00	.1840E+00	.0000E+00
40.00	64.00	10.053	0.020	.7700E-01	.3000E-02	.4664E+01	.4000E-02
40.00	96.00	15.080	0.020	.1050E+00	.4000E-02	.6329E+01	.6000E-02
40.00	128.00	20.106	0.020	.1320E+00	.4000E-02	.7992E+01	.7000E-02
60.00	144.00	15.080	0.020	.1740E+00	.7000E-02	.1207E+02	.1100E-01
60.00	191.00	20.001	0.020	.1900E+00	.9000E-02	.1233E+02	.1500E-01
100.00	319.00	20.043	0.020	.1048E+01	.2300E-01	.1321E+03	.5600E-01

Table 5.8: Ranges in predicted values of stratified near bottom load and transport for fine sand ($d = 0.02\ cm$). Predictions are grouped by wave bottom velocity. Load units are $\frac{cm^3}{cm^2}$; transport units are $cm^3/cm/sec$

Ub	Ab	T(sec)	d(cm)	load		transport	
				(max)	(min)	(max)	(min)
20.00	32.00	10.053	0.010	.7100E-01	.0000E+00	.4515E+01	.0000E+00
20.00	64.00	20.106	0.010	.4500E-01	.0000E+00	.2462E+01	.0000E+00
40.00	64.00	10.053	0.010	.1980E+00	.2000E-02	.1552E+02	.7000E-02
40.00	96.00	15.080	0.010	.2130E+00	.3000E-02	.1599E+02	.1000E-01
40.00	128.00	20.106	0.010	.2340E+00	.4000E-02	.1723E+02	.1300E-01
60.00	144.00	15.080	0.010	.6280E+00	.7000E-02	.7076E+02	.2000E-01
60.00	191.00	20.001	0.010	.5710E+00	.9000E-02	.5865E+02	.2300E-01
100.00	319.00	20.043	0.010	.4718E+01	.3900E-01	.1162E+04	.1730E+00

Table 5.9: Ranges in predicted values of stratified near bottom load and transport for very fine sand ($d = 0.01\ cm$). Predictions are grouped by wave bottom velocity. Load units are $\frac{cm^3}{cm^2}$; transport units are $cm^3/cm/sec$

Ub	Ab	T(sec)	d(cm)	load		transport	
				(max)	(min)	(max)	(min)
20.00	32.00	10.053	0.006	.1330E+00	.0000E+00	.7377E+01	.1000E-02
20.00	64.00	20.106	0.006	.1380E+00	.0000E+00	.7216E+01	.0000E+00
40.00	64.00	10.053	0.006	.6750E+00	.4000E-02	.7065E+02	.1900E-01
40.00	96.00	15.080	0.006	.5800E+00	.5000E-02	.5495E+02	.2200E-01
40.00	128.00	20.106	0.006	.5530E+00	.6000E-02	.4966E+02	.2500E-01
60.00	144.00	15.080	0.006	.2814E+01	.1400E-01	.5079E+03	.8300E-01
60.00	191.00	20.001	0.006	.2332E+01	.1500E-01	.3798E+03	.7600E-01
100.00	319.00	20.043	0.006	.2134E+02	.9300E-01	.8705E+04	.1297E+01

Table 5.10: Ranges in predicted values of stratified near bottom load and transport for coarse silt ($d = 0.006\ cm$). Predictions are grouped by wave bottom velocity. Load units are $\frac{cm^3}{cm^2}$; transport units are $cm^3/cm/sec$

Ub	Ab	T(sec)	d(cm)	load		transport	
				(max)	(min)	(max)	(min)
20.00	32.00	10.053	0.002	.3870E+00	.2000E-02	.2078E+02	.1200E-01
20.00	64.00	20.106	0.002	.3440E+00	.2000E-02	.1622E+02	.8000E-02
40.00	64.00	10.053	0.002	.5961E+01	.2300E-01	.9591E+03	.2990E+00
40.00	96.00	15.080	0.002	.4582E+01	.1900E-01	.6652E+03	.2160E+00
40.00	128.00	20.106	0.002	.3861E+01	.1800E-01	.5217E+03	.1830E+00
60.00	144.00	15.080	0.002	.2345E+02	.1020E+00	.6220E+04	.2464E+01
60.00	191.00	20.001	0.002	.1978E+02	.8800E-01	.4945E+04	.1845E+01
100.00	319.00	20.043	0.002	.1274E+03	.7550E+00	.8944E+04	.4288E+02

Table 5.11: Ranges in predicted values of stratified near bottom load and transport for medium silt ($d = 0.0025\ cm$). Predictions are grouped by wave bottom velocity. Load units are $\frac{cm^3}{cm^2}$; transport units are $cm^3/cm/sec$

marked). The predicted load rises somewhat for the stratified case with increasing period.

5.7 Summary

The sensitivity analysis has brought to light a number of considerations which should be kept in mind when applying the Grant-Madsen-Glenn model to questions of sediment transport and when interpreting the model's results. With these results in hand, the boundary layer model can be a useful geological tool; if the model is applied blindly it may be misleading and, in some cases, simply will not work.

The conclusions can be cast in terms of physical conditions at the seafloor under which caution should be used in applying the model:

- Large wave bottom velocities ($\geq\sim 40\frac{cm}{sec}$), especially when near-bottom currents are small ($\leq\sim 10\frac{cm}{sec}$), cause stratification effects which reduce load predictions by 50% or more. These predictions require field verification.

- Large wave bottom velocities occurring where the seafloor surface grains are silt sized or finer may lead to nonunique solutions to the stratified boundary layer model, depending on specified reference velocity. The predicted sediment load and transport may vary by an order of magnitude for the different solutions. If the model's representation of stratification is correct, this nonuniqueness requires specification of another boundary condition, either a current velocity higher in the water column or a suspended sediment concentration measurement.

- Large bottom currents ($\geq\sim 30\frac{cm}{sec}$ at $z = 1m$) can suspend sediments to heights in the water column greater than the near-bottom layer on which this model focuses. When estimates of load and transport volumes in the

outer Ekman layer are greater than or equal to the near bottom volumes, the model's predictions of total transport are less certain.

- In a related concern, the predicted bottom Ekman layer depth based on mean shear velocity can exceed the water column depth in strong current flows. If so, the outer Ekman layer predictions should be discarded.

- If wave shear stress is insufficient to move sediment without current input, then there exists a set of input conditions on which the model will not converge when grain roughness is used as the roughness length. In this case, a more realistic representation of roughness, based on existing bedforms, should be used instead of the moveable bed roughness.

- When grain sizes are large, bedload may be a significant factor in total transport. This model provides bedload estimates, but they should be used only for estimating the significance of bedload transport on a given shelf under given circumstances. If bedload is determined to be the primary transport mechanism, a transport model which focuses on bedload should be used.

The controlling influence of stratification on sediment load and transport that is predicted for large wave bottom velocities has important implications for sedimentology. In limiting upward transport of sediment from the seafloor, it could explain why storms do not move more sediment than they do. The stratification model requires testing and verification, however, before extensive application to geological questions is warranted. The next chapter provides some examples of ways the model can be used to explore patterns of sediment transport and deposition.

Chapter 6

Application of Model to Continental Shelves

By using input parameters from observed conditions on continental shelves, the boundary layer model is used here to make predictions about net sediment transport. The applications are to some extent an extension of the sensitivity analysis to two dimensions. A box model is applied to an area representing an idealized continental shelf. The box is used to determine the influence on net sediment transport exerted by variations of single parameters along and across the shelf. Input parameters are based loosely on observed shelf configurations and storm conditions, and results are discussed with respect to both observed patterns of deposition mechanics of the model.

The applications serve to suggest the usefulness of the model in explaining patterns of transport and deposition, but I emphasize that they are not meant to explain deposition patterns on the specific continental shelves considered. The climatological data and numerical modelling efforts required for such a project are beyond the scope of this work.

The four-point box model used to make estimates of net transport was described briefly in Section 3.4. Recall that the net transport rate for the area of the box is calculated by averaging the orthogonal components of the transport vector at each corner across the sides of the box, then summing the transport into and out of the box. If more sediment is entering the box than is leaving it, there is net

deposition; if more sediment is leaving, there is net erosion. The deposition rate for the box is determined by averaging the volume of net transport over the area of the grid square. The average reworking depth is the average of the values at the four corners, including both the near-bottom and outer Ekman layer predictions. This quantity represents the total volume of sediment moved by the waves and currents. Adding the reworking depth to the net transport for the duration of the storm gives the total depth to which sediment is affected by the storm.

In order to gauge the effects of specific parameters on deposition, the physical scenario is simplified. The continental shelf is considered in cross section, conceptualized as a series of boxes at intervals of ten meter changes in water depth (Figure 6.1). The x-direction is taken to be cross-shelf, and the unit length (Δx) is determined by the slope of the shelf. The y-direction is alongshelf, and the length of the box side in the y-direction (Δy) is taken to be the same as that in the x-direction. Note that adjacent boxes are autonomous; there is no assumption that what happens in one square in any way affects an adjacent square.

The directions of the wave and current (θ_w and θ_{cur}) are given with respect to the alongshelf direction, which is taken to be zero degrees. The angle between the wave and the current (ϕ_c) is the smallest angle between the direction of the wave and the direction of the mean bottom flow, so ϕ_c is at most ninety degrees. The effects of wave refraction on θ_w are not taken into account, so that the effects of wave shoaling on bottom velocity and excursion will be isolated; the influence of wave direction is small. The value of γ_0 is taken to be 0.002 in all cases.

The boxes in Figure 6.1 begin at a depth of thirty meters. This is because, for the storm cases considered here, shallower depths tend to have full Ekman depths greater than thirty meters; certainly the surface and bottom Ekman layers overlap, and this is a complication not addressed in this simple model. The offshore depth limit is constrained only by the depth at which sediment is no longer mobilized,

which is in turn controlled by the depth of influence of the wave (Section 5.1).

Depth contours are assumed to run alongshelf, so there is no variation in depth in the y-direction. This translates to no variation in the bottom wave parameters (u_b, A_b) with y. The ten meter variation in water depth introduces a significant change in bottom wave parameters in the x-direction, however, and the net transport introduced by this variation will be the focus of this discussion. Variation in wave parameters introduces no net transport in and of itself, of course, since the GMG model is based on a linear wave assumption; transport is carried out by the mean current, so if there is no current, there is no net transport. If the only variation in parameters is in the x-direction (e.g. depth change, variation in grain sizes across shelf) and all flow is alongshelf, there is transport but no *net* transport, since the same volume of sediment which flows into the square also flows out at the other end. If hydrodynamic and sedimentological parameters vary only perpendicular to the flow, then their variation will not contribute to the net transport of sediment.

In the presence of a cross-shelf component to the near-bottom mean flow, the variation in bottom wave parameters with depth can effect net transport by several means. The most obvious is the increasing bottom velocity of waves, due to shoaling. The maximum shear stress is expected to decline, so the sediment made available for transport by the current would also decline. The expected transport pattern in the presence of an offshore component of current would be a progressively declining offshore transport resulting in a net deposition of sediment at all locations where sediment was put in motion. To illustrate this point, consider Figure 6.1. For the same crosshelf current component at all depths, assumed directed offshore, the average offshore transport into a box at a depth of thirty meters would be greater than the transport out of the box at forty meters, since the wave bottom shear stress is smaller at the deeper location. Since more enters than leaves, this situation would result in deposition. The same would be true for each of the

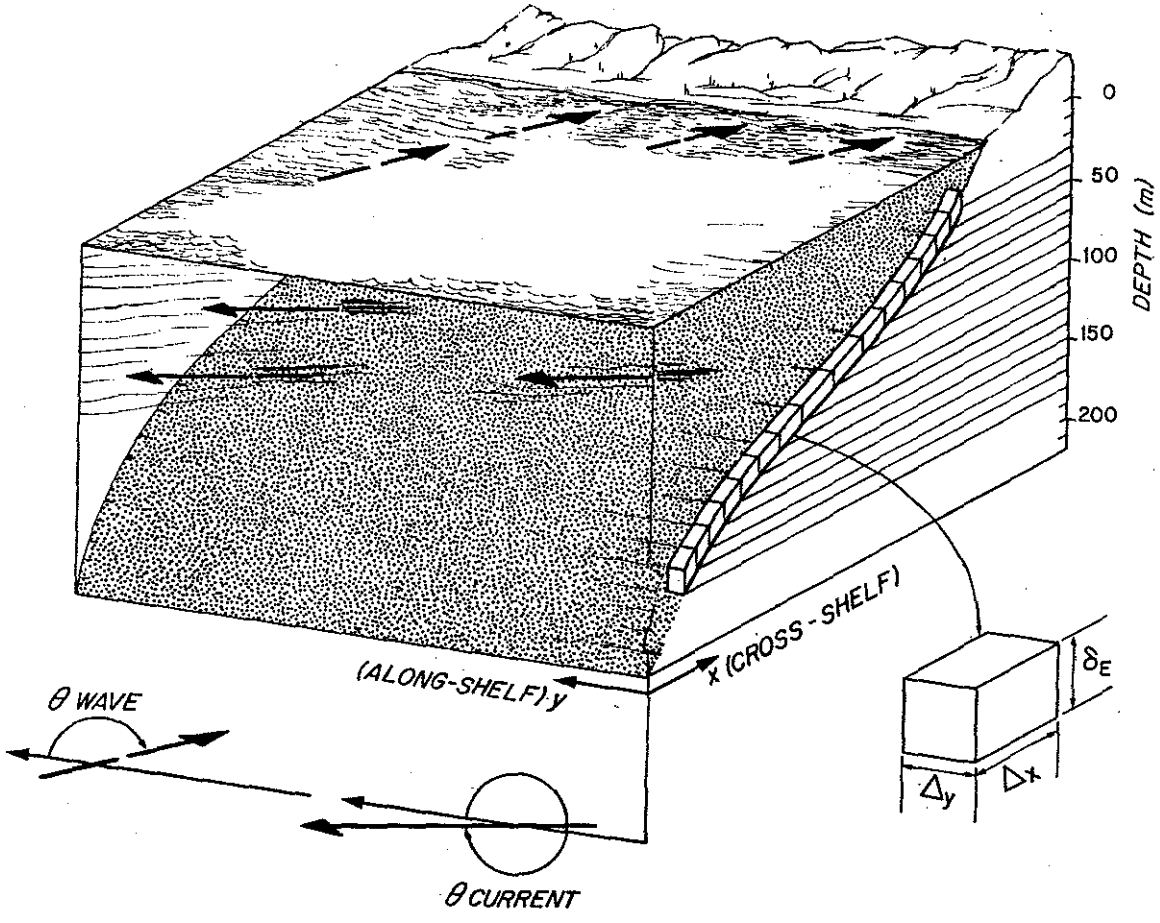

Figure 6.1: Schematic diagram of grid squares used to represent the continental shelf in cross section, beginning at a depth of thirty meters and extending across the shelf at depth intervals of ten meters. Scale in the x-direction (cross-shelf) determined by slope of shelf; scale in y-direction determined by alongshelf changes in input parameters, or by x-scale. Wave and current directions specified with respect to alongshelf direction.

other, deeper, boxes. In this situation, the only question is the amount of expected deposition. In the discussion which follows, this pattern of deposition is referred to as the 'expected' pattern.

As the sensitivity analysis showed, waves affect two other parameters important to sediment transport: bed roughness and sediment stratification. Wave shear stresses can create ripples; stronger stresses can wash them out. The lower roughness under larger wave velocities can lead to situations where the enhancement of sediment transport by waves is smaller at shallower depths than deeper. Likewise, stratification effects can be stronger under larger waves (see Section 5.3), which would also lead to a decrease in suspended sediment transport at smaller depths. These factors tend to counter the 'expected' pattern of wave effects described in the last paragraph. The significance of each one for deposition and erosion patterns is not obvious, however. The applications below explore some possible variations.

To exercise the model in a quasi-realistic way, net transport is estimated for areas of the continental shelf modelled on the mid-Atlantic region of the east coast of the U.S. and a region of the northern California coast where wave, current, and sediment conditions are reasonably well understood. These two shelves are used because they constitute a pair of very different shelf environments themselves, but contain features which are common to many shelves worldwide; each has been closely studied in recent years, with data including extensive near-bottom measurements of wave, current and sediment conditions. That data is the source for the storm conditions used in the model runs.

6.1 Mid-Atlantic Bight shelf type

The Mid-Atlantic Bight, encompassing the area north of Cape Hatteras and south of Cape Cod (Figure 6.2), is typical of continental shelves on passive continental

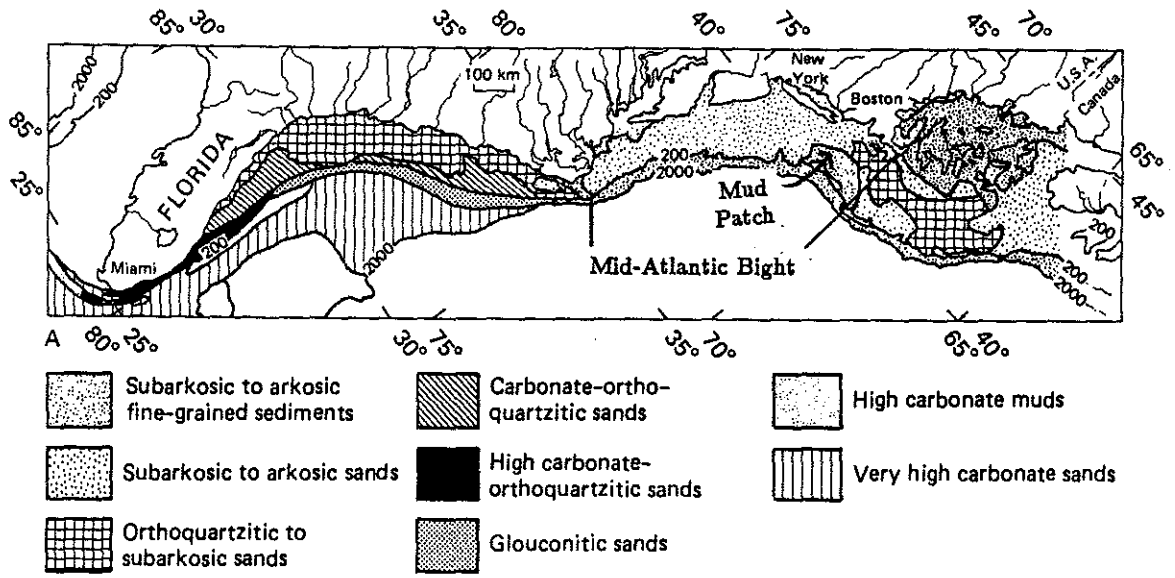

Figure 6.2: The Atlantic Continental shelf, showing the distribution of grain sizes and types. The Mid-Atlantic Bight is marked, and the location of the silty 'Mud Patch' area is shown. The 200m coutour shows the approximate location of the shelf edge (from Milliman et al., 1972).

margins. It is wide in most places, widening from about 23 km at Cape Hatteras to 150 -170 km off New Jersey and Cape Cod. Depth contours are generally shore-parallel. The shelf break is close to the world average of 130 m, and the average bottom slope ranges from about 5×10^{-3} to 3×10^{-4}. Outside of a few estuarine areas, the entire Atlantic margin, from Canada to Florida, is covered with sand-sized material, mostly relict from lower stands of sea level. The single exception is a region south of Cape Cod in water depths of sixty to one hundred meters where silt- and clay-sized grains make up 25 to 75 per cent of the surface bed material (Shepard and Cohee, 1936; Bothner, et al, 1981). It is referred to locally as the 'Mud Patch'.

Under everyday, non-storm conditions on the mid-to-outer Atlantic continental shelf, sediment does not move. Away from nearshore regions, tidal currents and mean flows are typically less than 10 cm/sec (Butman, 1987a). Waves are locally wind-generated; exclusive of storms they are too small to generate bottom velocities sufficient to move the coarse sediment typical of this margin. Using bottom pressure observations collected between 1975 and 1980 at depths of 60 and 80 meters on Georges Bank and at 80 meters in the Mud Patch, Butman (1987a) determines that maximum wave bottom velocities are almost never greater than 10 cm/sec during the summer months, and reach that velocity only one per cent of the time in the fall and five per cent of the time in spring. The winter is characterized by about two storms per month, however, and Butman suggests that wave-generated bottom velocities are greater than 10 cm/sec up to 15 per cent of the time in winter. Not even the silts of the Mud Patch, and certainly not the medium to coarse sands which make up the bulk of the surface sediment on the Atlantic continental margin respond to wave and current velocities less than 10 cm/sec. We therefore focus on representative storm conditions.

In studies from 1976 through the present, Butman has been measuring near-bottom conditions on the mid-Atlantic shelf, often in conjunction with physical oceanographic studies of shelf circulation (see, e.g. Butman, 1987a, 1987b; Butman, et al, 1979). Butman's data suggest that sediment resuspension is highly correlated with storm activity (Butman, 1987a). Sediment as coarse as fine sand has been found in sediment traps as high as three meters above the bottom (Parmenter, Bothner and Butman, 1983), and suspended sediment concentrations of at least 10 and perhaps 50 mg/l (equivalent to volumetric concentrations of 4×10^{-6} to 2×10^{-5}) have been observed at heights of two meters above the bottom (Butman, 1987a).

Storms affecting the mid-Atlantic shelf generally follow one of two patterns:

1) winds blow from the south, shifting to southwest over the course of the storm, setting up bottom currents which are generally alongshelf toward the north with a slight offshore component; or 2) winds blow from the northeast, shifting to northwest, setting up bottom currents which flow generally alongshelf toward the south, with a small offshore component (Butman, 1987b). Wave direction is likewise controlled by local winds. Storm effects last up to about three days.

These observations of shelf and storm conditions provide guides to the input conditions to this model and interpretations of results for the first application. It is to be emphasized that these are not specifically results for any location on the Atlantic continental margin, but are meant to illustrate the application of the techniques developed here as they can be applied to that margin or one like it.

Application One: Large storm, single grain size bed

The first application of the boundary layer model to a continental shelf uses wave and current conditions observed during a large storm on the Atlantic continental shelf. The seafloor is assumed to be covered with sediment of a single grain size. The range of water depths covered is thirty to one hundred meters, in a series of seven grid squares, each eighteen kilometers on a side and each spanning a ten meter change in water depth (Figure 6.3). This box configuration corresponds to a slope of 0.055 %. The wave and current conditions used are modeled after data collected in February, 1978, by Butman (1987a). This period represents an extreme winter storm for this region; the storm is locally referred to (still) as the 'Blizzard of '78' (always capitalized). The mean current was approximately 32 cm/sec for the duration of the storm, and had a cross-shelf component near the bed of about 5 cm/sec. This translates to a current direction of 161°, where 0° is the alongshelf direction. Since waves are wind-generated and the wind in this storm blew initially out of the northeast, a direction of 225° is used for the wave. The wave conditions

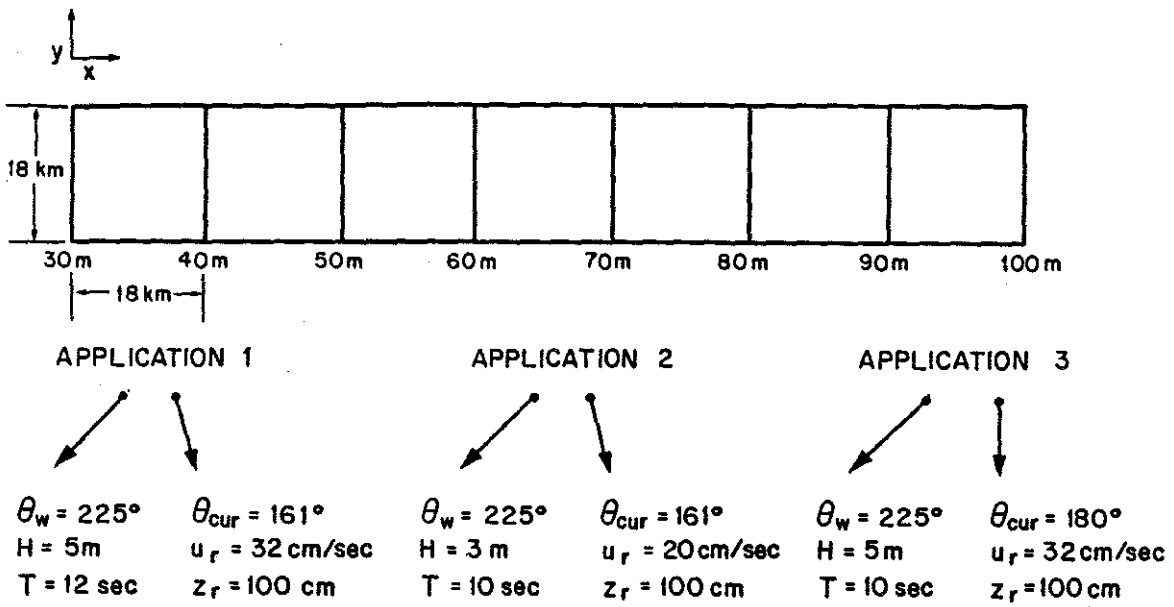

Figure 6.3: Schematic diagram of grid representing the Mid-Atlantic Bight continental shelf, and wave and current conditions used in applications described in text

over approximately three days sustained heights of five meters with twelve second periods. The model was run for each of four grain sizes ranging from medium silt to medium sand.

The results are shown in Figure 6.4. A lot of information is packed into each graph, so the format is explained in some detail here. Each part (a,b,c,d) of the figure shows the predictions for a single grain size for a row of seven boxes across the shelf, from thirty to one hundred meters water depth. The total deposition rate (or erosion rate if the value is negative), in cm/hr, is shown for each grid square in the left-hand bar graph, and repeated in the right-hand list. The other three bar graphs show the proportion of the total deposition rate attributable to each of the three contributions (bedload, near-bottom, and outer Ekman layer transports). A transport rate of 4×10^{-4} cm/hr translates to a net accumulation of about 0.1 mm/day. The average reworking depth is listed, suggesting gross transport through the square, as opposed to the net transport represented by deposition

rates.

The variation of wave parameters with water depth *can* introduce net cross-shelf transport in the presence of a steady current with even a small cross-shelf component. However, the depositional patterns vary dramatically from the intuitively 'expected' pattern of net deposition in all boxes. Particularly in the sand cases, the decrease in bottom wave velocity with depth leads to increase in roughness, because waves strong enough to wash ripples out at one depth are only strong enough to create ripples in water ten meters deeper. Predicted transport out of the box at the deeper end is thus increased relative to input at the shallower end. This can be augmented by a larger sediment stratification effect at the shallower end of the box, which limits input. The stratification effect dominates in silt cases. Recall that the deposition rates represent only cross-shelf transport; exactly as much sediment enters the square from the north as leaves toward the south, since there is, by assumption, no alongshelf variation in any parameter.

To illustrate the effects of stratification and roughness on the net transport predictions, two sets of results will be examined in more detail and related to the sensitivity results. First, we examine the strip from fifty to seventy meters depth in the medium sand case (Figure 6.4a). In the box covering fifty to sixty meters depth, a net erosion of 1×10^{-4} cm/hr (0.02 mm/day) is predicted; deposition of 1.3×10^{-4} cm/hr is predicted for the sixty to seventy meter box. This change results primarily from moveable bed roughness effects due to the change in maximum wave bottom velocity from 59 cm/sec to 36 cm/sec from 50 to 70 meters, and in wave excursion amplitude A_b from 113 to 68 cm over that distance. The skin friction shear stress is approximately equal to the breakoff value (Equation 3.55) at fifty meters, but lower than the breakoff value at sixty meters; wave-generated ripples are therefore washed out at the shallower depth, but not at the deeper location (see Section 3.3). The value of the boundary roughness z_0 is 0.8 cm at fifty meters

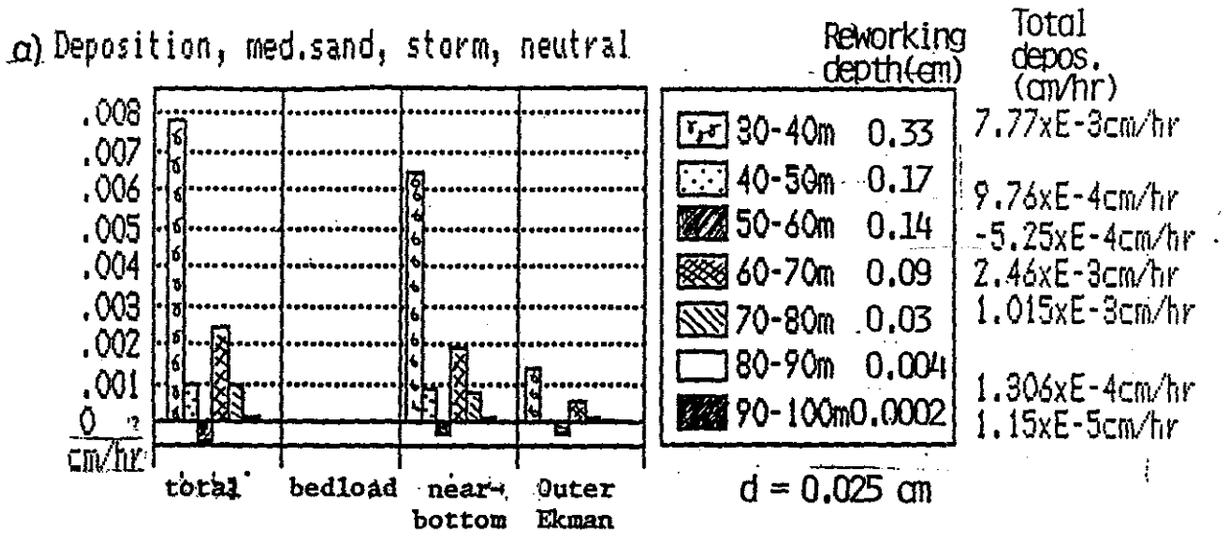

Figure 6.4: Predicted deposition/erosion rates and reworking depths for single-grain-size shelves, with shelf and storm description derived from conditions typical of continental shelf of the Mid-Atlantic Bight. Grid is shown in Figure 6.3.
$H = 5m, T = 12s, \theta_w = 225°, u_r = 32\ cm/sec, \theta_{cur} = 161°$
(a) Results for medium sand show variable deposition rates across the shelf, ranging no higher than 0.05 mm/day. Variation is due in large measure to variation in bed roughness. Very little variation in reworking depths is evident. Motion ceases at 100 m.

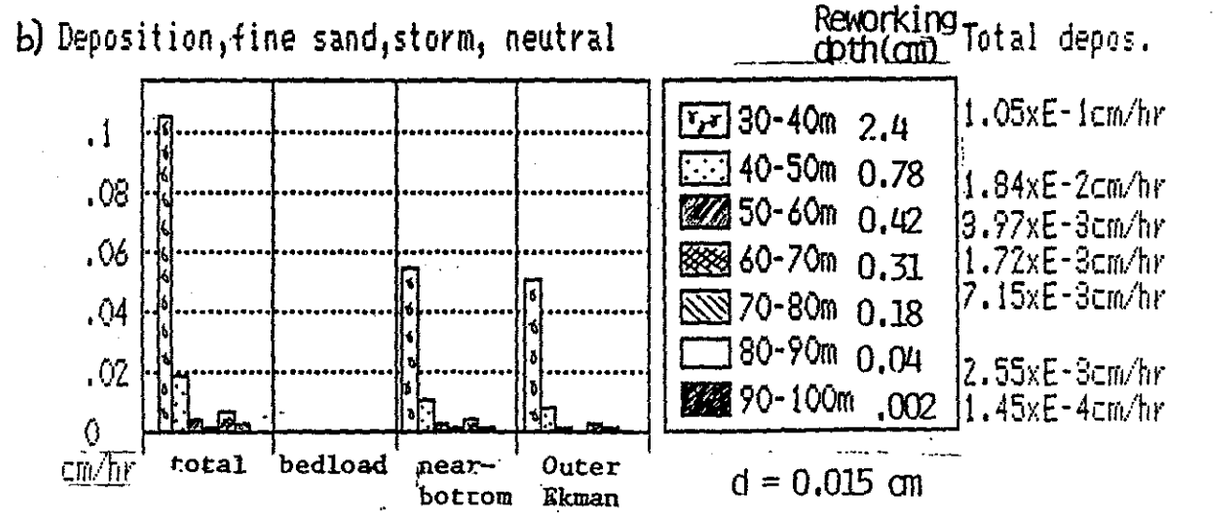

(b) Results for fine sand show deposition/erosion rates and reworking depths no higher than 0.3 mm/day, with variation due to roughness and stratification. Motion ceases at 100 m.

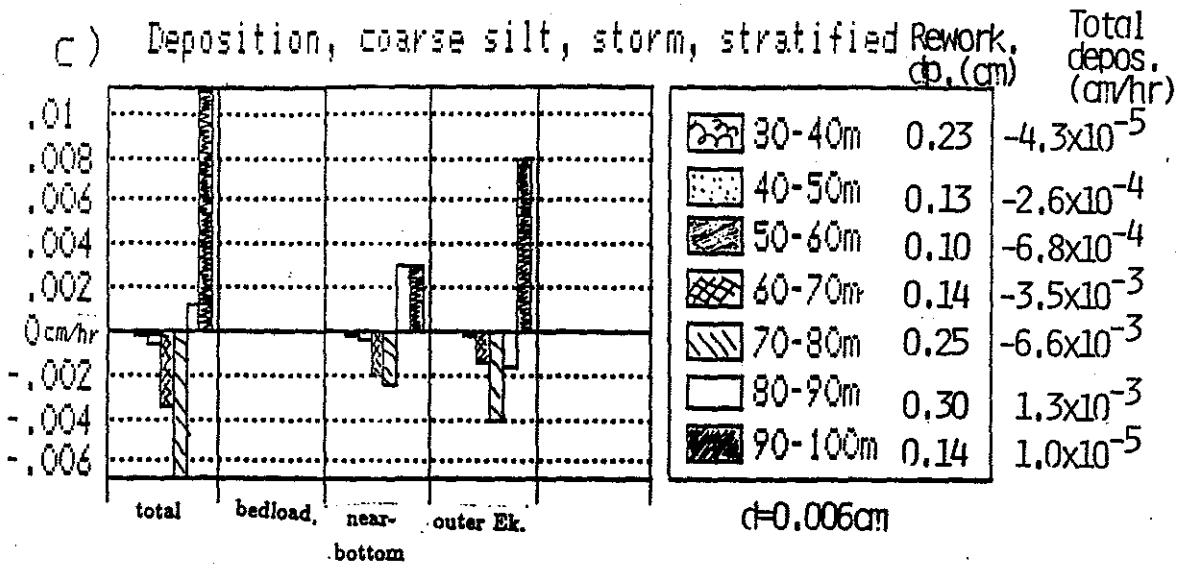

Figure 6.4: (c) Results for coarse silt show net transport rates generally increasing with depth, with erosion as high as 1.5 mm/day on the central shelf and deposition as high as 0.5 mm/day only 10-20 m deeper, as effects of stratification decline with wave strength in deeper water. Motion ceases at 100 m, leading to the large (and questionable) outer Ekman layer deposition in the deepest box.

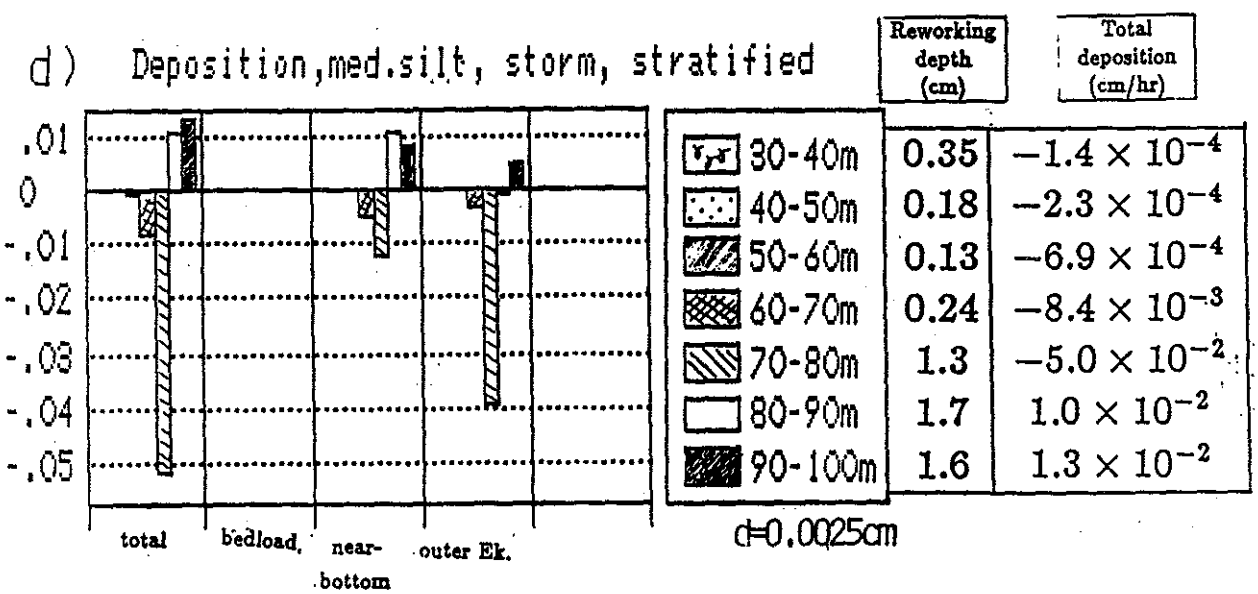

(d) Results for medium silt show similar effects of depth and stratification as the coarse silt case, with erosion as high as 2.5 mm/day. The largest predicted erosion results from an ambiguous stratification effect, discussed in text. Motion ceases at 110 m. Stratification effects limit reworking and net erosion to relatively small volumes on inner shelf.

and 1.8 cm at sixty meters, representing a change in ripple steepness ($\frac{\eta}{\lambda}$) from 0.08 to 0.13 as predicted using the Grant and Madsen (1982) moveable bed roughness model.

Because of the increased roughness, the wave-current shear velocity u_{*cw} is greater at sixty meters than at fifty meters, even though the maximum wave bottom velocity u_b drops from 59 to 46 cm/sec. The larger u_{*cw} increases the predicted load and transport in two ways. First, more sediment can be transported to the top of the wave boundary layer, so the current has more sediment available to suspend. Second, more low-momentum fluid is transported upward, so the wave-enhanced roughness felt by the mean flow (z_{0c}; Section 3.3) is greater. In this case, z_{0c} increases from 8 cm to 10 cm between fifty and sixty meters depth. The increase in roughness at sixty meters depth thus generates the conditions which lead to net erosion between fifty and sixty meters. By contrast, roughness lengths at sixty and seventy meters are approximately equal, so the expected pattern holds: the decrease in maximum wave bottom velocity leads to decreases in wave shear velocity, current roughness length, sediment concentration at the top of the wave boundary layer, and total load and transport. The transport into the box at sixty meters depth is therefore greater than the transport out at seventy meters, so there is net deposition.

The net erosion predicted between sixty and seventy meters on a shelf covered with medium silt (Figure 6.4d) is due to stratification effects, rather than roughness. The physical roughness lengths (z_0) at the two depths are nearly equal: 0.028 cm at sixty meters vs. 0.022 cm at seventy meters, reflecting ripple heights of less than a centimeter. The larger wave bottom velocities at the shallower location therefore lead to a concentration at the top of the wave boundary layer which is twice as large at sixty meters as at seventy. Recall from the sensitivity analysis discussion of stratification effects (Section 5.3.2) that an increase in $C(\delta_{cw})$ of a factor of two

could generate a substantial decrease in predicted transport by a given current due to increased stratification effects (Figure 5.5d). Stratification therefore limits transport into the box at sixty meters more than it limits transport out at seventy meters, and erosion results.

Under a large wave, large current and small grain size conditions of the sensitivity analysis results suggested caution, since results could be ambiguous. The sudden increase in reworking depth from 0.24 cm to 1.3 cm between the 60-70 meter box and the 70-80 meter box suggests that this case should be investigated (Figure 6.4d). Examination of the model results for that box reveals that this wave and current case at seventy meters has a non-unique solution (Section 5.3.2). The model converged on one solution at seventy meters for the shallower box, and a different solution for the deeper box. At 70 m in the 60-70 meter box, the predicted current shear velocity u_{*c} is 0.97 cm/sec, the predicted reworking depth is 0.35 cm and total predicted transport is 9.3 $cm^3/cm/sec$. At 70 m in the 70-80 meter box, stratification is less effective in reducing turbulence, and the predicted parameters are 1.3 cm/sec for current shear velocity, 0.85 cm predicted reworking depth, and 31.6 $cm^3/cm/sec$ predicted transport. The net transport rates are not affected by the inconsistency: either result gives erosion in each box. However, this example demonstrates again that caution must be used in applying this model to fine grain sizes in storm situations until field applications have resolved some of the uncertainties and refined the model, most importantly the treatment of stratification.

Stepping back from these detailed examinations of the mechanics of the theoretical model, some useful observations can be made about net transport in storms. The deposition and erosion rates in Figure 6.4 would introduce net erosion and deposition of a few tenths of a millimeter to a few millimeters over the course of a single, three-day storm. The exceptions are the deepest boxes in the silt cases, where a two-day storm might lead to one to two cm of erosion or deposition. In

the coarse silt case, this results because the deepest box has no sediment motion predicted at its offshore edge. This is the reason for large deposition rates at the offshore edge of a number of the profiles, particularly for fine sediments.

Comparison of deposition rates at similar depths shows a tendency for net transport rates to rise with decreasing grain size, especially in the deeper boxes where stratification effects are less limiting to silt resuspension. Stronger stratification effects where wave velocities are greater (i.e. shallower depths) explain the consistent erosion of silts in the shallower areas. Stratification effects keep the magnitudes of the total deposition rates fairly similar between grain sizes, though there is a slight tendency for net transport rates to rise with decreasing grain size. Reworking depth increases fairly consistently with decreasing grain size. The exceptions to this pattern follow from the observations in the sensitivity analysis that in some storm situations, load (and therefore reworking depth) is nearly independent of grain size.

Bedload transport is insignificant in every case, and near-bottom transport is more significant than outer Ekman layer transport in most cases. When outer Ekman layer transport is significant, however, net transport rates are suspect. The poor constraints on the outer Ekman transport direction could cause large errors.

For contrast, the predictions for the neutral case are shown in Figure 6.5. The pattern of deposition is much closer to the expected one: in general, there is net deposition in each box, decreasing in magnitude with depth. This pattern is changed only by roughness effects, most notably in the 50-60 meter box in the medium sand case where erosion is predicted (Figure 6.5a). This predicted erosion results from the same variation in roughness as in the stratified case discussed above, although the erosion rate is five times as great in the neutral case. The occurrence of an erosional region and the irregularity in deposition rates across the shelf for the sand cases testify to the significance of moveable bed roughness in combined

wave-current flows.

In general, the deposition rates are at least a factor of two, and more often an order of magnitude or more, greater when the effects of stratification are neglected. The same holds true for reworking depths. Stratification effects generally increase with smaller depths and smaller grain sizes, as discussed in the sensitivity analysis, where smaller depths correspond to larger waves.

A word should be said about the plausibility of some of the neutral case predictions listed. They have been included simply as predicted by the model, using it as a 'black box' for input and output; the results must be interpreted in light of known physical conditions. The reworking depths predicted for silt-sized grains are impossible, extending over a meter in some cases and over ten meters in one case (Figure 6.5c and d). The accompanying transport rates would build small mountains on the seafloor over the course of a storm, and predicted sediment concentrations as high as twenty meters above the seafloor are on the order of 10^{-2}, which is impossible. The near-bottom layer thickness is approximately equal to the water depth in the shallowest water depths, so the outer Ekman layer transport should be disregarded; this resolves some of the problems with the extreme deposition rates in the 30-50 m range, since the outer Ekman layer transport is 50 times the near-bottom transport at those depths, but not with the concentrations. The sediment concentration parameter, γ_0, used in these predictions has the value 0.002; decreasing it even by an order of magnitude would still give concentrations that are far too high. Comparisons of the neutral case predictions with observed concentrations demonstrates again that some modification to the steady flow modeling of suspended sediment transport must be included when there are strong wave effects.

The near-bottom sediment concentations, transport estimates, and reworking depths predicted by the stratified model, however, are plausible with respect to

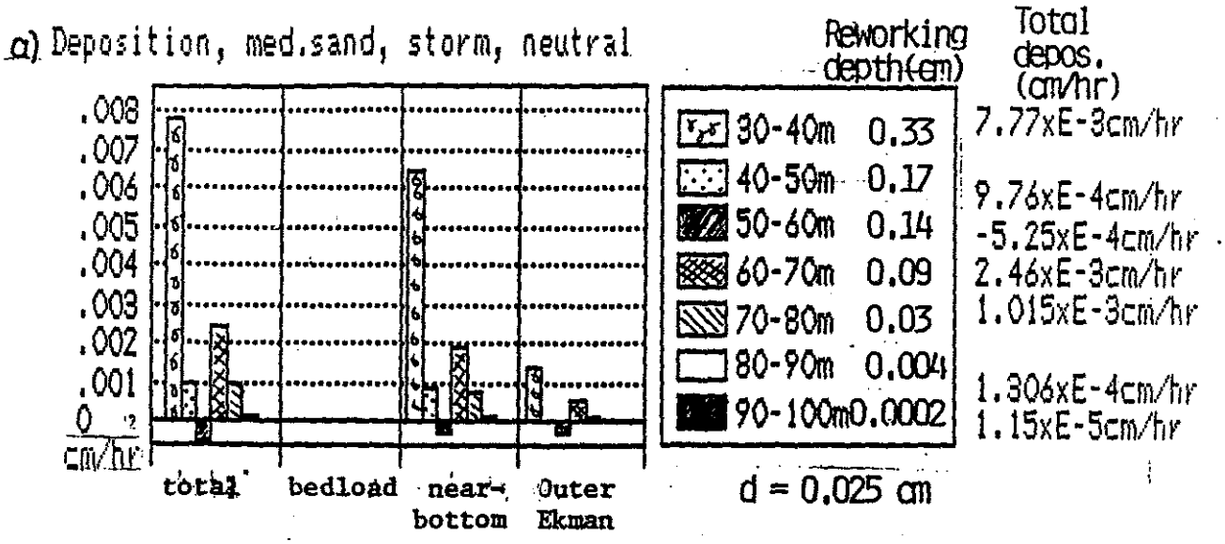

Figure 6.5: Predicted deposition/erosion rates and reworking depths for single-grain-size shelves, same conditions as Figure 6.4, but disregarding the effects of stratification. Reworking depths and maximum deposition rates are consistently higher in the neutral case, as expected.

$H = 5m, T = 12s, \theta_w = 225°, u_r = 32\ cm/sec, \theta_{cur} = 161°$

(a) Results for medium sand show deposition rates varying from the expected pattern due to bottom roughness variability (see text).

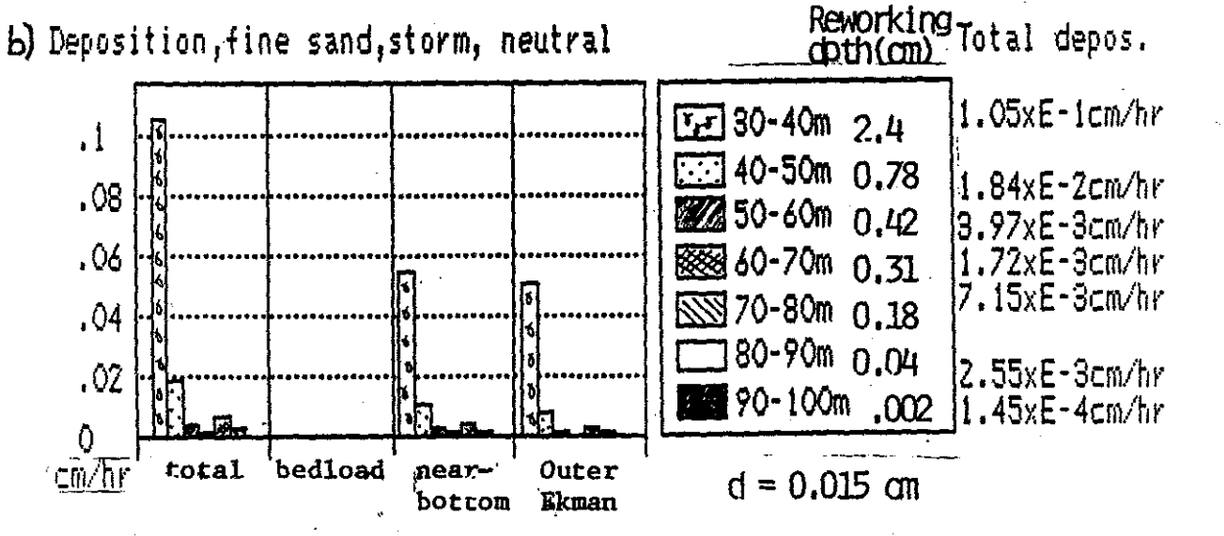

(b) Results for fine sand show deposition rates as high as 2.5 cm/day in shallow water, and some variation due to roughness.

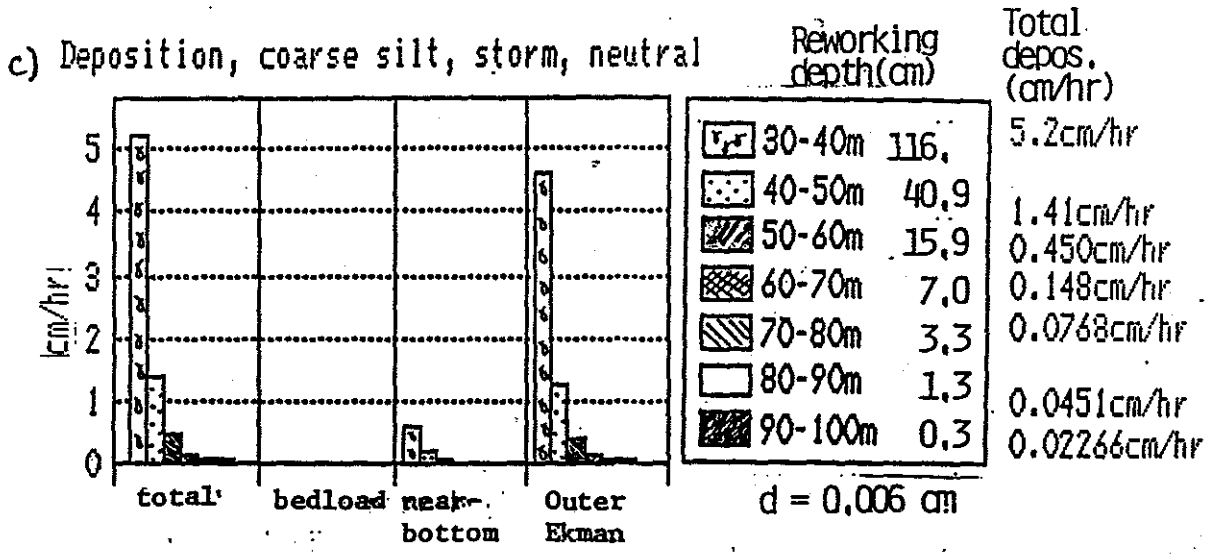

Figure 6.5: (c) Results for coarse silt show unrealistically high reworking depths and transport rates in shallow water, dominated by outer Ekman layer transport.

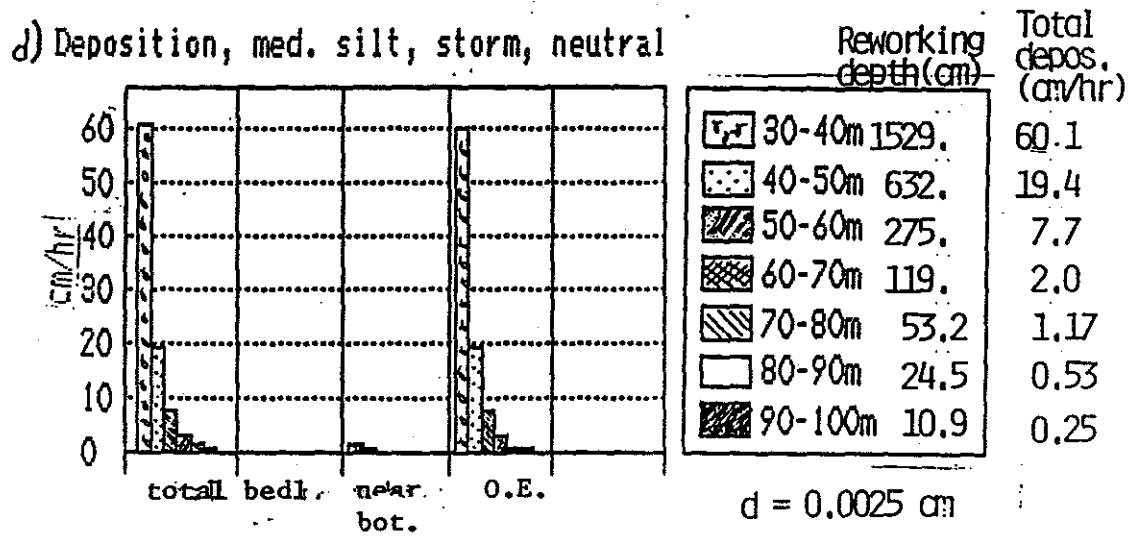

(d) Results for medium silt show similar effects of depth and stratification as the coarse silt case, with deposition as unrealistically high as a meter per day in shallow water. Most of this is due to the outer Ekman layer transport estimate.

storm observations. When strong storm waves are present on a continental shelf, particularly when sediment is fine-grained, the neutral case formulation for sediment transport predictions is unsatisfactory. Stratified effects, as modeled here, appear to provide a reasonable correction to the simple neutral case, though further work is necessary to see if this stratification effect can be observed in the field, or whether a similarly satisfactory correction can be achieved through revision of the eddy viscosity, reference concentration, or other model features.

Application Two: Small storm, single grain size bed

This case is the same as the previous one, except that the wave and current conditions represent a less violent storm. The wave height is three meters, wave period is ten seconds, and current velocity at one meter off the bottom is 20 cm/sec. Wave and current directions are the same: 161° for the current, 225° for the wave. The results are shown in Figure 6.6; for contrast, the neutral results are shown in Figure 6.7.

There is no sediment motion at depths greater than sixty or seventy meters, depending on grain size. The reworking depth is often smaller than the grain size for sand-sized grains (Figure 6.6a and b), indication that not even the entire surface layer is mobilized. There is mostly slight erosion of the silts. This contrasts with the neutral case (Figure 6.7), where there is at least some deposition in all regions, and substantial accumulation for medium silts. Even for this small storm, the reworking depths and concentrations high in the water column, predicted using the neutral formulation, are unreasonably high, indicating that stratification or some other mechanism must act to limit resuspension.

The principal result is that most sediment motion, especially on the mid- to outer-shelf results only from large storms. If, as Butman (1987b) suggests, along-shelf transport direction alternates between two primary storm directions, then one

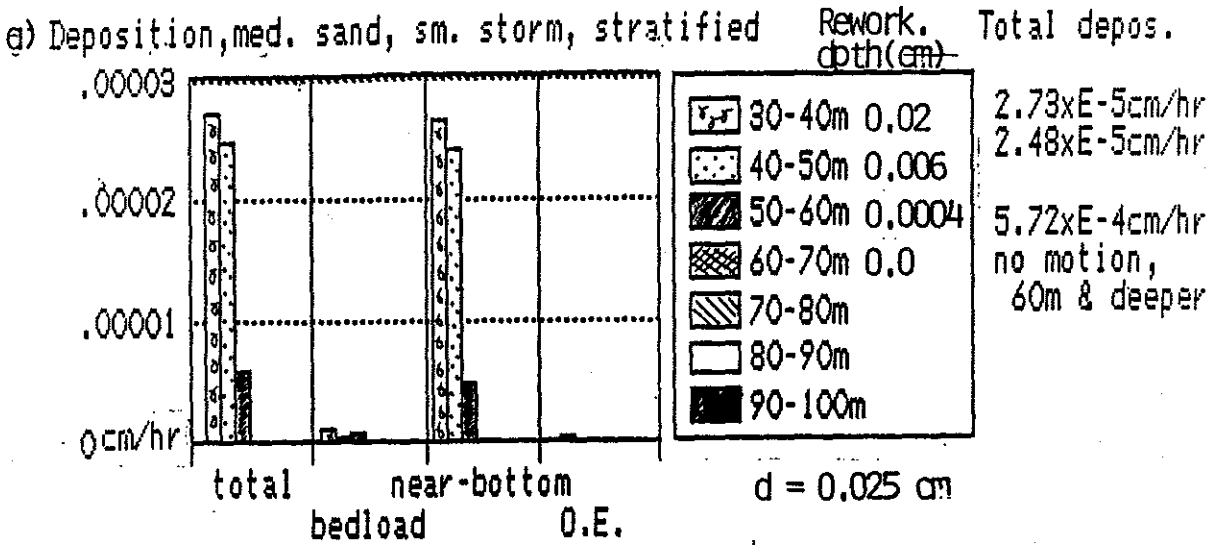

Figure 6.6: Predicted deposition/erosion rates and reworking depths for single-grain-size shelves, with shelf and storm description derived from conditions typical of a small storm on the Mid-Atlantic Bight. Grid is shown in Figure 6.3. Sediment is set in motion no deeper than 60-70 m, and net transport is no greater than 1 mm/day, demonstrating the ineffectiveness of small storms at transporting sediment.
$H = 3m, T = 10s, \theta_w = 225°, u_r = 20\ cm/sec, \theta_{cur} = 161°$
(a) Results for medium sand show insignificant net transport rates and reworking depths, following expected patterns of deposition variance with depth.

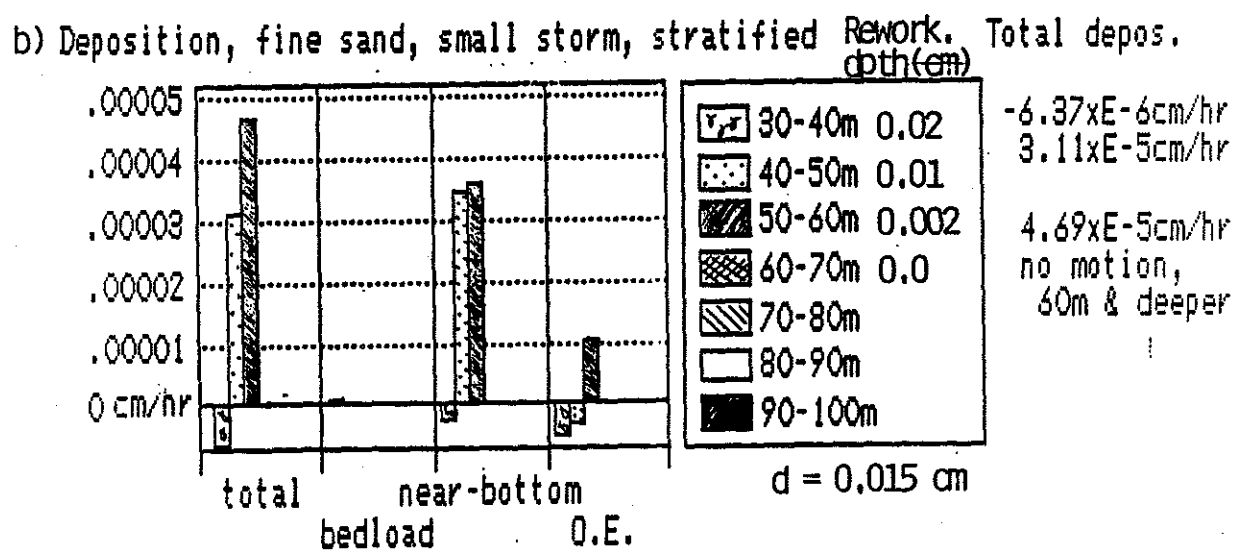

(b) Results for fine sand are very small, but the patterns are strongly affected by roughness and stratification.

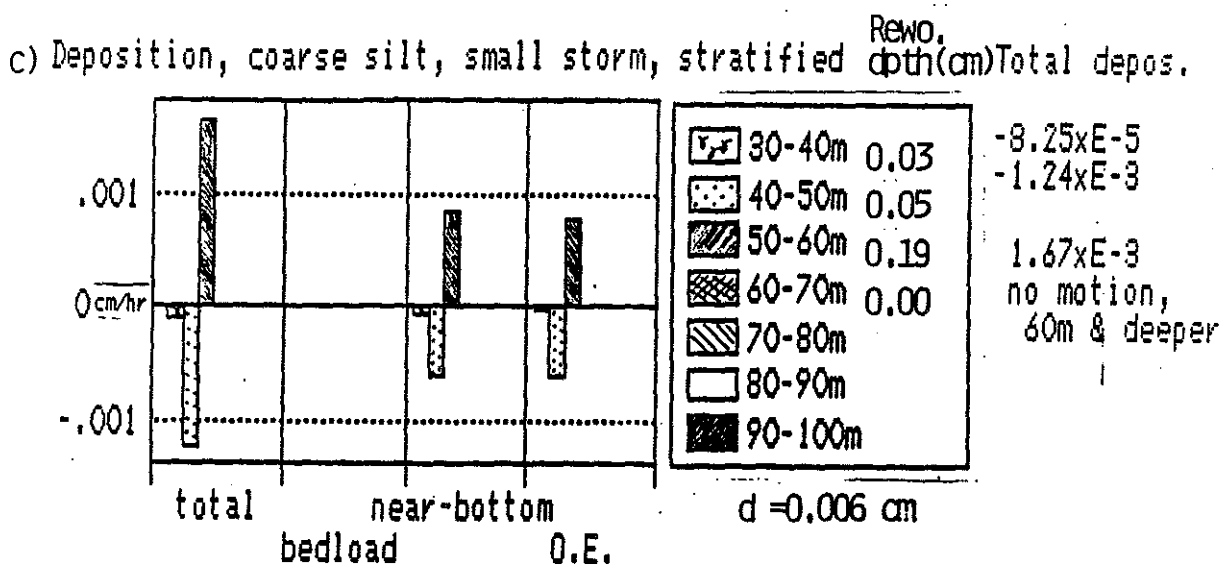

Figure 6.6: (c) Results for coarse silt show the effects of decreasing stratification with decreasing wave velocity in the reworking depth that increases with depth, and the 2 mm/day erosion rate on the central shelf.

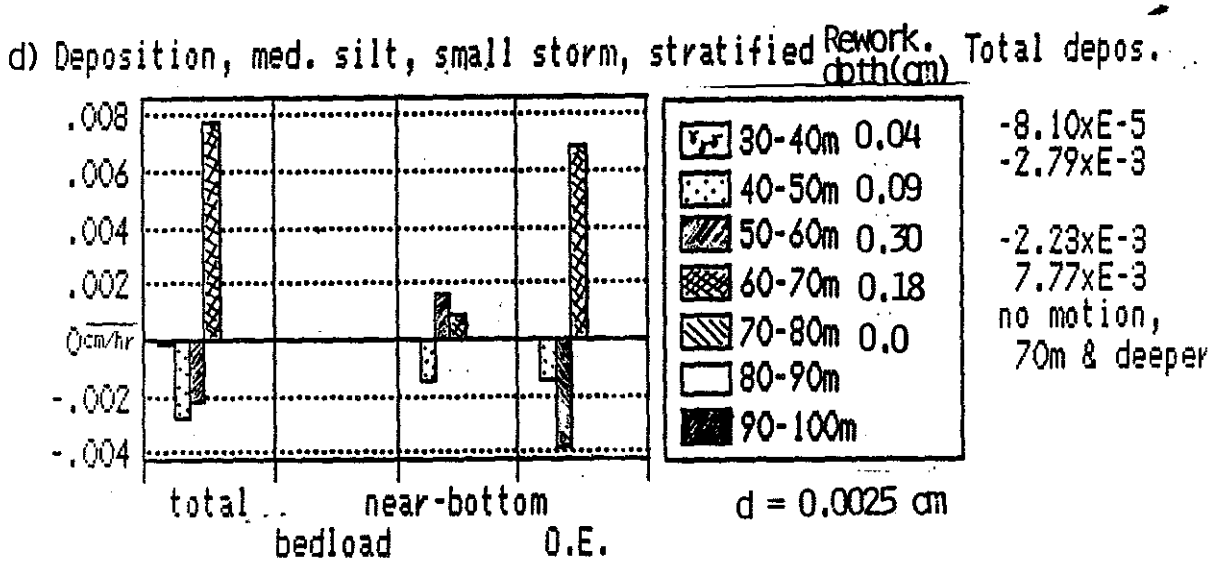

(d) Results for medium silt show similar effects of depth and stratification as the coarse silt case.

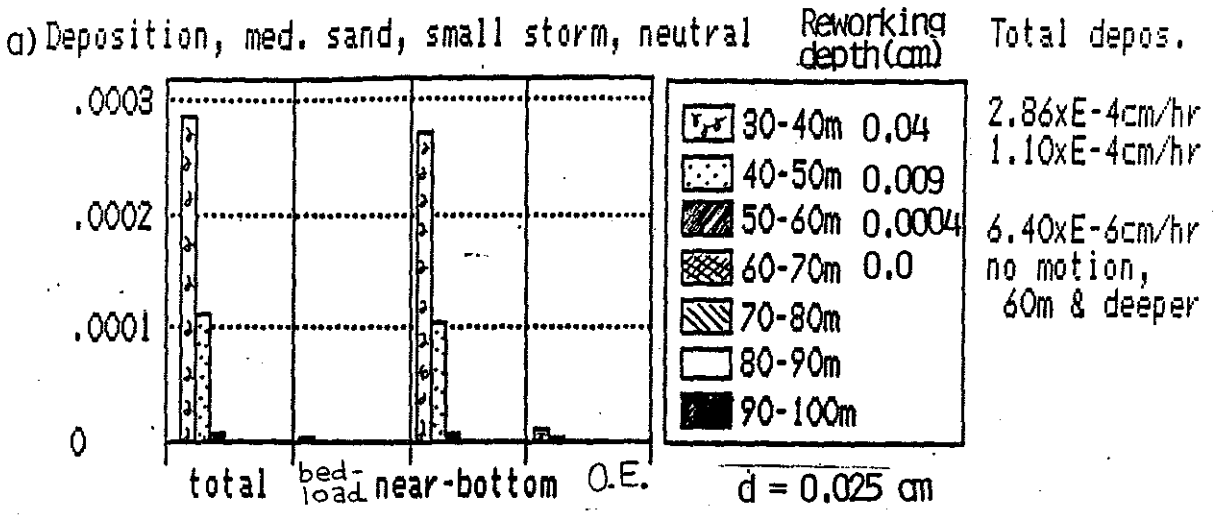

Figure 6.7: Predicted deposition/erosion rates and reworking depths for single-grain-size shelves, with shelf and storm description derived from conditions typical of a small storm on the Mid-Atlantic Bight, neglecting the effects of stratification. Sediment is set in motion no deeper than 60-70 m, and net transport is no greater than 1 mm/day, demonstrating the ineffectiveness of small storms at transporting sediment.
$H = 3m, T = 10s, \theta_w = 225°, u_r = 20\ cm/sec, \theta_{cur} = 161°$
(a) Results for medium sand show insignificant net transport rates and reworking depths, following expected patterns of deposition variance with depth.

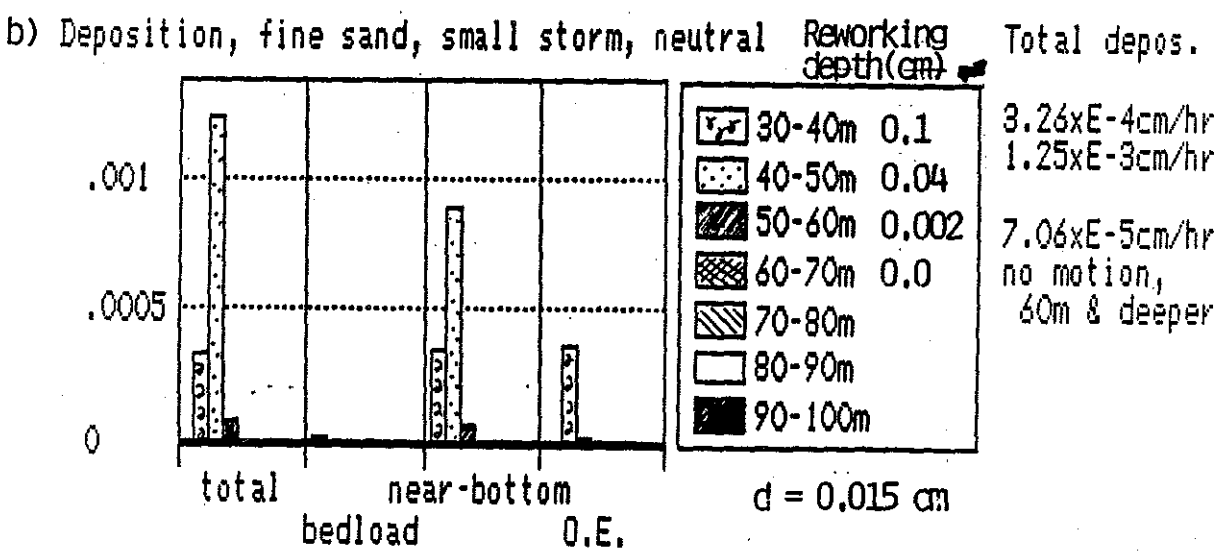

(b) Results for fine sand are very small, but the patterns are strongly affected by roughness and stratification.

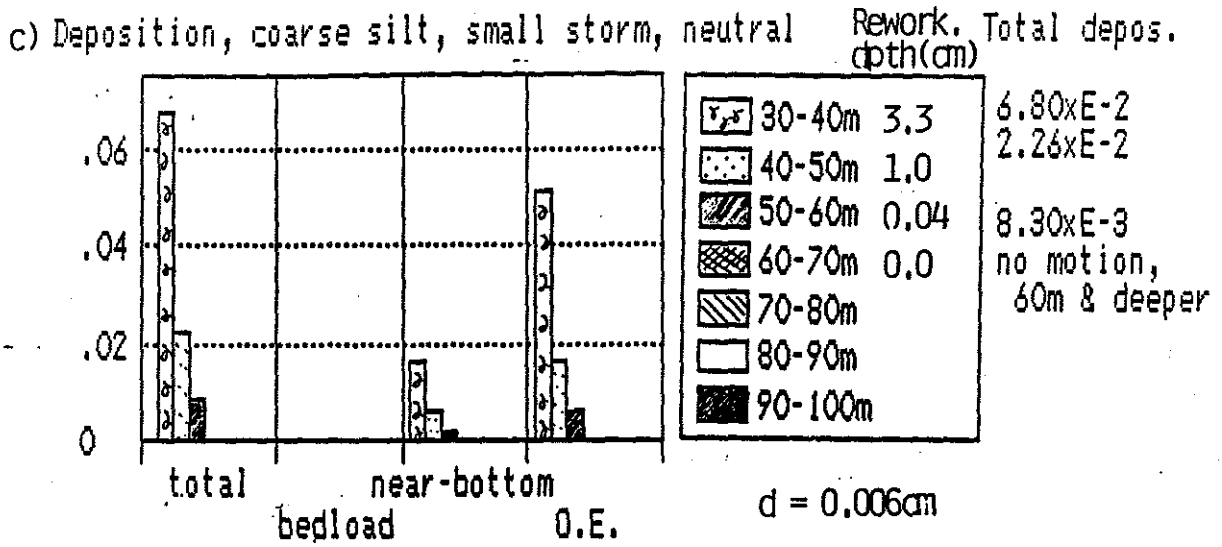

Figure 6.7: (c) Results for coarse silt correspond to expected deposition patterns. Outer Ekman layer transport in shallowest depths is suspect because of water depth limitations.

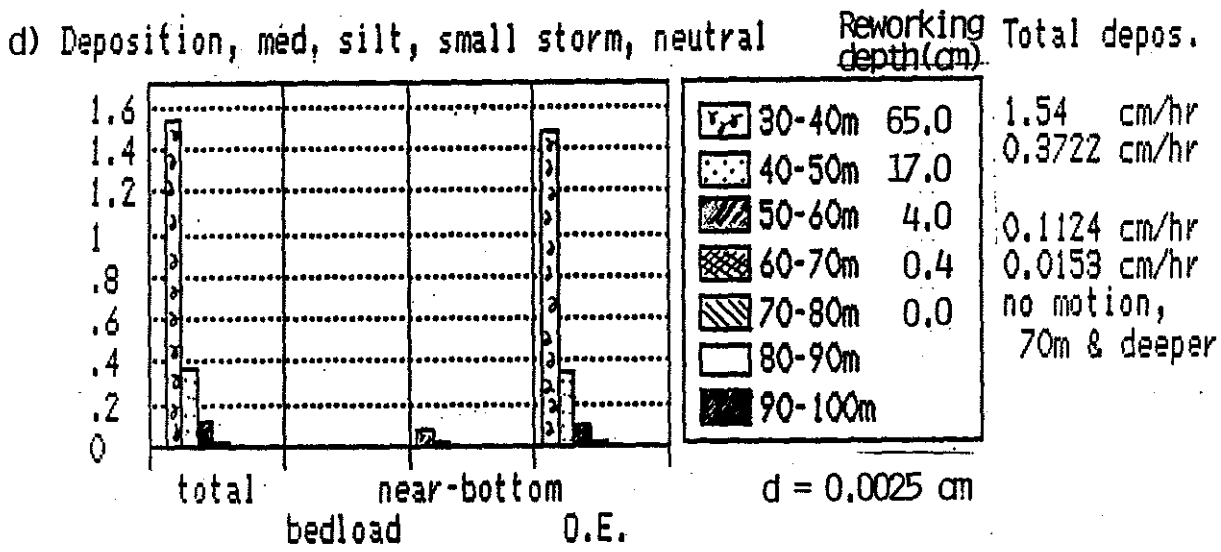

(d) Results for medium silt show similar expected deposition patterns as the coarse silt case, and the same depth limitation on the outer Ekman layer transport holds with respect to the unreasonably high reworking depths and deposition rates in the shallowest boxes.

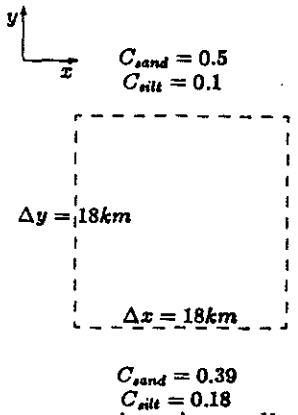

Figure 6.8: Initial grain bed concentrations in application with alongshelf grain texture changes. The sediment is silty sand with 17%silt upcurrent, 35% downcurrent.

might expect the top few millimeters of a sandy seafloor on the Atlantic margin to be transported back and forth alongshelf, with a slow accumulation or erosion of the sand-sized grains due to cross-shelf transport of perhaps a millimeter or two per year, depending on water depth.

Application Three: Alongshelf grain texture changes

On the Atlantic continental shelf as one approaches the 'Mud Patch', there is a perceptible fining of grain texture alongshelf. In order to test the effect of alongshelf grain texture changes, initial bed concentrations of 83% fine sand ($d = 0.015\ cm$) and 17% coarse silt ($d = 0.006\ cm$) at the upcurrent points and 65% fine sand with 35% coarse silt at the downcurrent points are assumed (Figure 6.8). The same 'Blizzard of '78' wave conditions are used ($H = 5m; T = 12sec; \theta_w = 225°$), but the 32 cm/sec current is taken as heading directly alongshelf ($\theta_{cur} = 180°$) so that all net transport results from grain texture changes.

The results are shown in Figure 6.1, both total deposition rates and reworking depths (Figure 6.1a) and by grain size (Figure 6.1b). Note that despite the fact that the bed is predominately sand, both total transport (as signaled by reworking depth) and net transport are predominately silt. Bedload is, again, insignificant, but outer Ekman layer transport plays a large role in the net transport in several

boxes. This is of less concern here, however, since net transport predictions are not dependent on a small component of the total flow as they were in the last cases; some veering in the outer Ekman layer will still leave the strongest component of transport alongshelf.

Intuitively, one expects net erosion, since the silt would be more likely to be transported and there is more silt on the south end of the box, which is the direction of transport. This pattern holds for areas deeper than sixty meters. Shallower than that, however, the larger wave bottom velocities generate larger suspended sediment concentrations at the top of the wave boundary layer, and stratification effects are pronounced. The larger proportion of silt farther south is more affected by the stratification effects, so much so that the net transport out at the southern end of the box is lower than the net transport in at the northern end. This explains the predicted deposition at depths less than sixty meters.

The predicted erosion rates are significant, representing a centimeter or more over the course of a large storm. A prevailing pattern of this sort would soon winnow away all fine sediment if there were no source of silts from the north.

6.2 Northern California shelf type

The northern California continental shelf is typical of continental shelves on narrow, swell and storm dominated continental margins. The region chosen for exercising the model is north of San Francisco, between Pt. Reyes at 38°N and Pt. Arena at 39°N (Figure 6.10. The shelf width ranges from about 16 km at Pt. Arena to about 30 km just north of Pt. Reyes. The shelf break is slightly deeper than the world average, at about 150-170 m. Bottom topography is simple and shore parallel. The region is subject to large wind stress variations and is exposed to open ocean swell. Sediment input comes primarily from a single source, the Russian River, and

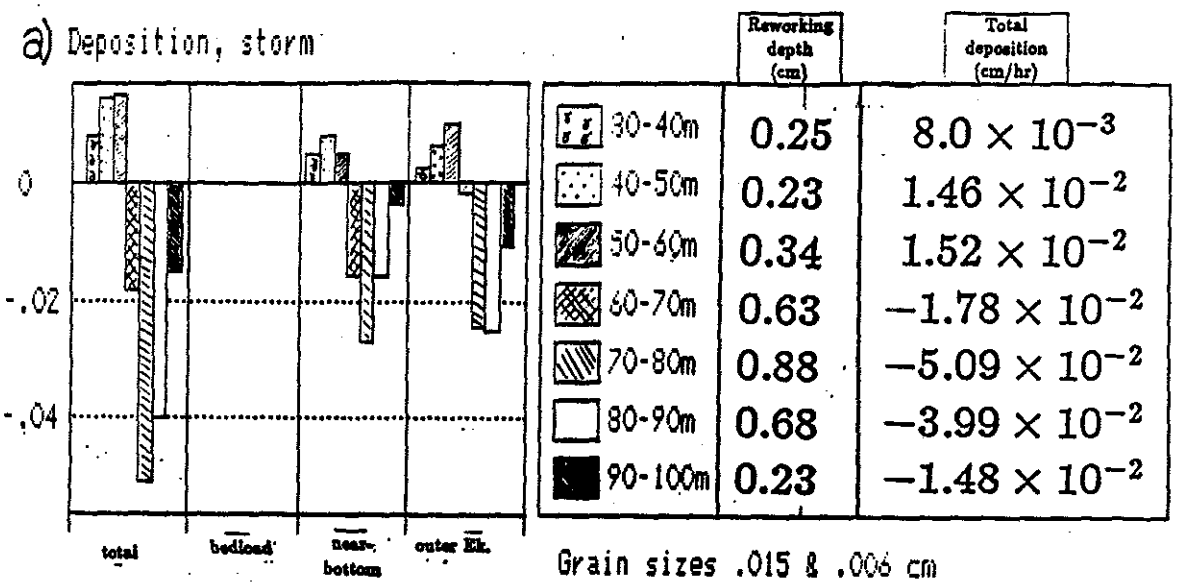

Figure 6.9: Predicted deposition/erosion rates and reworking depths for H=5m, T=12sec, when grain size distribution changes alongshelf (Figure 6.8). Transport of sand extends no farther than 90 m water depth; silt is transported to a depth of 100 m. All transport is alongshelf; there is no cross-shelf component of current. (a) Total erosion is up to 1 cm/day on the mid-to-outer shelf, and deposition of up to 3 mm/day occurs in the shallow parts of the shelf. Deposition results from the combined increase in stratification effects of waves at shallower depths and the increased effect of stratification on the larger silt component at the southern end of the box.

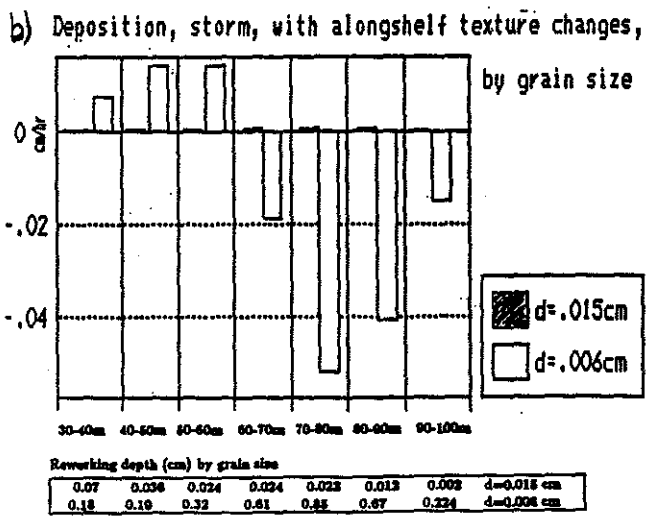

(b) Deposition and erosion rates by grain size show that nearly all of the net transport is in the silt size class, despite its small bed concentration. The reworking depths show that nearly all of the load is silt.

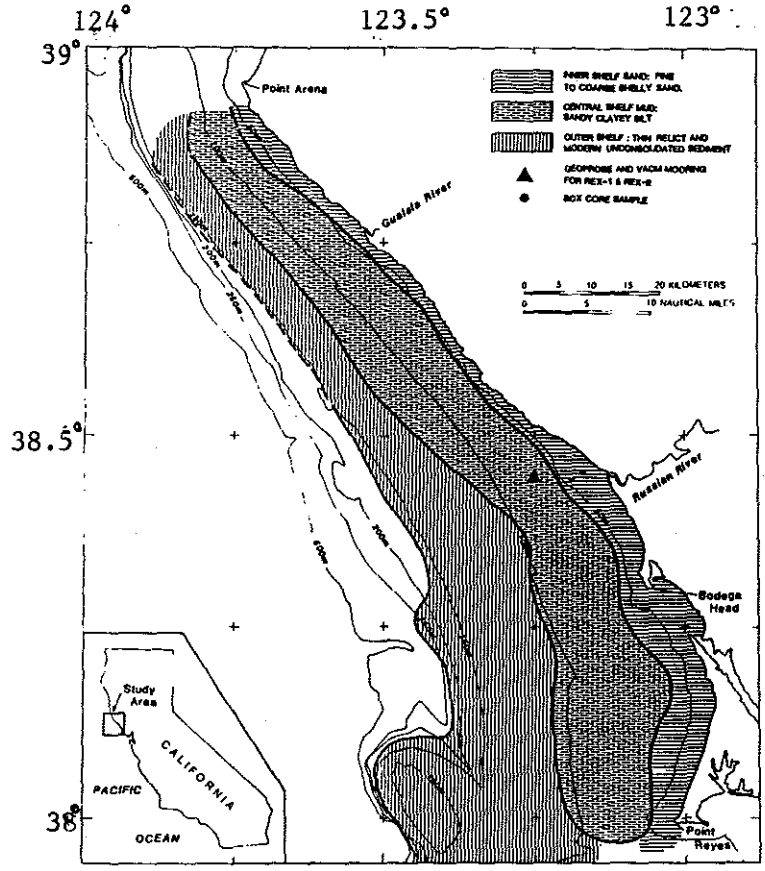

Figure 6.10: The Northern California Shelf, on which the second set of applications of the sediment transport model are based, showing the sand-silt-sand sediment distribution across the shelf (from Drake and Cacchione, 1984).

consists of about 12% sand and about 44% each silt and clay (Klise, 1983). Most of the sediment input occurs in winter as a result of seasonal storms.

In cross-section, the shelf can be divided into three zones, distinguished by bottom slope and sediment type (Cacchione et al, 1983). The inner shelf zone has a bottom slope of $1 - 2°$, extends to a depth of about 60 m, and is covered with fine- to coarse-grained sands. The slope decreases abruptly between 60 and 70 m to about $0.2 - 0.3°$. This central shelf region is covered with sandy silts, with a clay component of up to 15%. At depths of 130-140 m, the silty sediment thins to less than 0.5 m and the slope increases to about $0.5 - 1°$. The outer shelf-upper slope region is characterized by patchy, sandy sediment cover, of modern and relict

origin, to depths of about 200 m (Klise, 1983).

The physical oceanography and meteorology of this region were studied intensively in the Coastal Ocean Dynamics Experiment (CODE) from 1981-1983 (CODE Group, 1983), and studies of the near-bottom flow and sediment transport have been conducted both as part of CODE and independently (Drake and Cacchione, 1984; Cacchione and Drake, 1982; Cacchione et al, 1987). These studies provide essential first order data needed for the model.

Circulation on the northern California shelf is seasonal, primarily controlled by steady winds from the north in spring and summer (upwelling season) and cyclonic storm winds from the south interspersed with strong northerlies in winter. From about April through October, the shelf is subject to strong, steady equatorward winds. These winds control waves and currents, generating southerly currents with bottom velocities less than 15 cm/sec (Drake,1984) and windsea with periods less than 12 seconds and significant height less than 3 meters (U.S. Army Corps of Engineers, 1981-82). About October, winter wind and circulation patterns become dominant. Winds are generally lighter and more variable than in summer, but are interrupted by intermittent cyclonic storms whose strong winds lead to near-bottom currents up to 40 cm/sec (Drake and Cacchione, 1984). Waves associated with these storms commonly have periods of 14-18 seconds and significant heights of 3-5 m (H. Graber, unpub. data). During any season, swell generated by distant storms may affect the shelf with waves of periods up to 25 seconds or more; these waves may persist for durations of 12 to 24 hours (Cacchione, pers. comm.).

Like the Mid-Atlantic Bight, the northern California shelf under non-storm conditions, which includes most of the summer season, is characterized by little or no sediment motion (Drake and Cacchione, 1984). Winter storms are cyclonic, with winds initially from the southeast. The strong, poleward bottom currents they generate typically persist for one to three days. Transmissometer observations of

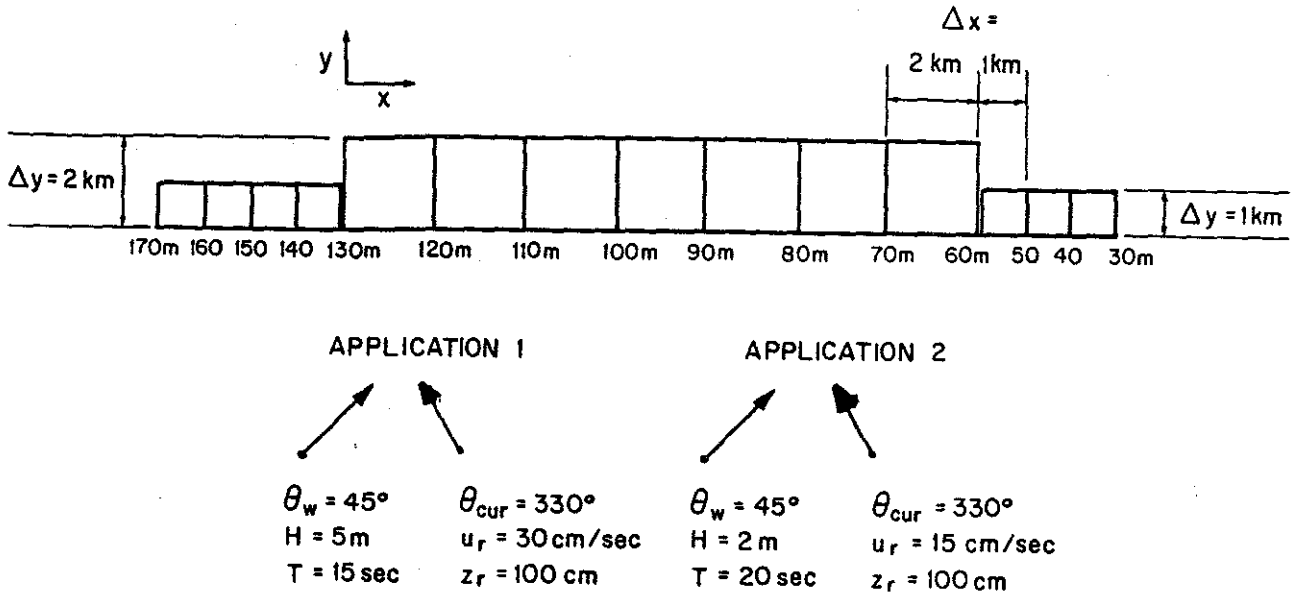

Figure 6.11: Schematic diagram of grid representing the N. California continental shelf and wave and current conditions used in applications described in text

suspended sediment, here like the Atlantic, are strongly correlated with storms (Drake and Cacchione, 1984).

Application One: Large storm, single grain size bed

The first application of the boundary layer model addresses the case of a single grain size bed under wave and current conditions typical of a large storm on the northern California shelf. The boxes begin at a depth of 30 meters and extend out to the depth at which sediment no longer is put in motion by the waves and currents being tested. However, in order to approximate the slope on the California shelf, the grid spacing is one kilometer in water depths of 30-60 m, two kilometers from 60-130 m, and one kilometer at depths greater than 130 m (Figure 6.11). The smaller grid magnifies the erosion/deposition rate due to net transport, since the difference in sediment volume entering and leaving the box at its boundaries is being distributed over a smaller area inside the box.

The wave used to represent a storm condition is five meters high, with a period of 15 seconds and a direction of 45° with respect to the alongshelf direction. The current at one meter above the bottom is 30 cm/sec with a direction of 330° with respect to the alongshelf direction (Figure 6.11). This represents a near-bottom current with a 26 cm/sec alongshelf component and a 15 cm/sec velocity in the offshore direction. This is typical of near-bottom storm current observations at depths of about 50 meters, although the cross-shelf component generally diminishes to about 7 cm/sec with increasing water depth (D. Cacchione, pers. comm.). The deeper estimates of erosion/deposition may, therefore, be excessive by a factor of two or more. This wave and current condition was applied to the same four single-grain-size shelf scenarios as the Mid-Atlantic Bight storm, with grain diameters ranging from medium sand to medium silt.

The results are shown in Figure 6.12. A detailed description of the figure's format was given in conjunction with the Atlantic Shelf application. The effects of roughness and stratification were discussed in detail in the Mid-Atlantic Bight results, so they will receive only cursory mention here. The points to note in these results are the increased transport rates resulting from the increased depth gradient and the increased transport depths due to the larger wave period.

Generally, all grain sizes show a similar depositional pattern as wave bottom velocities and excursion amplitudes decrease across the shelf (Figure 6.12). On the inner shelf, there is relatively small volume erosion, or near-equilibrium. A region of net cross-shelf erosion, increasing in volume with depth, is consistently found on the central shelf. The outer shelf is an area of deposition for all grain sizes, with the increase or decrease controlled by the influence of outer Ekman layer transport. These trends mirror trends in reworking depths, which begin fairly high, decrease on the mid-shelf where stratification effects are strong, increase again on the outer shelf where stratification effects decrease, and decrease toward no motion as wave

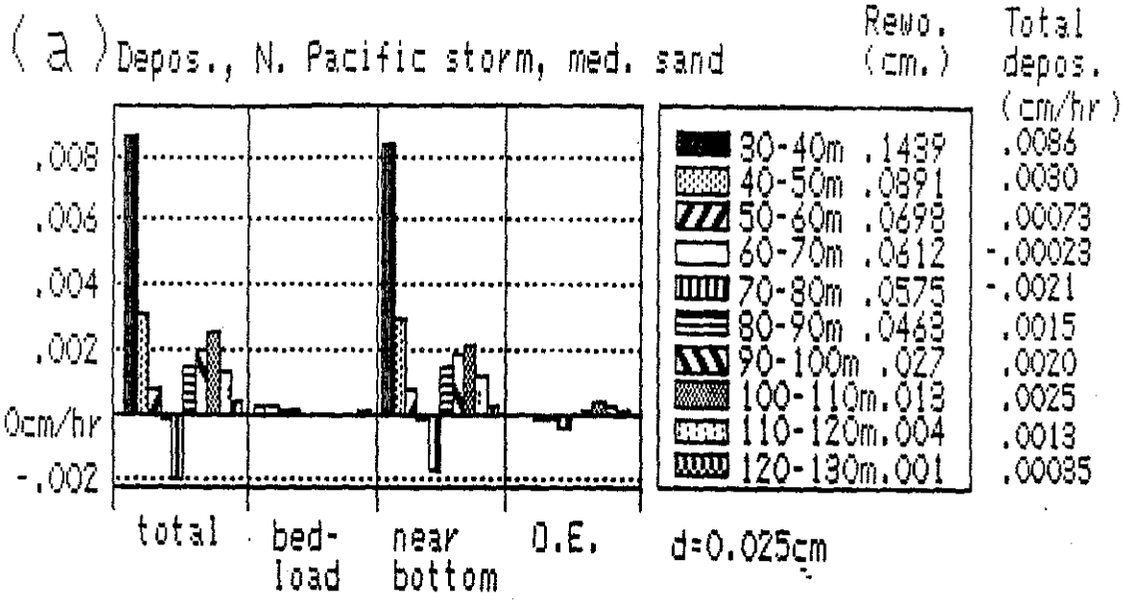

Figure 6.12: Predicted deposition/erosion rates and reworking depths for single-grain-size shelves, with shelf and storm description derived from conditions typical of N. California continental shelf. Grid and wave-current conditions shown in Figure 6.11.
$H = 5m, T = 15s, \theta_w = 45°, u_r = 30\ cm/sec, \theta_{cur} = 330°$
(a) Results for medium sand show variable deposition rates across the shelf, ranging as high as 2 mm/day, with erosion or deposition of 0.5 mm/day or less being more typical. Motion ceases at 130 m depths.

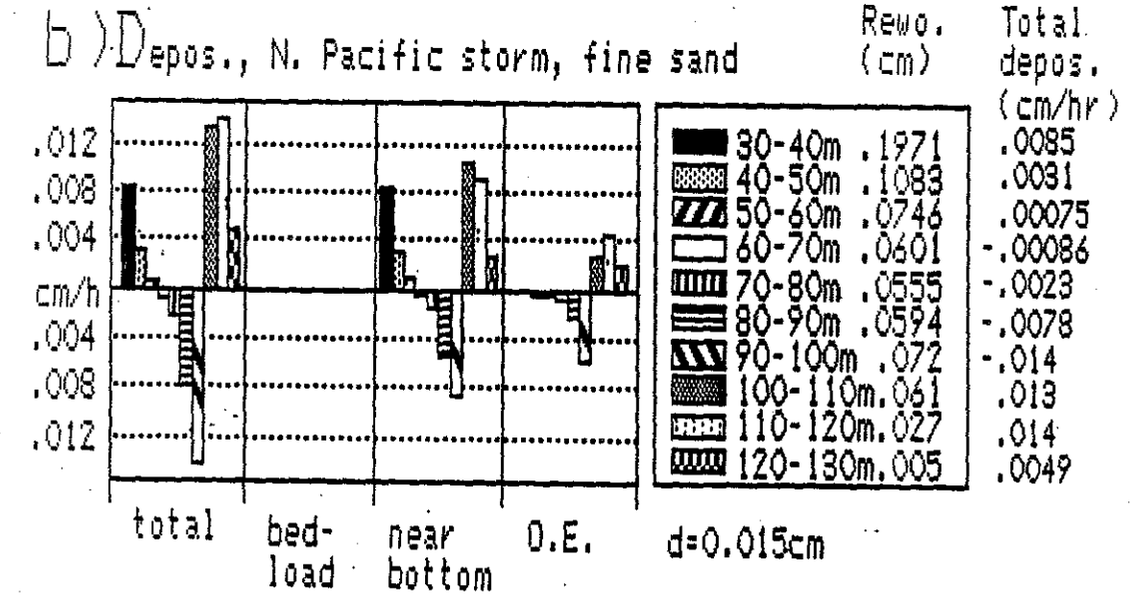

(b) Results for fine sand show deposition and erosion rates as high as 3 mm/day. Motion ceases at 130 m.

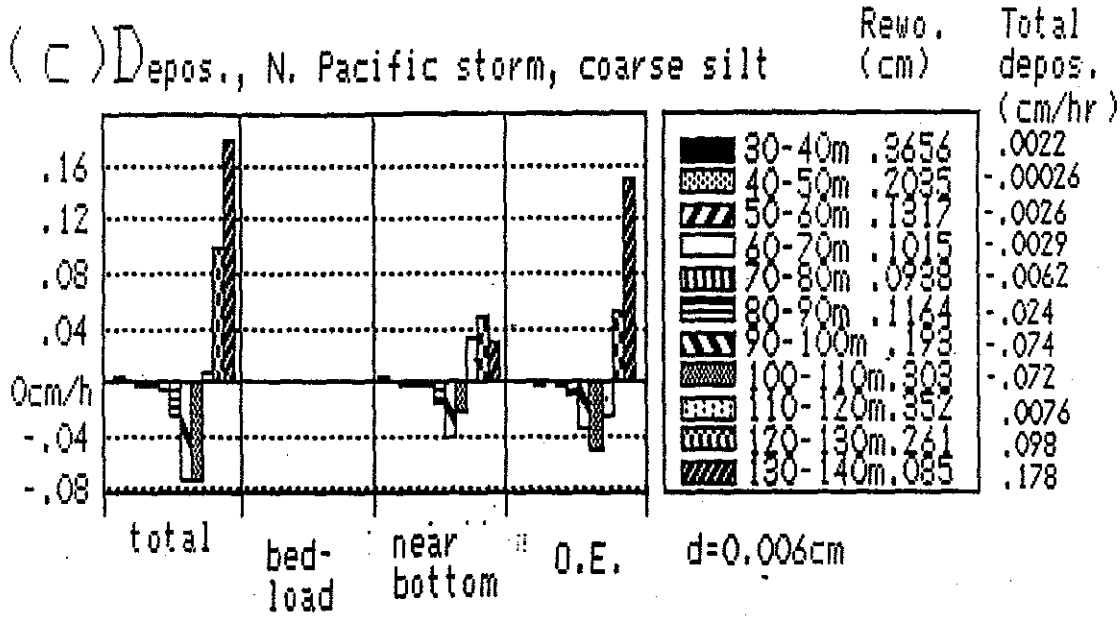

Figure 6.12: (c) Results for coarse silt show net transport rates generally increasing with depth, with erosion as high as 1.5 cm/day in the central shelf and deposition as high as 3 cm/day 30 m deeper.

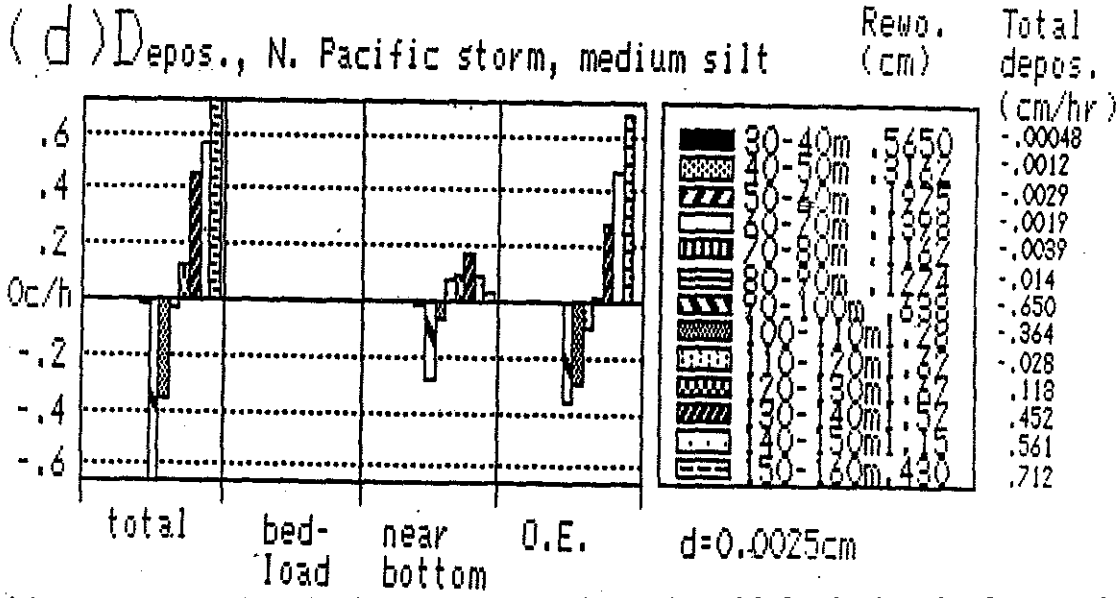

(d) **Results for medium silt show net transport increasing with depth, changing from erosion to deposition as the effects of stratification weaken with decreasing bottom wave velocities. Deposition of as much as 14 cm/day is predicted for the outer shelf, though the large outer Ekman layer contribution is unreliable.**

influence dies out with depth. The location on the shelf at which each of these transitions occurs is a function of grain size.

Deposition and erosion rates on the Pacific shelf (Figure 6.12) exceed those for a typical large storm on the Atlantic shelf (Figure 6.4) by at least a factor of two and generally an order of magnitude or more. There are three controlling factors: increased wave period, increased cross-shelf component of velocity, and increased shelf depth gradient. The increase due to the difference in shelf gradient is the overriding factor, and is easy to determine. Since the change in depth over 18 km on the Atlantic shelf corresponds to 1 or 2 km on the Pacific shelf, the net transport rate for similar depths is immediately raised by a factor of 18 or 9 for 1 or 2 km grid spacings, respectively. The increased cross-shelf component of current velocity adds to the net transport slightly, but the changes in stratification and roughness effects caused by the increased wave period can temper the expected increases due to the other two factors.

The same patterns of transport are evident on both the Pacific and Atlantic shelves, except that the increased wave period causes the shallow water (large u_b) patterns to reach farther out on the shelf. Bedload transport is, again, of minor importance relative to suspended transport in storms. The outer Ekman layer contribution to the net transport is small for medium sand and, at relatively shallow depths, for smaller diameter sediments as well. The sudden decrease in stratification effects can be tracked at 90-100 m for all three smaller grain sizes, where increased effects of outer Ekman layer transport become noticable. This occurs because both the height of the Ekman layer and the sediment transporting capacity of the current boundary layer above the wave boundary layer are decreased when stratification effects are strong. These combine to enhance erosion when stratification is stronger at the shallower end of the grid square, as is the case between 90 and 100 m for these three grain sizes in this wave-current setting.

The patterns of deposition and erosion are interesting with respect to the observed sediment distributions on the Pacific shelf. The net deposition of sands, decreasing to a depth of 60 m, and erosion of silts in the onshore boxes predicts the sandy nearshore zone of the California shelf. The predicted small volumes of erosion and deposition of sand out to depths of 130 m is likewise reflected in the small percentages of sand found in the mid-shelf mud zone. The predicted pattern of distribution for silts likewise mimics the observed: there is nearshore erosion, then deposition out to a depth at which all sediment motion suddenly ends. The predicted zones of deposition are shifted seaward by $\sim$ 20 m relative to the observed, especially with respect to the medium silt. However, if a smaller wave had been used -four meters rather than five meters in height perhaps- the zones would shift landward. The results suggest that the offshore limits of the mud belt may be probably defined by seasonal storm wave characteristics.

Application Two: Moderate swell, single grain size bed

This application corresponds to the occurrence of moderate swell on the continental shelf on a day of average currents. The wave height is two meters; period is twenty seconds; direction is out of the South Pacific at 45°. The current velocity is 15 cm/sec at one meter above the bottom in a direction 330°, corresponding to a cross-shelf component of 7.5 cm/sec and an alongshelf component of 13 cm/sec.

Because of the 20 second wave period, the maximum depth of sediment motion is only 30 -40 m less than the five meter waves of the first application (Figure 6.13). The patterns of deposition across the shelf are similar: deposition or steady state holds in the shallowest reaches; increasing effects of stratification in the mid-shelf lead to erosion for the three finer grain sizes; and decreasing stratification causes deposition on the outer shelf. The medium sand predictions follow the 'expected' deposition pattern entirely, demonstrating negligible effects of either roughness or

stratification changes with depth. The negligible deposition and reworking rates for fine sand and coarse silt suggest that storm transport dominates mid- and outer-shelf deposition patterns for these grain sizes. In the mid-shelf areas, however, the deposition rates for medium silt is similar for the storm and swell conditions. Stratification effects under the large waves limit the transport of the fine grains, leading to a case where deposition patterns are as dependent on swell as on storm conditions.

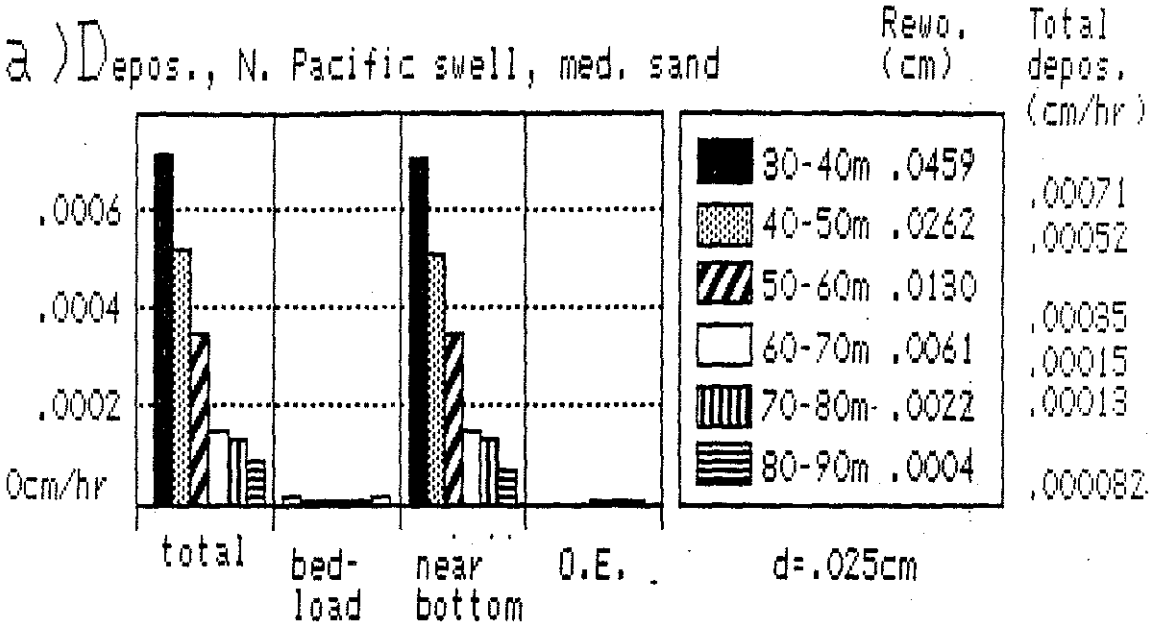

Figure 6.13: Predicted deposition/erosion rates and reworking depths for single-grain-size shelves, with shelf and swell description derived from conditions typical of N. California continental shelf. Grid is shown in Figure 6.11.

$H = 2m, T = 20s, \theta_w = 45°, u_r = 20\ cm/sec, \theta_{cur} = 330°$

(a) Results for medium sand show expected deposition rates, demonstrating that the wave-generated shear stresses are neither high enough to wash out ripples nor to set up stratification effects strong enough to counter the expected pattern. Deposition rates are no more than .2 mm/day. Motion ceases at 90 m depths.

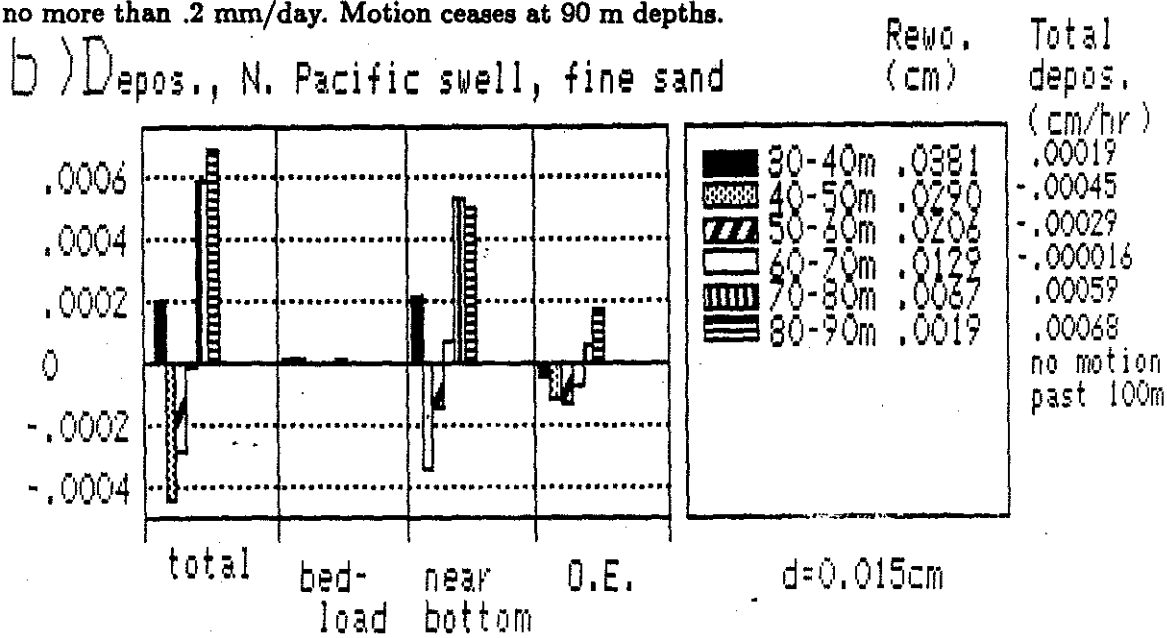

(b) Results for fine sand show deposition and erosion rates no more than 0.2 mm/day. Motion ceases at 90 m.

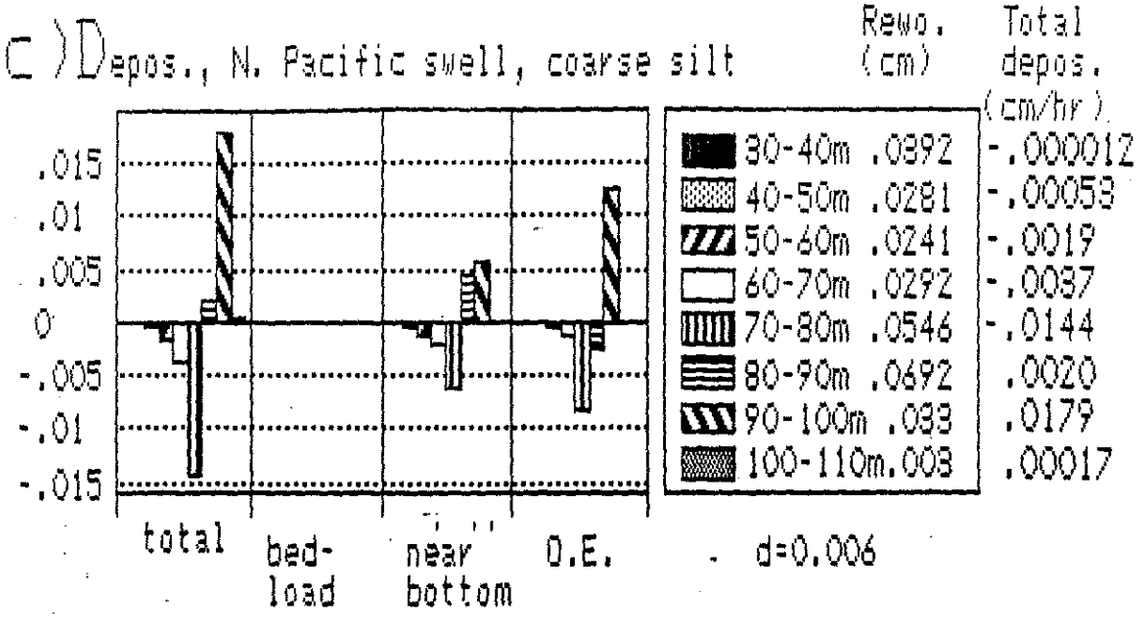

Figure 6.13: (c) Results for coarse silt show net transport rates generally increasing with depth, with erosion as high as 3.0 mm/day in the central shelf and deposition as high as 3 mm/day 30 m deeper. Motion ceases at 110 m.

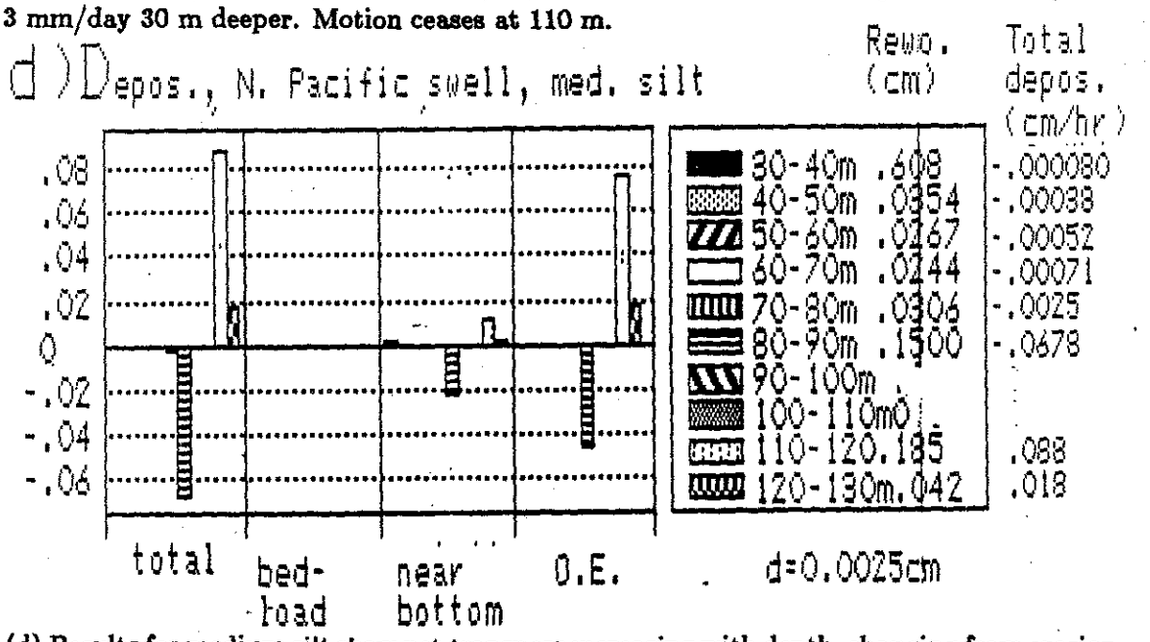

(d) Results for medium silt show net transport increasing with depth, changing from erosion to deposition as the effects of stratification weaken with decreasing bottom wave velocities. Deposition of as much as 2.1 cm/day predicted for the outer shelf is comparable with the storm case. Motion ceases at 130 m

Chapter 7

Conclusions and Future Work

The purpose of this work has been to apply a theoretical wave-current boundary layer model to the prediction of sediment transport on the continental shelf, to test the sensitivity of the model to some of the many parameters and assumptions necessary to represent the physical processes, and to use the model to predict patterns of sediment transport and deposition under conditions representative of some found on different continental shelves. This work may be seen as a step toward the ultimate sedimentological goal of producing a general predictive model which reliably explains existing patterns of sediment deposition and distribution, and which can be used to characterize the depositional environment of elements of the stratigraphic record.

A physical explanation and a mathematical treatment of the fluid dynamic theory were offered separately so that a reader unfamiliar with boundary layer theory could follow the explanations of the results. The equations, however, provide precise demonstrations of the relations of the forcing and sediment response.

A presentation of the response of the model to variation in the input parameters and some of the assumptions, presented in the Chapter 5, demonstrated a number of consistent results and limitations which were stated in the summary to that chapter. Some of them are repeated here:

- Large wave bottom velocities ($\geq\sim 40\frac{cm}{sec}$), especially when near-bottom currents are small ($\leq\sim 10\frac{cm}{sec}$), cause stratification effects which reduce load predictions by 50% or more. These predictions require field verification.

- Large wave bottom velocities occurring where the seafloor surface grains are silt sized or finer may lead to nonunique solutions to the stratified boundary layer model, depending on specified reference velocity. The predicted sediment load and transport may vary by an order of magnitude for the different solutions. If the model's representation of stratification is correct, this nonuniqueness requires specification of another boundary condition.

- Large bottom currents ($\geq\sim 30\frac{cm}{sec}$ at $z = 1m$) can suspend sediments to heights in the water column greater than the near-bottom layer on which this model focuses. When estimates of load and transport volumes in the outer Ekman layer are greater than or equal to the near bottom volumes, the model's predictions of total transport are less certain.

- In a related concern, the predicted bottom Ekman layer depth based on mean shear velocity can exceed the water column depth in strong current flows. If so, the outer Ekman layer predictions should be discarded.

To test the wave-current boundary layer model in more realistic situations, it was inserted into a simple numerical box model and used to calculate net transport under conditions representative of two very different continental shelves. Data from the Mid-Atlantic Bight were consulted to determine storm conditions representative of that area. The model was run to test the effects on sediment load and transport predictions of intensification of wave bottom velocities due to cross-shelf slope on the mid-to-outer shelf. One might expect a uniform increase in sediment load and transport in the onshore direction, caused by the increase in wave bottom velocity

as the wave shoals. In the presence of an offshore current, this would generate a prediction of net deposition at all depths, declining in volume with increasing water depth. This pattern is not observed, however, for two reasons:

- Sediment stratification effects intensify with increased wave bottom velocity. Predicted transport is sometimes smaller at the onshore side of the grid square, leading to predicted erosion in the presence of an offshore component of flow;

- Sediment roughness responds to the flow; in particular, larger wave bottom velocities can wash out ripples on sand beds, leading to lessening of wave-generated turbulence. This can lead to smaller deposition than expected under the wave.

Storm conditions typical of the Northern California shelf were applied to a narrow continental shelf. The shelf's depth gradient itself amplified the erosion and deposion predictions. The predicted patterns of deposition were in general agreement with the observed sand-silt-sand patterns on the California margin. The results suggest that the outer limit of the mud belt found on that shelf may be defined by seasonal storm wave characteristics, and in this area that storm transport plays a more important part in moving sediment through the area than do the average conditions.

In conclusion, the analysis performed using the Grant-Madsen-Glenn wave-current boundary layer model showed that the model gives realistic predictions of sediment resuspension and transport when stratification effects are included. Stratification is an important effect in this model, and field tests are needed to determine how realistic the model's treatment of stratification is.

7.1 Future Work

There are a number of questions raised by the model which require field experiment to answer. They are:

- The model predicts intense sediment stratification effects when wave bottom velocities are high, resulting from large sediment concentrations inside the wave boundary layer. Are these real, or are they artifacts of the model? How can they be observed in the storm wave environment?
- The model predicts very large sediment concentrations in the wave boundary layer. Are they real?
- The model predicts reworking depths of sediments up to several centimeters. Can those be observed?
- The model predicts net erosion/deposition based on observable parameters (i.e. cross-shelf components of currents). Can such deposition be detected, or is it buried in the noise of other variables and uncertainties?
- The model represents the surface wave spectrum as a single, monochromatic wave velocity at the bottom. How is the spectrum best represented?

If this model is to be useful in geological studies, these questions need answers. Measurement technology has lagged behind theory, so that most models have to base their verification on gross measurements when fine ones are needed. New instrumentation and techniques may be applicable, however, and field verification is unquestionably the next step in applying this model.

REFERENCES

Businger, J. A., and S. P. S. Arya, 1974. Height of the mixed layer in the stably stratified planetary boundary layer. *Adv. Geophys.*, **18A**, 73-92.

Bothner, M. H., E. C. Spiker, P. P. Johnson, R. R. Rendigs, and P. J. Aruscavage, 1981. Geochamical evidence for modern sediment accumulation on the continental shelf off southern New England, *J. Sed. Petrol.*, **51**, 281-292.

Butman, B., 1987a. Physical processes causing surficial-sediment movement. in *Georges Bank* , edited by R. H. Backus: MIT Press, Cambridge, 146-162.

Butman, B., 1987b. The effect of winter storms on the bottom, in in *Georges Bank* , edited by R. H. Backus: MIT Press, Cambridge, 73-77.

Butman, B. and D. W. Folger, 1979. An instrument system for long-term sediment transport studies on the continental shelf, *J. Geophys. Res.*, **84**, 1215-1220.

Butman, B., M. Noble and D. W. Folger, 1979. Long-term observations of bottom current and bottom sediment movement on the Mid-Atlantic continental shelf, *J. Geophys. Res.*, bf 84, 1182-1205.

Cacchione, D. A., D. E. Drake, W. D. Grant, A. J. Williams, and G. B. Tate, 1983. Variability of sea-floor roughness within the Coastal Ocean Dynamics Experiment (CODE) region, *Woods Hole Oceanog. Inst. Tech. Rept. WHOI-83-25*, 50pp.

Cacchione, D. A., and D. E. Drake, 1979. A new instrument system to investigate sediment dynamics on continental shelves, *Mar. Geol.*, **30**, 299-312.

Cacchione, D. A., and D. E. Drake, 1982. Measurements of storm-generated bottom stresses on the continental shelf, *J. Geophys. Res.*, **87**, 1952-1960.

Cacchione, D. A., W. D. Grant, D. E. Drake, and S. M. Glenn, 1987. Storm-dominated bottom boundary layer dynamics on the northern California continental shelf: Measurements and predictions, *J. Geophys. Res.*, **92**, 1280-1291.

Carstens, M. R., R. M. Nielson, and H. D. Altinbilek, 1969. Bed forms generated in the laboratory under oscillatory flow: analytical and experimental study. *Tech. Memo. 28*, US Army Corps. Engr., Coastal Eng. Rsch. Ctr.

Clark, T., and C. Stearn, 1960. *Geological evolution of North America*: New York, Ronald Press Co., 434pp.

Clauser, F. H., 1956. The Turbulent Boundary Layer, in *Advances in Applied Mechanics*, **4**, H. C. Dryden and J. vonKarman, editors: Academic Press, New York, 1-51.

CODE Group, 1983. Coastal Ocean Dynamics, *Trans., Amer. Geophys. Union*, *64*, 36, 538-540.

Dietz, R. S., 1963. Wave-base, marine profile of equilibrium, and wave-built terraces: a critical appraisal. *Geol. Soc. Am. Bull.*, **74**, 971-990.

Dietz, R. S., 1964. Wave-base, marine profile of equilibrium, and wave-built terraces: reply. *Geol. Soc. Am. Bull.*, **75**, 1275-1281.

Downing, J. P. , R. W. Sternberg, and C. R. B. Lister, 1981. New instrumentation for the investigation of sediment suspension processes in the shallow marine environment, *Mar. Geol.*, **42**, 19-34. 1985

Drake, D. E. and D. A. Cacchione, 1984. Seasonal variation in sediment transport on the Russian River shelf, California, *Cont. Shelf Res.*, **4**, 5, 494-514.

Ellison, T. H., 1956. Atmospheric Turbulence in *Surveys in Mechanics*, edited by Batchelor, G. K. and R. M. Davies: Cambridge Univ Press, 400-430.

Emery, K. O., 1968. Relict sediments on continental shelves of the world, Bull. Amer. Assn. Petrol. Geologists, **52**, 3, 445-464.

Garrels, R., 1951. *Textbook of geology*: New York, Harper and Bros., 511pp.

Glenn, S. M., 1983. A Continental Shelf Bottom Boundary Layer Model: The Effects of Waves, Currents, and a Moveable Bed. Sc. D. thesis, Woods Hole Oceanographic Institution/Massachusetts Institute of Technology, 237pp.

Glenn, S. M., 1987. A suspended sediment stratification correction for combined wave and current flows. *J. Geophys. Res.*, **92**, C8, 8244-8264.

Grant, W.D., L.F. Boyer, and L.P. Sanford, 1982. The effects of bioturbation on the initiation of motion of intertidal sands. *J. Mar. Rsch*,**40**,(3), 659-677.

Grant, W. D. and S. M. Glenn, 1983a. A continental shelf bottom boundary layer model. Vol. I: Theoretical model development *Technical report to the American Gas Association*, 167 pp.

Grant, W. D. and S. M. Glenn, 1983b. A continental shelf bottom boundary layer model. Vol. II: Model/data comparison. *Technical report to the American Gas Association*, 63 pp.

Grant, W. D. and S. M. Glenn, 1983c. A continental shelf bottom boundary layer model. Vol. III: Users manual. *Technical report to the American Gas Association*, 189 pp.

Grant, W. D. and O. S. Madsen, 1979. Combined Wave and Current Interaction with a Rough Bottom. *J. Geophys. Res.*, **84**, C4, 1797-1808.

Grant, W. D. and O. S. Madsen, 1982. Movable bed roughness in unsteady oscillatory flow. *J. Geophys. Res.*, **87**, C1, 469-481.

Grant, W. D. and O. S. Madsen, 1986. The continental shelf bottom boundary layer. *Ann. Rev. Fluid Mech.*, **18**, 265-305.

Grant, W. D., A. J. Williams, S. M. Glenn, D. A. Cacchione, and D. E. Drake, 1983. High frequency bottom stress variability and its prediction in the CODE region, *Woods Hole Oceanog. Inst. Tech. Rept. WHOI-83-19*, 72pp.

Jonsson, I. G., 1966. Wave boundary layers and friction factors, *Proceedings of the Tenth Congress of the International Association for Hydraulic Research*, 85-92.

Kachel, N. B., 1980. A time dependent model of sediment transport and strata formation on a continental shelf. Ph.D. thesis, Univ. of Washington, 123pp.

Kachel, N. B., 1987. Modeling wave-current-sediment interaction events to develop a sediment transport budget for the Washington continental shelf, in *Coastal Oceanography of the Pacific Northwest*, edited by M. R. Landry and B. H. Hickey: Wiley-Interscience, New York.

Klise, D. K., 1983. Modern sedimentation on the California continental margin adjacent to the Russian River, M. S. Thesis, San Jose State Univ., 143pp.

Kulm, L. D., R. C. Roush, J. C. Harlett, R. H. Neudeck, D. M. Chambers, and E. J. Runge, 1975. Oregon continental shelf sedimentation: interrelationships of facies distribution and sedimentary processes, *Jour. of Geol.*, **83**, 145-175.

LeBlond, P. H., and L. A. Mysak, 1978. *Waves in the Ocean*: Elsevier, 602pp.

Leet, L. D. and S. Judson, 1958. *Physical Geology, 2nd edition:*, Englewood Cliffs, N.J., Prentice Hall, inc., 502pp.

Long, C. E., 1981. A simple model for time-dependent stably stratified turbulent boundary layers, *Special Report No. 95*, Univ. of Washington, Seattle, Wa., 170pp.

Longwell, C, A. D. Knopf, and R. Flint, 1948. *Physical Geology*: New York, John Wiley and Sons, inc., 543 pp.

Madsen, O. S., and W. D. Grant, 1976. Quantitative description of sediment transport by waves. *Proc. Coastal Engr. Conf., 15th*, **2**, 1093-1112. *J. Phys. Oceanogr.*, **7**, 248-255.

Mantz, P. A., 1977. Incipient transport of fine grains and flakes by fluids- extended Shields Diagram, *Jour. of the Hydr. Div., ASCE*, **103**, HY6, 601-615.

McCave, I. N., 1984. Erosion, transport and deposition of fine-grained sediments. in *Fine-Grained Sediments*, edited by D. A. V. Stow and D. J. W. Piper: Geol. Soc. of London, Special Pub. 15, 35-70.

Meyer-Peter, E. and R. Müller, 1948. Formulas for Bed-Load Transport. *Proc. Intl. Assn. Hydraulic Struc. Rsch., 2nd*, 39-64.

Milliman, J. D., O. H. Pilkey, and D. A. Ross,, 1972. Sediments of the continental margin off the Eastern United States, *Geol. Soc. Amer. Bull.*, **83**, 1315-1334.

Moore, D.G. and J. R. Curray, 1964. Wave-base, marine profile of equilibrium, and wave-built terraces: discussion. *Geol. Soc. Am. Bull.*, **75**, 1267-1273.

Nowell, A. R. M., 1983, The Benthic Boundary Layer and Sediment Transport, *Rev.Geophys. and Space Phys.*,**21**, 5, 1181-1192.

Nowell, A. R. M., P. A. Jumars and J. E. Eckman, 1981. Effects of biological activity on the entrainment of marine sediments, *Mar. Geol.*, **42**, 133-153.

Owen, P.R., 1964. Saltation of uniform grains in air. *J. Fluid Mech.*, **20**, 225-242.

Parmenter, C. M., M. H. Bothner, and B. Butman, 1983. Characteristics of resuspended material from Georges Bank collected with a sediment trap, *Est., Coastal and Shelf Sci*, **17**, 521-533.

Shepard, F. P. and G. V. Cohee, 1936. Continental shelf sediments off the Mid-Atlantic states, *Geol. Soc. Amer. Bull.*, **47**, 441-458.

Shields, H., 1936. Application of similarity principles and turbulence research to bed-load movement (in German), *Mitteilungen der Preuss, Versuchsanst. Fur Wasserbau and Schiffbau,* Berlin

Smith, J. D., 1977. Modeling of sediment transport on continental shelves. in *The Sea,* **vol. 6**, edited by E.D. Goldberg, I.N.McCave, J.J. O'Brien, and J.H. Steele: Interscience, N.Y., 123-151.

Smith, J. D. and C. E. Long, 1976. The effect of turning in the bottom boundary layer on continental shelf sediment transport, *Mémoires Société Royale des Sciences de Liège*, **6**, 10, 369-396.

Smith, J. D. and S. R. McLean, 1977. Spatially averaged flow over a wavy surface. *J. Geophys. Res.*, **82**, 12, 1735-1746.

Swift, D. J. P., 1974, Continental Shelf Sedimentation, in *Geology of Continental Margins*: Springer-Verlag, New York, 117-135.

Swift, D. J. P.,D. B. Duane, and O. H. Pilkey, eds., 1972, *Shelf Sediment Transport: Process and Pattern*: Dowden, Hutchinson and Ross, Stroudsburg, Penn., 656pp.

Thorne, P. D., 1986. A potentially new instrument for measuring the in-situ concentration of fine sediments in suspension. *Mar. Geol.*, **73**, 343-348.

Trowbridge, J. and O. S. Madsen, 1984. Turbulent wave boundary layers Model formulation and first-order solution, *J. Geophys. Res.*, **89**, 7989-7997.

U. S. Army Corps of Engineers, Coastal Data Information Program Monthly Reports, 1981-1982.

Von Engeln, O., 1942. *Geomorphology*: New York, MacMillan and Co., 665pp.

Wiberg, P. and J.D. Smith, 1983. A comparison of field data and theoretical models for wave-current interactions at the bed on the continental shrlf. *Cont. Shelf. Res.*, **2**, 2/3, 147-162.

White, S. J., 1970. Plane bed thresholds of fine grained sediments. *Nature*, **228**, 152-153.

Wooding, R. A., E. F. Bradley, and J. K. Marshall, 1973. Drag due to regular arrays of roughness elements of varying geometry, *Boundary Layer Meteorology*, **5**, 285-308.

Yalin, M. S. and E. Karahan, 1979. Inception of sediment transport, *Jour. of the Hydr. Div., ASCE*, **105**, HY11, 1433-1443.

Yalin, M. S., 1972. *Mechanics of Sediment Transport*: Pergamon Press, New York, 290 pp.

Appendix A

Modelling approach

The diagram of Figure A.1 outlines the approach driving the modelling effort described in this dissertation. Each box contains a model element. The guiding premise is that each element is autonomous within the model, and can be replaced as advances in the appropriate field outmode the approach being used. The shaded boxes indicate model elements included in this dissertation.

A complete continental shelf model requires input from a wide range of scientific disciplines (Figure A.1). Work is now underway attempting to characterize wave fields from satellite observations and shelf circulation from meteorological and topographic data. At the same time, studies are underway to characterize the response of sediments to shear stresses caused by flows, the influence of bottom benthos on those responses and the influence of the responses (i.e. bed roughness and suspended sediment-induced stratification) on the bottom boundary layer flows.

To clarify the interactions illustrated in the diagram, the generation and effects of surface waves will be traced through the diagram. A similar exercise for currents might be a worthwhile investment of time for the reader: these diagrams contain a great deal of information on the complex interactions in the shelf system and studying them can provide some insight.

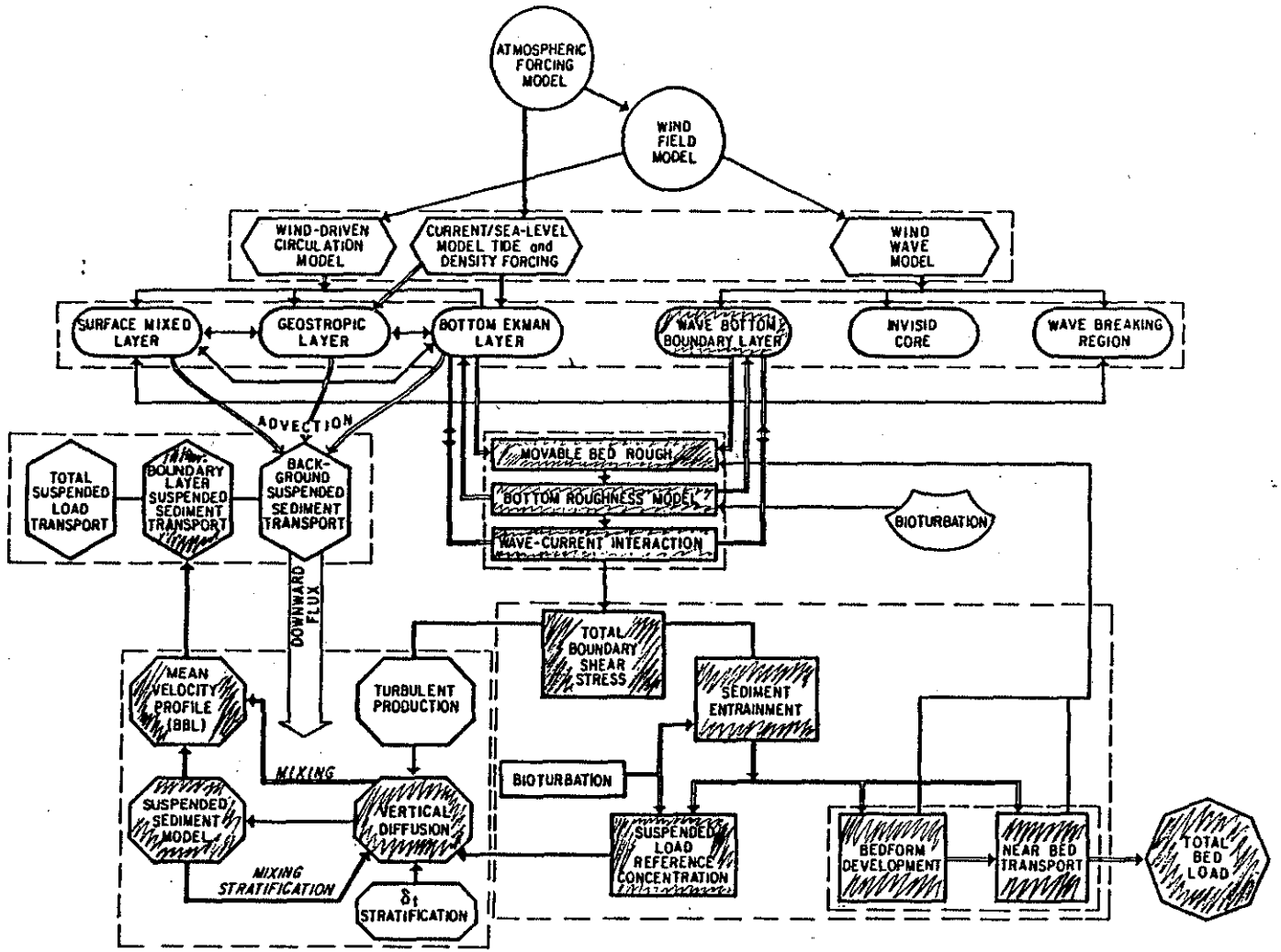

Figure A.1: Detailed diagram of model elements necessary for the continental shelf physical system. Dashed boxes refer to the general system diagram in Figure 1.2. Hatched boxes indicate elements included in the model presented in this thesis. (Grant and Graber, unpublished)

Starting at the top of Figure A.1, note that large-scale *atmospheric models* drive predictions of *wind fields*, which then can be applied to the prediction of *wind-generated waves*. The elements of the diagram are emphasized so that it is easier to place the discussion in context of the figure. Depending on the wave height and period and the water depth, the wave may break, it may generate oscillatory motion to some depth in the inviscid core, or it may generate significant velocities (up to 100 cm/sec or more) at the seafloor. In the latter case, the effects of the wave can be modelled as a *wave boundary layer* in the bottom few centimeters of the water column. If the bottom velocities are sufficiently large, bottom sediments will be moved, perhaps forming ripples. These effects are included in a *movable bed roughness* model, which combines with other elements of bottom roughness to influence the form of the wave bottom boundary layer. This is the first element of feedback in the system. If currents are present, the nonlinear *interaction of waves and currents* also must be modelled, along with its effect on the roughness and the wave boundary layer.(The roughness model is in part a derivative of semi-empirical models of *bedform development* and *near bed transport*, which explains the connection to the bottom boundary condition models of the lower right-hand corner.)

Having determined the bottom roughness and wave bottom velocities, the *total boundary shear stress* can be calculated using a friction factor or drag coefficient model. Empirical initiation of motion models use the skin friction component of the shear stress to calculate conditions for *sediment entrainment*; other semi-empirical models are used to calculate the bottom boundary condition for suspended load, the *reference concentration*. The total shear stress is also used in an eddy viscosity model of *turbulent production* and *vertical diffusion* of mass and momentum. The vertical diffusion and reference

concentration are combined in a *suspended sediment model.* Stratification by sediments can influence vertical diffusion, in another feedback mechanism, and they jointly influence the calculation of the *mean velocity profile.* The mean velocity profile has been generated using models of *geostrophic* and *Ekman layer* flow.

Appendix B

Friction Factor, Shear Stress and Shear Velocity Solutions

The characteristic boundary shear stresses and shear velocities are calculated from the instantaneous boundary shear stress. The instantaneous boundary shear stress is defined in GMG using a quadratic drag law, as defined in Equation 3.21:

$$\vec{\tau_0} = \frac{1}{2}\rho f_{cw}(u^2+v^2)[\frac{u}{(u^2+v^2)^{\frac{1}{2}}}, \frac{v}{(u^2+v^2)^{\frac{1}{2}}}]$$

where u, v are the x, y components of a combined wave and current reference velocity close to the bottom (though we are, for the moment, assuming that the wave and near-bottom current are collinear in the x-direction). f_{cw} is the combined wave and current friction factor. The characteristic shear stress in the wave boundary layer ($\tau_{0cw} = \rho\ u_{*cw}^2$) is defined as the maximum value of Equation 3.21. For the current boundary layer, τ_{0c} ($= \rho u_{*c}^2$) is calculated by time averaging equation 3.21. The solutions for the shear velocities are:

$$u_{*cw} = [\frac{1}{2}f_{cw}\alpha(\frac{u_a}{u_b})]^{\frac{1}{2}}u_b$$

$$u_{*c} = [\frac{1}{2}f_{cw}V_2(\frac{u_a}{u_b})]^{\frac{1}{2}}u_b$$

where α and V_2 are functions of the maximum and time-averaged velocities, respectively, in the wave boundary layer. u_a is a representation of the velocity of the mean flow in the wave boundary layer, so $\frac{u_a}{u_b}$ is a representation of the relative strength of the mean versus the maximum oscillatory flow in the wave boundary layer. The value of f_{cw} is determined using these definitions and the wave velocity profile. The value of f_{cw}, is calculated implicitly from the equation:

$$[0.097(\frac{k_b}{A_b})^{\frac{1}{2}}\frac{K}{f_{cw}^{\frac{3}{4}}}]^2 + 2[0.097(\frac{k_b}{A_b})^{\frac{1}{2}}\frac{K}{f_{cw}^{\frac{3}{4}}}][\frac{V_2}{2\alpha^{\frac{1}{4}}}]\cos\phi_c = \frac{\alpha^{\frac{3}{4}}}{4} - \frac{V_2^2}{4\alpha^{\frac{1}{2}}} \qquad \text{(B.1)}$$

where ϕ_c is the angle between the wave and current directions, A_b is the bottom excursion amplitude for the wave, defined in Equation 3.26, and K is derived from the equation for the wave velocity (Equation B.2) to be:

$$K = \frac{1}{2\varsigma_0^{\frac{1}{2}}}\frac{1}{(\mathrm{ker}^2\, 2\varsigma_0^{\frac{1}{2}} + \mathrm{kei}^2 2\varsigma_0^{\frac{1}{2}})^{\frac{1}{2}}}$$

The solution for the wave momentum equation inside the wave boundary layer is not explicitly of interest for the present problem, though it is necessary for the calculation of the boundary shear stress. The solution immediately above the bottom is:

$$u_w = u_b[1 + \frac{1}{2}\frac{\ln\xi + 1.154 + \imath\frac{\pi}{2}}{\mathrm{ker}\, 2\xi_0^{\frac{1}{2}} + \imath\mathrm{kei}\, 2\xi_0^{\frac{1}{2}}}e^{\imath\omega t}] \qquad \text{(B.2)}$$

where $\xi = \frac{z}{\delta_w}$ and $\xi_0 = \frac{z_0}{\delta_w}$. Ker and kei are Bessel Functions: tabulated solutions to a particular form of differential equation. The derivation and background for the wave velocity profile and friction factor equation are covered in some detail in Grant and Madsen, 1979.

Appendix C

Model Results: Five More Wave Cases

Plots of results for five wave conditions discussed in the Sensitivity section (Section 5) are included here. The list of wave and sediment conditions represented in these plots is presented in Table 5.2 on page 88. The five wave conditions represented are: moderate windsea, large storm with small fetch, moderate swell, large storm with large fetch, and extreme swell.

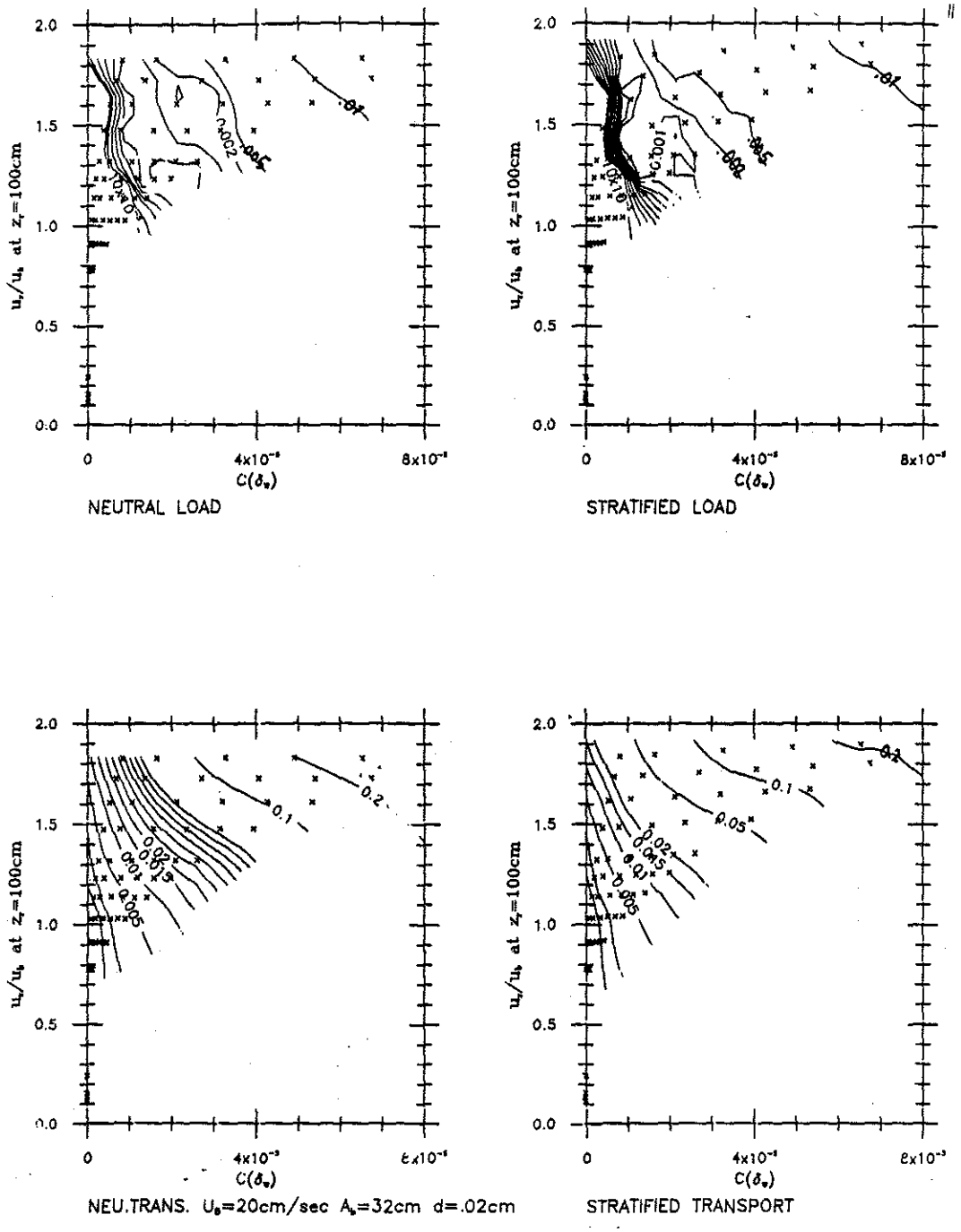

Figure C.1: Predicted near-bottom load ($\frac{cm^3}{cm^2}$) and transport ($cm^3/cm/sec$) values for fine sand in moderate windsea. T=10 sec, and the wave height in 50 m of water would be 2.5m. u_r is reference current velocity. δ_w ranges from 2-11 cm; $\frac{\ell}{\delta}$ ranges from 1 to 28 m.

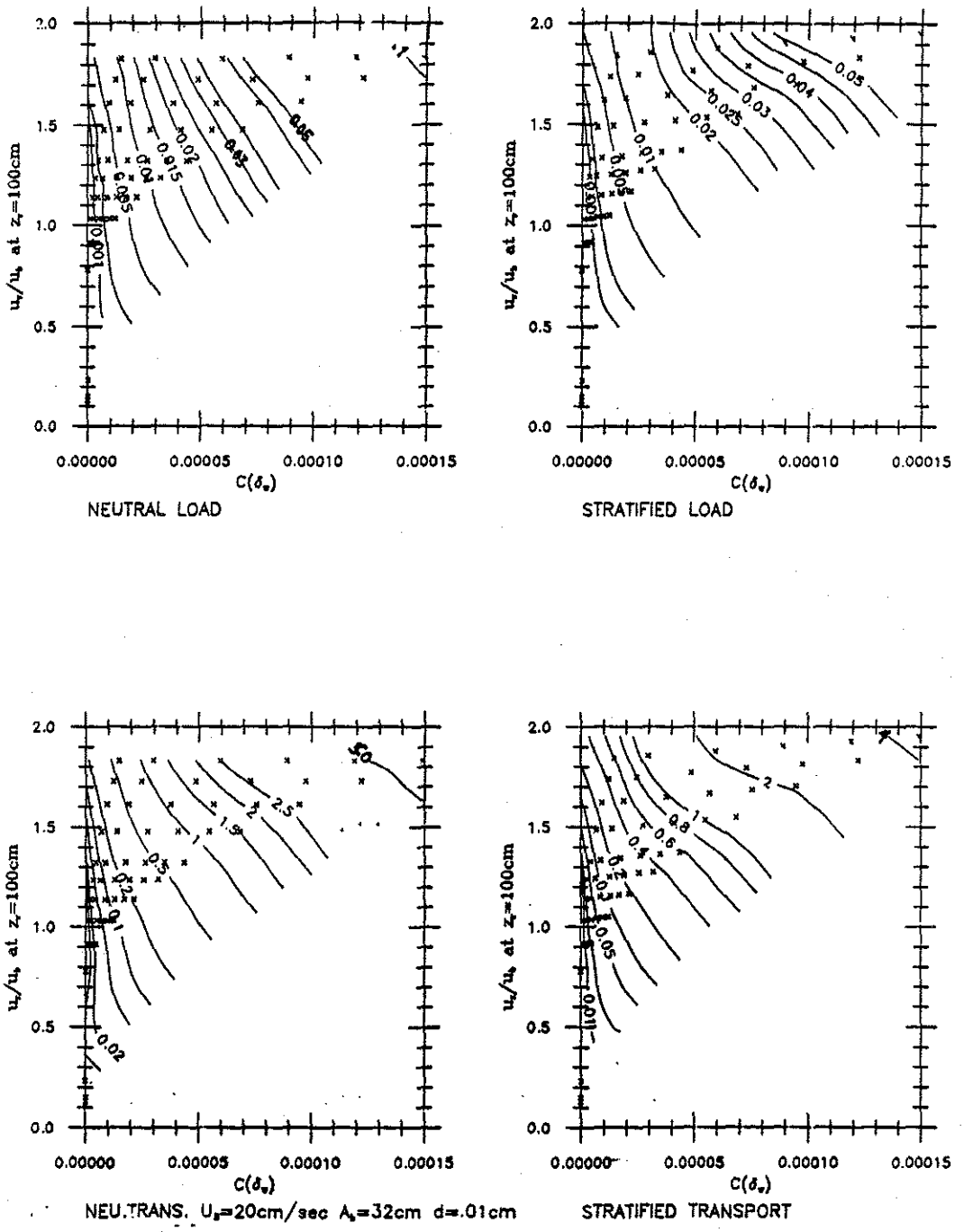

Figure C.2: Predicted near-bottom load ($\frac{cm^3}{cm^2}$) and transport ($cm^3/cm/sec$) values for very fine sand in moderate windsea. δ_w ranges from 2-10 cm; $\frac{\ell}{\delta}$ ranges from 1 to 28 m.

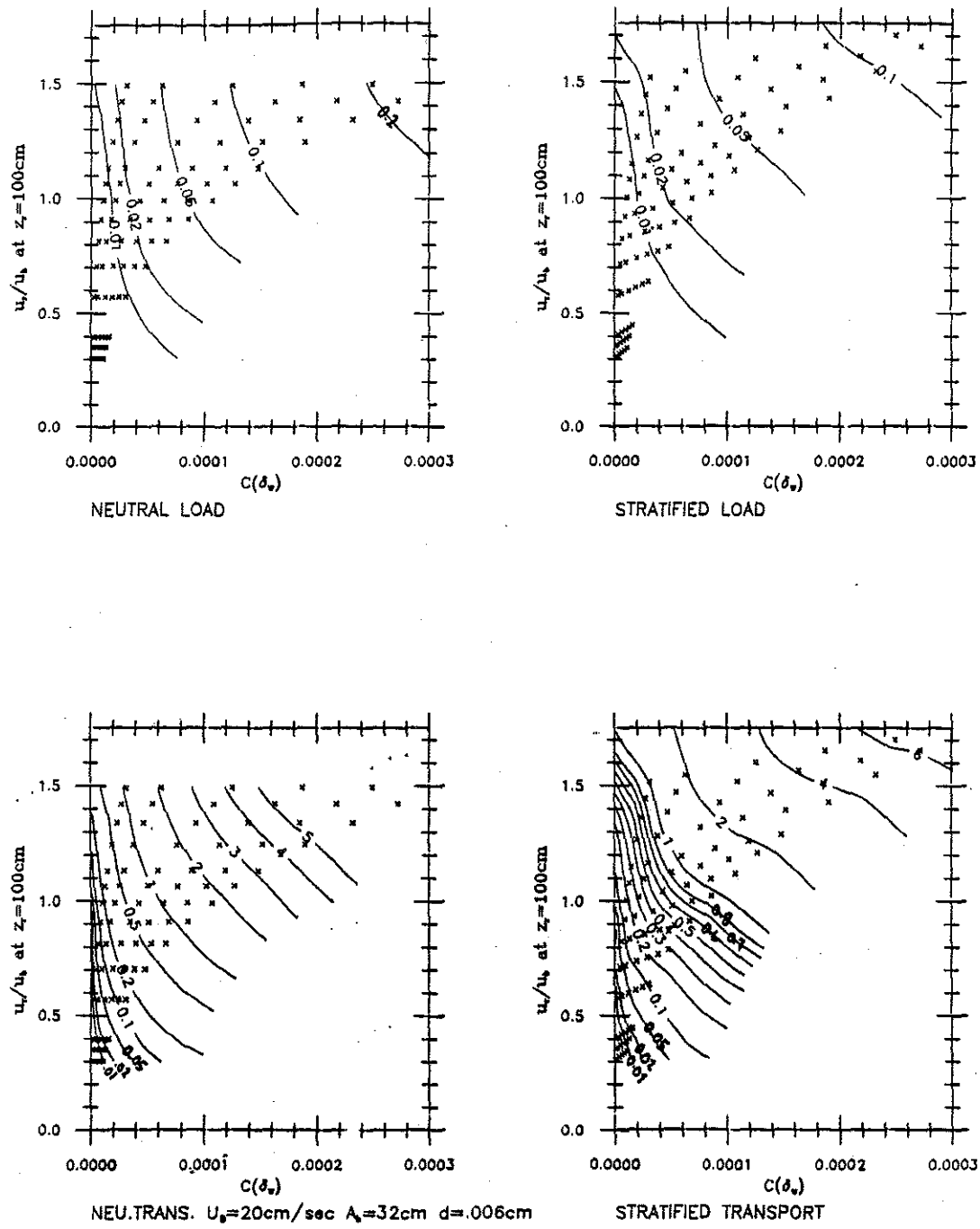

Figure C.3: Predicted near-bottom load ($\frac{cm^3}{cm^2}$) and transport ($cm^3/cm/sec$) values for coarse silt in moderate windsea. δ_w ranges from 7-8 cm; $\frac{\ell}{\delta}$ ranges from 6 to 18 m.

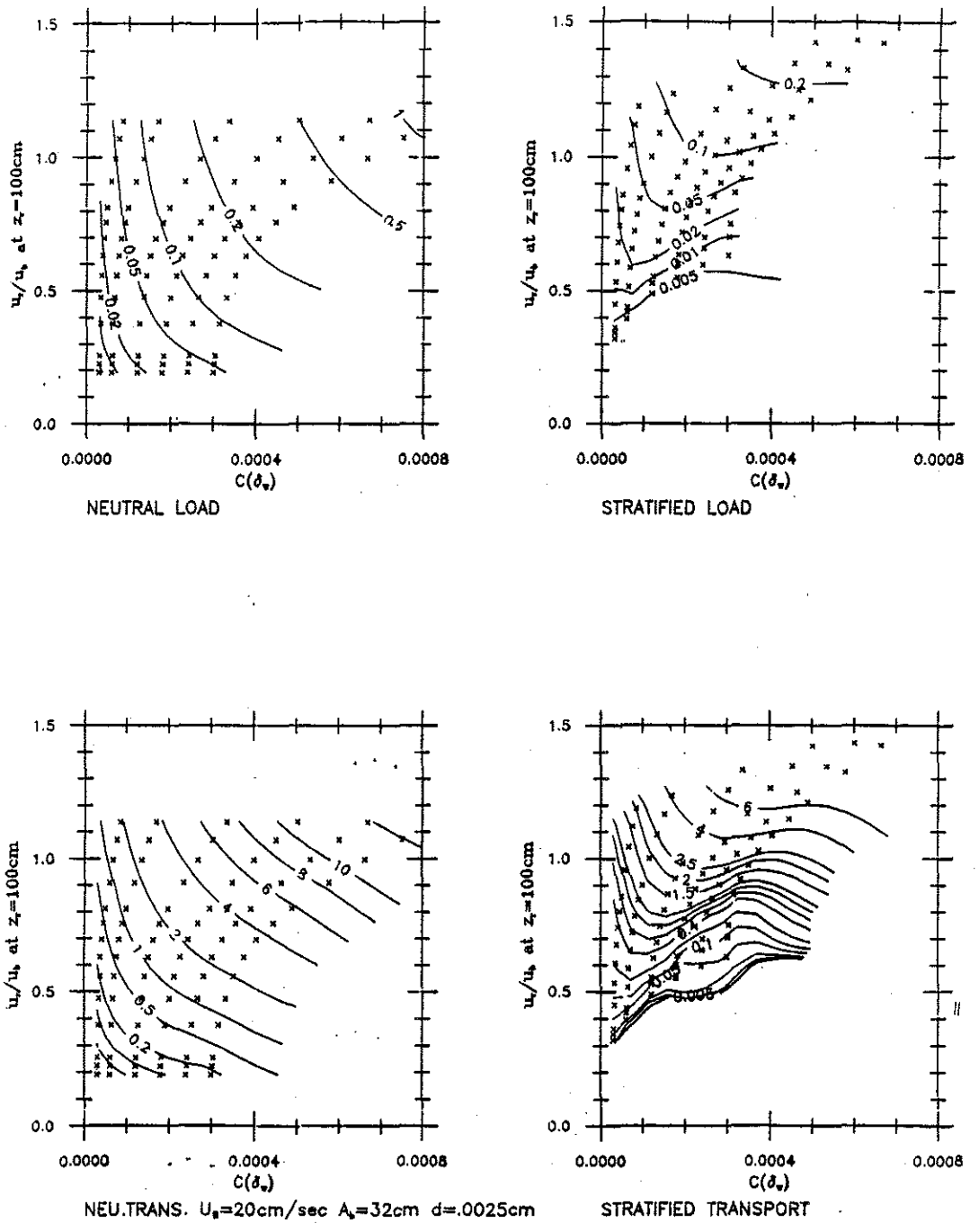

Figure C.4: Predicted near-bottom load ($\frac{cm^3}{cm^2}$) and transport ($cm^3/cm/sec$) values for medium silt in moderate windsea. δ_w ranges from 3.7-3.8 cm; $\frac{\ell}{\delta}$ ranges from 3 to 10 m.

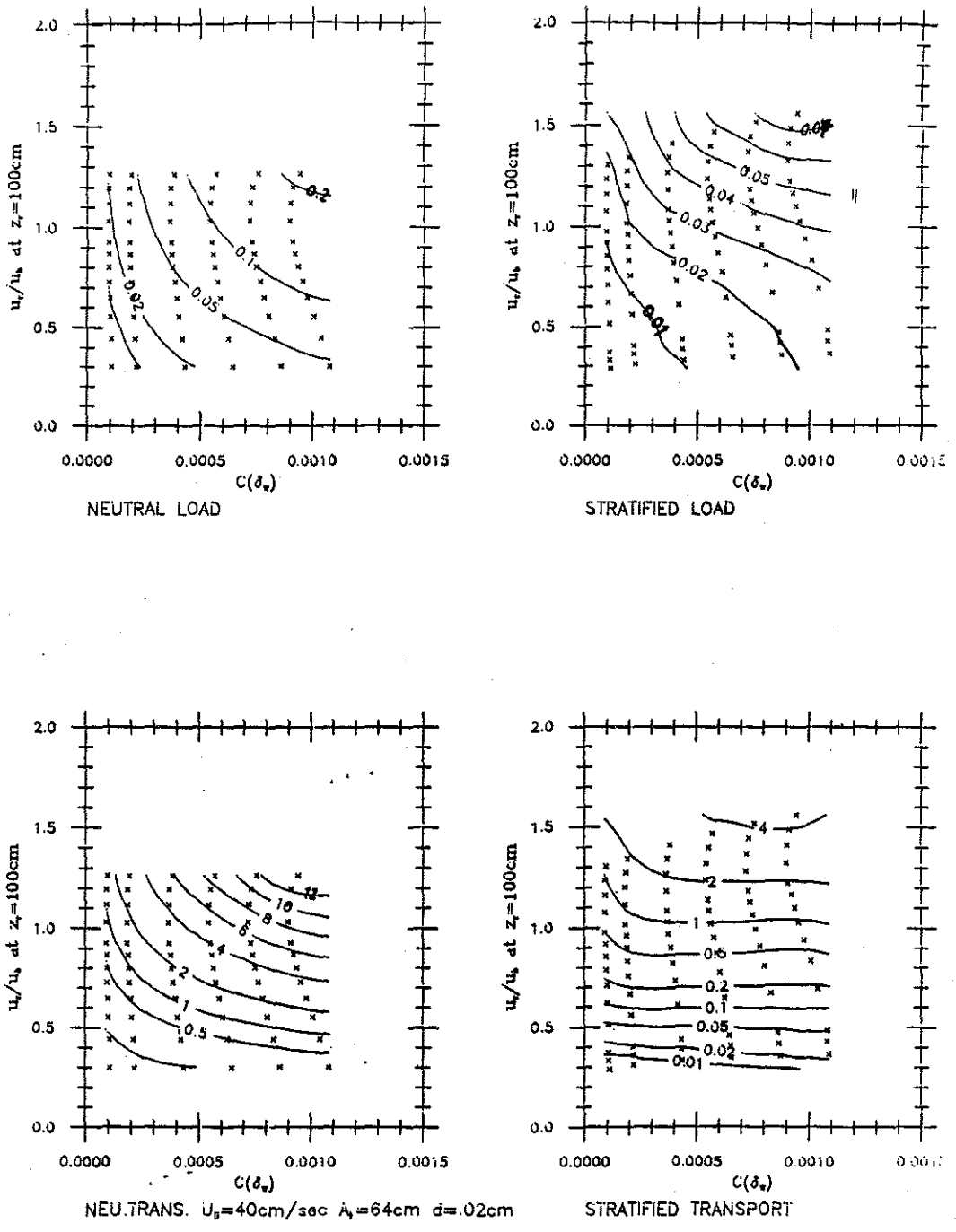

Figure C.5: Predicted near-bottom load ($\frac{cm^3}{cm^2}$) and transport ($cm^3/cm/sec$) values for fine sand in a large storm, early stages. T=10 sec, and the wave height in 50 m of water would be 5.0m. u_r is reference current velocity. δ_w ranges from 13 to 16 cm; $\frac{\ell}{\delta}$ ranges from 11 to 36 m.

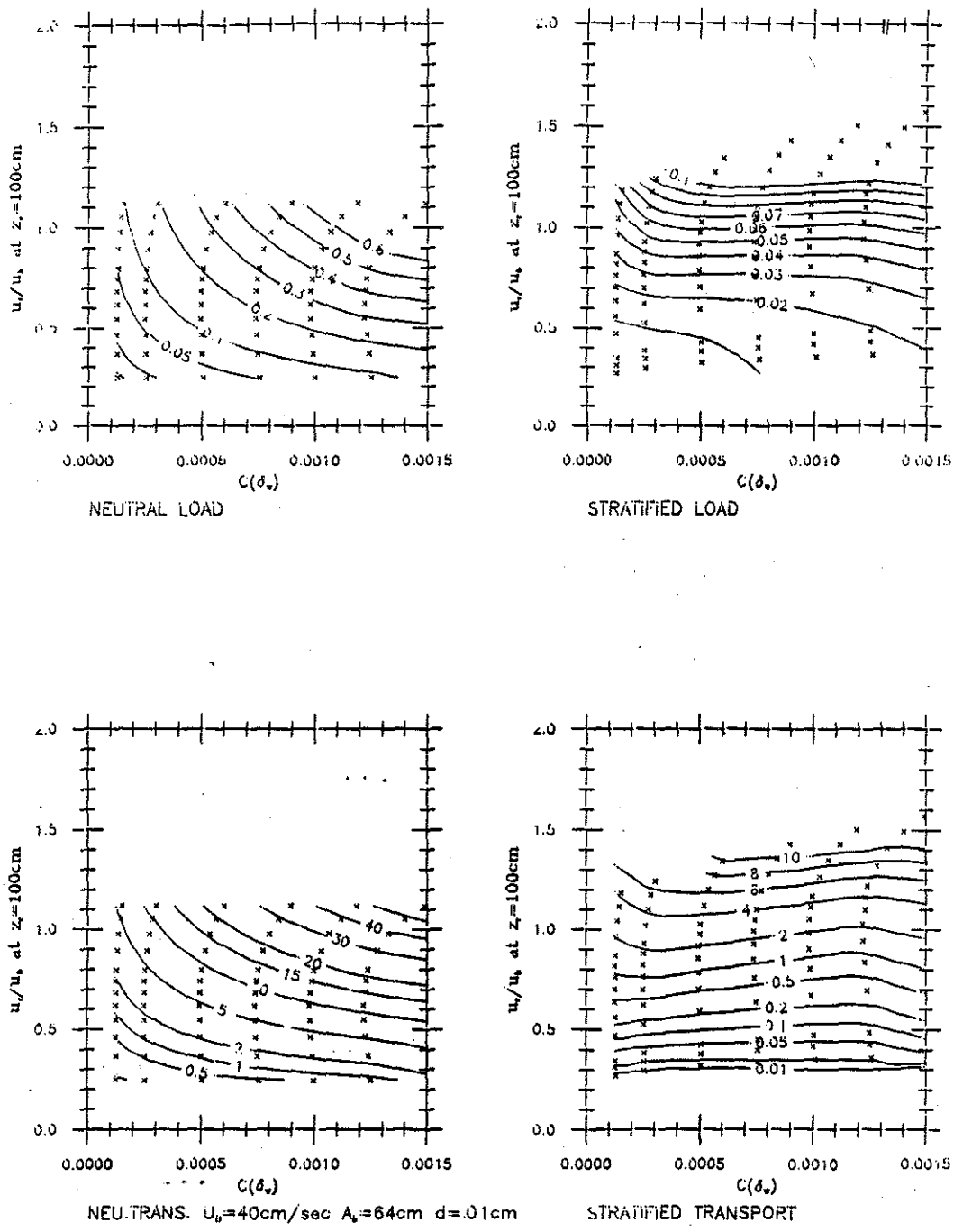

Figure C.6: Predicted near-bottom load ($\frac{cm^3}{cm^2}$) and transport ($cm^3/cm/sec$) values for very fine sand in a large storm, early stages. δ_w ranges from 9-10 cm; $\frac{\ell}{\delta}$ ranges from 7 to 26 m.

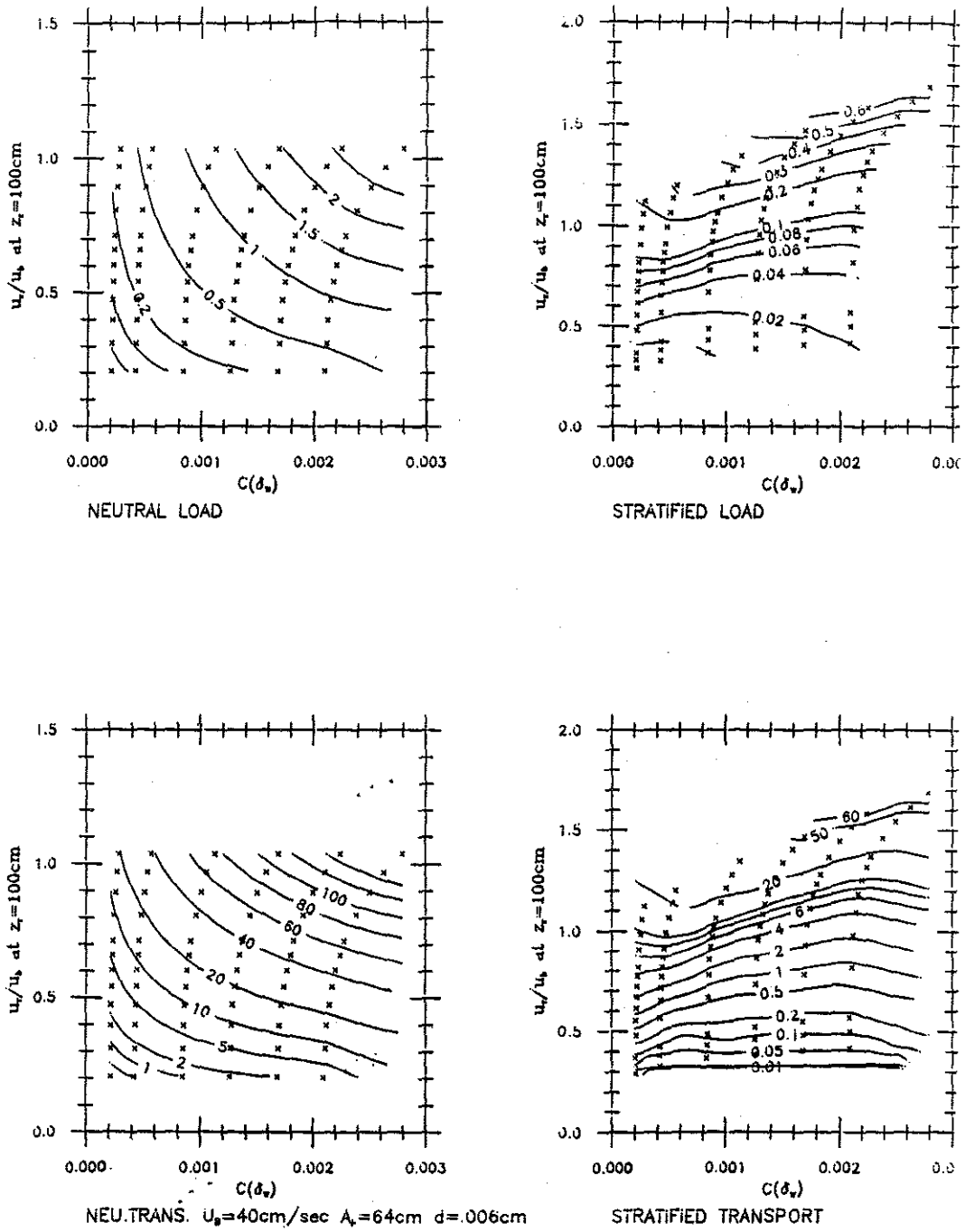

Figure C.7: Predicted near-bottom load ($\frac{cm^3}{cm^2}$) and transport ($cm^3/cm/sec$) values for coarse silt in a large storm, early stages. δ_w ranges from 7-8 cm; $\frac{\ell}{\delta}$ ranges from 5 to 22 m.

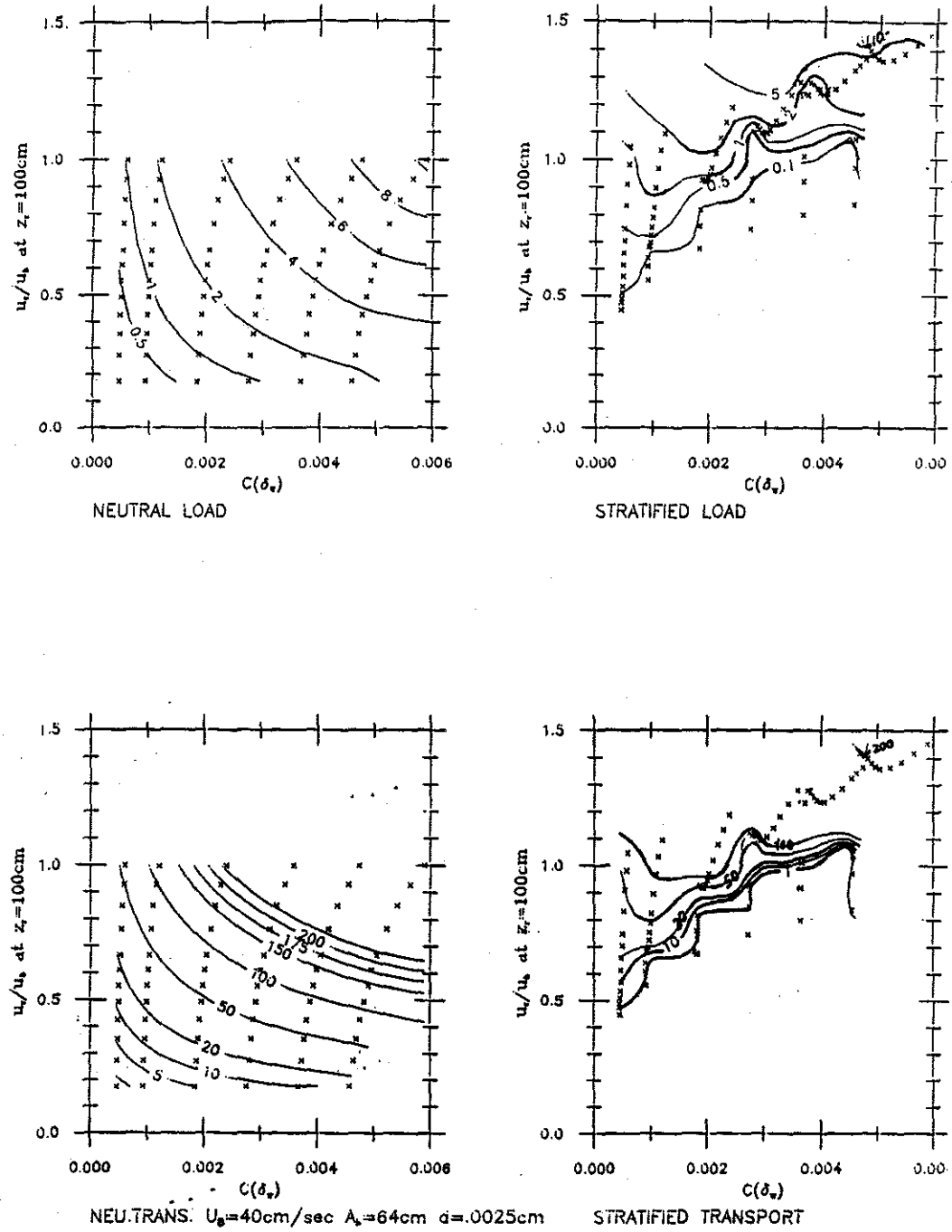

Figure C.8: Predicted near-bottom load ($\frac{cm^3}{cm^2}$) and transport ($cm^3/cm/sec$) values for medium silt in a large storm, early stages. δ_w ranges from 5-7 cm; $\frac{\ell}{\delta}$ ranges from 4 to 20 m.

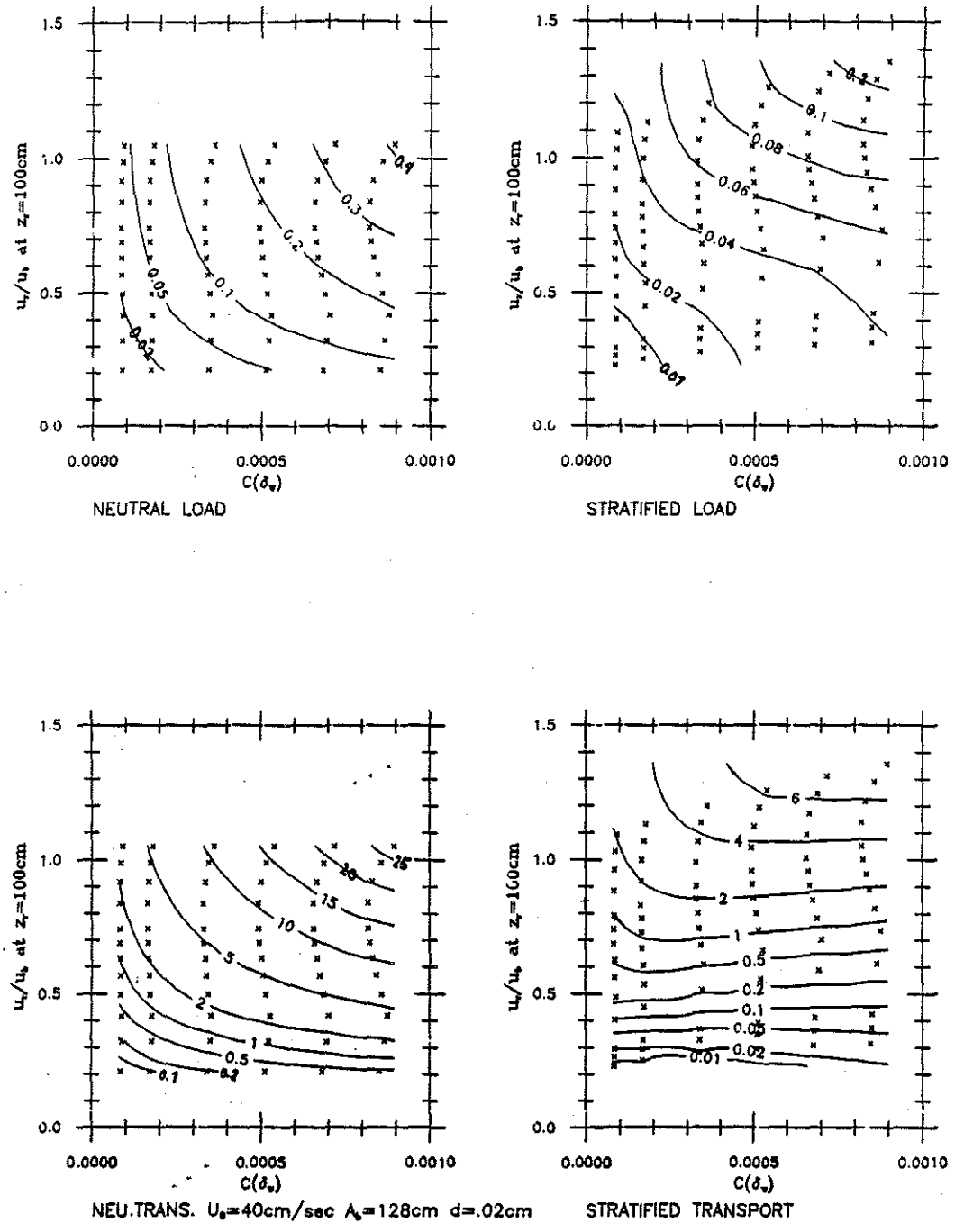

Figure C.9: Predicted near-bottom load ($\frac{cm^3}{cm^2}$) and transport ($cm^3/cm/sec$) values for fine sand in moderate swell. T=20 sec, and the wave height in 50 m of water would be 2.2 m. u_r is reference current velocity. δ_w ranges from 29 to 34 cm; $\frac{\ell}{\delta}$ ranges from 12 to 39 m.

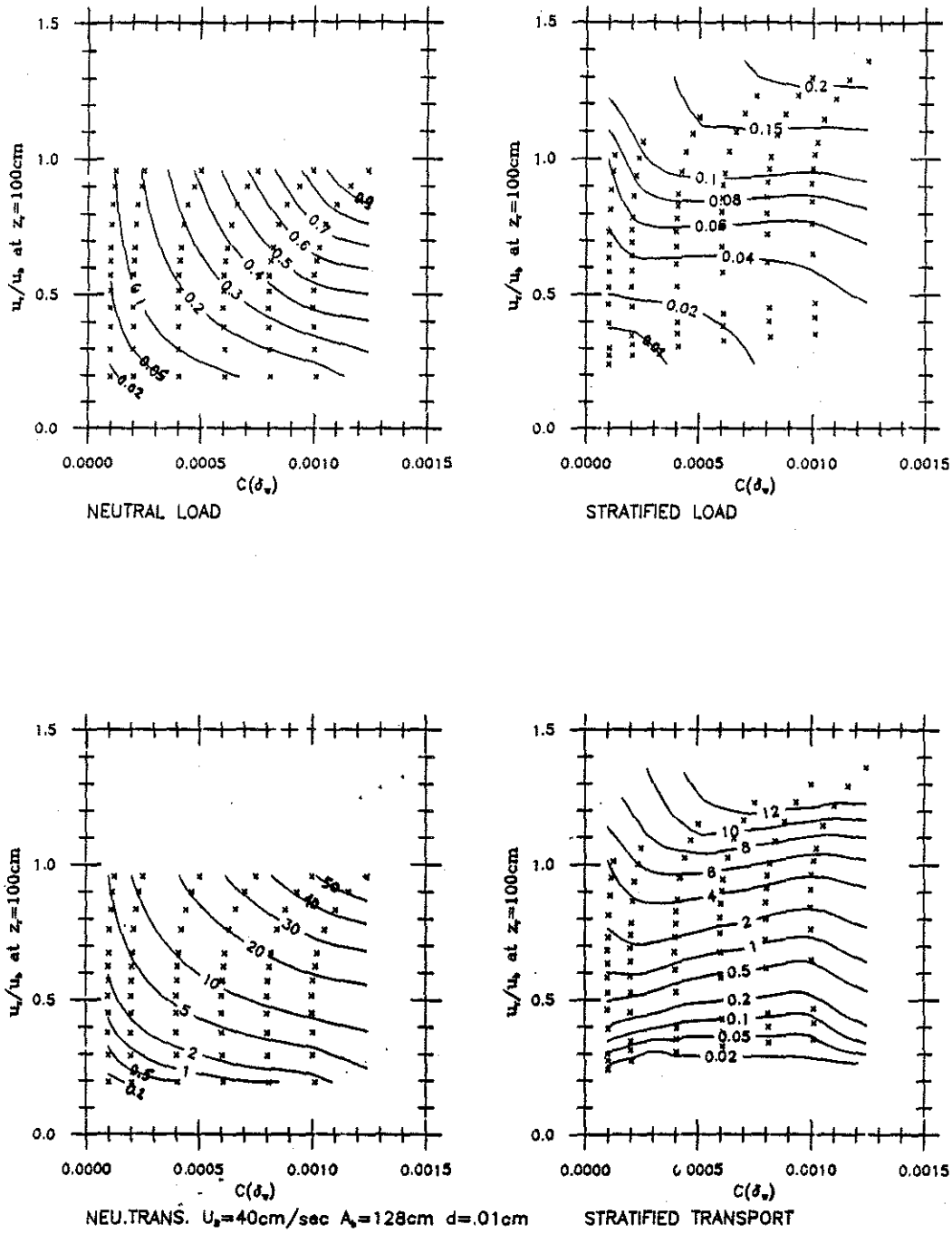

Figure C.10: Predicted near-bottom load ($\frac{cm^3}{cm^2}$) and transport ($cm^3/cm/sec$) values for very fine sand in moderate swell. δ_w ranges from 20-23 cm; $\frac{\ell}{\delta}$ ranges from 8 to 27 m.

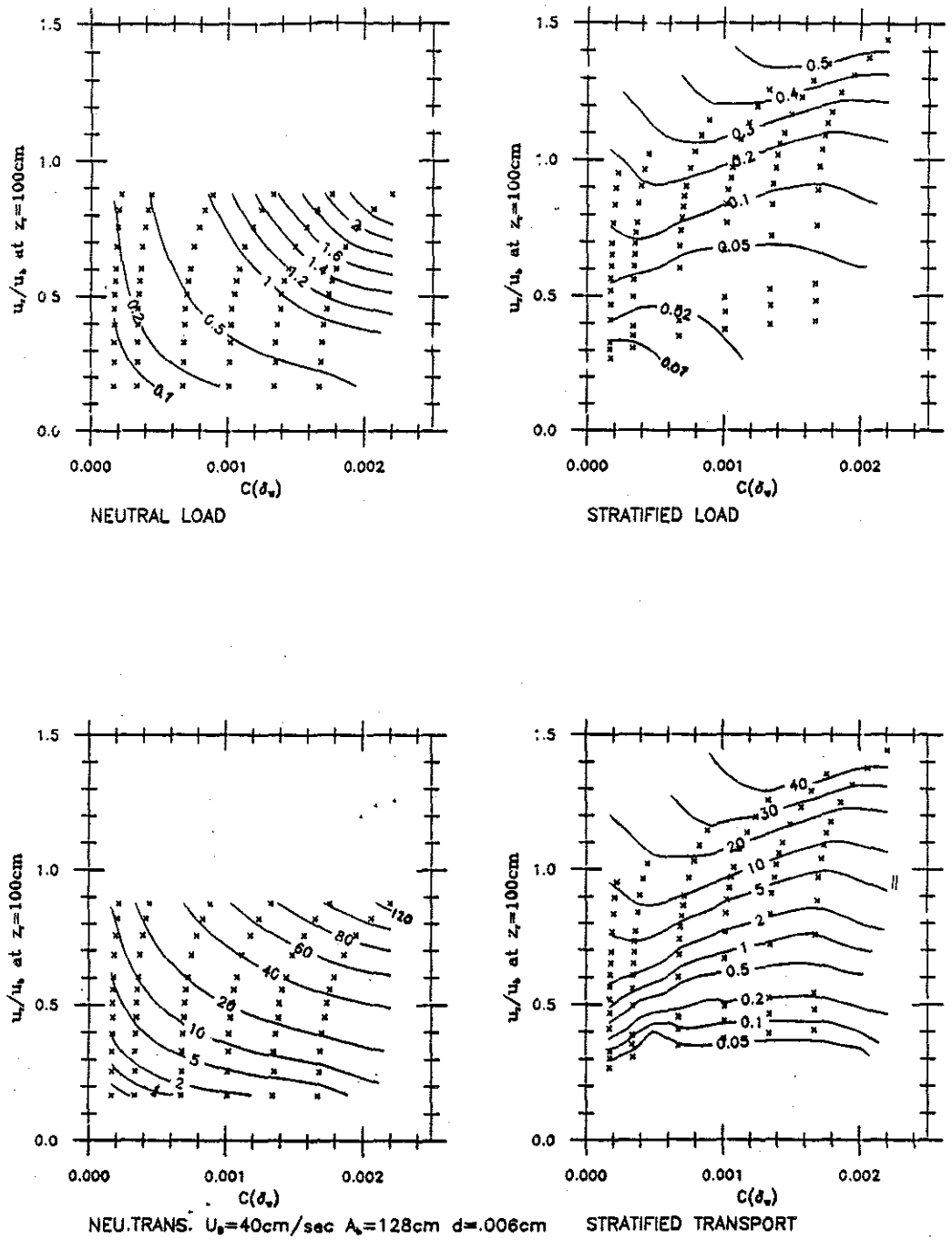

Figure C.11: Predicted near-bottom load ($\frac{cm^3}{cm^2}$) and transport ($cm^3/cm/sec$) values for coarse silt in moderate swell. δ_w ranges from 14.8-15.3 cm; $\frac{\ell}{\delta}$ ranges from 5 to 21 m.

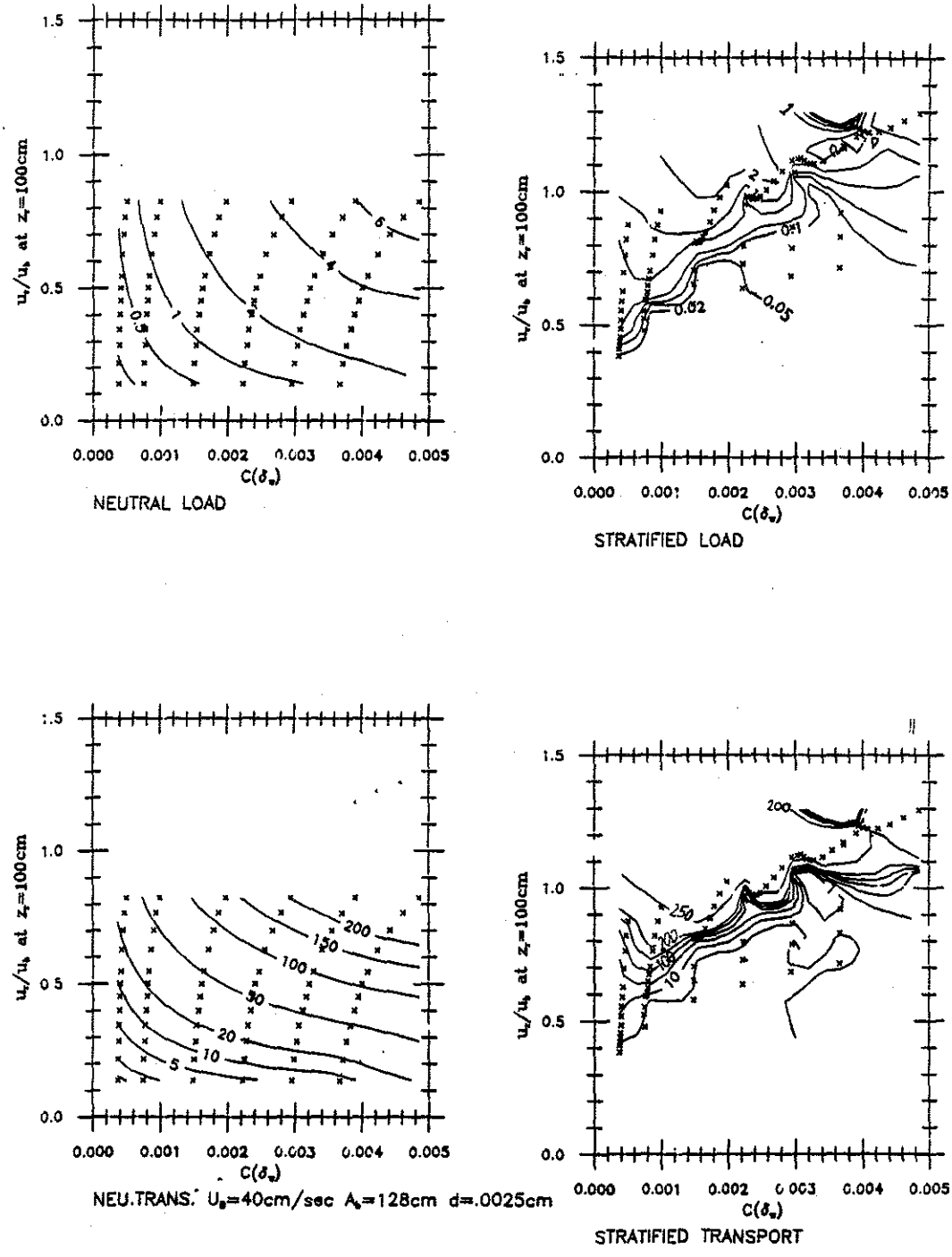

Figure C.12: Predicted near-bottom load ($\frac{cm^3}{cm^2}$) and transport ($cm^3/cm/sec$) values for medium silt in moderate swell. δ_w ranges from 10-12 cm; $\frac{\ell}{\delta}$ ranges from 3 to 17 m.

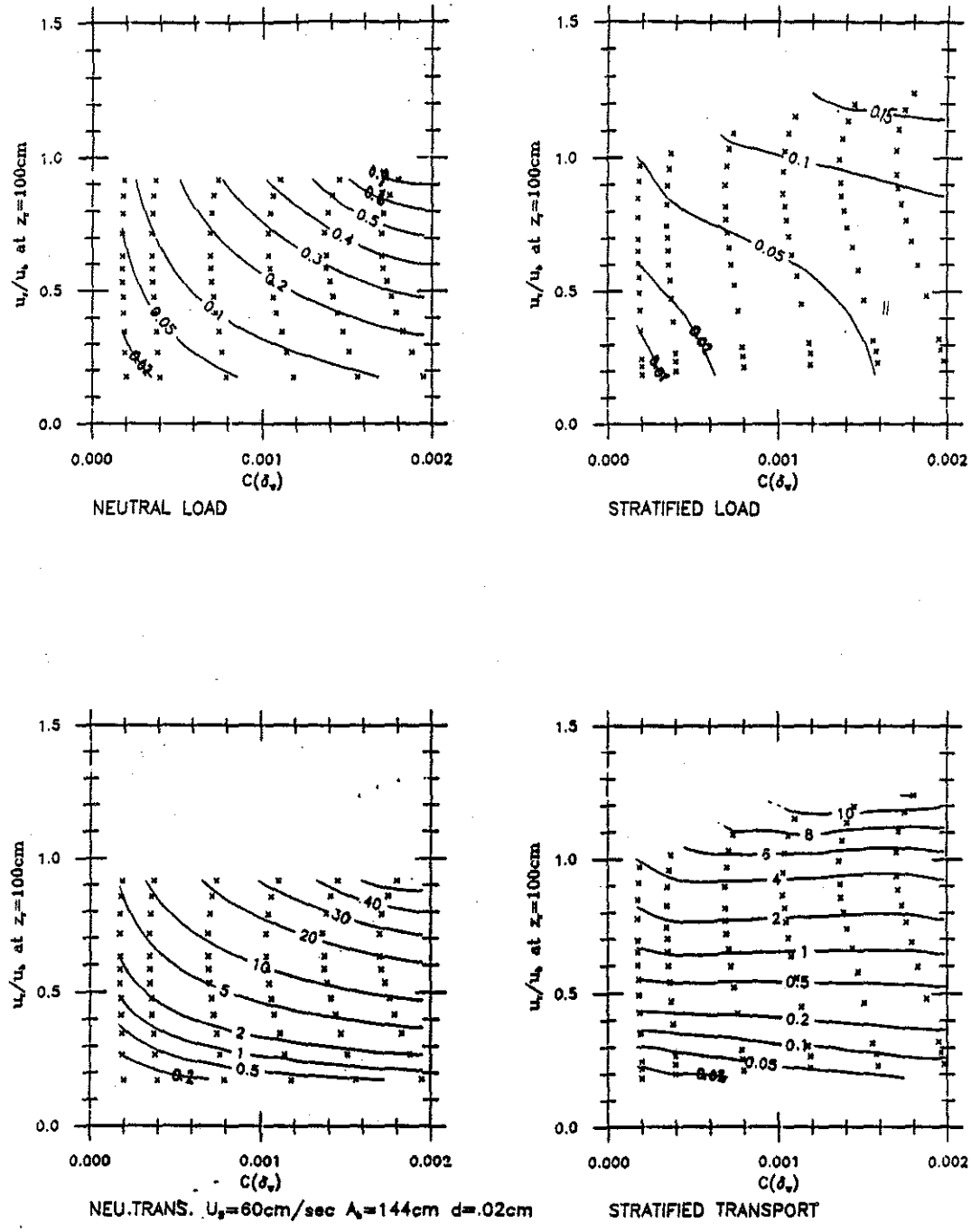

Figure C.13: Predicted near-bottom load ($\frac{cm^3}{cm^2}$) and transport ($cm^3/cm/sec$) values for fine sand in a large storm, late stages. T=15 sec, and the wave height in 50 m of water would be 3.9 m. u_r is reference current velocity. δ_w ranges from 21 to 22 cm; $\frac{\ell}{\delta}$ ranges from 10 to 39 m.

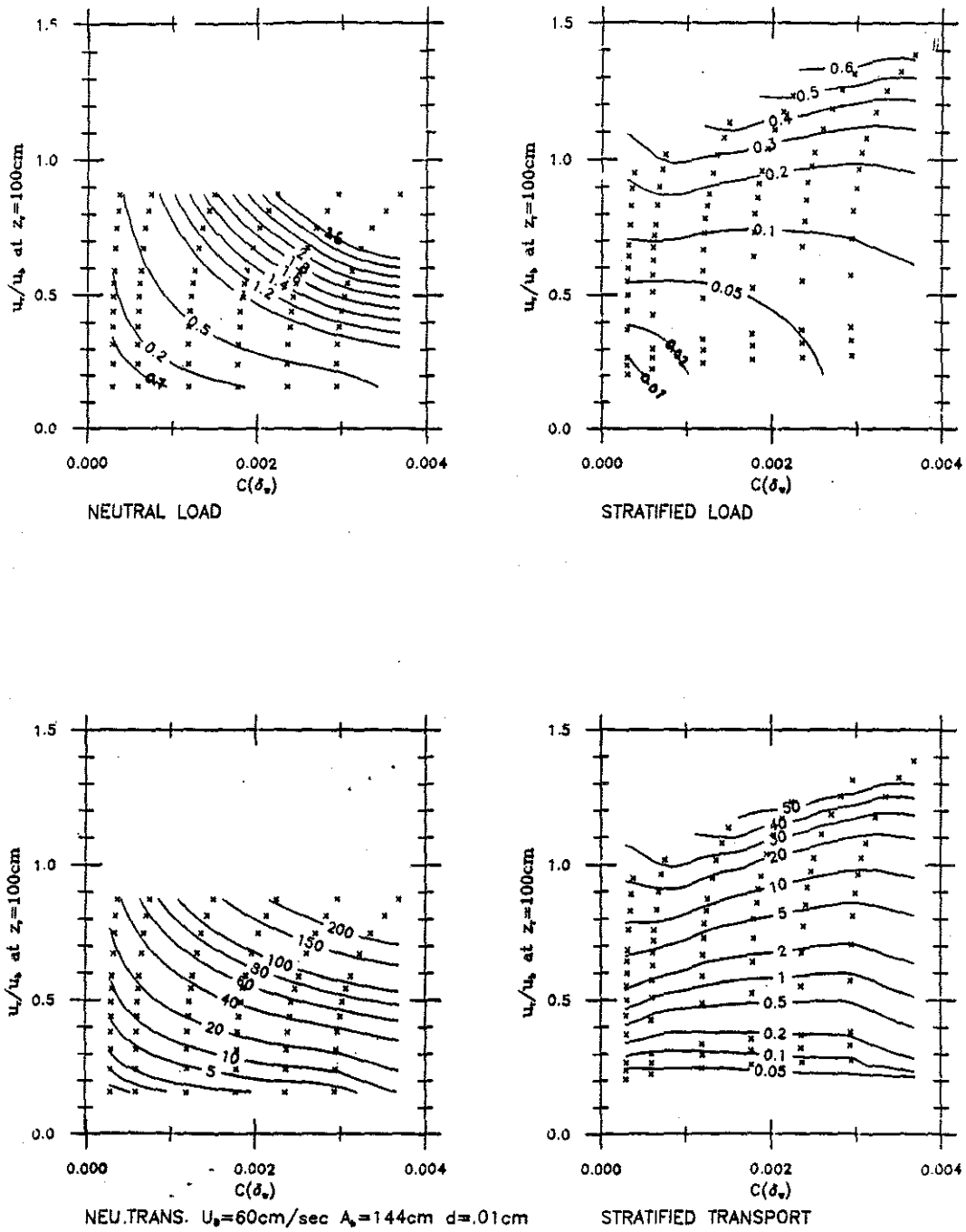

Figure C.14: Predicted near-bottom load ($\frac{cm^3}{cm^2}$) and transport ($cm^3/cm/sec$) values for very fine sand in a large storm, late stages. δ_w ranges from 18-16 cm; $\frac{\ell}{\delta}$ ranges from 8 to 33 m.

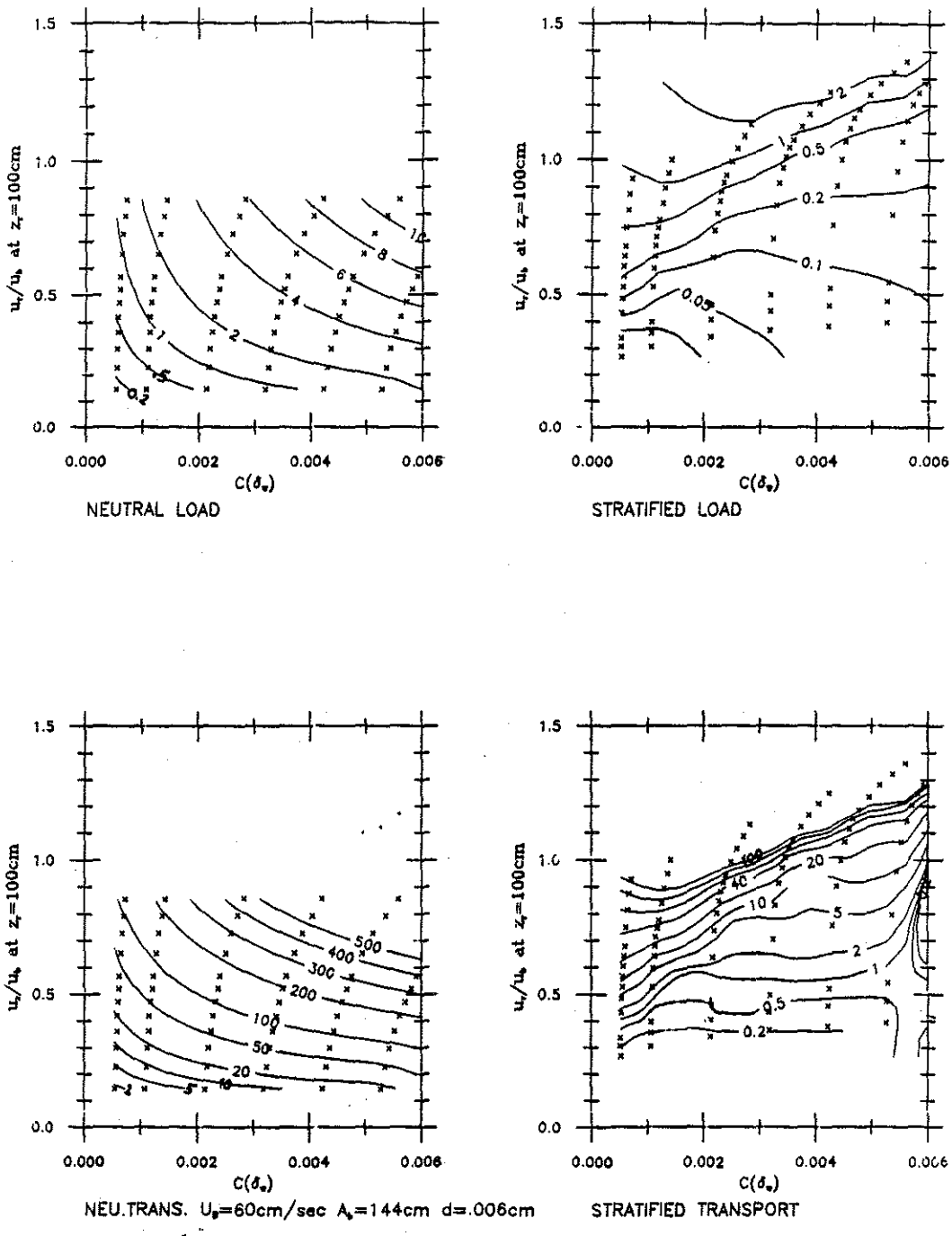

Figure C.15: Predicted near-bottom load ($\frac{cm^3}{cm^2}$) and transport ($cm^3/cm/sec$) values for coarse silt in a large storm, late stages. δ_w ranges from 13-17 cm; $\frac{\ell}{\delta}$ ranges from 6 to 31 m.

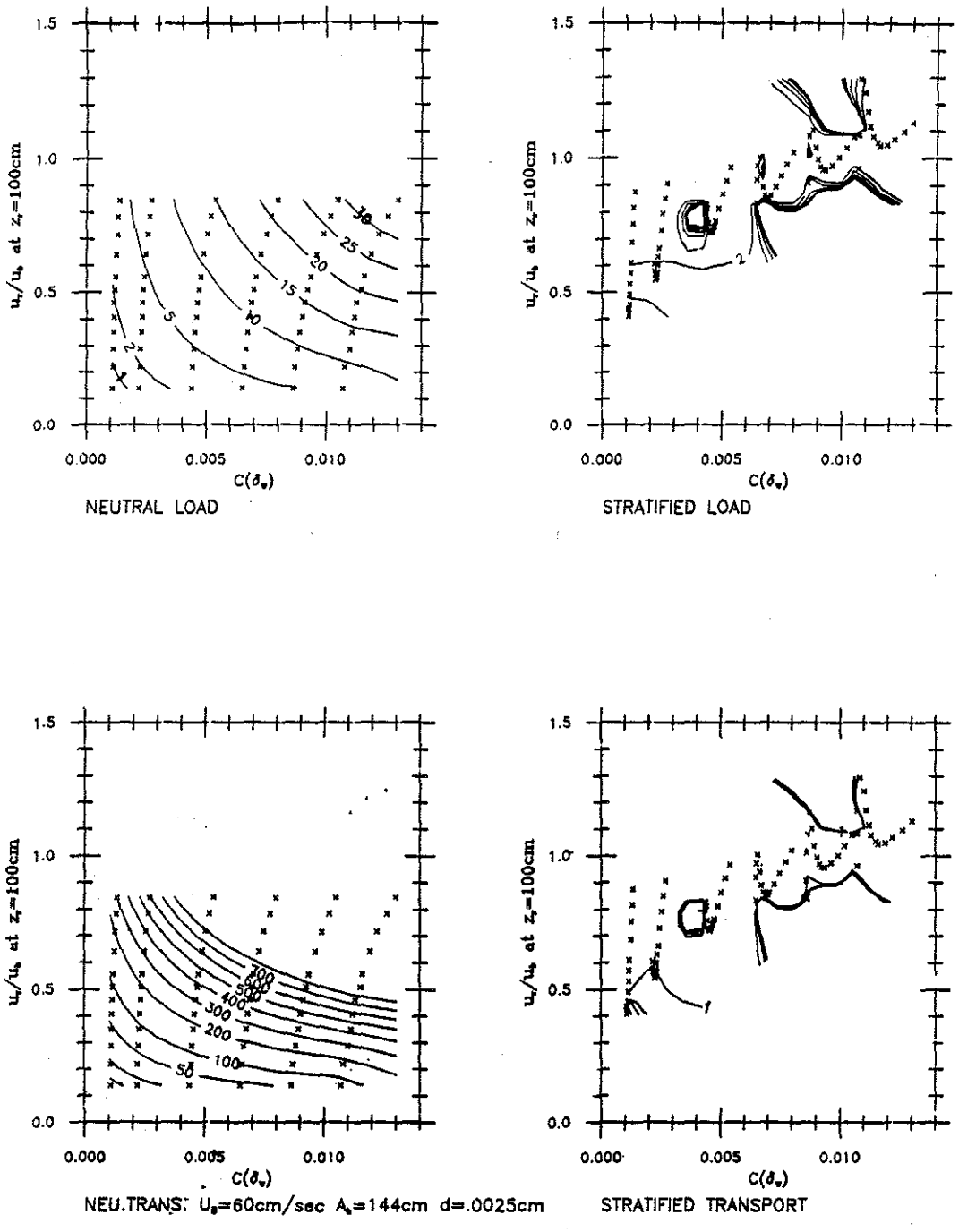

Figure C.16: Predicted near-bottom load ($\frac{cm^3}{cm^2}$) and transport ($cm^3/cm/sec$) values for medium silt in a large storm, late stages. δ_w ranges from 12-17 cm; $\frac{\ell}{\delta}$ ranges from 6 to 30 m.

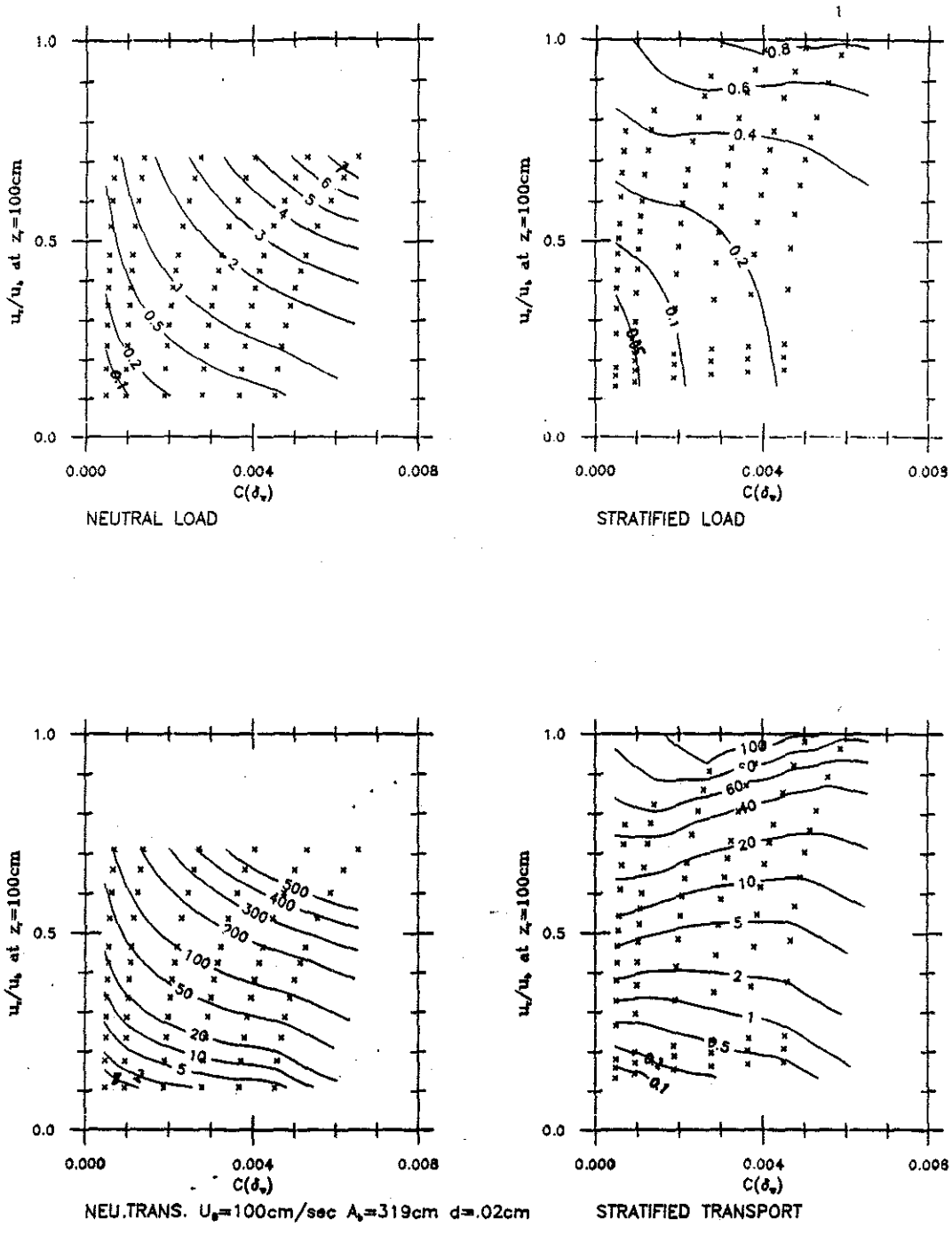

Figure C.17: Predicted near-bottom load ($\frac{cm^3}{cm^2}$) and transport ($cm^3/cm/sec$) values for fine sand in extreme swell. T=20 sec, and the wave height in 50 m of water would be 5.4 m. u_r is reference current velocity. δ_w ranges from 34 to 42 cm; $\frac{\ell}{\delta}$ ranges from 12 to 57 m.

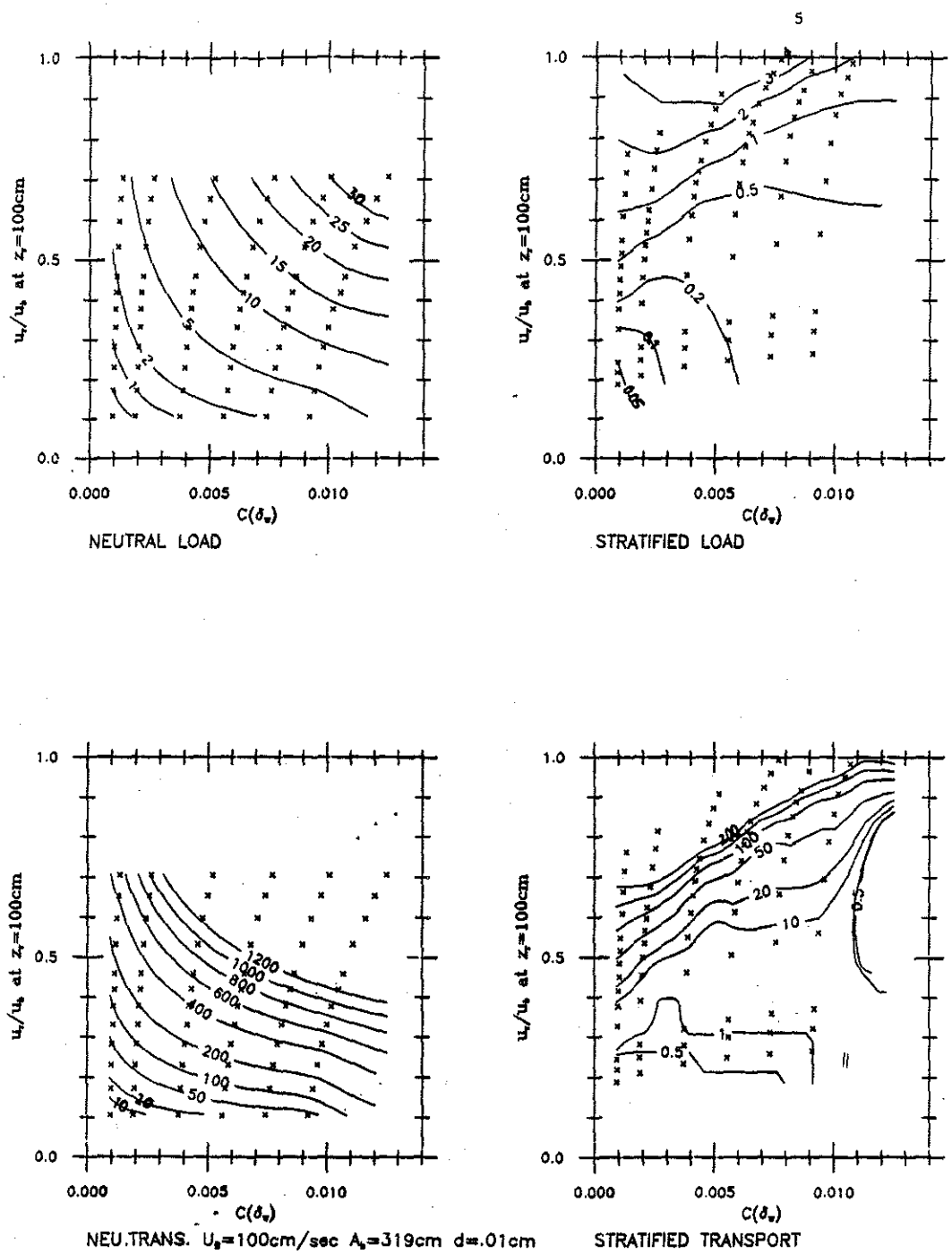

Figure C.18: Predicted near-bottom load ($\frac{cm^3}{cm^2}$) and transport ($cm^3/cm/sec$) values for very fine sand in extreme swell. δ_w ranges from 29-40 cm; $\frac{\ell}{\delta}$ ranges from 10 to 54 m.

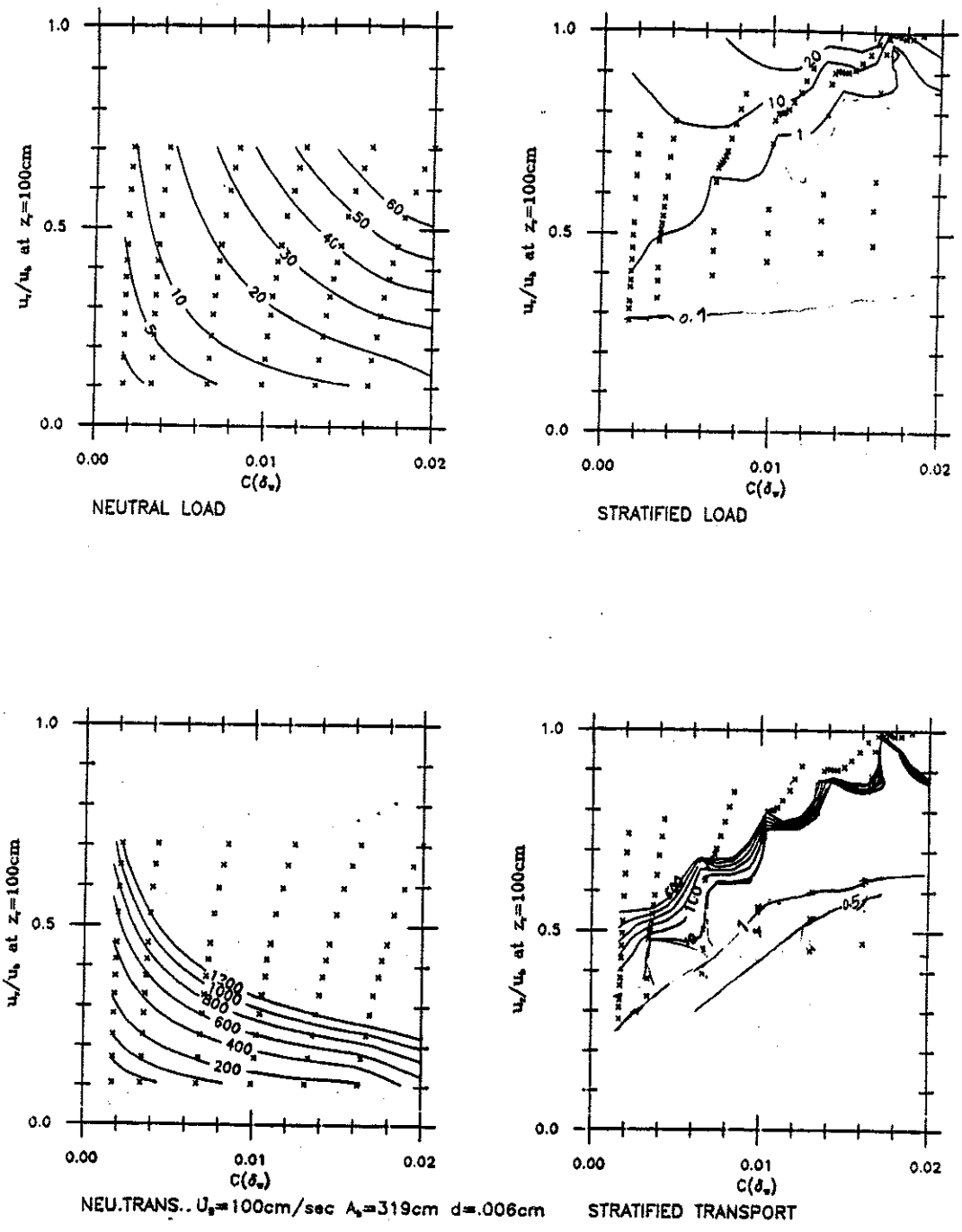

Figure C.19: Predicted near-bottom load ($\frac{cm^3}{cm^2}$) and transport ($cm^3/cm/sec$) values for coarse silt in extreme swell. δ_w ranges from 28-39 cm; $\frac{\ell}{\delta}$ ranges from 10 to 53 m.